Evaluation of Micro Electro Discharge Machining Performance: the Effect of Process Parameters and Electrode Material

Cristina Merla

Department of Management, Information and Production Engineering
University of Bergamo

Submitted in fulfilment of the requirements for the degree of Philosophiae Doctor in Mechatronics, Innovative Manufacturing Technologies, Information Technology and Mathematical Methods, ING-IND/16, XXVII cycle, AYs 2012-2014

Supervisor: Prof. Giancarlo Maccarini
Co-supervisor: Prof. Gianluca D'Urso

February 2015

Abstract

The use of micro components has become a widespread technological trend and it has been characterised by a continuous growth over the years: already in 2000 the surveys predicted an increase in the market from 30 billion USD to 60 billion USD in 2005 (Mounier 2002).

In general, the word micro-engineering deals with the development and manufacture of products characterised by functional features in the order of magnitude of microns. These products are usually characterised by a high level of components and functionalities integration because of the small dimensions of the final product (Alting L 2003).

From the technological point of view, the miniaturization of components enhances the difficulties related to their production with conventional technologies. At the same time this miniaturization trend opens the possibility to employ new non-conventional technologies that, like micro-EDM, laser beam machining and focused ion beam etching, are able to fulfil the market requirements and the technological challenges associated with the realization of micro components.

Micro-EDM is characterised by a series of advantages that over the years contributed to make it one of the most appealing micro-technologies especially for micro-drilling, thanks to its flexibility.

Micro-EDM is able to machine any conductive material regardless of the hardness and high strength of the workpiece material and, thanks to the contact-less nature of the process, it leaves no residual stresses in the workpiece. It allows the realization of high aspect ratio micro features, especially micro holes, with an excellent surface finishing and 3D micro structures without the need of any mask, with considerable advantages from the set up point of view (Reynaerts D 1997).

In micro-EDM, the erosion mechanism is based on electrical discharges that melt and vaporise the material. Tool and workpiece electrodes are separated by a gap, called “sparking gap”: between them the dielectric fluid helps controlling the environmental

electrical conditions in which the discharges take place. The dielectric fluid acts as insulator for certain voltage conditions and as conductor when the electric field reaches certain values. Thus, the erosion phenomenon is not limited to the workpiece material, but involves the electrode, too. Although it is not possible to eliminate this drawback, it is possible to control it by means of a proper regulation of the process parameters.

The influence of the process parameters is of great importance, not only for an effective control of the wear phenomenon, but especially because they have an influence on the final geometrical characteristics of the through holes and on the process performances.

Several studies have investigated the influence of the process parameters on micro-EDM drilling process (Jahan 2013, Kumar S 2009, Mahendran S 2010), nevertheless a lack of information emerges from the literature: no effective formalization of the input-output relationship in micro-EDM drilling has been carried out so far.

The aim of the present work is to deepen the knowledge of the influence of the real process parameters on the final geometrical characteristics of the holes and on the process performances.

Since complete information about the real value of fundamental process parameters (namely, the peak current and the exchanged energy and power) is not available, a signal acquisition system was implemented. This system is aimed at the recording and filtering of the real process parameters involved in the machining.

Moreover, one of the purposes of the study was to determine a formal relationship between the micro drilling process inputs, such as the power exchanged between the electrodes, and the outputs, like the geometrical characteristics of the holes and the process performance.

With the collected information it was possible to determine a formal equation for the prediction of the electrode wear and the machining time.

The experimental campaign was executed with a Sarix SX 200 machine. Through holes have been carried out with tungsten carbide (TC) and copper (Cu) tubular electrodes having external diameter equal to 300 and 150 μm. A DOE approach was implemented,

and the analysis of variance helped understanding the real influence of the parameters on the selected indicators for the geometrical characteristics and process performances.

The experimental campaign has been carried out with an automatic drilling program. During the execution of every hole the oscilloscope recorded the electric signals of peak current and voltage. The automatic drilling program allowed the recording of the electrode wear and the machining time. After the execution of each hole, the electrode has been cut with the Sarix Arianne wire EDM unit, in order to carry out all the holes with the same electrode geometrical conditions.

After the execution of the campaign, the holes top diameter (corresponding to the electrode entrance) and bottom diameter (electrode exit) have been measured with an optical microscope in order to carry out the geometrical analysis of the holes. Two parameters have been taken into account in order to evaluate the geometrical characteristics of the holes: the diametrical overcut (DOC) and the taper rate (TR). Similarly, two different indicators were considered for process performances, the material removal rate (MRR) and the tool wear ratio (TWR).

At the same time, the collected data referring to peak current, voltage and discharge energy has been analysed, in order to obtain reliable information about the peak current, the peak voltage, the number of sparks, the energy and the power exchanged during the process.

Once the data has been collected for all the electrodes materials and diameters, and for all the process parameters combinations, a regression analysis has been carried out. A comparison between linear and non-linear regression was carried out. Predictive equations based on the real values of the process parameters were obtained in order to forecast the machining time and the electrode wear, as well as the geometrical characteristics of the holes.

Acknowledgements

First and foremost I want to thank my supervisor Professor Giancarlo Maccarini. He provided a great example as a successful man, both in research and in life. Secondly, I must thank Professor Claudio Giardini, Gianluca D'Urso and Chiara Ravasio. I appreciated the contributions and the commitment they dedicated to make my experience productive, focused and stimulating.

I am also grateful for the chance I had to undertake the most challenging work experience so far. My stay in Cardiff has been a source of inspiration, knowledge, friendship, professional growth and personal improvement. I give my gratitude to professor Samuel Bigot of the Cardiff University, for his humanity, professionalism and for his scientific contribution. I had the pleasure to work with Anthony Surleraux, that revealed himself to be one of the greatest men I have ever met. I owe my good time in Cardiff to the many friends I had the luck meet during my experience abroad: Tracy, Gary and Jack for the family life and for the memorable human experiences we have shared. What you gave to me is inestimable. Aimee and Natalia, my fellow housemates, you were unique, I miss our time together.

A sincere gratitude goes to Michele Caldara for his fundamental contribution to my experimental activity at University of Bergamo and to Daniele Di Marco, for the precious and constant help. To all the friends I found along my path at University of Bergamo, thank you.

I would like to thank my father, Luciano, for his love, for his courage, for his openness and honesty, for his precious guidance and constant support. For all the things we have been through, always together.

Finally, I dedicate my work, my sacrifices, my improvements to honour my mother's memory, my first teacher at school and my first guide in life. I hope that everything I have done is up to the great human example she gave to me.

Cristina Merla
Università degli Studi di Bergamo
27th February 2015

Table of Contents

Chapter 1

Introduction

"The ability to see, use and include the possibilities brought by micro and nanotechnologies can be considered core competences for the companies in future, as well as product design and development" (Alting L 2003).

It appears clear from this statement that the use of micro components has become a widespread trend and it has been characterised by a continuous growth over the years: already in 2000 the surveys predicted an increase in the market from 30 billion USD to 60 billion USD in 2005 (Mounier 2002).

In general the word micro-engineering deals with the development and manufacture of products characterised by dimensions or functional features in the order of magnitude of the micron (10^{-6} m). Moreover, these products are usually characterised by a high level of integration of components and functionalities (Alting L 2003).

The technologies employed to produce this kind of micro components are defined micro-technologies. Originally, the definition "micro technologies" was related to the production of micro components made of silicon. The connection between this material and micro technologies was due to the microprocessors market (which is based on silicon) and its rapid growth. Usually, the technologies employed for the manufacturing of silicon resulted in a higher level of development if compared with the micro technologies, which were dedicated to the manufacturing of micro-products made of metals or ceramic materials (Menz 2002). For this reason the technologies dedicated to silicon machining started to be employed in other fields of mechanics.

Progressively, the products have been characterised by a reduction of their dimensions and the same trend has inevitably characterised the dimensions of the components, too. Thanks to the improvements achieved in product design, new and innovative products have been made available to a growing number of customers. This resulted in a growing pressure on manufacturing technologies because the increasing number of products

requires the development of technologies able to guarantee a mass production of the components.

It is common knowledge that many micro-products and micro-components have been produced as prototypes by using dedicated technologies and production chains in laboratory, but the majority of the technologies is still not suitable for mass production, which is inevitably delayed because of the absence of a cost effective production process (Alting L 2003). This is the most critical aspect in micro manufacturing, since the machining times are usually longer than in conventional technologies, with a consequent reduction of the productivity.

The downscaling of the product dimensions, as well as the micro-technology development, has been investigated by several researchers, starting from an overview of the main machining technologies (Masuzawa 2000) and a description of the production of parts having at least two dimensions in the order of magnitude of the sub-millimetre range (Geiger 2001).

These studies were extended to several aspects of micro-manufacturing as, for example, the micro-assembly (Van Brussel 2000) and the micro-scale process for the realization of products by means of electroforming (MacGeogh J A 2001).

As a general remark, it is possible to affirm that all the works about micro-machining are characterised by a common issue emerging from the down scaling of the conventional machining processes (Alting L 2003).

In fact, the term micro-manufacturing refers to a wider set of aspects that include the design, the machining, the handling and in general all the activities related to the production of the components. It is not possible to consider micro manufacturing an only size-related process, as if it is only a simple downsizing of the dimensions of the components, since it involves numerous other aspects of the design and manufacturing process.

Moreover, for the realization of micro products it is necessary to use micro components that must be assembled in order to guarantee a certain level of functionality in final micro product: the integration of the components ensures a certain integration of functions, different functioning principles and intelligence into the products (for example, in sensors and actuators). The reduction of the dimensions of the components results in an inevitable complication of the overall handling process. It is thus desirable

that the same component carries out more than one function in order to fulfil different tasks in the product and minimise the operational effort.

According to the literature, micro-components can be classified into three main categories as reported below (Alting L 2003):

1. Two dimensional structures (2D), for example optical gratings;
2. Two and a half dimensional structures ($2^1/_2$D), like fluid sensors;
3. Three dimensional structures (3D), for example components for hearing aids.

As mentioned before, independently from the specific application of the single product, the components which are characterised by single or multiple functional elements in the order of magnitude of micron can be considered micro-components.

Since the micro products and components are characterised by these micro features another issue relates to the interface relationship existing between micro components and other macro scale components (Alting L 2003). All these aspects give a great contribution to the complexity of both design and manufacturing of final products.

From the technological point of view, the miniaturization of components enhances the difficulties related to their production with conventional technologies but at the same time it opens the possibility to employ new non-conventional promising technologies like micro-EDM and laser beam machining.

The micro-machining processes have been classified in categories by several researchers, one of the most comprehensive is reported in Table 1.

In recent years a new series of innovative materials has been developed. In particular, base materials with unique mechanical and thermal properties have been introduced in several fields, and thanks to their high wear resistance they are particularly useful, especially for the realization of tools and moulds. The most diffused innovative materials are for example tungsten carbide and its composites, titanium based alloys, nickel based alloys, tool steels, and other super alloys. But, even though these materials are characterised by excellent mechanical properties, a higher hardness and a lower heat and corrosion sensitivity, they are characterised by great difficulties of being machined with conventional technologies (Jahan, Rahman and Wong, 2011). And since these materials are not used only in sectors characterised by an advanced level of research (like the aerospace) but are currently employed for the realization of consumable goods, the relevance of the technologies able to machine these materials is growing.

Table 1: Technology overview for the manufacturing of micro products (Alting L 2003), (Masuzawa 2000).

Working Principle	**Material Interaction**			
	Subtractive	Mass Containing	Additive	Joining
Mechanical force	-cutting -grinding -blasting -ultasonic machining	-rolling -deep drawing -forging -punching		-ultrasound -cold pressure welding
Melting/ Vaporization (Thermal)	-EDM -LBM -EBM		-CVD -PVD	-welding -soldering -bonding
Ablation	-LBM			
Dissolution	-ECM -isotropic/ anisotropic etching -reactive ion etching			
Solidification		-casting -injection moulding		
Polymerisation/ Lamination			-stereolithography -photoforming -polymer deposition	-gluing
Sintering		-combination of mechanical and thermal principles		

Technologies able to machine these materials can open the applicability of "difficult to cut" materials on a wider scale, opening up opportunities in different fields of application.

Several key technologies able to machine the so called "difficult to cut" materials have been developed in the micro manufacturing field, one of the most promising is micro-EDM. Many challenges characterise the development of micro-EDM technology, especially its application to industrial scale production.

Between the technologies reported in Table 1, micro-EDM can be considered one of the most promising, thanks to its contact less nature that preserves the workpiece from any kind of residual stresses left on the workpiece surface.

The use of micro-EDM in an industrial context is continuously growing thanks to its own characteristics that can be summarised as follows:

- Possibility to machine hard and high strength materials (like titanium, all kind of steels and stainless steels, ceramic conductive materials) or materials hardened with thermic or chemical treatments (like tempered materials). As mentioned before, with this technology, the base material hardness is a secondary aspect as refers the machining speed and the machining energy;
- Possibility to machine the workpiece for the realization of any 3D feature: in this case it is possible to use both rotating tools (for the realization of 3D micro-EDM milling) and steady tools (in this case it is about plunge micro-EDM with a shaped tool, which corresponds to the negative shape of the feature to be realised). It is possible to obtain nearly sharp edges (unless the electrode radius), to create cavities and protrusions with shapes difficult to realize with conventional technologies.
- The machining speed is lower than other technologies, for example micro-laser or conventional technologies characterised by contact between the tool and the workpiece;
- The tool wear is in general considerable if compared with conventional technologies: this is due to the intrinsic characteristics of the technology, because the erosion mechanism, based on melting and vaporizing of the material, involves the tool electrode as well. Moreover, the wear phenomenon is

inevitable and it is hardly predictable because it depends on both the electrode material and the workpiece material.

- Surface final roughness: this phenomenon is strictly dependent on the process parameters used for the realization of the micro features and it is due to the micro-craters left on the surface by the electric sparks occurring between the tool and the workpiece.

Based on the previous consideration and on the common practice, the main micro-EDM machining techniques can be summarized as follows (Jahan, Rahman and Wong, A review on the conventional and micro-electro discharge machining of tungsten carbide 2011):

1. Micro-EDM drilling: micro-electrodes are kept in rotation during the machining process and are used to realize micro holes having different aspect ratios;
2. Micro-EDM milling: in this case, micro electrodes are used towards the workpiece and kept rotation in order to create 3D micro features;
3. Die-sinking micro-EDM: in this case, an electrode having a certain shape is used to create a mirrored feature on the workpiece material;
4. Micro-wire EDM: a wire is used to cut through a conductive workpiece in order to realize different shapes micro components;

Micro-drilling is one of the most diffused applications of micro-EDM: manufacturing of cylindrical features or nearly cylindrical cavities with diameter lower than 0.5 mm is a field of great interest both in research and in industrial application (Sanchez, et al. (2013)). In recent years, an active field of research has been focused on micro-drilling. In particular, the research has been focused on the definition and optimization of different manufacturing methods depending on the component diameter, aspect ratio, geometry and material (Masuzawa 2000).

A wide variety of components is characterized by small diameter cylindrical geometry. For example, holes of 0.3 - 0.4 mm diameter and large depths are typical features in aerospace components of Ni-based and Ti-based alloys.

The most diffused components characterized by micro-holes are gear shafts, valves, shafts and channels of micro-fluidic systems, parts for micro-pumps and turbines, mechanical and electrical contact probes, micro-ejector pins in injection moulds, micro-tools, or micro-structured rolls (Sanchez, et al. (2013)).

Micro-EDM is, as well as micro-laser, the most used manufacturing method for this type of precision micro features realized in difficult-to-machine materials. The optimization of this technology imposes to consider different aspects, especially the process parameters, electrode material and electrode set-up. As a matter of fact, especially the process parameters affect process performance, in terms of processing time, dimensional tolerances and electrode wear (Sanchez, et al. (2013)).
A lack of information regards the existence of a formal relationship between the "inputs" and "outputs" of the micro-EDM drilling process.

The aim of the present work is to deepen the knowledge in the field of micro-EDM drilling. In particular, the focus of the analysis refers to the relationship between the process parameters and the final output, expressed in terms of geometrical characteristics of the micro holes and process performances. The micro drilling process has been carried out with copper and tungsten carbide tubular electrodes on 316L stainless steel.

Since a real knowledge of the process parameters is not available, an acquisition system able to collect in real time the process parameters, namely peak current (I) and voltage (V), has been designed and implemented. Based on the peak current, voltage and energy data collected during the machining, the power exchanged during the process has been estimated and correlated to the geometrical characteristics of the micro-holes and to the process performances.
The following chapter describes in detail the historical background and the basic principle of the micro-EDM machining process. Special attention has been dedicated to the Sarix SX 200 machine and on the process parameters information.

Chapter 2

Historical background and basic principle of EDM

Electrical discharges represent nowadays a known phenomenon in nature, nevertheless it was described and studied by a considerable number of researchers since the XVIIIth century.

The first formal attempt to describe the EDM (Electro Discharge Machining) erosion phenomenon was made by Robert Boyle in the mid 1600s: he tried to create metal powder from a solid rod and described the effects of the material removal caused by the discharges (Schumacher B M 2013).

Later, in 1751, Benjamin Priestley recognized the presence of the so called "footprints" left by the discharges on both the electrodes (Schumacher B M 2013).

In 1881 Meritens introduced the use of spark discharges aimed at arc-welding with the contribution of material transfer and in 1917 Prof. Kohlschutter developed a system, at university of Bern, able to use the discharges for the metal pulverization and for implementation of colloidal chemistry. During the experiments the researcher found the presence of gas emissions, especially when machined with high electric tension.

Later, in 1930s the electrical discharges were used for the machining of diamond and steel (US-Pat. 20035) and in the same years a machine for the removal of burrs from valuable workpiece was introduced: the American company Elox (US-Pat. 1.556.325) developed the so called "Disintegrator" (Schumacher B M 2013).

But only during World War II electrical discharges became one of the earliest non-traditional machining technologies. The Russian physicist couple Natalya and Boris Lazarenko studied extensively the electrical erosion phenomenon (Lazarenko B R 1944): they were asked to find a solution to the considerable erosion of the electric power contacts and to find substitutes to precious materials used for that kind of connections and their idea was described in the well-known thesis published in 1943 titled "Inversion of the effect of wear on electric power contacts for machining purposes". In this publication is well described how applying an RC-circuit and

charging defined energies in the capacitor allowed a more stable machining process and the drawbacks of the negative electric contact were turned into a positive effect of the electrical machining to erode metals.

Originally, EDM was applied to a machine aimed at the stock removal (N. S. Ho K H 2004). Although the first applications of the technologies allowed a certain material removal, these two scientists faced the need of maintaining a certain distance between the tool and the workpiece, the so called "gap", able to guarantee a more stable process.

This was achieved by a servo-control that helped maintaining the gap between tool and workpiece. In late forties Lazarenko's assistant Solotych provided a description of the discharge ignition through the emission of cold electrons (Solotych 1952).

But only in the fifties EDM technology became a technology able to fulfil the needs of the market, and it became progressively a real "workshop technology".

In fact, the capability of using EDM without the drawbacks of arcing, made EDM more profitable and industrially more usable. Such an improvement represented the turning point of the development of EDM technology: from its initial status of simple machine used for the removal of the taps and drills, EDM became an actual industrial process through the introduction of RC (resistor and capacitance or relaxation) power supplies and vacuum tubes first, to solid state transistors, from hand fed electrodes to CNC controlled 6 axis machining (Jaham 2013).

In late fifties the EDM machining capabilities made this technology widespread in industry and at the same time researchers focused on several aspects of the technology in order to achieve two targets: first of all to deepen their knowledge of the technology and secondarily to answer the needs of the market, in a so called "market pull" and "science push" approach (Schumacher B M 2013).

The main aspects of the process that were scientifically investigated by the researchers are the physics principle of the material removal and the control of the gap during the machining. As a matter of fact, in the fifties the pioneers of EDM technology, were located in the so called socialist countries starting from Russia itself: for example, the ENIMS Research Institute of Moscow in cooperation with other institutes for machine-tool design developed machinery, tools and accessories for the technology; in the same

years a study on the different variants of electro-machining, with a special focus on EDM and its applications was published (Livshiz 1957).

The technological evolution of EDM continued in the sixties, led both by the Russians, that changed RC-circuits into RCL-circuits to increase the discharge rate and the machining efficiency, despite the higher instability of the system.

On the other side, the Americans as well focused on the circuit control and spark generation improvement, mainly led by Colt Industries (Schumacher B M 2013).
Especially USA and Great Britain had after the war the means to conduct massive research and innovation on technologies like micro-EDM.

In these years the main micro-EDM machine builders like Elox (USA), Sparcatron (GB) and AGIE with Charmilles (Suisse) developed new machines for the technology. The same research and industrial trend came from western Europe too: the CIRP (Collège International de Recherche de Production) committee found in the early 1950s and in 1960s started a scientific committee dedicated to electro-machining. From this starting point the eastern-Europe countries, that were originally leading the EDM technology development, were overcame by the western countries, and in the end Japan (Mitsubishi, Fanuc, Sodick and Seibu Denki) took their place as a new EDM developing country. The main reason for this trend is due to the spread of three fundamental technological developments of the sixties, namely the introduction of planar transistors, the integrated circuit technology (for the generation of static pulses) and the microprocessors, to develop numerical controls and programming methods (Schumacher B M 2013).

Wire-EDM machining was characterized by a similar developing path. The technology was known since 1940s, but only the introduction of stepping motors to control X and Y axes allowed the development of the technology in the modern form, although reasonable cutting speeds were achieved only after the seventies. In the same years, the introduction of the double X-Y slide made possible to realize electrodes characterized by a certain taper by means of an independent movement of the upper and lower wire guide.

As a general remark, it is possible to say that the evolution and the spread of wire EDM depended on the introduction of powerful generators, new wire electrodes, better flushing conditions and the employment of CNC machines (N. S. Ho K H 2004).
Thanks to all these improvements it has been possible to reduce the machining costs of the 30% and the wire speed by a factor of 20, to increase the discharge current by a factor of 10 and improve the surface finishing by a factor of 15 (Arbizu I D s.d.).

Although EDM found a widespread application range in the last seventy years, a different path of diffusion characterized micro-EDM process. In this case, the technology had a slow industrial acceptance until it became necessary for the realization of progressively miniaturized products. The first advent of EDM process on a micro-scale came in 1968 when Karafuji and Masuzawa executed the first micro-hole on a 50 μm thick carbide plate (Karafuji H 1968).

Despite the high level of innovation, this process gained a high industrial relevance only in recent years, when the need for progressively smaller products forced the identification and the development of novel technologies able to fulfil the market technological requirements.

In micro-EDM, like in macro scale EDM, the electrical discharges cause the material removal by means of melting and vaporizing. The controlled sparks occur between the tool and the workpiece separated by a small gap called “sparking gap” in the presence of a dielectric fluid. Micro-EDM process is similar to the macro scale one, except for the dimension of the tool used, the power supply of the discharge energy and the resolution of the axis (Jaham 2013). In particular, micro-EDM is characterized by high frequencies (>200 Hz) and small energies (10^{-6}-10^{-7} J) for every discharge for a surface roughness of about 0.1 μ (Jaham 2013).
But for the effective final development of the technology, in the form it is known nowadays, only the advent of software ensured the introduction of new functions like the electrode planetary movement as well as the possibility of the simultaneous movement of the axis. In the following section a brief description of the basic principle of EDM, and consequently micro-EDM, is reported.

2.1 Overview of the EDM and micro-EDM basic principle

As a matter of fact, the basic principle of micro-EDM and EDM is the same: the material is removed from the workpiece by means of controlled electrical discharges that leave craters and micro-craters on the workpiece surface. The erosion mechanism takes place in the presence of the dielectric fluid, deionized water or mineral oil (like kerosene) (Jaham 2013).

As mentioned before, in the micro-EDM process the sparks occur between a positively charged anode and a negatively charged cathode, similarly to the macro scale process. The machining starts with the application of an electric field between the two electrodes, the tool electrode and the workpiece that must be necessarily made of electrically conductive materials: at this point the cathode starts emitting electrons.

The voltage applied to the electrodes results in an electric field, also known as energy column, whose intensity increases as the distance between the electrodes decreases. The electrons start a series of collisions with neutral atoms that result in the release of others ions and electrons immediately attracted in areas characterized by the higher value of the electrical field.

The space between the electrodes is always filled with a dielectric that is deteriorated by the increasing electric field. The accumulation of ions and electrons enhances the formation of the so called “bridging effect” that helps reducing the gap between the electrodes.

The dielectric is now characterized by a lowered resistivity and for this reason the spark can take place between the two electrodes.

Once the spark has occurred, the voltage is reduced to zero and the spark can effectively vaporize the material (metal composing the tool, the workpiece as well as the dielectric between them). The spark is followed by the formation of bubbles of gases like hydrogen, carbon and various oxides.

The material composing the workpiece is melted and vaporized: the melted particles rapidly solidify thanks to the flushing dielectric, which in this technology fulfils the cleaning of the machining zone, as well. Nevertheless, some of the solidified particles

stay in the machining zone increasing the electrical resistivity of the area and because of this phenomenon the voltage rises, too.

The dielectric at this point can no longer sustain the current that drops between the electrodes, and for this reason the current must be dropped off: this pause represent the pulse interval, the so called t_{off}. During this pause, the source of heat is no longer present in the machining area and for this reason the vapour bubble in the working zone collapses, the fresh dielectric takes the place of the deteriorated one and the area is cooled. Once the new dielectric is repositioned, the process can take place again, the voltage is applied, the electric field restored and a new spark takes place (Takahata 2009). Figure 1, Figure 2 and Figure 3 illustrate the principle of EDM: in particular in Figure 1 is reported the pre-discharge phase, in Figure 2 the discharge phase and in Figure 3 the post-discharge phase. The erosion mechanism can be divided into three main phases: the preparation for ignition, the discharge phase and the interval between the discharges (Jaham 2013).

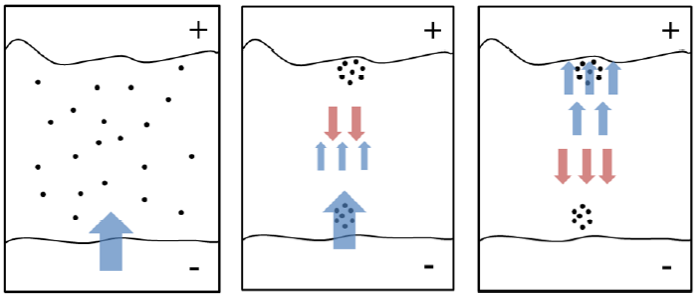

Figure 1: Pre-discharge phase in EDM process (Deshmukh 2013)

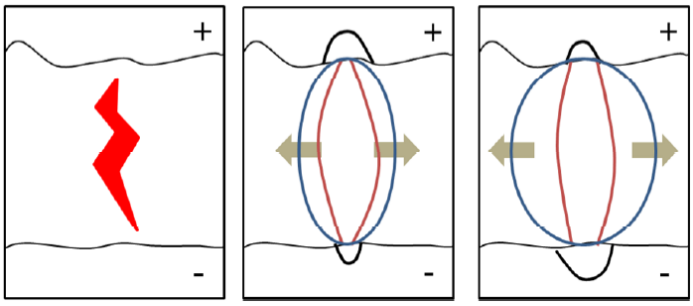

Figure 2: Discharge phase in EDM process (Deshmukh 2013)

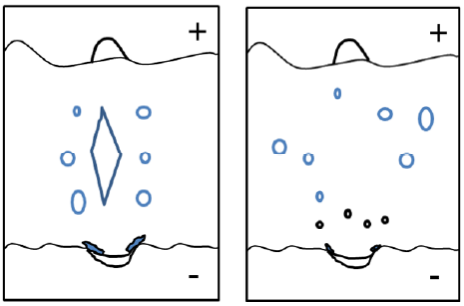

Figure 3: Post-discharge phase in EDM process (Deshmukh 2013)

The material removal involves the tool as well: the electrical discharges cause the melting, vaporising and, for this reason, the removal of the material from the tool, which is inevitably damaged. With a proper study and setting of the process parameters it is possible to enhance the workpiece material removal and minimize the tool material removal.

The sparks formation is governed by the setting of several process parameters namely peak current, voltage, frequency and energy of the discharges, just to mention the most relevant having an influence on the workpiece material removal.

In order to ensure the right position of the electrode a servo-system is employed: it operates moving the electrode towards the workpiece, it restores the proper gap if a short circuit occurs and in general it moves the electrode of the proper feed rate during the machining. In parallel, the pulse generator provides with the discharge energy.

2.2 EDM and Micro-EDM: main differences

Although micro-EDM and EDM share the same machining principle based on electrical spark discharges, substantial differences characterise the micro scale process if compared to the conventional one.

The main differences rely on the size of the tool electrode and subsequently the technologies necessary to realise the electrodes: smaller electrodes can be characterised by a lowered heat conductivity and the small mass that characterises the tool ignition and burning of the electrode or wire breakage during the machining that can be avoided imposing appropriate wire traction force (Innovaciòn s.d.).

Secondarily, the micro scale process is characterised by lower discharge energies that must be limited in order to control the unit removal rate per spark (UR) and result in smaller discharge craters if compared with those in EDM erosion process (Uhlmann E 2005).

Moreover, in micro-EDM the erosion phenomenon is sensibly higher than in conventional EDM because of the electrode softening (Jaham 2013). A recent study investigated the different behaviour of micro-EDM and EDM for the energy density point of view. In particular, it was demonstrated that the power density, defined as the ratio between the energy amount absorbed by the workpiece and the area of the plasma channel, is a good indicator of the machining efficiency (Zahiruddin M 2012).

In EDM, even under the same energy conditions, it is possible to observe different performances between high peak current discharges characterised by a short duration and low peak current discharges with a longer discharge duration (Kunieda M 2005). It was possible to conclude that, although the principle of micro-EDM and EDM is the same, substantial differences characterise their machining conditions, especially in terms of efficiency which is greatly affected by the power density. In micro-EDM the absolute value of the power is lower than the one recorded in conventional EDM.

In Table 2 a comparison between micro-EDM and EDM parameters is shown. The discharge duration in micro-EDM is significantly shorter than in conventional EDM; for this reason the plasma is limited in its expanding and this phenomenon results in a higher value of the power density, which is about 30 times compared with the conventional EDM process.

For the same reasons the energy consumption for the material removal in micro-EDM is higher because of the higher level of the power density, on the contrary the energy dissipated because of the heat conduction in micro-EDM is considerably lower than in conventional EDM.

Finally, in micro-EDM the higher power density also results in higher removal efficiency: in macro-EDM more material is melted and re-solidifies in the machining area, which inevitably results in more energy lost and higher consumption.

Table 2: Comparison between micro-EDM and EDM parameters (Zahiruddin M 2012).

Parameters	Micro-EDM	Conventional EDM
Discharge current [A]	1.14	10.36
Discharge voltage [V]	24	17.19
Discharge duration [10^{-6} s]	0.07	17
Crater diameter [μm]	4.25	68.4
Removal volume per pulse [μm^3]	1.90	972.5
Energy distribution in workpiece [%]	10.37	34
Energy lost for heat conduction [%]	6.02	30
Energy absorbed by debris [%]	4.35	1
Plasma diameter [μm]	13.7	342.24

Together with the energy, the dielectric flushing is a distinctive aspect of the micro scale process. In micro-EDM due to the small gap between workpiece and tool and because of the reduced dimensions of the features, the debris flushing is consequently more difficult if compared with the macro scale process (Katz Z 2005).

The most important difference between the two processes is due to the dimensions of the plasma channel radius during the spark that is considerably smaller than the macro scale electrode diameter. Finally, another important distinctive aspect is the accuracy of the axis repositioning that, in micro-EDM, is in the order of magnitude of the micron.

2.3 Why micro-EDM?

Micro-EDM is characterised by a series of important advantages that make this technology one of the more appealing in micro-machining, especially for its flexibility. Some of the most important distinctive features are summarised as follows:

- Micro-EDM is able to machine any conductive material, regardless of the hardness and high strength. This technology in fact, is contact less and for this reason the electrodes are always separated by a certain gap. This distinctive property gives a great potential to micro-EDM that is able to machine hard metals normally used for the fabrication of tools otherwise hardly workable with conventional technologies.
- No residual stress and no force exchange characterise micro-EDM. The gap between the tool and the workpiece helps avoiding any residual stress on the workpiece during the machining and for this reason it helps in preserving the integrity of the workpiece. Moreover, in micro-EDM the workpiece can be extremely small and the absence of contact between the electrodes can help maintaining the reciprocate position of the electrodes.
- Micro-EDM allows the realization of high aspect ratios holes with the help of ceramic guides that prevent possible electrode bending during the drilling process

Based on the previously described characteristics, it is possible to highlight the following advantages that make micro-EDM suitable for the majority of the complex 3D micro machining.

Micro-EDM is more flexible than lithographic technologies and for this reason it is suitable for small batch production. Moreover, it requires low set up costs if compared with lithographic techniques and it can easily machine 3D complex shapes (it is more flexible than etching for example).

Finally, micro-EDM does not need masks for the realization of 3D shapes so it can be considered faster especially for the setup point of view (Reynaerts D 1997).
In order to make micro-EDM a real industrial process it is necessary to increase the material removal rate and to reduce the machining time, one of the main drawbacks of the technology.

Some other points of possible improvement are the possibility of increasing the automation in micro-EDM machining with the introduction of CAM approach to the machining.

2.4 Micro-EDM system main components

Micro-EDM machines are composed by several systems that perform different tasks during the machining.

The most important systems are the pulse generator, servo control, for the determination of the correct position of the electrode in respect to the workpiece, the dielectric flushing and the filtering system for the correct flushing of the machining zone and the filtering of the dielectric in order to remove the solid debris of the machining, and the central control unit, that manages all the functions of the systems and all the interfaces between the operator and the machine itself.

In the following sections all the system composing the micro-EDM machine will be described in detail.

2.4.1 Pulse generator

The basic principle of micro-EDM removal is the use of electrical discharges aimed at material removal by means of melting and vaporising of the material composing the workpiece.

In micro-EDM, differently from EDM, the realization of components having dimensions in the order of magnitude of tens or hundreds of microns, requires the minimization of the energy per pulse especially in case of the finishing process, which is executed with certain process parameters combination aimed at the best finishing (and for this reason particularly not “aggressive”).

The choice of the pulse generator then, depends on this particular necessity and the difference between EDM and micro-EDM regards this aspect, too. In macro scale EDM in fact, the peak current and the tension reach higher levels and the melting of the tool with the workpiece is frequent. The most critical component from the finishing and feature dimensions point of view is the DC power supply.

The different discharge generators can be classified in several different types (Mahendran S 2010):

1. Rotary impulse generator: the sinusoidal waveform of the voltage is generated by the DC motor principle;

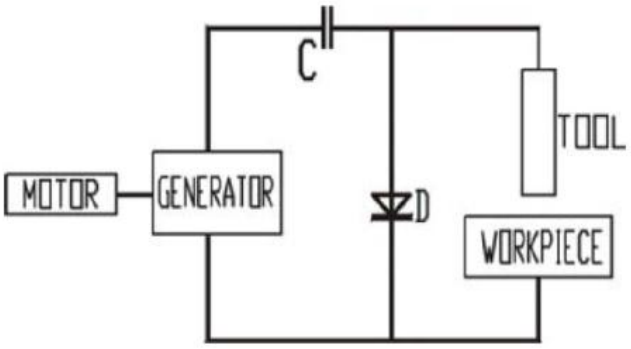

Figure 4: Rotary impulse generator (Mahendran S 2010)

2. Relaxation generator: the basic principle consists in the charging and discharging of the capacitor connected with the power supply in order to generate a voltage saw tooth wave. During the spark creation, the capacitor is allowed to charge and then discharge when put in contact with the piece. The discharge pulse duration is dominated by the capacitance of the capacitor and for this reason the frequency of discharge depends on charging times. This particular type of circuit results in extremely low removal rates: the low machining frequency is due to the time needed by the capacitor to charge after each discharge. Moreover, the electrical charge is not uniform and this results in non-uniform discharge energies (Jaham 2013). These draw backs can be overcome by the employment of transistor-type generators, which functionalities are described as follows.

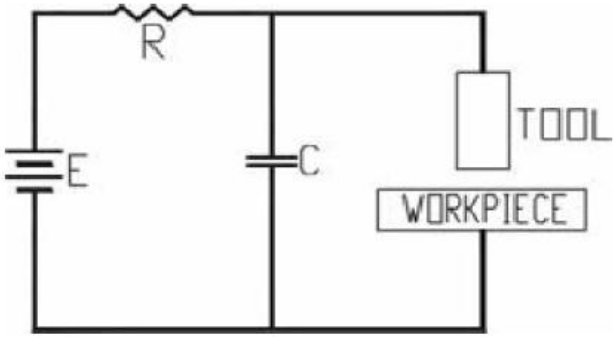

Figure 5: Relaxation generator (Mahendran S 2010)

3. Transistor-type pulse generator: in this case a series of resistances and transistors are connected in parallel to the power supply. The current intensity for this reason is a function of the number of transistors switched on in the circuit. In particular, in this case and differently from the other cases, the voltage is switched between zero and the set voltage with a rectangular wave. It is possible to increase the efficiency of the production, if compared with relaxation type generator. The dramatic improvement made by the introduction of this type of generator is mainly due to the absence of any condenser, for this reason there is no need to wait for the condenser charge before the occurrence of the discharge. Moreover, it is possible to change the duration and the peak current depending on the required machining performance (Jaham 2013).

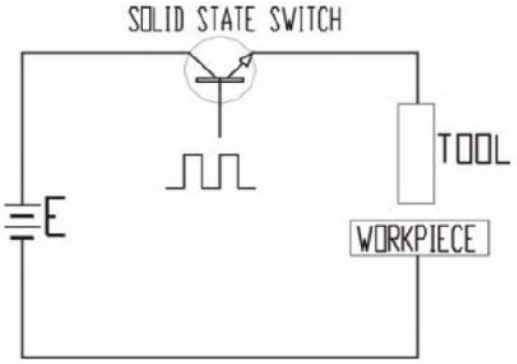

Figure 6: Relaxation generator (Mahendran S 2010)

2.4.2 Servo control systems

In micro-EDM, the control of the gap between the tool and the electrode is a strategic aspect of the process because it is demonstrated that the gap between the tool electrode and the workpiece is directly responsible of the surface finishing and of the accuracy of the machined features.

For this reason, in order to implement a repeatable machining system it is important to develop an accurate and stable gap control system (L. G. Rajurkar K P 2006), (Zhang L 2012).

In micro-EDM machining the gap is usually in the order of magnitude of tens or hundreds of microns, which is notably lower than the usual gap in macro scale EDM machining. For this reason, in micro-EDM the servo control system must accomplish a more accurate control of the digital signal.

In general, the servo control can be operated based on different algorithms that try to predict the gap distance, the tool position, the delay time and the gap voltage, just to mention the most important. A larger gap causes a delayed discharge and a higher value of the average gap voltage; on the contrary smaller gaps result in smaller delays of the ignition and a gap voltage smaller than the required servo reference voltage.

For this reason, the electrode is retracted and thanks to this the voltage can increase allowing the discharge to happen in the right boundary conditions. This system is very useful, especially to avoid short circuits due to potential debris in the machining area (W. W. Rajurkar K P 1991).

2.4.3 Dielectric circulation systems

The dielectric circulation system is one of the most important parts of the micro-EDM machining systems because it allows not only the proper adduction of the dielectric in the machining area during the erosion but also the filtering of the dielectric and the monitoring of its temperature. This last aspect is one of the most important because of the inflammable nature of the majority of the dielectric fluids (kerosene is the most used).

The dielectric circulation system is composed by the following parts:

- Dielectric fluid (generally kerosene or deionized water) and it is provided to machining area by means of dedicated nozzles;
- Dielectric container;
- Low pressure pump;
- High pressure dielectric pump;
- Filtering system.

This last component helps keeping the dielectric clean: during the machining some solidified metal particles (coming from the workpiece and from the tool, too). As a general remark, it is possible to affirm that the dielectric supply system carries out several tasks: first of all it ensures the continuous distribution of the dielectric in the machining area in order to remove solidified debris from the machining area. Moreover, it helps the contribution of always fresh dielectric to the machining area, the maintenance of the dielectric fluid temperature below the ignition point and helps reducing the electrode and workpiece temperature, as well (Jaham 2013). In the following section the process parameters will be described in details.

2.5 Micro-EDM process parameters

Since the working principle of EDM and micro-EDM is mostly the same, it is possible to state that the process parameters governing EDM and micro-EDM process are the same, even though they assume significantly different values, as explained before. The principal process parameters are described in detail in the following sections.

2.5.1 Discharge voltage

The gap voltage (measured in volts) applied between the tool and the workpiece determines the total energy exchanged between the two electrodes, for this reason higher values of the voltage result in higher removal rates but at the same time in poorer surface finishing (Jaham 2013).

This parameter is one of the most important as regards the occurring of the spark discharge: the spark in fact, can find a “path” between the electrodes and the dielectric only when the voltage has reached a certain minimum value. When the discharge finds the proper “ionization path” the current can flow and the gap voltage drops to a lower level and stabilizes at the working gap level.

Increasing the voltage value corresponds to an increased value of the gap condition that allows a better flushing of the machining zone and a more stable erosion process (Kumar S 2009).

2.5.2 Peak Current

Together with the spark voltage, the peak current (measured in amperes) is another parameter which is representative of the erosive capability of the sparks. During the machining, and especially during the t_{on} duration, the peak current reaches the target value.

High values of the current, as for the voltage, result in a higher volume removed from the workpiece and worse surface finishing.

Usually, the only parameter that is settable on the micro-EDM machines (for example Sarix machines) is the peak current, in other words the maximum value of the current reached during the machining.

It is noteworthy that, setting the peak current to a high value results in an improved material removal rate (MRR) but inevitably results in a higher tool wear phenomenon.

2.5.3 T_{on} (pulse on time)

The cycle of the machining process, in both EDM and micro-EDM, is composed of two main durations: the time made available to the spark to occur (t_{on}) and the time needed to re-establish the boundary conditions necessary for the spark to happen (t_{off}), in other words, the time needed to set the voltage and set the electric field in the machining area.

In the first phase, corresponding to the t_{on}, the effective material removal can take place. It is demonstrated that the volume removed from the workpiece is directly function of the amount of energy transferred between the electrodes, and for this reason it is a direct function of the peak current and the time duration of the spark (Mahendran S 2010).

As for the peak current, it is known that the MRR is directly proportional to the pulse duration. The surface finishing is itself directly proportional to the ton duration: the higher the t_{on} the worse the surface finishing, for the same reasons explained for the peak current.

2.5.4 T_{off} (pulse off time)

The pulse off time is the time between two following sparks, in other words the time when the pulse generator is turned off.

From a different point of view, the t_{off} is the time needed by the system to re-ionize the dielectric and to prepare the conditions to the spark to occur again. This pause time allows the ablated particles to solidify and to be removed from the machining area.

The shorter the pulse off time the higher the number of the discharges occurring between the tool and the electrode. It is an important parameter, especially for the control of the short circuit: if the pulse off time is too low, short circuit can occur.

Although a reduced pulse off time makes the process slower, it allows at the same time a better control and stability of the machining (Jaham 2013). Both these two durations are expressed in microseconds.

2.5.5 Polarity

In micro-EDM machining the polarity can be set to positive or negative value and the two different settings are representative of two different erosion strategies.

As mentioned before, the plasma channel is made of ions and electrons. These particles are characterised by a smaller mass if compared to atoms composing both the workpiece and tool material. Because of the electric field between the electrodes, when the polarity is set to negative mode, these particles are led between the electrodes in order to erode the anode predominantly.

In this case the erosion involves the workpiece preferentially. The changing in the polarity results in a higher erosion of the tool, which is preferable in case of tool electrode machining. Finally, a recent trend consists in a periodic changing of the polarity, the so called “swing pulse” aimed at reducing the negative effects of short circuiting during the machining (N. S. Ho K H 2003).

2.5.6 Machining gap

Another important process parameter in micro-EDM machining is the sparking gap. This parameter is representative of the distance between the tool and the workpiece during the machining and it is responsible of the surface finishing of the machined features. For this reason, the reduction and the monitoring of the sparking gap are important factors especially from the surface finishing point of view.

It is known from the literature that decreasing the distance between the electrodes enhances the probability of the spark occurrence and for this reason it is important to maintain the gap to a constant value during the machining, in order to control the erosion aggressiveness. A constant gap is not representative of the real machining process, which is characterised by a variation of the gap during the machining because of the debris formation between the electrodes.

For this reason, micro-EDM machines are characterised by a monitoring system that periodically measures and eventually corrects the gap value, in a feedback control approach.

The process parameters that are measured and controlled in order to change the gap are the voltage and the delay. The tension parameter has been described before and the delay is a percentage parameter (with values between 1 and 100) that is directly measured by the generator.

This parameter is calculated as the ratio between two characteristic durations in micro-EDM machining:

- The t_{on}, in other words the time that the generator gives to the spark to occur
- The difference between the time required by the spark to occur and the time available (t_{on})

This indicator gives information about the real distance between the tool and the electrode. For example, if the electrode is in contact with the workpiece, the delay will be equal to zero, because when the electrodes are in contact the machine detects a short circuit and the discharge cannot occur; on the contrary, if the tool is too far from the workpiece (in other words, it is at a distance higher than the minimum required) the

spark cannot occur and the numerator is identical to the denominator and the ratio is equal to 100% (Pham D T 2004).

2.5.7 Other process parameters

Other important process parameters are the machining frequency (usually expressed in kHz) which is a direct function of the discharge duration, and finally the regulation that is a code identifying a particular algorithm of short circuits suppression and the gain. This last parameter has a direct influence on the speed of the process because it influences the gain of the feedback control system: low values of the parameter can lead to a slow machining process, on the contrary a high value of the indicator can result in a very instable machining process.

2.5.8 Dielectric fluid

The dielectric fluid has a relevant role in micro-EDM machining. It allows the occurring of spark discharges under certain conditions, besides it helps keeping the machining area clean, removing the solid debris from the machining zone thanks to the dielectric flushing.

Several types of dielectric fluids have been studied and their properties were described in detail (Kibria G 2010). In particular, the influence of the dielectric fluid on the machining performance (MRR, material removal rate and TWR, tool wear ratio) was investigated. Traditionally, the most used dielectric fluids in micro-EDM are mineral oil (kerosene) and deionized water.

Kerosene, which is used as dielectric fluid in the conventional EDM machines too, is characterised by a certain degradation of its properties during the machining; moreover, it produces harmful vapours (like CO and CH_4) that result from the erosion process, which make the machining environment harmful and toxic (Zhang Q H 2006).

On the contrary, deionized water ensures a safer machining environment, a faster cooling of the machining area and a better tool wear ratio but at the same time worse geometrical characteristics of the machined holes (L 1981). It is common knowledge

that the debris in the machining area are unwanted effects of the erosion process mechanism. In this case in fact, the discharges that involve the debris cause a certain tool wear that doesn't result in an effective erosion of the workpiece itself. The discharges in fact can be defined inefficient. In parallel with this common assumption, some researchers have investigated possible positive effect of the debris in the machining area. According with this assumption in fact, the debris help the discharge ignition process improving the overall erosion conditions (Luo 1997).

The absence of debris in the machining area on the contrary can result in unwanted arcing that has a bad influence on the precision of the feeding mechanism. On the other hand, a high amount of debris in the machining zone can result in short-circuiting, ineffective machining mechanism and uneven surface of the workpiece.

Other studies demonstrated that a certain amount of debris in the machining are is always wanted because it ensures a good discharge transitivity and breakdown strength, besides a good deionization and gap size (Jeswani 1981).

Based on these considerations and in order to investigate the influence of the debris on the machining phenomenon, some researchers have used powder-mixed dielectrics in micro-EDM machining of micro-holes. In these studies the role of the debris particles is investigated by mixing powders with certain characteristics like the particles size, the density and other physical characteristics of the powder. Some experimentations have been carried out using Al, SiC powder-mixed kerosene in different concentrations for the machining of titanium alloys. The authors investigated different polarity settings too, for the machining of titanium alloys with the same powder-mixed dielectric (Y. B. Chow H M 2000) (Y. L. Chow H M 2008).

Other works studied different mixes of powder and dielectric as for example Al, Cr, Cu, graphite, silicon and silicon carbide mixed in different dielectrics (Kansal H K 2007). Finally, an exhaustive comparative study on pure kerosene, pure deionized water, B_4C mixed kerosene and B_4C mixed deionized water was carried out (Kibria G 2010). It was demonstrated that different dielectrics have a different influence on the final result expressed as material removal rate, tool wear rate, overcut and micro-hole accuracy.

Recently, other studies have investigated the possibility to use gases as dielectric fluids. In micro-EDM machining the most commonly used dielectrics are liquids characterised

by different dielectric permittivity (like deionized water and mineral oil). As a matter of fact, the use of these dielectrics, especially mineral oil, requires proper air filtering and a correct dismissal of the used dielectric. The spread of an environment friendly approach for a more conscious manufacturing enhanced the study of micro-EDM technology in different dielectric conditions. In particular, it was underlined the possibility to conduct EDM and micro-EDM tests with different dielectrics, the so called "dry" conditions. It was demonstrated that in dry micro-EDM on magnesium, compressed air is preferable to O_2: it ensures better surface quality and higher MRR, the same geometrical characteristics and slightly worse tool wear performance. From the comparison between oil and dry micro-EDM (with air), a similar influence of the electrode geometry is recorded. Oil ensures a higher material removal rate if compared with air thanks to its larger inertia and higher viscosity: this increases the bubble expansion force and material removal per discharge and air demonstrated to produce the best surface characteristics (D'Urso, et al. 2015).

2.5.9 Electrodes

In micro-EDM several different electrodes materials can be employed: copper, tungsten carbide, brass and graphite are the most used. It possible to classify the electrode geometry as follows:

- Tubular electrode: brass, copper, tungsten carbide, having diameter bigger than 0.12 mm
- Coreless electrode: copper and brass with external diameter bugger than 0.5 mm
- Cylindrical electrode: brass, copper, tungsten carbide and graphite

(a) (b) (c)

Figure 7: electrode geometry, tubular (a), coreless (b) and cylindrical (c)

In general, the coreless electrode is employed for the execution of blind holes, on the contrary the tubular one is used for the through holes. The cylindrical electrode is

suggested for the execution of holes but only with low thicknesses of the workpiece material (SA 2012). The correct choice of the electrode material is fundamental for the execution of the machining. Many aspects need to be taken into account, for example the electrode material, the removal rate, the wear resistance, the surface finishing the machinability and the cost of the material.

As a general remark, it is possible to assert that different electrode materials can ensure different process performances, which strongly depend on the "wear resistance" characteristics of the material composing the electrode. Graphite electrodes have been demonstrated to have good performance for the wear resistance (N. S. Ho K H 2003).

Some researchers investigated the influence the electrode can have on the final result (like the process performances and, in case of drilling machining, on the geometrical characteristics of the micro holes) in terms physical and chemical properties.

2.6 Micro-EDM Drilling

Micro-EDM technology can be successfully used to drill micro holes in a wide range of materials, on the only condition that the workpiece is made of an electro-conductive material: this is the only necessary condition to allow the electrons flow between the electrodes and the material to be removed by melting and vaporizing.

Since micro-EDM is a micro machining process the main problems in micro machining refer to the clamping and the centring of the electrodes. Although several sizes of electrode clamping system are available, sometimes it can be necessary to further reduce the diameter of the electrodes. In these cases, the majority of the micro-EDM machines are equipped with a wire-EDM dressing unit that allows the machining of the micro-electrodes that are directly clamped in the spindle, avoiding possible electrode re-centring problems (Lim H S 2003).

Several papers refer to experimental researches carried out to investigate micro-EDM drilling process. In micro-EDM, in fact, there are many factors affecting the process performance; these factors can be related either to the process parameters (such as voltage, peak current, pulse duration, spark gap and flushing conditions) or to the

system (such as type of dielectric fluid, tool properties, chemical and physical material properties). The main aspects here considered are summarized in the following sections.

2.6.1 Electrode characteristics (diameter, material and geometry)

As regards the electrode, both geometry and material have an influence on MRR and electrode wear. In (Yilmaz e Okka 2010) it has been demonstrated that the optimum electro discharge drilling parameters can only be obtained with properly selected electrode geometries and material. Moreover, experimental results revealed that the single-channel electrode provides better material removal rates and lower electrode wear ratios than multi-channel tubular electrode. However multi-channel electrodes produce better surfaces and lower hardness values than single-channel electrodes (Yilmaz e Okka 2010). In micro-EDM drilling the tool wear can be considered a more serious problem than for conventional drilling. Therefore, many researches have dealt with the optimization of the micro-drilling process by adequate experiments (Denkena, et al. 2006). Compensation methods of the electrode wear, in order to achieve the required accuracy of the machined holes, have been investigated by several researchers: in (Pham, et al. 2007) a simple model for volumetric wear ratio estimation in micro-EDM drilling was proposed and in (Lim, et al. 2007) the authors developed an "on-the-machine" measuring device to inspect dimensions and wear of the fabricated tool electrodes. A useful method to improve the reduction of the wear phenomenon in micro-drilling process is the planetary movement of the electrode, which provides extra space for debris removal. In this way, the material removal rate increases and the electrode wear can be reduced (Yu, Rajurkar and Shen, High aspect ratio and complex shaped blind micro holes by micro EDM 2002). Moreover, also the performance parameters are greatly influenced by the thermal and electrical properties of the workpiece material. In (Pham, et al. 2007) it was demonstrated that also the workpiece material microstructure have a relevant influence on the final tool wear, for both tubular and cylindrical electrodes. In fact, workpiece materials having small grain size result in a better removal of the debris from the working zone and in a lower number of secondary discharges which bring to a lower electrode wear

In (D'Urso G. 2014) three different electrode materials (copper, brass and tungsten carbide) and two different electrode geometries (cylindrical and tubular) were investigated. It was demonstrated that the electrode material shows a relevant influence on the final value of the TWR (Tool Wear Ratio) indicator. In particular, it was demonstrated that the tungsten carbide electrode can be considered the best in terms of tool wear; on the contrary, the brass electrode shows the worst performance and wear resistance. Moreover, a possible relation existing between the tool wear behaviour and the characteristics of the material composing the tool itself and the workpiece material, was investigated. Figure 8 reports an example of the relationship found between the electrode material characteristics and the electrode wear. As regards the relation existing between workpiece material characteristics and tool wear, it was demonstrated that the relation between the two is well described by a logarithmic tendency, as reported in Figure 9.

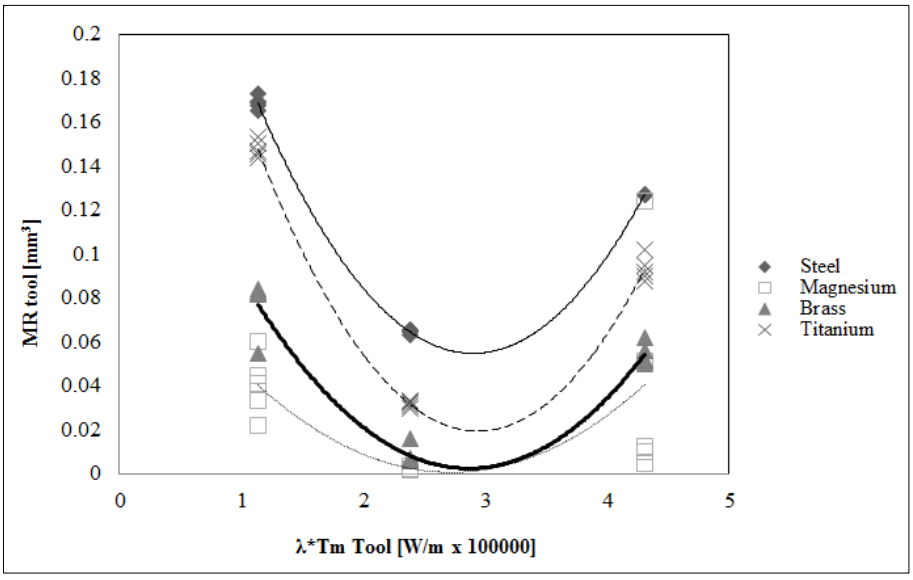

Figure 8: Material removed from the tool as a function of the tool wear resistance

As a general remark, since micro-EDM is an electric spark based technology, the physical and thermal characteristics of the electrode material must be considered relevant. (D'Urso, Maccarini, et al., The influence of electrode shape and material on micro-EDM drilling process 2012) investigated the effects of several types of electrodes (different materials and shapes) in drilling micro-holes using micro-EDM technology on the most industrial used materials such as stainless steel, titanium and brass. As regards

the geometrical characteristics of the electrode, in (D'Urso, Maccarini and Merla, 2013) the authors studied the micro-EDM drilling process of metal plates.

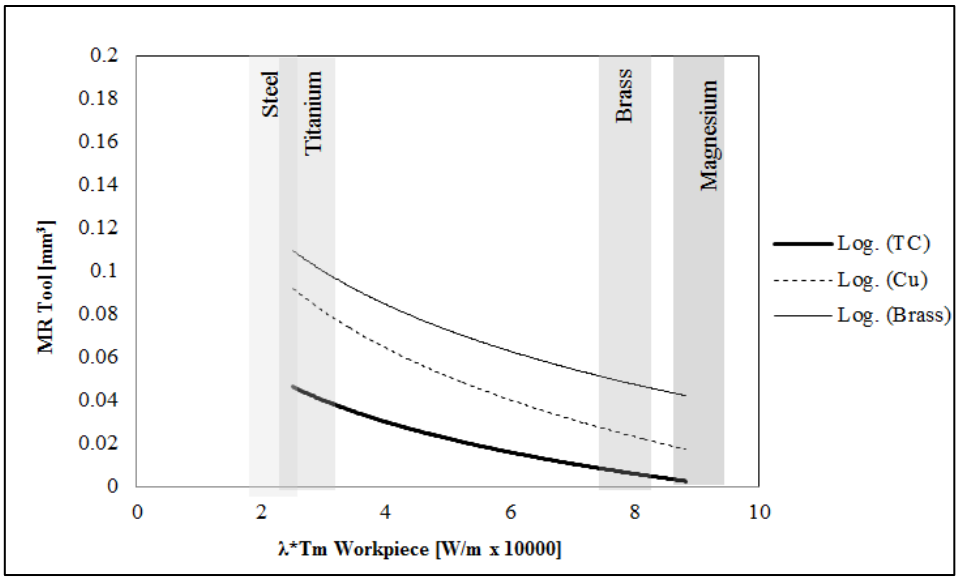

Figure 9: Material removed from the tool as a function of the workpiece material wear resistance

In particular, the aim of the work was to investigate the effects of the "downsizing" of the micro holes diameter on the drilling performances. The influence of the reduction of the diameters in terms of both process performances (e.g., tool wear, taper rate, diametrical overcut) and general quality of the holes was investigated. Steel plates having thickness equal to 0.8 mm were taken into account. The drilling process was carried out using carbide electrodes having diameter equal to 300, 200, 100 and 50 μm. Since the standard electrodes adopted in this study had a diameter equal to 300 μm, a wire EDM unit was used to obtain the other electrodes. The relationship between the process parameters considered the most significant and the final output, was studied. Furthermore, the geometrical and dimensional properties of the micro-holes were analysed using both optical and scanning electron microscopes. In particular, it is demonstrated that the diameter size has a significant influence on the final value of the diametrical overcut while peak current and frequency parameters have a negligible effect.

Finally, the realization of high aspect micro holes was studied as well. Since micro-EDM is able to guarantee the latest market requirements both in terms of miniaturization capabilities and quality of the features obtained, it was possible to fabricate several types of features such as, small 3D milled features or HAR (High Aspect Ratio) micro holes. One of the main concerns in micro machining, and most of all in HAR micro holes machining, is the geometrical and dimensional qualification of the drilled features. Since inner HAR micro holes can be considered an almost inaccessible environment, in some cases it is important to carry out a non-destructive investigation procedure, in order to preserve the quality and the integrity of the micro holes obtained. In (D'Urso, Merla and Maccarini, EDM drilling of high aspect ratio micro holes 2013) the authors investigated the micro-EDM machining of HAR micro holes (both through and blind holes) with different aspect ratios. Moreover, a preliminary non-destructive geometrical characterization of the holes was carried out. The experimental campaign was executed using a specific ceramic guide system for the deep hole drilling process. The emphasis of the study was on the evaluation of both the process performances and the dimensional properties of the holes depending on both the hole aspect ratio and the process parameters. This study confirmed the micro-EDM capabilities in deep drilling; in particular, holes having AR equal to 100 were obtained. The drilling time under the worst working conditions was longer than two hours with relevant tool wear. Certain deviations from the ideal hole profile, like tapered and barrelled holes, were observed. (Yilmaz e Okka 2010)

2.6.2 Dielectric flushing conditions

A relevant aspect having an influence on the process performance refers to the flushing conditions. It was demonstrated that the introduction of vibration (characterized by high frequency and constant amplitude) at the workpiece surface can ensure a considerable reduction of the machining time of micro-EDM (Garn, Schubert and Zeidler 2011). As already mentioned, in (D'Urso, et al. 2015) a comparison between the kerosene dielectric and the unconventional oxygen and compressed air was carried out. Moreover, in (Kibria G 2010) different dielectric fluids for micro-hole machining of Ti-6Al-4V were taken into account. In this case the machining performance (expressed in

terms of MRR, tool wear rate, overcut, diameter variance at entry and exit, machining surface integrity and accuracy) are greatly influenced by the nature of the dielectric used.

2.6.3 Workpiece material

In (Jahan, Wong and Rahman, A comparative experimental investigation of deep-hole micro-EDM drilling capability for cemented carbide (WC-Co) against austenitic stainless steel (SUS 304) 2010) it was pointed out that the thermal properties of the workpiece material have a significant influence on the quality and accuracy of micro-EDM holes. Micro electro discharge drilling of a titanium super alloy was investigated in (Pradhan, et al. 2009) and in (D'Urso, Longo, et al. 2011) in order to optimize the process parameters. The most significant process parameters and the optimal combination level of machining parameters were found, showing a common result for titanium workpiece. In (Kuppan, Rajadurai and Narayanan 2008) small deep hole drilling of Inconel 718, using EDM technology with a pure electrolytic copper electrode, was carried out varying peak current, pulse on time, duty factor and electrode speed. The results revealed that MRR is more influenced by peak current, duty factor and electrode rotation, whereas depth average surface roughness is strongly influenced by peak current and pulse on time. Using a desirability function approach, the parameters were optimized for the maximum MRR with a specified surface roughness. In (D'Urso G. 2014) the influence of workpiece material properties, electrodes properties and process parameters on the final output (expressed in terms of geometrical characteristics of the micro holes and process performance) when realizing micro holes on different workpiece materials with micro-EDM technology was investigated. In particular, different combinations of workpiece materials, electrode materials and electrode geometries were tested. The electrode material showed a relevant influence on the final value of the TWR indicator, in particular, the tungsten carbide electrode can be considered the best from this point of view. The process parameters and the workpiece material properties have an influence on the final value of the TWR too, although the effect of the workpiece material is extensively relevant if compared with the peak current/voltage level. As relates to the electrode wear, the minimum value is recorded

for the tungsten carbide electrode, for all the workpiece materials. Regarding the relation existing between workpiece material characteristics and tool wear, it was demonstrated that the relation between the two is well described by a logarithmic equation tendency.

Both the electrode geometry and the physical properties of the material show a relevant effect on the DOC and as regards the TR, only the electrode geometry seems to have an influence. The workpiece material properties (especially in terms of melting point), as well as the electrode material and geometry, demonstrated to have a relevant effect on the surface finishing. In general, the tubular electrode and workpiece materials with high melting points ensure a better surface finishing.

Other studies investigated the micro-EDM drilling process of magnesium, a particularly relevant material for medical applications. Medical devices require an excellent surface integrity of the produced parts to reduce friction or to increase cell adhesion for optimal fitting, mechanical stability and biocompatibility to reduce the risk of inflammatory reactions. Magnesium is a promising material to be used for biodegradable orthopaedic implants. These implants are only temporary; in fact the corrosive environment of the human body absorbs the implant. Due to the natural regenerative capacities of the human body, new natural bone tissue grows into the space occupied by the implant. In this way, a second surgery for the removal of temporary implant can be avoided (Klocke, et al. 2011). In (Klocke, et al. 2011) surface roughness of magnesium alloy obtained using Wire EDM was investigated while in (Ponappa, et al. 2010) the effect of some process parameters on drilled-hole quality of microwave-sintered magnesium nano composites are evaluated.

Magnesium alloys are very difficult to machine with conventional process especially for complex 3D shapes. These limits are overcome by Electrical Discharge Machining (EDM) technologies where the material is removed by a series of rapid electric spark discharges between the cutting tool (electrode) and the workpiece. In (D'Urso, Maccarini, et al., Micro-EDM machining of small features on magnesium plates 2012) the effects of process parameters in drilling micro holes on magnesium plates were investigated. Magnesium plates having a thickness equal to 1 mm were used as well as carbide electrodes having a diameter equal to 0.3 mm. The Design Of Experiment

(DOE) was used for planning the experimental campaign and ANOVA techniques were applied to study the relationship between process parameters and final output. In particular, the process parameters considered the most significant were investigated as a function of material removal rate and wear rate. Geometrical and dimensional properties of the micro-features were also investigated using both optical and SEM microscopes.

As a matter of fact, no significant information about the real process parameters involved during the process was recorded so far. Consequently, all the investigations carried out were focused on the nominal values of the parameters, without a real knowledge of the sparks characteristics. Moreover, no real formalization of the relationship existing between the expected hole diameter and geometrical characteristics is available. The same can be said for the forecast of the machining duration. The following section describes in detail the experimental set up for the signal recording and for the automatic drilling procedure. In the following chapters the analysis of the results and possible regression equations for the forecasting of the machining duration, the hole geometrical characteristics and the electrode wear are given.

Chapter 3

Experimental campaign

The present chapter is about the acquisition system set up and the drilling experimental procedure, describing in detail the preliminary tests, the machine setting and the automatic drilling procedure. After having taken into account the machine builder's suggested parameters and the common practice, the experimental campaign has been designed with a DOE approach. Once the final process parameters have been selected, the automatic drilling procedure has been implemented.

3.1 Micro-EDM machine

The experimental campaign was carried out with a Sarix SX 200 micro-EDM machine and with tubular tungsten carbide (TC) and copper (Cu) electrodes. Figure 10 represents the overall equipment, with particular focus on the units composing the machine.

The most important units of the machine are the generator, which is responsible for the spark formation, the spindle, where the electrode is positioned and held during the machining, the wire EDM unit, able to cut and dress electrodes, and the controller.

The machine allows the execution of both micro drilling and micro milling on all conductive materials, regardless of the hardness or high strength of the workpiece, thanks to the "contact-less" nature of this technology.

The machine is equipped with a wire micro-EDM unit, which is helpful for the electrode cut and dressing. In wire micro-EDM electrode dressing the usual negative polarity of the machining is always inverted: by doing this, the electrode plays the role of the workpiece and the wire acts like a real tool while machining the electrode. In Figure 11 it is possible to notice the wire, made of brass and having a diameter equal to 200 micron.

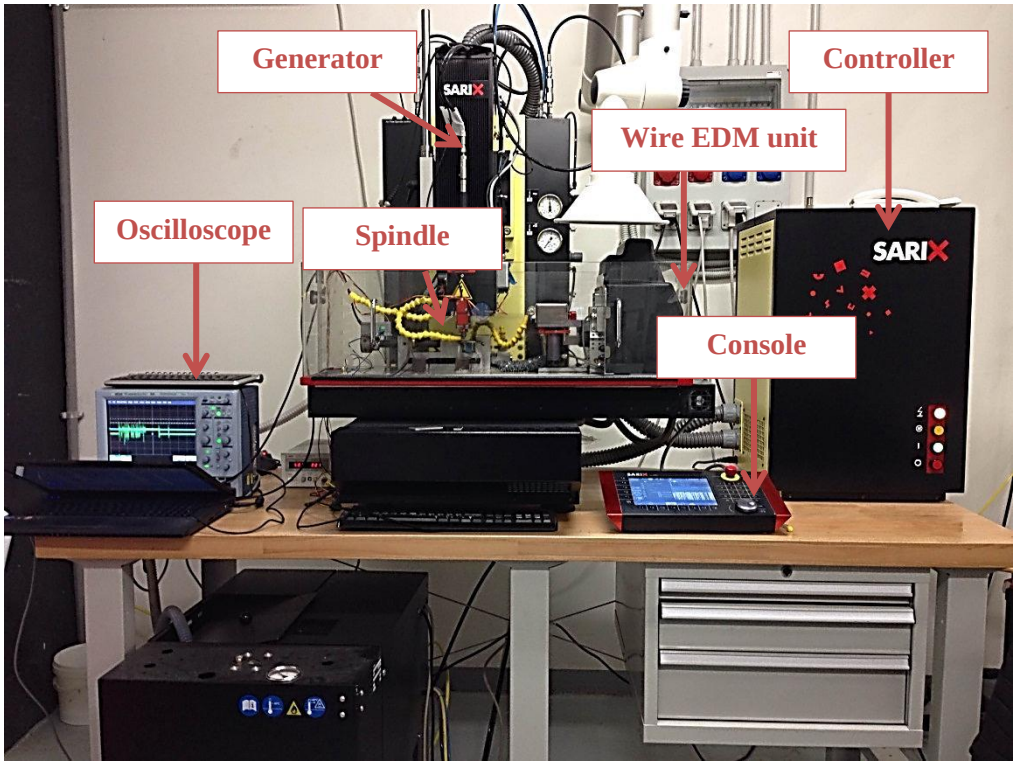

Figure 10: Sarix SX 200 micro-EDM machine

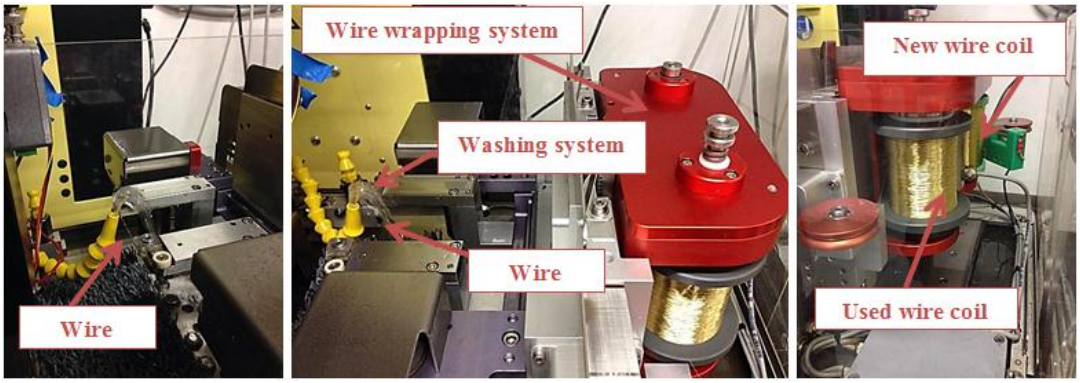

(a) (b) (c)

Figure 11: Wire micro-EDM machine "Arianne" (b), detail of the wire cutting system (a) and of the wire winding system (c)

With the so called "Arianne" wire unit it is possible to cut the electrode after the execution of every micro hole in order to restore the geometrical characteristics of the electrode. In the micro-EDM process, the electrode is affected by an inevitable wear due to the spark discharges occurring between the electrode and the workpiece. The final shape of the electrode is consequently tapered.

Besides the simple electrode cut, with the wire micro-EDM unit it is possible to dress the electrodes in order to reduce the initial standard diameter, in other words to carry out the so called "micro-electrodes". Alternatively, it is possible to shape the cylindrical electrodes into different geometries (namely, triangular, rectangular, conical and spherical), reported in Figure 12.

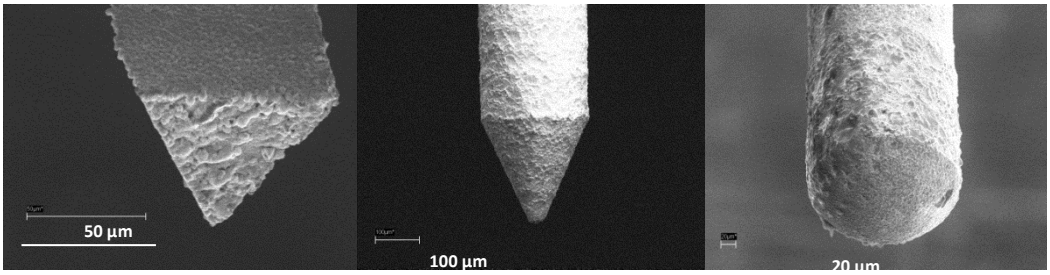

(a) (b) (c)

Figure 12: Wire micro-EDM unit shaped electrodes obtained from a cylindrical TC electrode having diameter equal to 300 micron, triangular (a), conical (b) and hemi-spherical (c).

The electrode wear is function of the electrode material, of the workpiece material and of the process parameters. Since this phenomenon cannot be avoided, it is necessary to control it and to limit it, by means of a proper choice of the process parameters.

The choice of the process parameters is thus fundamental for the limitation of the tool wear. At the same time, the identification of a correct match between tool and workpiece material is able to guarantee a minimization of the tool wear.
In both cases, before starting the machining process, it is necessary to set a referential point on the workpiece, which is also used during the machining for the electrode wear measurement. Since the machine functioning is based on a closed electric circuit, it is possible to detect every short circuit during the machining.
The short circuit corresponds to the physical touch between the electrode and the workpiece, which prevents any discharge to occur.

In order to carry out the machining in fact, it is necessary to keep a certain distance between the electrode and the workpiece, when the electrode and the tool are in contact a short circuit is detected. The capability of the machine to detect short circuits is used to measure the electrode wear: a referential touch is executed before and after the

machining and the corresponding z quote difference corresponds exactly to the electrode consumption.

Figure 13 reports a picture of the detail of the spindle. It is possible to notice the electrode and the holding system, which is dedicated for each diameter. Moreover, with a regulation screw it is possible to set the closure strength of the spindle, which directly affects the holding pressure on the electrode.

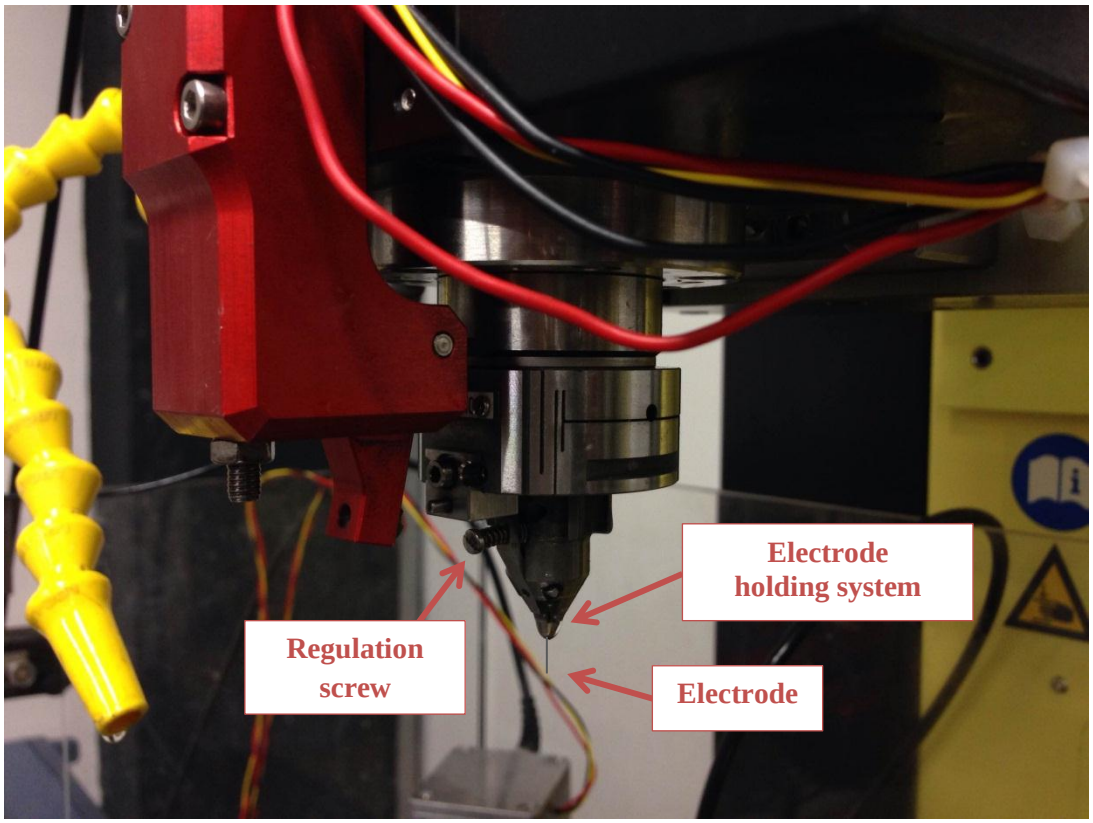

Figure 13: Micro-EDM spindle system

Since the clamping system is dedicated for each diameter and the experimental campaign is executed with two different diameters, two different electrode clamping systems have been used, respectively for the 300 and 150 micron electrodes. The main components of the chuck head system (Figure 14) are reported below:

- Rectified clamps: they have dimensions directly dependant on the electrode diameter. For the present experimental campaign the 300-340 micron was used for the 300 micron electrode and the 150-190 micron for the 150 micron;

- Electrode guide: it has the same diameter as the electrode and it helps keeping the electrode in place between the two clamps;

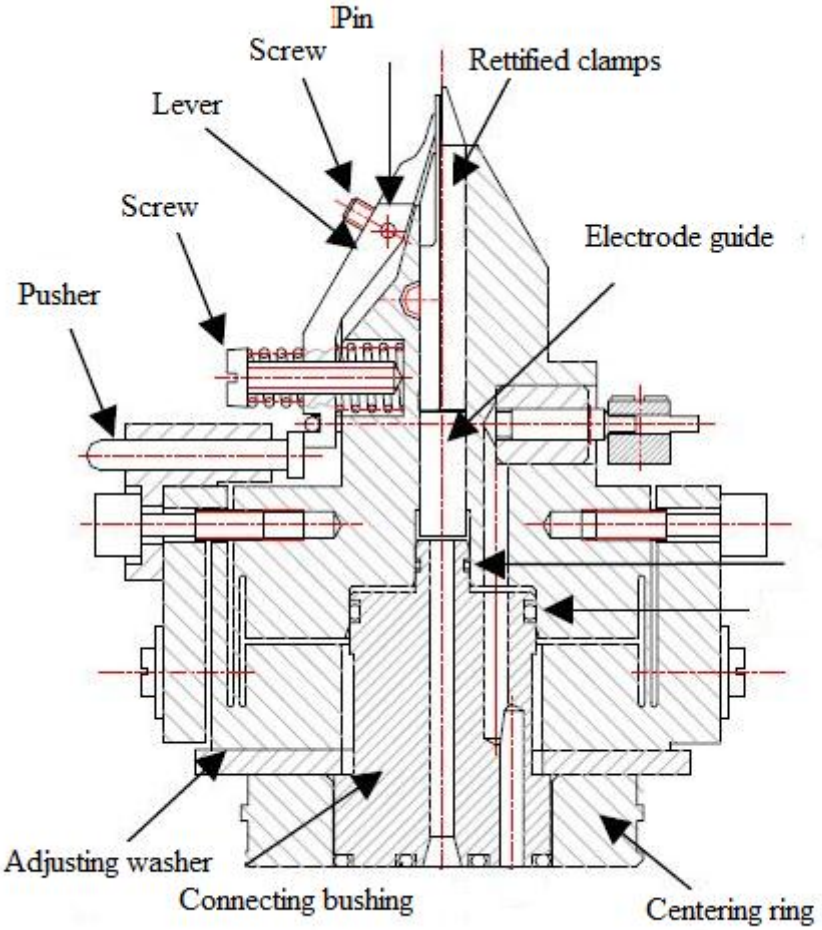

Figure 14: Chuck head system

In order to use one electrode, it is necessary to set the clamping system with the proper holding system, for this reason it is necessary to remove the rectified clamps and the electrode guide, to substitute these components with the correct diameters ones and to execute the electrode-centring procedure, which results to have a great influence on the geometrical characteristics of the holes.

Without any centring procedure in fact the electrodes is affected by an uncontrolled run-out from the electrode axis, which directly affects the micro-holes geometry. The centring procedure is executed using a microscope dedicated to the purpose. The microscope is mounted on the x-y axis and it is able to magnify the electrode clamping

system area allowing the estimation and regulation of the electrode position referred to the z axis. In Figure 15 the microscope experimental set up is reported, and Figure 16 describes the basics of the centring procedure.

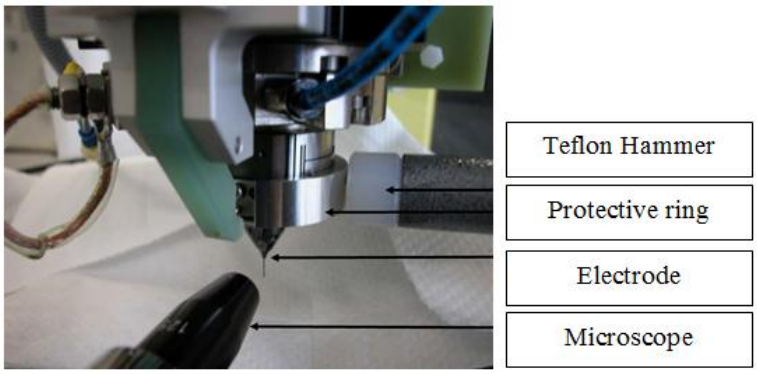

Figure 15: Centring procedure set up

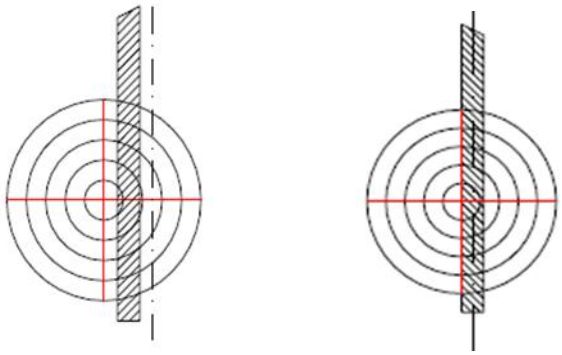

Figure 16: Electrode centring principle

The execution of the centring procedure is very helpful for the estimation of the electrode run-out and for its minimization with the use of proper screws on the clamping system itself.

Finally, for the execution of the smaller diameters, especially 150 micron electrodes, it was necessary to employ some deep drilling ceramic guide. For this kind of machining in fact, it was necessary to have a longer portion of the electrode out of the clamping system. The electrode length combined with the small electrode diameter and the dielectric flushing can have a negative influence on the final holes diameters.

The ceramic guide instead, minimizes these effects, in order to carry out a more reliable and fast drilling procedure. Figure 17 represents the ceramic guide support for deep

drilling procedures and Figure 18 represents the ceramic guide during the drilling procedure.

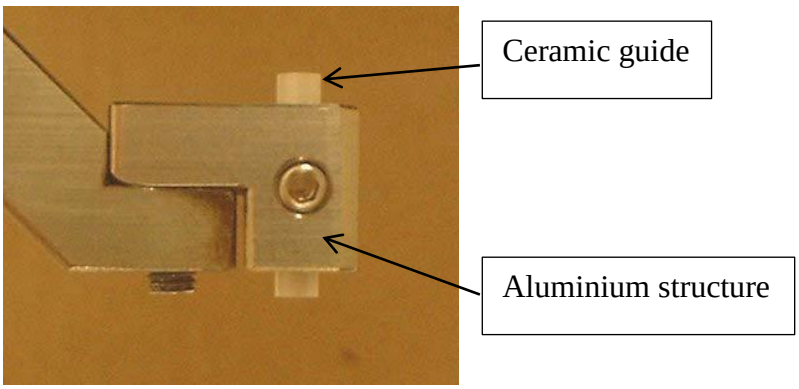

Figure 17: Ceramic guide mounted in the aluminium support for the deep drilling procedure

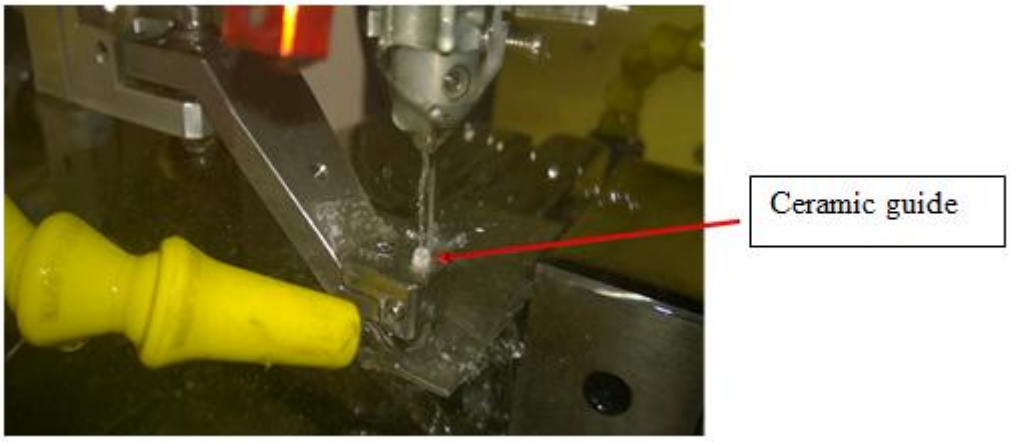

Figure 18: Ceramic guide with electrode during EDM micro drilling

The centring procedure for the ceramic guide is very similar to the procedure implemented for the clamping system.

Also in this case it is necessary to use a microscope in order to align the ceramic guide and the electrode (in other words, align the ceramic guide with the clamping system). In this case, the microscope reported in Figure 19, is used to regulate the ceramic guide position by means of two regulating screws on the aluminium structure of the ceramic guide system. The screws help positioning the ceramic guide from the initial out of axes position to the final correct position, as reported in Figure 19.

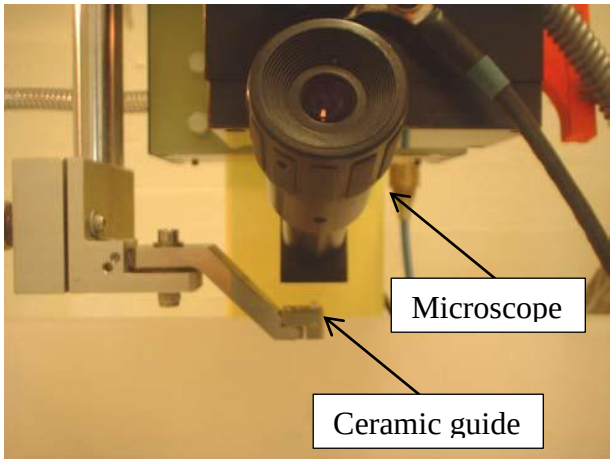

Figure 19: Microscope for the ceramic guide alignment

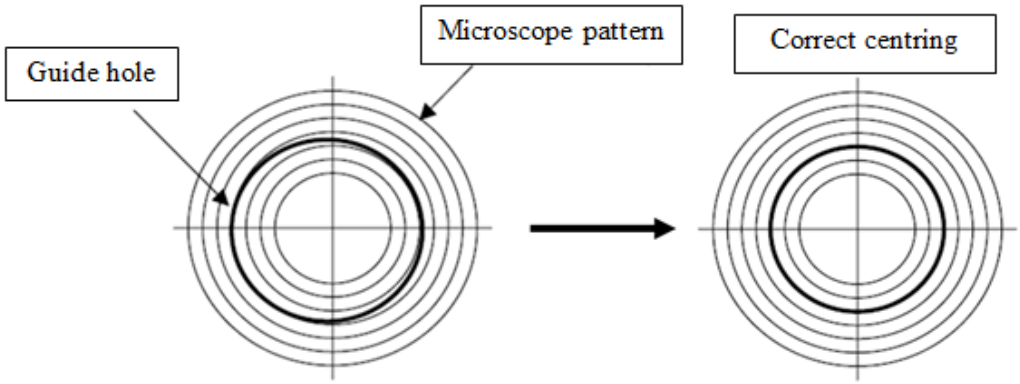

Figure 20: Ceramic guide alignment microscope detail

3.2 Process parameters

The Sarix SX 200 machine can be used both manually and automatically, by means of the Icon Editor program that allows the creation of an automatic drilling program.

The machine builder provides a general guide about the mutual influence of the process parameters. Table 3 reports the general relationship between the parameters. The meaning of the symbols is reported below:

- ↑ directly proportional;
- ↓ inversely proportional;
- ↗ directly proportional (influence of other process parameters)
- ↘ inversely proportional (influence of other process parameters)
- ≈ constant;
- - no effect.

The selection of the process parameters can be defined as "diameter dependent": this means that, since the electrode diameter is progressively reduced (300 and 150 micron) during the campaign, the choice of the process parameters must be adapted to the different geometrical condition of the electrode. For example, for smaller diameters the energy level and the intensity of the current are lower, in order to maximize the material removal and minimize the electrode wear.

Based on these suggestions, the first process parameter that was chosen was the energy, that has a great influence on I and V. Secondly the tension and last the peak current, I. It is important to underline that the energy parameter is not representative of a real physical entity, but it is just representative of the wave shape of the discharges. The same happens for the peak current, which is not expressed in ampere. The tension instead is expressed in volts.

Once selected the energy levels for each diameter and material, some preliminary tests have been carried out in order to identify the final process parameters. The preliminary tests were based on the machine builder suggested parameters. These parameters were selected taking into account the electrode material, geometry and diameter, the workpiece material and the required surface finishing.

Table 3: Mutual effect of the process parameters

Parameter	Diameter	Conicity	Roughness	Electrode wear	Time
Frequency ↑	≈	-	-	-	↓
Pulse width ↑	≈	-	-	-	↘
Gap ↑	≈	≈	-	↗	↘
Gain ↑	-	≈	-	↗	↘
Peak Voltage (V) ↑	↗	↑	↑	↑	↑
Energy ↑	↗	≈	↑	↗	↓
Time ↑	-	-	-	≈	↗
Polarity	≈	≈	-	↑	↑

In Table 4 are reported the energy parameters for each electrode diameter and material.

Table 4: Energy parameter per electrode diameter and material

Diameter [mm]	Material [-]	Energy level [-]
0.3	TC	365
		206
0.15	Cu	365
		206

Before the execution of the proper experimental campaign, extensive preliminary tests were carried out in order to find the optimal process parameters' set. For every process parameter a certain range was taken into account and all the collected results have been compared. In this phase of the experimental activity, the selection of the process parameters was aimed at the minimization of the tool wear and the machining time. Moreover, the selection of the final process parameters have been based on the "quality"

of the machining graph, representing the plotting of the voltage in real time during the process. A quality evaluation of the machining can be based on the number of short circuits occurring during the machining, as reported in Figure 21.

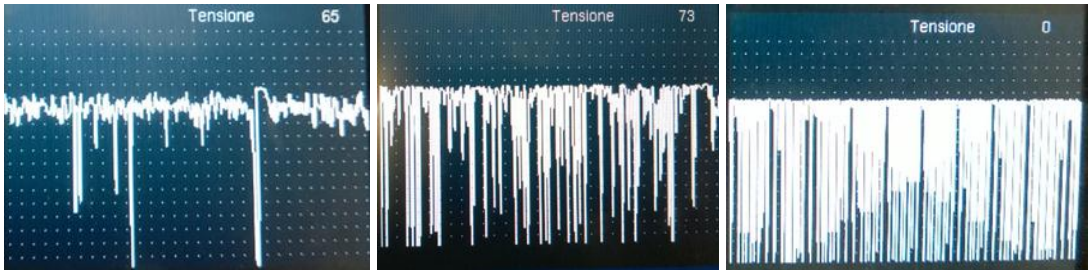

(a) (b) (c)

Figure 21: Real-time machining quality evaluation

It is possible to notice that the quality of the graph strongly depends on the number of short circuits occurring during the machining.

In Figure 21 (a), the number of short circuit in the time unit is limited, in this case the machining is very effective and the sparks occurring between the tool and workpiece are aimed at the melting and vaporizing of the material of the workpiece and not to the debris still present in the machining area. In Figure 21 (b) the number of short circuits is higher, the machining is not as efficient as before and the machining time as well results to be higher. Finally, an example of the worst machining condition is reported in Figure 21 (c). If the preliminary tests were characterized by this conditions, the preliminary test was executed a second time, and only if in this case the result was the same the process parameter have been varied within the range identified. On the contrary, if the preliminary tests were characterized by a graph as reported in (a) and (b) and at the same time the machining time was considered “acceptable” (based on the common practice and on the machine builder suggestions), the process parameters combination was selected for the final experimental campaign.

For the execution of the final experimental campaign, a full factorial DOE approach was adopted: two process parameters (namely, peak current - I and voltage - V) were varied on three levels, codified as “low”, “medium” and “high” and they were dedicated for each electrode and parameters combination. Five repetitions for every experimental conditions were executed. For the 300 and 150 micron electrode diameters, a total

amount of 45 holes was carried out for each energy level. In total, 360 through micro holes were carried out.

The selected parameters correspond to the following machining characteristics:

- Energy (wave shape): the energy selection corresponds to two different shapes of the pulses. Different levels of the energy parameters correspond to different pulse characteristics that in this case correspond to long pulses (E 365) and long retarded pulses (E 206);
- Frequency and T_{on}: they regulate the number of sparks occurring during the process, and in some ways the process material removal attitude. For high values of frequency the possibility to have sparks increases. The same cannot be said for the time duration T_{on} which, because of the machine algorithms, regulates the time available for the spark to occur, but not the real spark duration.
- Gain and Gap: they regulate the reactivity of the process; in this case, the low values for the parameters ensure a very reactive process;
- Peak Current (I): this value is known to have a direct influence on the erosion mechanism, but is anyway dependent on the energy level and on the electrode diameter. In this case, with long pulses, it has a great influence on the energetic content of the sparks;
- Voltage (V): for long pulses it is known to have the same influence of the peak current, so the selected values are expected to have an influence on the energy content.

As mentioned before, only some of the process parameters are expressed as physical quantity. A brief resume is reported in Table 5. Table 6 and Table 7 report the fixed and varied process parameters for every electrode diameter and for every energy level. For each electrode diameter, two different energy levels were investigated.

As a matter of fact, for each electrode a certain set of energy levels is available. This means that some limitations still exist about the choice of the energy levels for each electrode diameters. For example, with the 300 micron electrode all the energy levels are available: it is possible to machine with an energy level starting from 13, the minimum available, to 365 which ensures the fastest machining but at the same time the worse surface finishing. On the contrary, with small diameters (100 μm or lower) only the lower energy levels are usable (13, 100).

Table 5: Process parameters and their typology

Parameter	Unity of measurement	Non-dimensional
Energy	-	•
Frequency	kHz	
T_{on}	µs	
Gap	-	•
Gain	-	•
Peak Current (I)	-	•
Tension (V)	V	
Regulation	-	•
Polarity	-	•

Nevertheless, only certain energy levels are able to ensure the best results in term of trade-off between machining time and electrode erosion, namely between 365 and 200 for 300 and 150 micron electrode diameters.

Table 6: Fixed process parameters

Mat.	Diam [µm]	En [-]	Freq [kHz]	T_{on} [µs]	Gap [-]	Gain [-]	Reg. [-]	Pol. [-]
TC/Cu	300	206	120	5	60	100	03_01	-
		365	120	5	60/75	100	03_01	-
TC/Cu	150	206	120	5	60	100	03_01	-
		365	120	5	60	100	03_01	-

Table 7: Varied process parameters

Mat.	Diameter [µm]	Energy level [-]	I [-]			V [-]		
TC/Cu	300	206	10	35	50	80	110	140
		365	40	60	80	80	100	120
TC/Cu	150	206	15	30	50	80	110	140
		365	20	40	60	70	95	110

3.3 Acquisition of electrical spark data during micro-EDM processes

When considering the various input and output parameters of micro-EDM in the context of the Sarix SX200 machine, a problem concerning the energy and current machine parameters arises. Those parameters aren't given or in other cases they are expressed as "index levels". Those levels are in fact without any measurement unit and they only give an indication of the magnitude of the energy and current parameters. Moreover, the correlation between these levels and the real dimensional values is not verified. Considering those facts, it is possible to conclude that the existing degree of uncertainty related to those parameters makes them unreliable if they were to be used in various regression methods.

In order to overcome this limitation, the acquisition and processing of actual electrical data was decided. The collected data will then be used in place of the nominal current and energy values set on the machine.

3.3.1 Overview

Before going into the details of each element comprising the data acquisition and processing chain, a global description is given in Figure 22. The function of data

acquisition in itself is performed with a Teledyne LeCroy Wavesurfer oscilloscope. The input of the oscilloscope is the electric signal between both electrodes that has been pre-processed through the use of two electrical boxes that effectively act as active probes. The automation of the acquisition process is done with the use of Matlab software on a personal computer connected to the oscilloscope via a local Ethernet network. A timer in a Matlab script will fetch the data from the oscilloscope at regular intervals of time and save the data as Matlab figures files.

The analysis of the electrical graphs is also made with the use of a specially designed Matlab script that will iterate over all the data figures and compute values such as energy per spark, peak current, peak voltage and number of sparks per second.

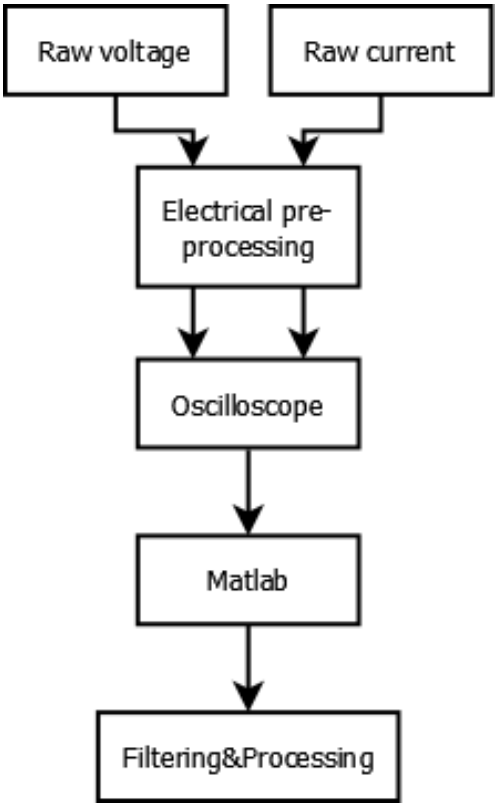

Figure 22: Overview of the data acquisition process.

3.3.2 The electric signal pre-processing

Two electrical circuits are used in order to pre-process the voltage and current signals. Those circuits are shown in Figure 23. The frequencies being dealt with in the case of

micro-EDM discharges are quite high as a single discharge's duration can be less than a microsecond. The input of an oscilloscope is usually set with a very high impedance of usually 1 MΩ in parallel with a small but known capacitance. However, for high frequencies, it is advised to use the 50 Ω setting and ensure that the source signal has an equivalent output impedance of 50 Ω as well as for the coaxial cable (the line). Impedance matching for the source, line and load will minimize reflections that are bound to modify the measured signal.

The use of the 50 Ω input impedance on the oscilloscope requires the input signals to have a low voltage. Using a low impedance will cause an overload for anything more than a few volts, therefore the signal has to be scaled down. The topmost circuit is the one used to process the voltage while the bottom one processes the current as a current.

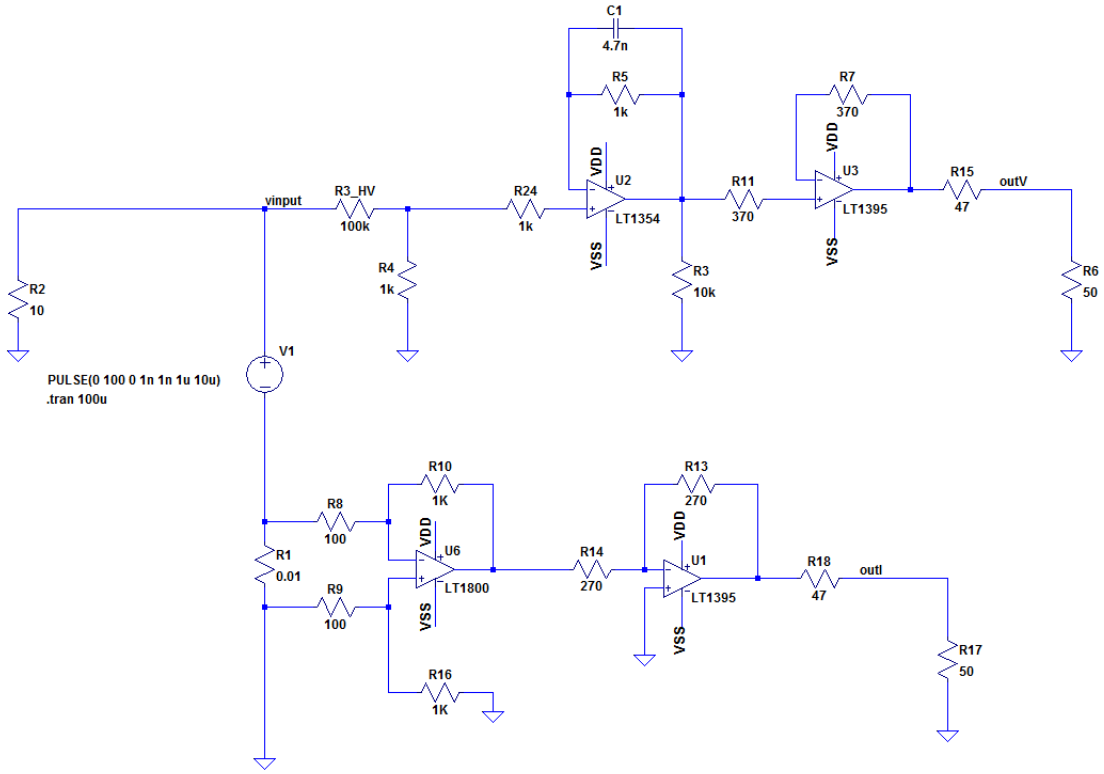

Figure 23: Detail of the electrical circuits used to pre-process the current and voltage signals

The first section of the voltage stage is a resistive voltage divider. The coefficient between the input voltage and output voltage in this passive linear circuit is:

$$K_{v1} = \frac{R_4}{R_2 + R_4} = 0.0099 \approx 0.01$$

The second to last section of the voltage stage is a unity gain amplifier whose purpose is to isolate the influence of the oscilloscope from the measured signal. It prevents the measuring circuitry from loading the first circuit in an unacceptable manner.

The last part of the voltage stage is another voltage divider with the following coefficient:

$$K_{v2} = \frac{R_6}{R_{15} + R_6} = 0.51$$

As a result, the output voltage, V_{out} follows the following relationship with the measured voltage, V:

$$V_{out} = V.K_v$$

With $K_v = K_{v1}.K_{v2} = 0.005$

Note that this last stage also provides with the termination impedance of 50 Ω and insures impedance matching.

The current stage comprises a current sense amplifier that will convert the current at the terminals of V1 into a voltage through the use of a sense resistor (R1: 0.01 Ω) giving a gain of 0.1 $V.A^{-1}$. Similarly to the voltage stage, the current stage then possesses a voltage buffer amplifier. In this case, the voltage is also inverted (essentially the voltage gain is -1). Finally, the impedance matching is ensured by a voltage converter with a gain of 0.51. The relationship between the output voltage for the current and the measured current I is:

$$V_{iout} = I.K_i$$

Where K_i = 0.05 $V.A^{-1}$. In that manner, both signals have the same order of magnitude. All the operational amplifiers are supplied with +/- 5VDC. Figure 24 and Figure 25 show the simulation of the voltage and the current probe circuit.

As regards the voltage, the input (in blue) is a square signal of amplitude 100 V, time on of 1 µs and a period of 10µs. For the current, the input current is in red, the output voltage in green.

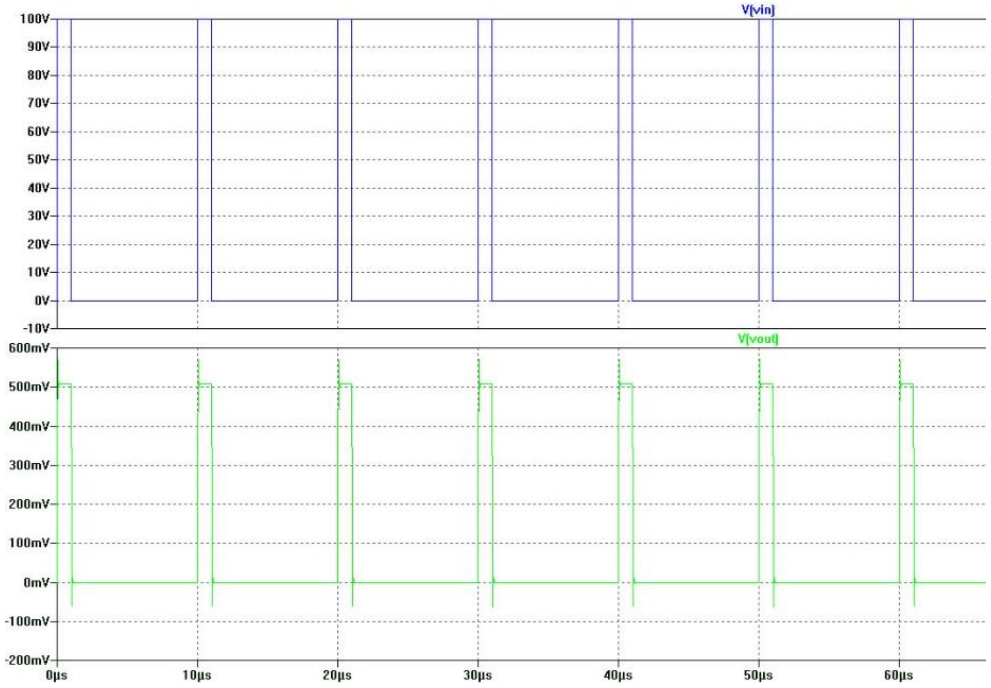

Figure 24: Simulation of the voltage probe circuit

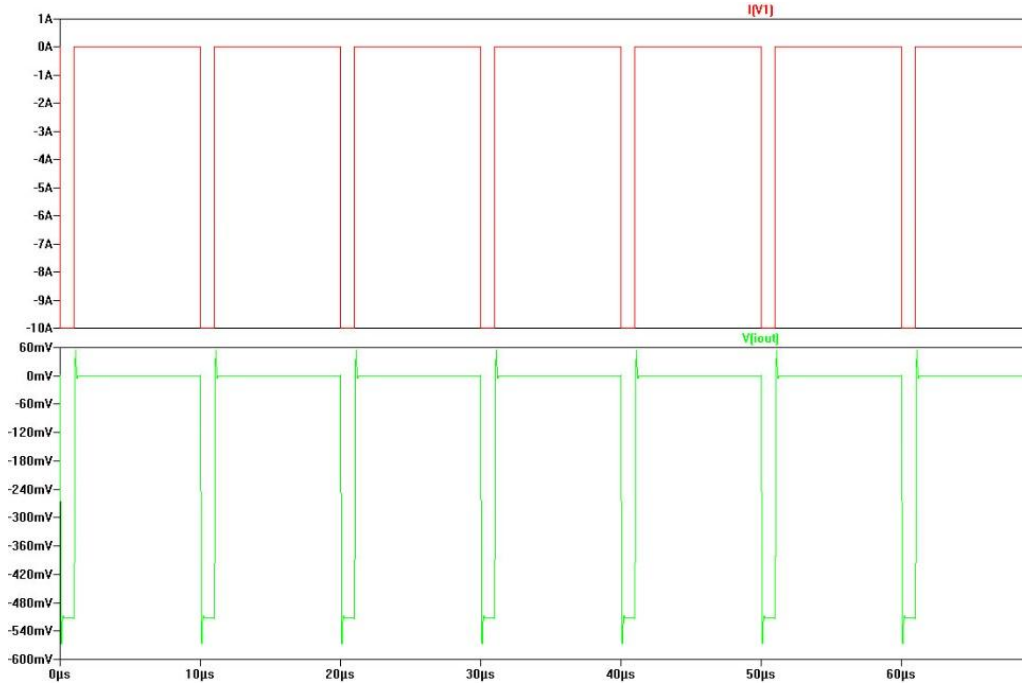

Figure 25: Simulation of the current probe circuit

Regarding the configuration of the oscilloscope's channels, both input impedances are set to 50 Ω considering the fact that the signal to be captured has a very high frequency.

3.3.3 The data acquisition automation

A Matlab script file was designed in order to automatize the acquisition of data. The script contains a Matlab timer object that executes a function at regular intervals which are set to five seconds. Additionally, numerous options concerning the timer can be set, more particularly the "BusyMode" and "ExecutionMode" parameters.

The "BusyMode" parameter defines what happens if the timer tries to launch the acquisition function before the completion of a previously launched acquisition function. The options available are *drop*, *error* and *queue*. The *drop* option enables the timer to skip the launch of the acquisition function, the *error* option throws an error and stops the timer while the *queue* option adds the launch of the acquisition function to a queue of tasks to do. It also adjusts the value of the timer's period. In order to avoid the change of the period value, the timer's BusyMode parameter has been set to *drop*. The "ExecutionMode" parameters define when the period value starts ticking. The different options, "fixedDelay", "fixedRate" and "fixedSpacing" are illustrated in Figure 26. The timer here uses the "fixedSpacing" mode.

Once the connection is established, the data from the oscilloscope for both channels is fetched sequentially. The points are then used to create a Matlab figure depicting the unaltered current and voltage function of time. The figures are saved under the following format:

$$dd - mm - yy - -HH - MM - SS.fig$$

An example is given in Figure 27. The tension is here negative due to the inverted polarity of the machine.

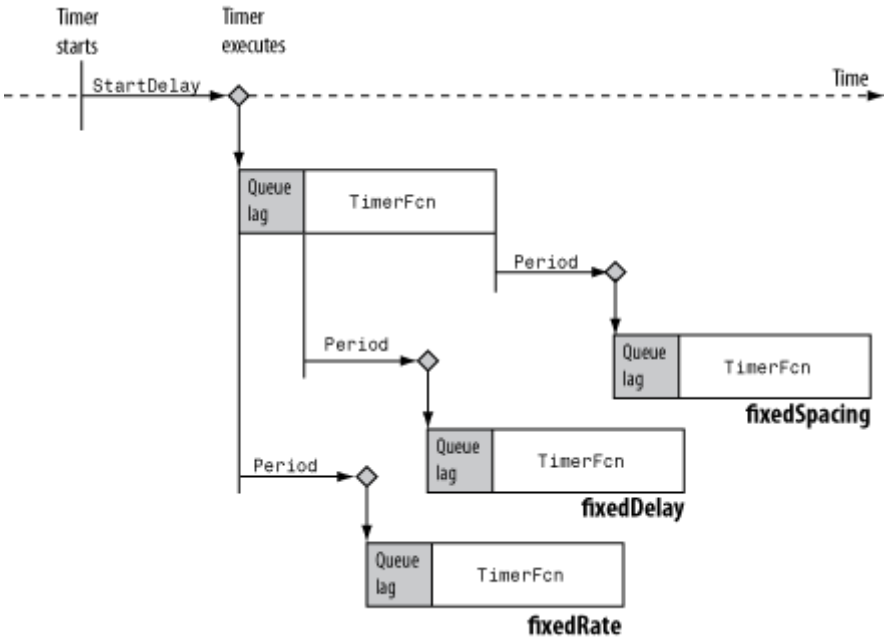

Figure 26: Matlab Timer object execution modes available

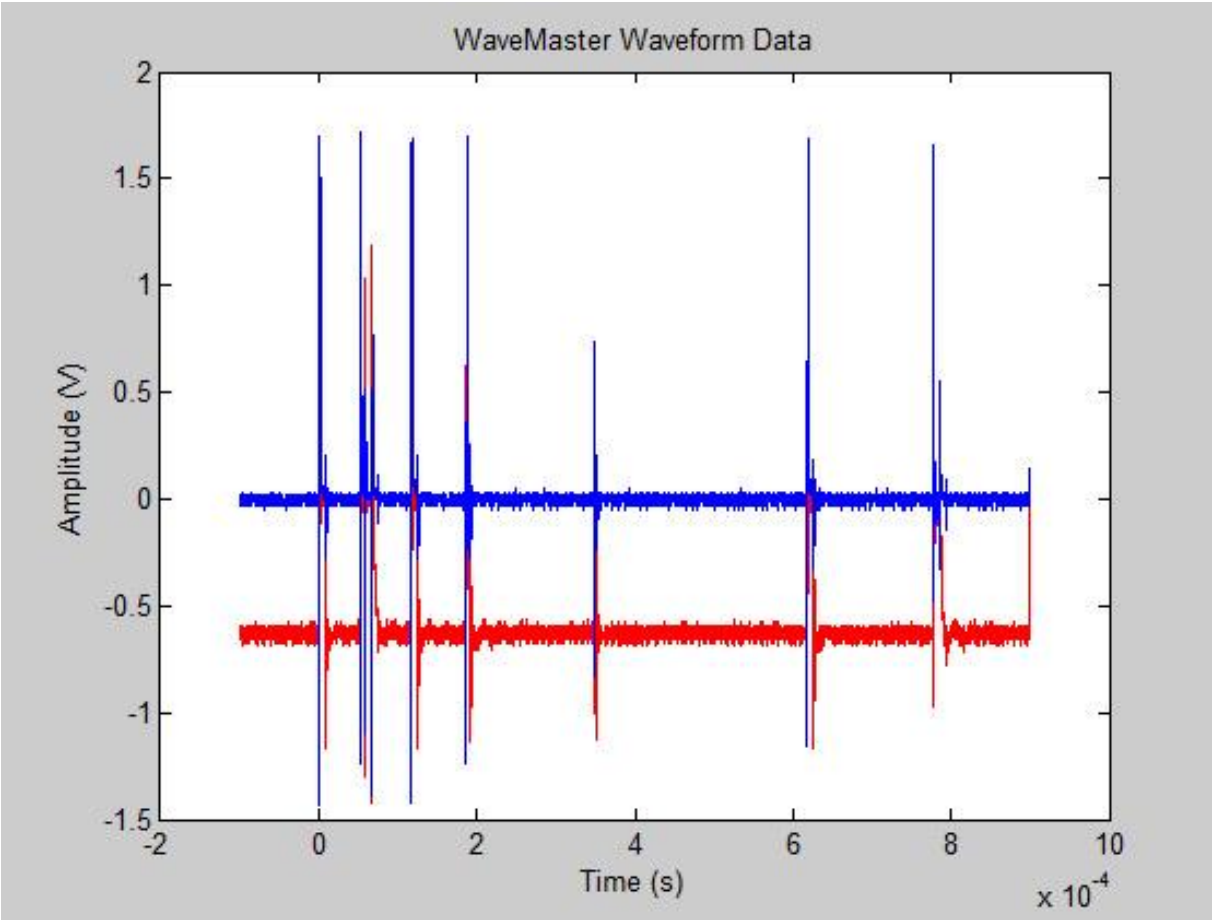

Figure 27: Raw current (blue) and voltage (red) data

3.3.4 Data analysis

Before being able to analyse the thousands of captured figures, it is necessary to identify which figures corresponds to which machined hole. This is made possible by the fact that the Sarix machine is able to generate a file with time information concerning each machined hole. As a result, for each material, diameter and energy combinations, there are 45 or 27 folders (depending on the number of repetitions) containing the data.

As seen previously, two coefficients to apply to the measured electrical data in order to obtain the true values exist. The first step is to apply the coefficients of -200 and 20 for the voltage and current, respectively.

3.3.5 Filtering the data

Before further processing, the data needs to be filtered to remove the noise. This task needs to take into account the fact that the sparks are very short in duration and can be confused as noise by a filtering algorithm. However the frequency bands of the noise and of the sparks are sufficiently different to not pose any significant problem during the filtering process. The data sample resolution makes it possible to use a simple moving average filter with a window size of 1000 for the current and voltage. Figure 28 shows an example of data before and after filtering. After filtering, power data (P(t)) is created through the multiplication of the filtered current and voltage data.

3.3.6 The sparks presence function

The sparks presence function is at the core of the analysis process since the way it is built will be decisive in the computation of all the values extracted from the data.
The sparks presence function is as follows:

$$Sp(t) = \begin{cases} 0 \; if \; there \; isn't \; a \; spark \; at \; t \\ 1 \; if \; there \; is \; a \; spark \; at \; t \end{cases}$$

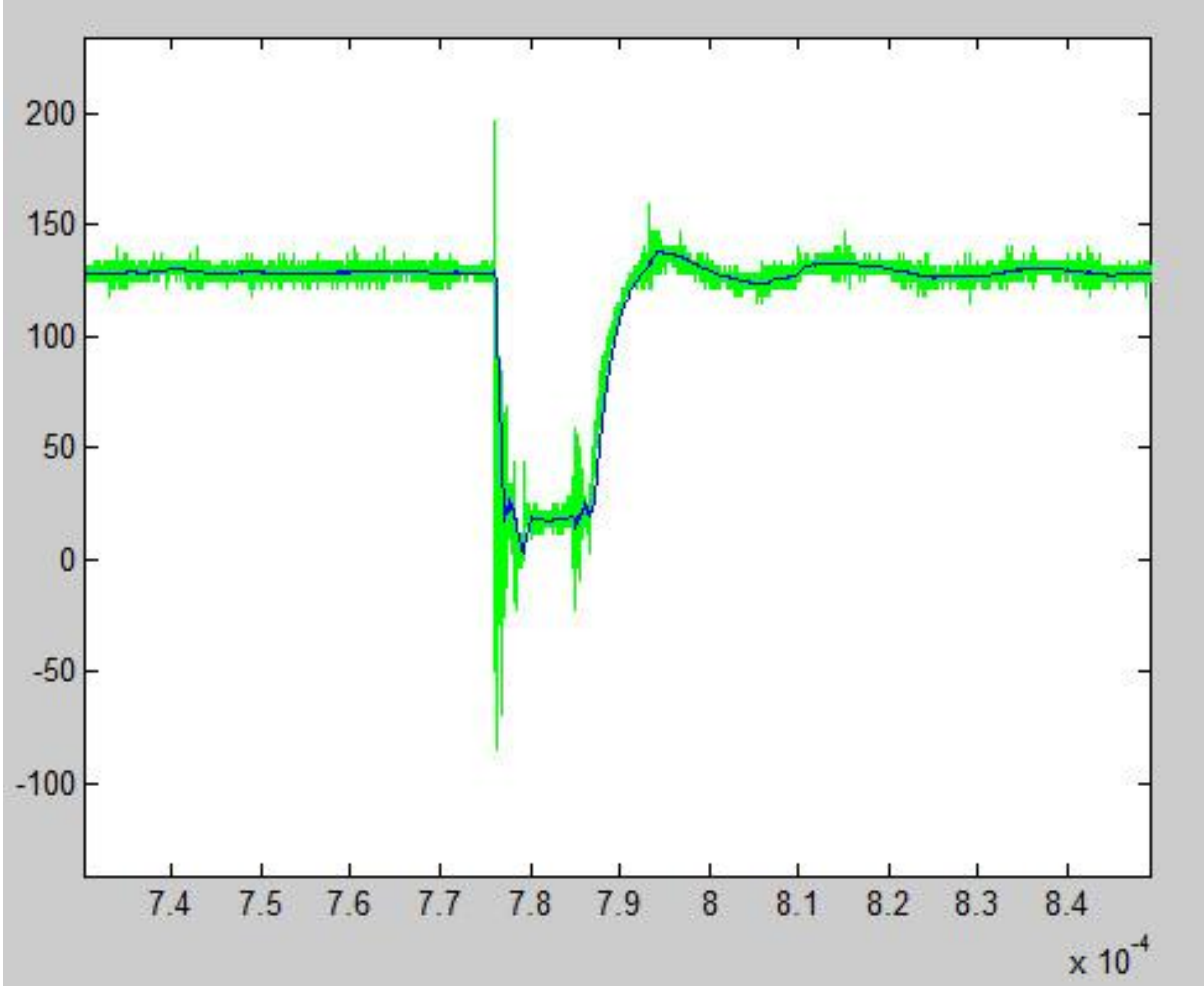

Figure 28: Voltage (in V) against time (in s). Green: unfiltered, blue: filtered.

In order to build that function, we have to consider what a spark actually is. Observation of the graphs tell us that the beginning of spark is characterized by:

- A sudden decrease in the voltage accompanied by:
- An increase in the current.

In the same way we can say that a spark ends when the current is back to a value close to zero.

Taking into account these observations, the beginning of a spark happens:

- When the voltage is below a certain level $V_{threshold}$ and:
- When the current is above a certain level I_{start}

A spark ends when:

- A spark is currently on going
- The current is below a certain level I_{end}

The choice of these three parameters, $V_{treshold}$, I_{start} and I_{end} is crucial since the sparks presence function needs to return the correct number of sparks. Additionally, it needs to do so while making the sparks detected be comparable between themselves and, therefore, achieve a certain level of consistency. Those parameters need to be chosen such as:

- The correct number of sparks is returned,
- The sparks detected maximize their energy.

Those values are also dependent on the experimental parameters and therefore would be different for each hole that is machined.

A procedure was defined to choose those values with the use of particle swarm optimization. For each set of parameters that was used in the experimental campaign, a figure was selected and the sparks contained in it counted. With the knowledge of the correct number of sparks and using it as a constraint in the optimization process, the algorithm was capable of finding the values of $V_{treshold}$, I_{start} and I_{end} that maximized the energy of all sparks. Those values were then used for the remainder of the figures.

3.3.7 Values computed from the data

With the sparks presence function $S_p(t)$ and the power function $P(t)$, the multiplication of both of them gives the power information during the discharges. The data analysis computes for each figure:

- The number of discharges.
- The amount energy transferred during the discharges through integration.
- The peak voltage for each discharge.
- The peak current for each discharge.

As a result, for each hole, it is possible to compute:

- The average energy transferred per spark.
- The total number of sparks.
- The average peak current.
- The average peak voltage.
- The number of sparks per second.
- The average energy transferred per second.

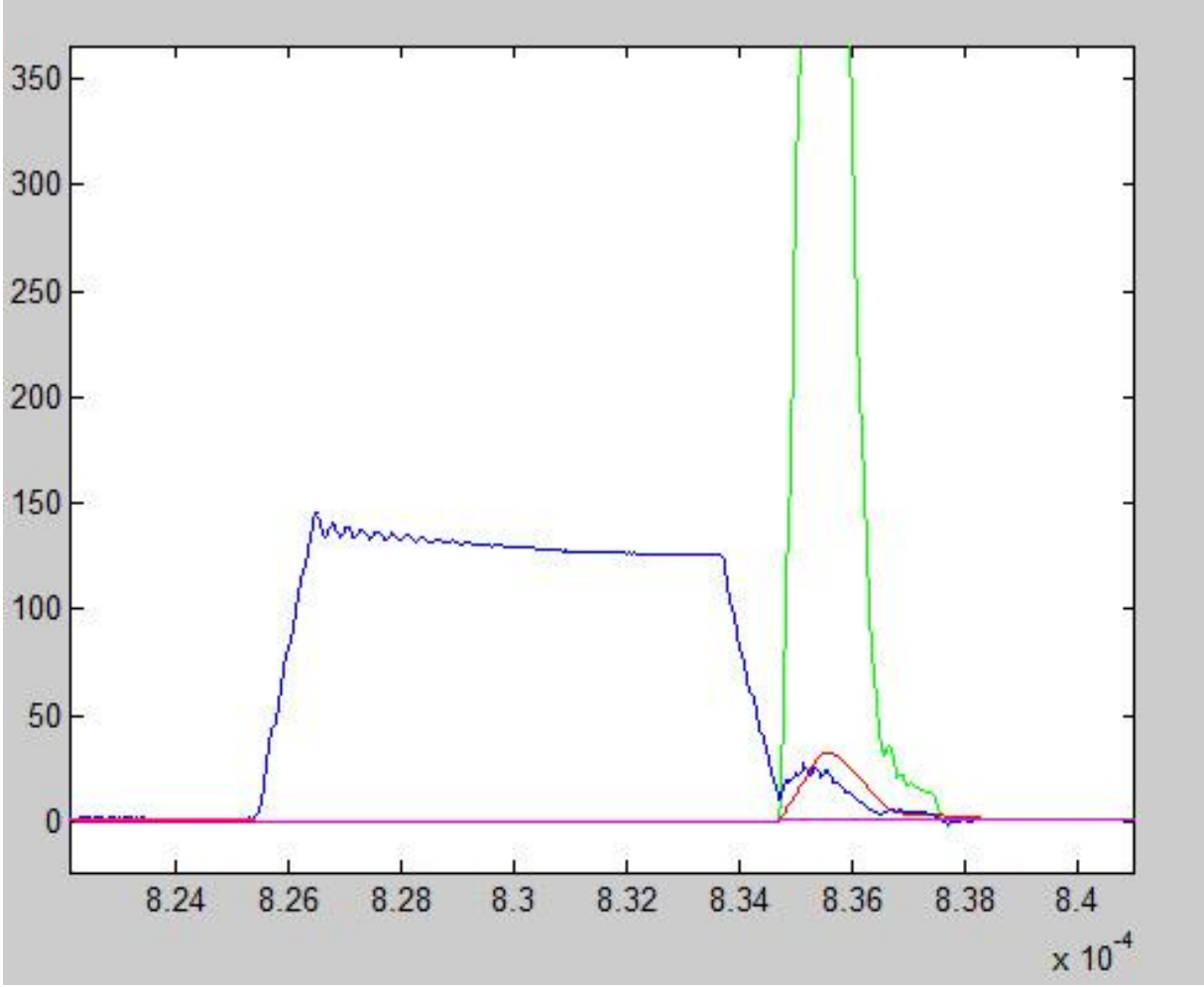

Figure 29: Voltage (in V, blue), Current (in A, red), Power (in W, green) and sparks presence function (magenta) function of time (in seconds).

For each hole, the data analysis algorithm generates a figure similar to Figure 29 for each of the original figures. In addition, a file called analysis.txt is generated with the

numerical values of “total energy”, “energy per spark”, “peak voltage”, “peak current”, “number of sparks” for each of the original figures.

For the whole Material/Diameter/Energy level combination, an excel file containing the average values of that data for each hole is generated.

3.4 Experimental Procedure

In order to find a possible relationship between the electrode and the hole diameter, holes with different diameters were carried out.

The experimental campaign has been executed starting from the bigger diameters (300 micron) followed by the execution of the smaller ones. The campaign was carried out with tubular electrodes made of two different materials, tungsten carbide and copper, in order to investigate the influence of the electrode material, as well as the process parameters, on the final results (geometrical properties of the holes and process performance). The experimental campaign consisted in the execution of through micro holes on 316L stainless steel plates having thickness equal to 1 mm. In order to carry out the campaign, stainless steel samples having dimensions of 30x60 mm were obtained from a 1 m^2 steel sheet by means of a conventional cutting machine. Table 8, Table 9 and Table 10 report the mechanical, electrical and thermal properties of the workpiece material. The planarity of the samples has been verified using the micro-EDM machine capability to detect short circuits by means of electrode touches in referential points selected on the samples.

Table 8: Workpiece material mechanical properties

Mechanical Properties	Metric value
Density [g/cm^3]	7.99
Modulus of Elasticity [GPa]	193
Yield Tensile Strength [MPa]	290
Ultimate Tensile Strength [MPa]	558

Table 9: Workpiece material electrical properties

Electrical Properties	**Metric value**
Electrical Resistivity [ohm-cm]	0.0000740
Magnetic permeability	<= 1.02

Table 10: Workpiece material thermal properties

Thermal properties	**Metric value**
Thermal conductivity [W/m K]	16.2
Melting point [°C]	1380
Specific Heat Capacity [J/g °C]	0.5

In particular, two or more electrode touches have been executed varying the x quote along the sample. The delta quote on the z axis was recorded in every x position along the sample: in order to consider the plate planar, the value must have been lower than 25 micron.

As a matter of fact, the sample planarity is a very relevant aspect, especially as regards the electrode wear measurement. This involves the electrode touch in a referential point on the plate, usually low left extremity of the sample. For this reason the planarity of the sample is of the utmost importance, in order to guarantee a reliable measurement of the electrode wear after the execution of each hole.

As mentioned before, the experimental campaign was executed with two different electrode materials, tungsten carbide and copper. Table 11 reports the details of the electrode dimensions and Table 12 reports the properties of the material composing the electrodes. Kerosene dielectric oil was employed for the micro-EDM tests.

Table 11: electrode material characteristics

Material	TC (WC94Co6)	Cu
Density [g/cm^3]	14.8	7.764
Melting Temperature [°C]	2867	1083
Electrical Resistivity [Ωcm]	$20x10^{-6}$	$0.17x10^{-6}$
Thermal conductivity [W/mK]	70	385
Specific Heat [J/(g°C)]	0.3	0.385

Table 12: dielectric characteristics

Dielectric fluid	Kerosene oil
Dielectric strength [MV/m]	14-22
Dielectric constant [-]	1.8
Thermal conductivity [W/mK]	0.149
Heat capacity [J/gK]	2.16
Dynamic viscosity [g/ms]	1.64

An automatic program was implemented to allow the execution of the micro holes, the wear measurement and the consequent electrode cut with the wire micro-EDM unit. The automatic program executes the following operations:

- Electrode lengthening in the referential point;
- Hole drilling;
- Time recording;
- Electrode touch in a referential point;
- Recording of the electrode wear;

- Electrode cut with the wire-EDM unit;
- Electrode lengthening in the referential point;

Automatically the machine produces a report file with the electrode wear and machining duration for each hole. A typical hole matrix is reported in Figure 30.

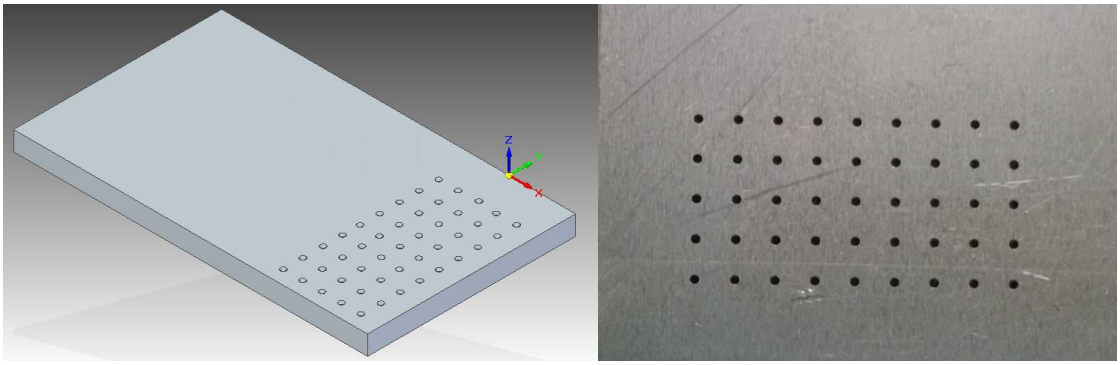

Figure 30: Typical micro-hole matrix

3.5 Indicators

Once the experimental campaign has been executed and all the data collected, it was possible to implement the data analysis in order to investigate the influence of the process parameters on the process indicators. The indicators can be divided in two main categories:

- Hole geometrical characteristics;
- Drilling process performances.

3.5.1 Hole geometrical characteristics

In order to investigate the hole geometrical characteristics, two different indicators were used. The first one is the Diametrical Over cut (*DOC*), calculated as the difference between the electrode nominal diameter (D_{nom}) and the hole top diameter (D_{top}), as reported below:

$$DOC = D_{top} - D_{nom}$$

The second indicator is the Taper Rate (*TR*) calculated as the difference between the hole's top and bottom diameters (D_{top} and D_{bottom}) and the plate thickness, h, as reported in the following equation:

$$TR = \frac{D_{top} - D_{bottom}}{h}$$

In micro-EDM drilling in fact, the wear phenomenon involves not only the workpiece but also the electrode. As a matter of fact the electrode, which is characterized by a cylindrical shape at the beginning of the machining, after a series of sparks it assumes a conical shape, that can have a negative effect on the micro-holes geometry. For this reason, these two indicators represent the hole enlargement due to the sparks' effect, the side discharges and the hole conicity. The hole typical geometry is reported in Figure 31.

3.5.2 Drilling process performances

As regards the drilling process performances, two different indicators were taken into account. The first one, the Material Removal Rate (MRR), gives information about the machining speed. It is calculated as the ratio between the material removed from the workpiece (MR_{wp}) and the recorded machining time (*t*), as reported below:

$$MRR = \frac{MR_{wp}}{t}$$

The material removed from the workpiece is calculated as the volume of the frustum of cone having diameters equal to the hole top and bottom diameters (D_{top} and D_{bottom}) as reported below:

$$MR_{wp} = \frac{1}{3}\pi h(R^2 + R \cdot r + r^2)$$

Since micro-EDM is based on electrical discharges and since the tool electrode is involved in the erosion process, the second indicator gives a measurement of the electrode wear. The Tool Wear Ratio (TWR) is calculated as the ratio between the

material removed from the tool (MR_{tool}) and the material removed from the workpiece (MR_{tool}), as reported below:

$$TWR = \frac{MR_{tool}}{MR_{wp}}$$

Where the material removed from the tool is calculated as the volume of the electrode taking into account the electrode cavity.

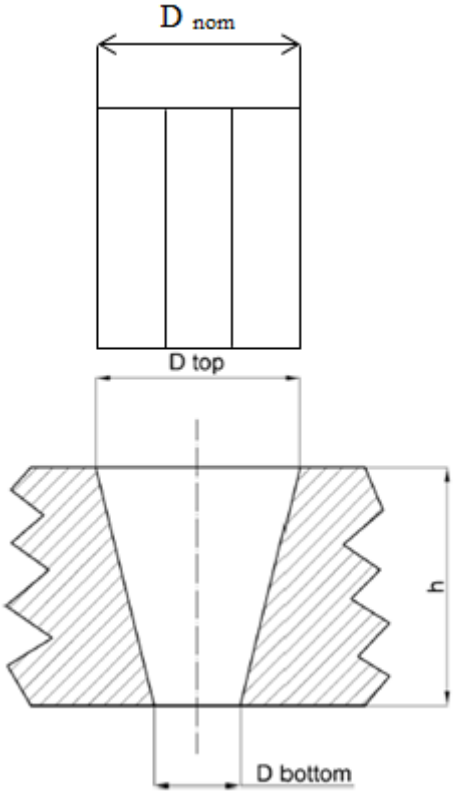

Figure 31: Hole typical frustum conical shape

3.6 Measurement procedure

Once the experimental campaign has been executed, the measurement procedure have been carried out using an optical and a scanning electron microscope. The measurement of the hole diameters involved both the top diameter, corresponding to the entrance of the electrode, and the bottom diameter, corresponding to the electrode exit.

As mentioned before, the top diameter is always bigger than the bottom diameter, because of the conicity of the hole. Typical pictures of the measures of the top and bottom holes are reported in Figure 32.

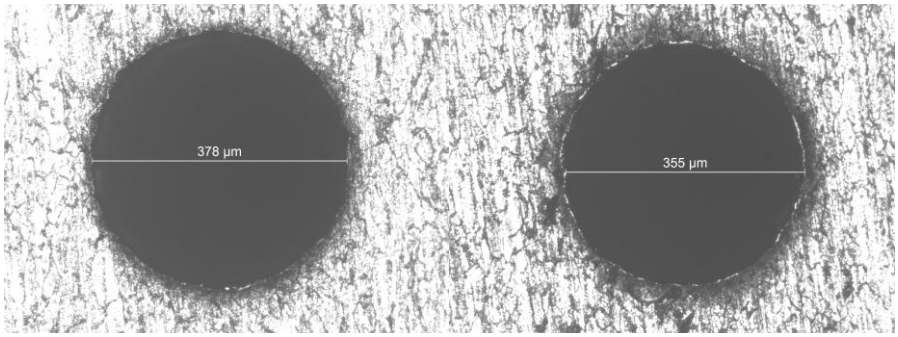

(a) (b)

Figure 32: Hole top (a) and bottom (b) diameters on steel plates drilled with tungsten carbide electrode

After the hole diameters measurement, the calculation of the indicators have been executed and the data analysis have been carried out. All the preliminary data preparation and the data analysis are described in detail in the following chapter.

Chapter 4

Data Analysis

The present chapter describes in detail the data analysis strategy and procedure. The first part of the work, consisted in the data preparation, aimed at the elimination of the outliers. After this preliminary part, the data have been analysed on three different levels of analysis: the first one is aimed at the individuation of a certain influence between the process parameters and the final output indicators, the second one is aimed at the evaluation of the actual trends of the indicators as a function of the exchanged power and the last level of analysis is aimed at the individuation of a relationship between the factors influencing the process and the final output.

4.1 Outliers

As mentioned before, the first step towards the execution of the data analysis consisted in the elimination of the outliers from the initial raw data regarding:

- Top diameter measured data - D_{top}
- Bottom diameter measured data - D_{bottom}
- Machining time - t
- Tool wear - w

The elimination of the outliers is fundamental in order to avoid any possible negative influence of aberrant values on the calculation of the final indicators (machining time, electrode wear, DOC, TR, MRR and TWR). The outliers can be defined as experimental measured values that are significantly different from the other observations, in other words they represent statistically incoherent data. This incoherence can be due to the intrinsic process variability that characterises micro-EDM.

As a matter of fact, in big data samples, a small amount of outliers can be considered physiological and for this reason it is not necessarily due to wrong experimental conditions. In general, in these cases the data is eliminated from the data sample, and

are excluded from the analysis. The first aspect to consider in this case is the identification of the outliers.

In the present work the outlier data has been eliminated considering the modified Thompson tau – τ approach. First of all, the collected data have been grouped in excel files divided in categories (electrode material, diameter and machining energy).
The τ indicator has been evaluated for all the collected data. First of all, the mean of the five repetitions for each process parameters combination has been calculated with the following equation:

$$x_m = \frac{1}{5}\sum_{i=1}^{5} x_i$$

Knowing the mean value for each of the five repetitions for every parameter combination it was possible to calculate the delta between the singular data and the mean data, as reported below:

$$\Delta = |x_i - x_m|$$

The following step consisted in the calculation of the standard deviation of the collected data, as reported in the following equation:

$$\bar{s}_x = \frac{1}{5}\sum_{i=1}^{n}(x_i - x_m)^2$$

At this point of the analysis the last needed information is the value of the Thompson tau value, that can be obtained from the dedicated statistical tables, as reported in Table 13. In this case, the selected value was 1.5712 since the number of repetitions was equal to five. Finally, in order to determine if the value is an outlier it is necessary to execute the comparison summarized below:

- If $\Delta > \tau \cdot \bar{s}_x$ the data is an outlier
- If $\Delta < \tau \cdot \bar{s}_x$ the data is not an outlier

If the second condition is satisfied, the data is kept and the analysis can be carried out, on the contrary the data must be eliminated and substituted with the data collected from another experimental test with the same process conditions.

Table 13: Modified Thompson tau table

n	τ	N	τ	n	τ
3	1,1511	**21**	1,8891	**40**	1,9240
4	1,4250	**22**	1,8926	**42**	1,9257
5	1,5712	**23**	1,8957	**44**	1,9273
6	1,6563	**24**	1,8985	**46**	1,9288
7	1,7110	**25**	1,9011	**48**	1,9301
8	1,7491	**26**	1,9035	**50**	1,9314
9	1,7770	**27**	1,9057	**55**	1,9340
10	1,7984	**28**	1,9078	**60**	1,9362
11	1,8153	**29**	1,9096	**65**	1,9381
12	1,8290	**30**	1,9114	**70**	1,9397
13	1,8403	**31**	1,9130	**80**	1,9423
14	1,8498	**32**	1,9146	**90**	1,9443
15	1,8579	**33**	1,9160	**100**	1,9459
16	1,8649	**34**	1,9174	**200**	1,9530
17	1,8710	**35**	1,9186	**500**	1,9572
18	1,8764	**36**	1,9198	**1000**	1,9586
19	1,8811	**37**	1,9209	**5000**	1,9597
20	1,8853	**38**	1,9220	**(→∞)**	1,9600

As a matter of fact, in order to eliminate the outliers from all the recorded data, the outliers removal procedure has been executed on all the collected data, in particular it involved:

- peak current (I);
- peak voltage (V);
- energy per spark (E/s);
- captured time (t);
- number of sparks (S);
- sparks per second (S/s);
- energy per second(E/s).

Once all the outliers were removed, the calculation of the indicators and the analysis of the results can be carried out.

The analysis of variance (ANOVA) approach was used. The typical ANOVA approach is based on the acceptance or the rejection of the null hypothesis, according to which all the considered groups of data represent random samples of the same population.

This statistical hypothesis test approach was helpful in order to make decisions using the collected data: it was possible to evaluate the influence of the factors on the final response, in other words, the machining time (t), electrode wear (w), DOC, TR, MRR and TWR indicators. The factors here considered were the peak current (I) and the voltage (V), varied on three levels, the energy (E), varied on two levels, and the electrode material, varied on two levels. The ANOVA analysis was originated by the already implemented DOE (Design of Experiments): the factors were assigned to the experimental units by means of randomization to avoid any repetitive error during the experimental campaigns. In this case, the effect of multiple factors was considered in a "full factorial" approach, meaning that the experiment included observations at all combinations of level of each factor. This approach resulted in the investigation of the single factors and at the same time their interaction: for example, for the initial factors I and V the effect of combination I*V on the final response was considered, too. The following section summarizes the results obtained by the analysis of variance for the tungsten carbide (TC) and for the copper (Cu) electrode.

4.2 Analysis of Variance

The analysis of variance approach was applied on three different levels, which considered progressively more factors in the analysis:

- First level of analysis: peak current (I) and voltage (V);
- Second level of analysis: since a common phenomenon is found behind the interaction between I and V, another relevant factors has been introduced, namely the energy level (E);
- Third level of analysis: electrode material (m).

Not only the geometrical and performance indicators were considered in the analysis: the plan has been evaluated in order to identify the influence of the factors on the final value of the machining time (t) and electrode wear (w), which can be considered interesting aspects of the machining process, especially from an industrial point of view.

As a matter of fact, the electrode wear and the TWR are directly proportional since the formulation of the TWR indicator, for this reason the results reported for the electrode wear are representative of the results obtained for the TWR or vice versa.

On the contrary, the machining time and MRR are inversely proportional, and for this reason they are not characterized by the same pattern. This aspect will be relevant while evaluating the main trends for the indicators as a function of the process parameters.

The following sections describe in detail the procedure and the results obtained from the analysis of variance approach for the tungsten carbide electrode. The same analysis has been executed for the copper electrode, too.

It is important to underline that, for the sake of simplicity, the other following sections report only the results that were obtained with the same procedure. Finally, the detailed statistical information about all the cases here investigated is reported in the Appendix.

4.2.1 Tungsten Carbide (TC) Electrode

4.2.1.1 First level of Analysis: I and V

TC, d 300 μm, E 365

The present section describes the results obtained from the analysis of variance for the TC electrode having nominal diameter equal to 300 μm. Table 14 reports the details concerning the machining time (t) response. It is possible to obtain information about:

- DF:
  - degrees of freedom of the considered factor which is equal to the number of levels (n) -1
  - degrees of freedom of the error, in this case equal to the observation subtracted by the number of levels of the factors
- Seq SS: represents the sequential sum of squares. It depends on the order the terms are entered into the model and it is the unique portion of the sum of squares explained by a term, given any previously entered terms;
- Adj SS: it is the adjusted sum of squares and does not depend on the order the factors are entered into the model. It is the unique portion of SS Regression explained by a factor, given all other factors in the model, regardless of the order they were entered into the model.

Table 14: abstract of the analysis of variance for the machining time response

Source	DF	Seq SS	Adj SS	F	P
I	2	50198	5019	8.55	**0.001**
V	2	57801	57801	9.85	**0.000**
I*V	4	17121	17121	1.46	0.235
Error	36	105674	105674		
Total	44				

The factor having a consistent influence on the final value of the machining time are the voltage (V) and the peak current (I), which are characterized by a p-value lower than the cut-off (α) value, set equal to 0.05.

In this case it is possible to reject the null hypothesis: in other words, the statistical series can be considered significant and the tension and the peak current have a consistent influence on the machining time. From a statistical point of view, the difference in the groups' mean values is a direct effect of the variation of the level of the factors. The analysis of variance approach is based on the assumption that the raw data is normally distributed. In order to verify this aspect, the normality test was executed for all the levels of the analysis and for all the data. An example is shown in Figure 33. In this case the normality of the data is verified since the histogram of the residuals has a typical Gaussian shape and the residuals as a function of the observation order do not show particular trends. Since the normality has been verified, the conclusions drawn from the analysis of variance can be considered consistent. It is important to underline that for all the indicators (time, wear, DOC, TR, MRR and TWR) the normality test gave positive results, comparable to the one shown in Figure 33.

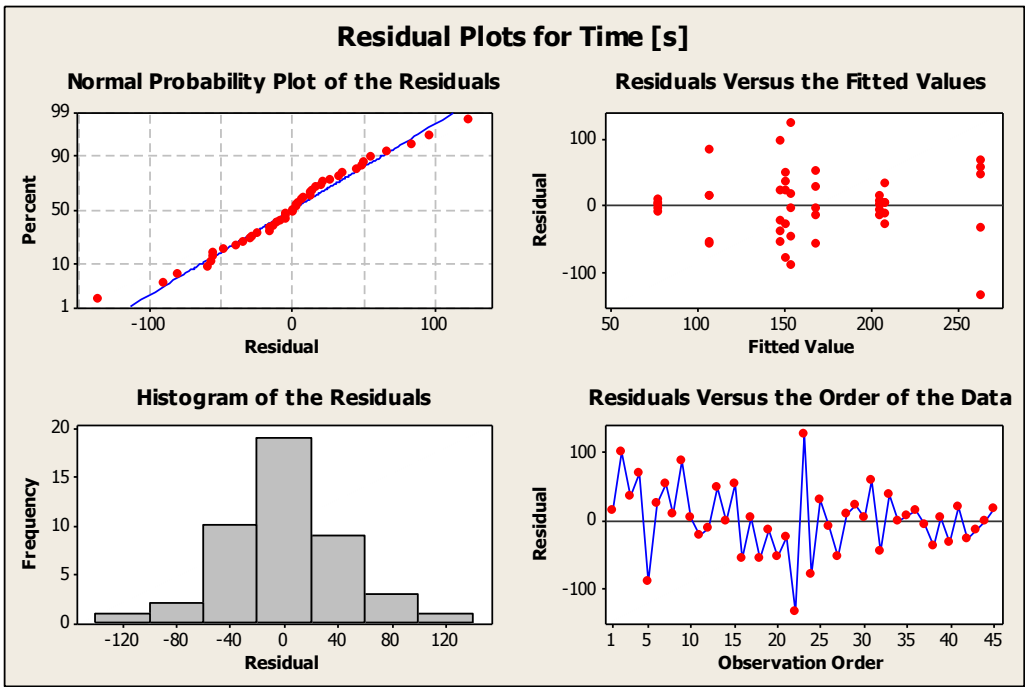

Figure 33: Normality test for the machining time response, d 300 µm, E 365

As regards the electrode wear (Table 15) it is possible to draw the same conclusions: both peak current and voltage have a consistent influence on the electrode wear final response. For the geometrical indicators, both DOC and TR are influenced by I, V and the parameters' combination I*V, as reported in Table 16 and Table 17. The results for MRR and TWR are shown in Table 18 and Table 19. For both of them, I and V resulted relevant factors. In order to summarize all the results, Table 20 shows only the p-values calculated for all the indicators. Considering the process performance indicators, MRR and TWR, it is possible to notice a strong relationship with I and V.

Table 15: Analysis of variance for the electrode wear, d 300 μm E 365

Source	DF	Seq SS	Adj SS	F	P
I	2	0.54518	0.54518	28.94	**0.000**
V	2	1.01400	1.01400	53.82	**0.000**
I*V	4	0.02116	0.02116	0.56	0.692
Error	36	0.33913	0.33913		
Total	44	1.91947			

Table 16: Analysis of variance for the DOC, d 300 μm E 365

Source	DF	Seq SS	Adj SS	F	P
I	2	0.0011173	0.0011173	10.77	**0.000**
V	2	0.0005689	0.0005689	5.48	**0.008**
I*V	4	0.0056669	0.0056669	27.30	**0.000**
Error	36	0.0018682	0.0018682		
Total	44	0.0092213			

Table 17: Analysis of variance for the TR, d 300 μm E 365

Source	DF	Seq SS	Adj SS	F	P
I	2	0.0001562	0.0001562	5.03	**0.012**
V	2	0.0000745	0.0000745	2.40	0.105
I*V	4	0.0019408	0.0019408	31.21	**0.000**
Error	36	0.0005596	0.0005596		
Total	44	0.0027312			

Figure 34 shows the interaction plot for the MRR indicator. The interaction plot has been used in order to describe the relationship existing between the response (in this case MRR) and the factors of the model (I, V and their interaction).

Table 18: Analysis of variance for the MRR, d 300 μm E 365

Source	DF	Seq SS	Adj SS	F	P
I	2	0.0000022	0.0000022	11.21	**0.000**
V	2	0.0000020	0.0000020	10.12	**0.000**
I*V	4	0.0000006	0.0000006	1.59	0.198
Error	36	0.0000035	0.0000035		
Total	44	0.0000082			

In order to summarize all the results, Table 20 shows only the p-values calculated for all the indicators. Considering the process performance indicators, MRR and TWR, it is possible to notice a strong relationship with I and V. Figure 34 shows the interaction plot for the MRR indicator. The interaction plot has been used in order to describe the

relationship existing between the response (in this case MRR) and the factors of the model (I, V and their interaction).

Table 19: Analysis of variance of the TWR, d 300 μm E 365

Source	DF	Seq SS	Adj SS	F	P
I	2	0.245006	0.245006	34.56	**0.000**
V	2	0.443255	0.443255	62.52	**0.000**
I*V	4	0.027001	0.027001	1.90	0.131
Error	36	0.127621	0.127621		
Total	44	0.842884			

As a general remark, an interaction is identified when the response at a certain factor level depends on the level (or the levels) of other factors. From a graphical point of view, parallel lines, or in general non-intersected lines, indicate absence of interaction; on the contrary, the greater the departure of the lines from the parallel state (that causes intersection of the curves), the higher the degree of interaction.

In this case, as regards the MRR indicator, it is possible to notice that the curves have different inclination but no real interaction between them is recorded. This means that a little interaction between the variation of peak current and the voltage variation is recorded, but as testified by the p-values, its effect on the response is negligible if compared with I and V factors' effect.

Table 20: Analysis of variance, p-values, d 300 μm, E 365

	t	Wear	DOC	TR	MRR	TWR
I	**0.001**	**0.000**	**0.000**	**0.012**	**0.000**	**0.000**
V	**0.000**	**0.000**	**0.008**	0.105	**0.000**	**0.000**
I*V	0.235	0.692	**0.000**	**0.000**	0.198	0.131

Figure 35 plots the data means at each level of both I and V factors. This kind of graph is useful to compare the strength of factor's effect. In this case both I and V have a considerable influence on the final result. Moreover, it is clear that the MRR is directly influenced by the peak current, differently from the voltage for which a non-monotone trend is recorded.

Figure 36 and Figure 37 show the results for the TWR indicator: no relevant interaction between I and V is found to have an influence on the final response, and an inversely proportional effect of the factors on the mean values of TWR is recorded. A possible interpretation of this result is that higher process parameters result in a more efficient workpiece material removal: in other words, for this energy level and electrode type, the portion of material removed from the workpiece with high process parameters is higher than with low process parameters. Similar influence of I and V was obtained for the machining time and the electrode wear, as an example Figure 38 shows the results for the electrode wear: since the electrode wear and the TWR are directly proportional, the same patter has been found. For the machining time indicator, even though I and V can be considered both relevant considered singularly, no influence of the interactions between the factors is recorded.

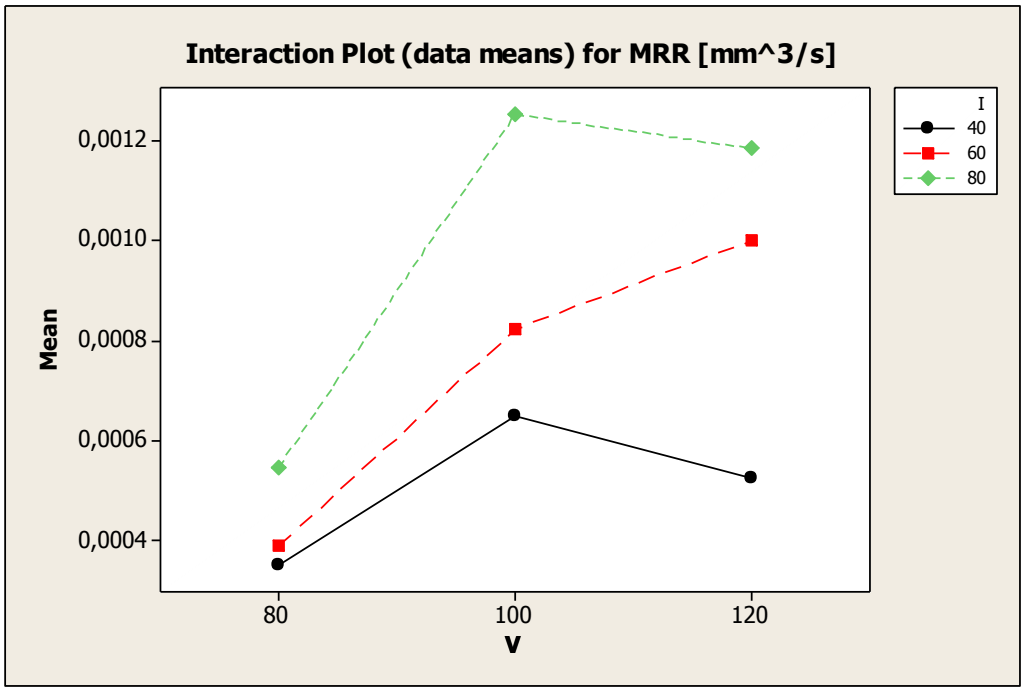

Figure 34: Interaction plot for MRR mean data as a function of I and V, d 300 µm E 365

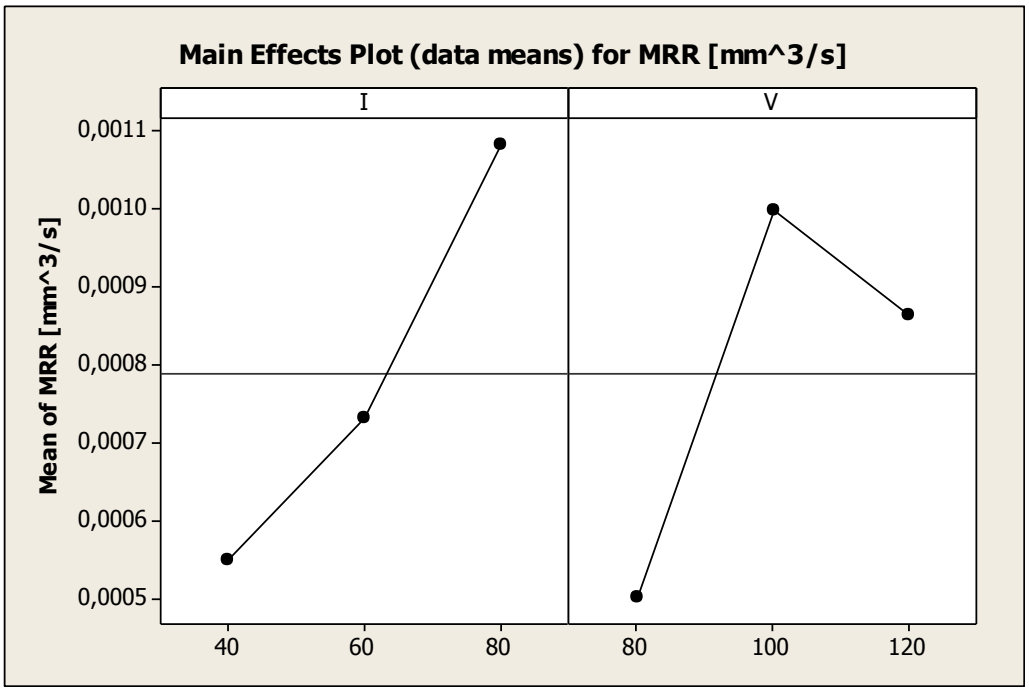

Figure 35: Main effects plot for MRR mean data as a function of I and V, d 300 µm E 365

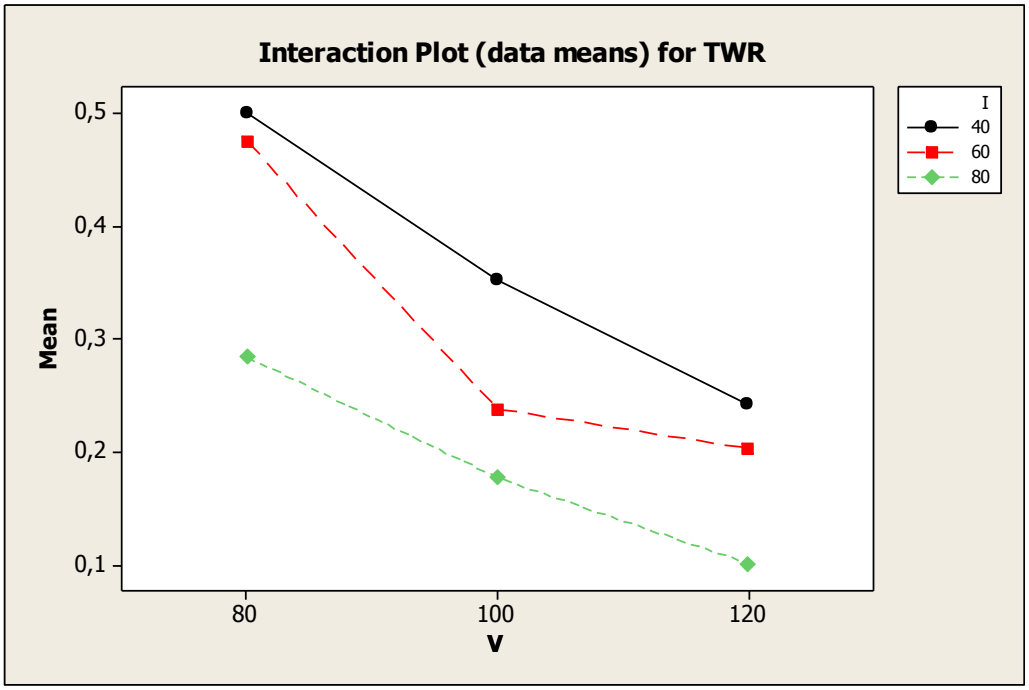

Figure 36: Interaction plot for TWR mean data as a function of I and V, d 300 µm, E 365

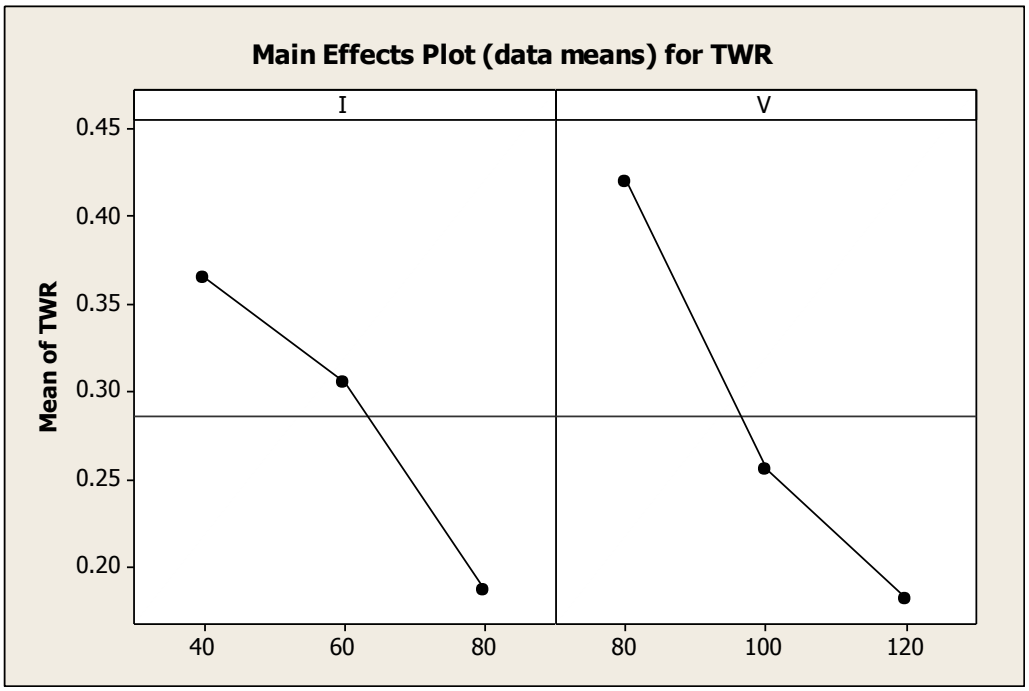

Figure 37: Main effects plot for TWR mean data as a function of I and V, d 300 µm, E 365

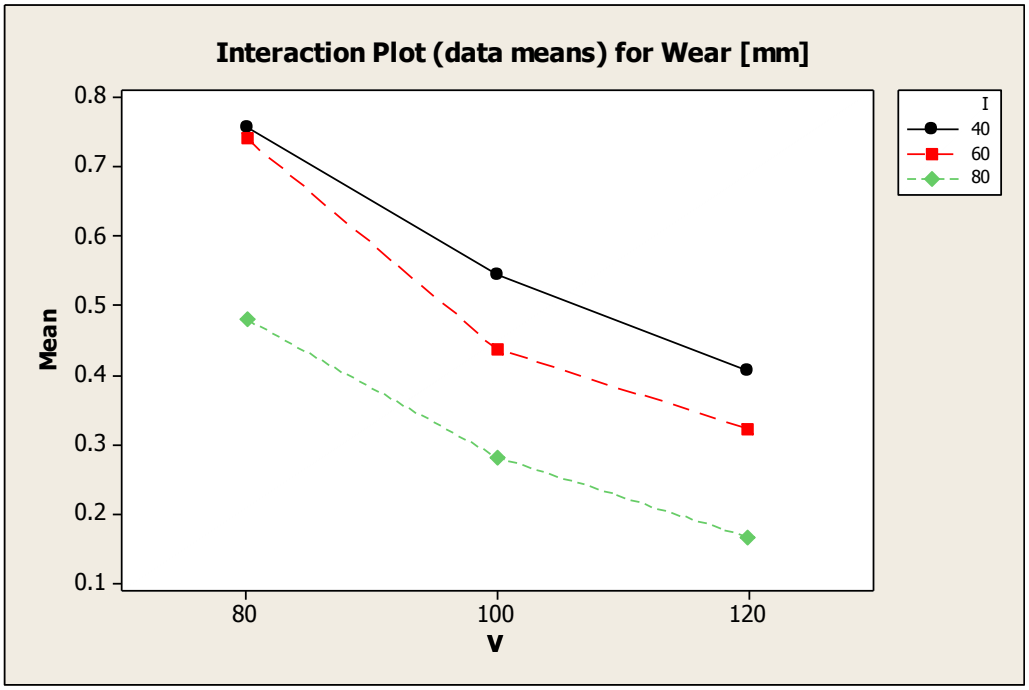

Figure 38: Interaction plot for tool wear mean data as a function of I and V, d 300 µm, E365

Considering the main effects plot for the electrode wear (Figure 39), it is possible to notice a decreasing monotone trend of the variable mean values for the peak current and a similar effect for the voltage. A different result is recorder for the machining time (Figure 40). The interaction effect is a "non-additive effect", in other words, something unexpected happens for particular combinations of levels of I and V factors. As regards the geometrical characteristics, different results have been found. Regarding the DOC, it is possible to notice from Figure 41 not only a lack of parallelism between the curves but also intersections, representing considerable interaction between the factors: this means that neither the peak current nor the voltage considered alone have a significant relevance on the final result. This is confirmed by the p-value analysis, from which the effect of I and V's interaction for the geometrical characteristics resulted to be relevant. The same conclusion can be drawn for the TR indicator, as seen in Figure 42.

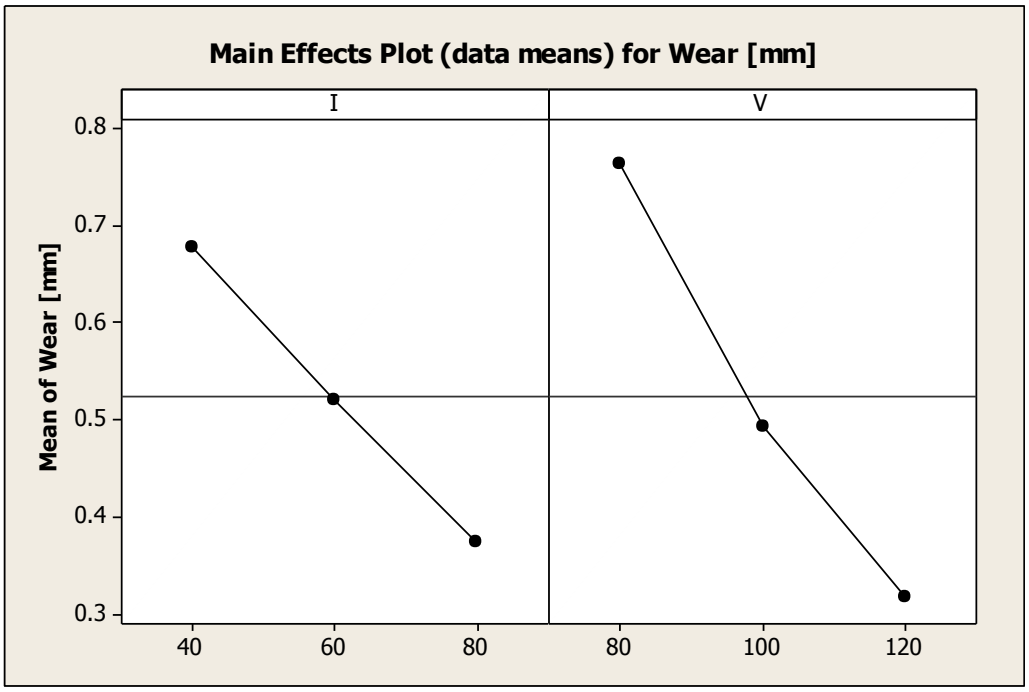

Figure 39: Main effects plot for electrode wear mean data as a function of I and V, d 300 μm, E 365

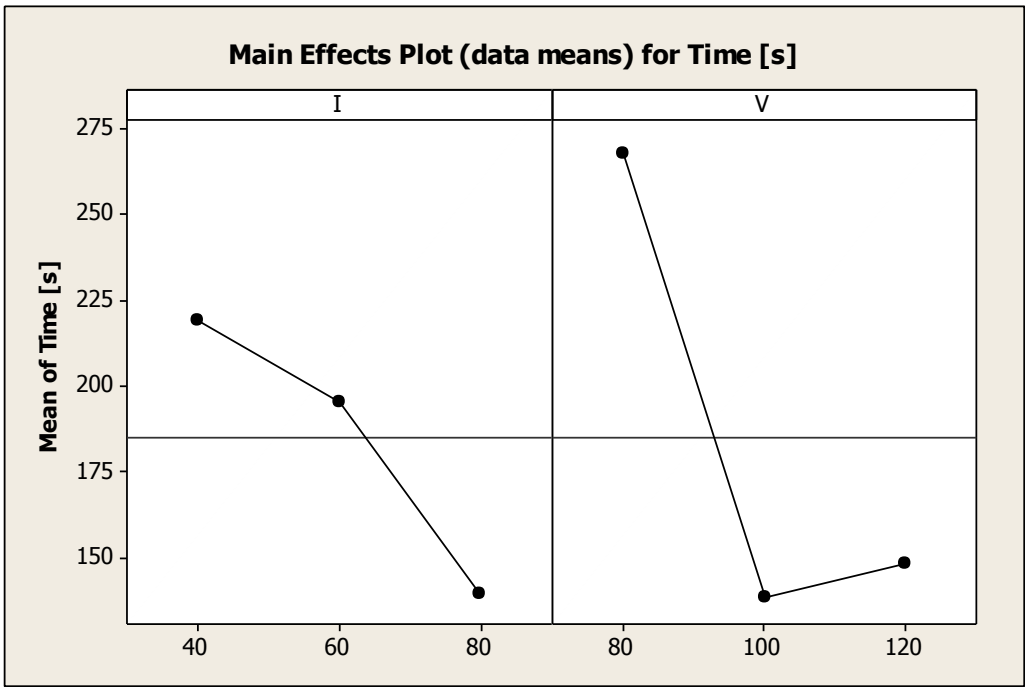

Figure 40: Main effects plot for machining time mean data as a function of I and V, d 300 µm, E 365

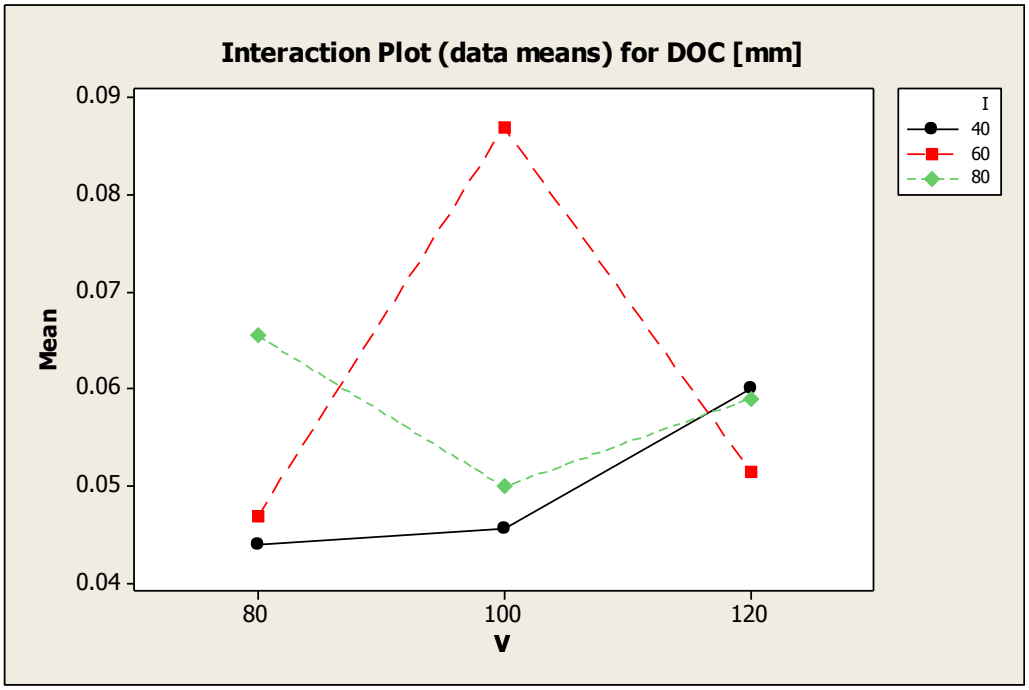

Figure 41: Interaction plot for DOC mean data as a function of I and V, d 300 µm, E 365

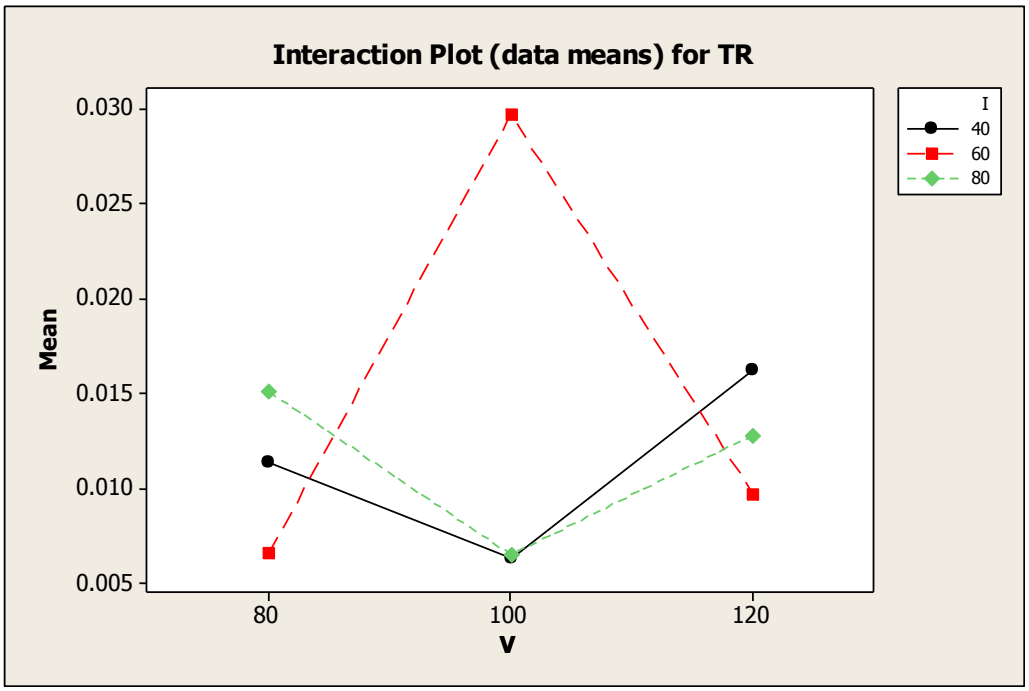

Figure 42: Interaction plot for TR mean data as a function of I and V, d 300 μm, E 365

The DOC and TR main effects plots clarify the effective influence of the factors on the final value of the indicator: in both cases the trend for the two is completely different, since for the voltage the maximum corresponds to the “medium” level of the factor (Figure 43 and Figure 44).

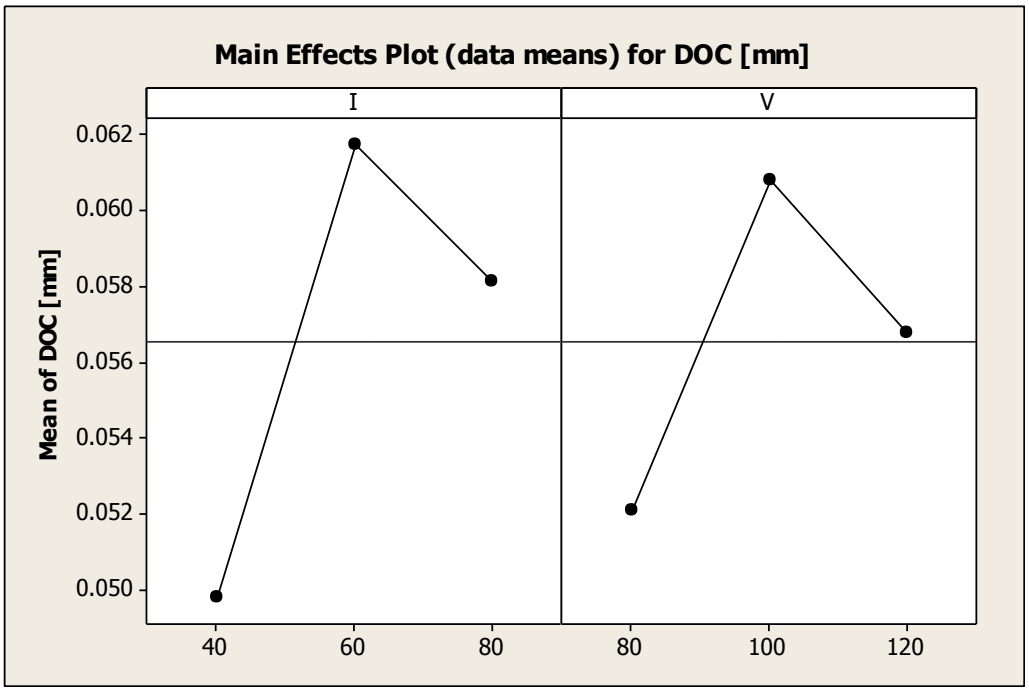

Figure 43: Main effects plot for DOC mean data as a function of I and V, d 300, µm E 365

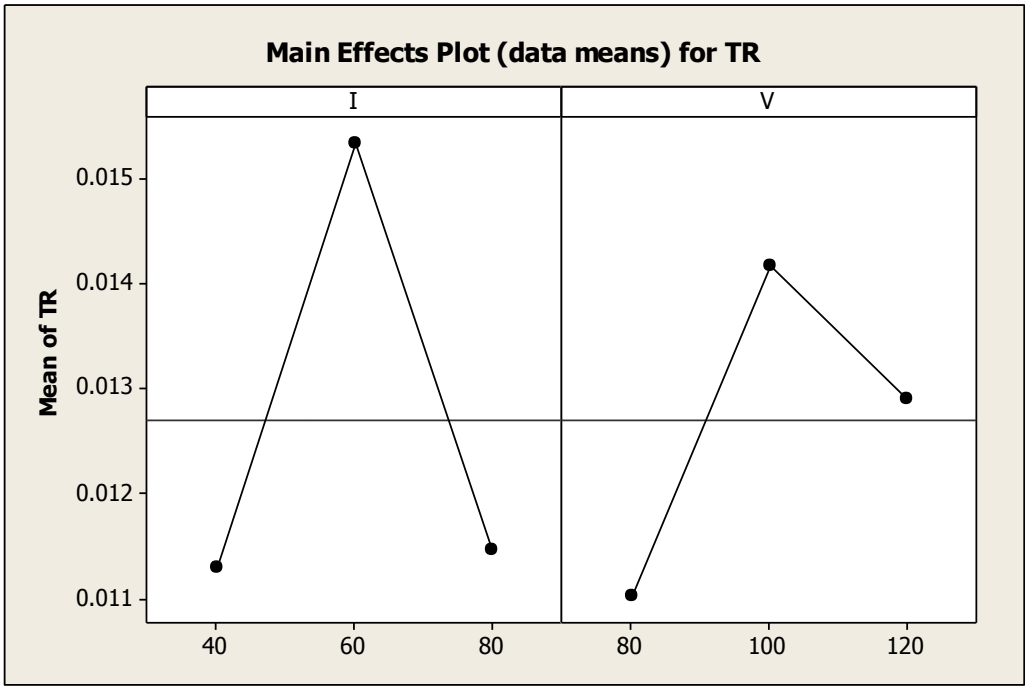

Figure 44: Main effects plot for TR mean data as a function of I and V, d 300 µm, E 365

TC, d 300 μm, E 206

The same analysis has been carried out for the experiments executed with the same electrode diameter (300 μm) and with low energy level (206).
Starting from this point of the dissertation, only the p-values from the analysis of variance will be shown and discussed since they are the most representative indicator of the factors' relevance. As mentioned before, the detailed data referring to the statistical analysis of variance is reported in the Appendix.

Table 21 reports the p-values for all the indicators. The machining time is influenced by the peak current (I), the voltage (V) and their combination (I*V) while the electrode wear and the DOC are only influenced by the combination of the factors, I*V. TR and MRR are not affected by the variation of I and V and their combination, while the TWR is only influenced by the voltage and I*V. The interaction effect of I and V is thus recorded even with the low level of energy. For the machining time, the peak current, the voltage and their combination have a relevant effect on the indicator, confirmed by the p-values that are all lower than the alpha limit. The interaction effect is shown in Figure 45, were curve's intersections are shown. The same conclusions can be drawn for the electrode wear (Figure 46).

Table 21: Analysis of variance p-values for d 300 μm and E 206

	t	Wear	DOC	TR	MRR	TWR
I	**0.028**	0.105	0.688	0.386	0.062	0.203
V	**0.018**	0.065	0.688	0.622	0.075	**0.046**
I*V	**0.009**	**0.002**	**0.021**	0.259	0.072	**0.028**

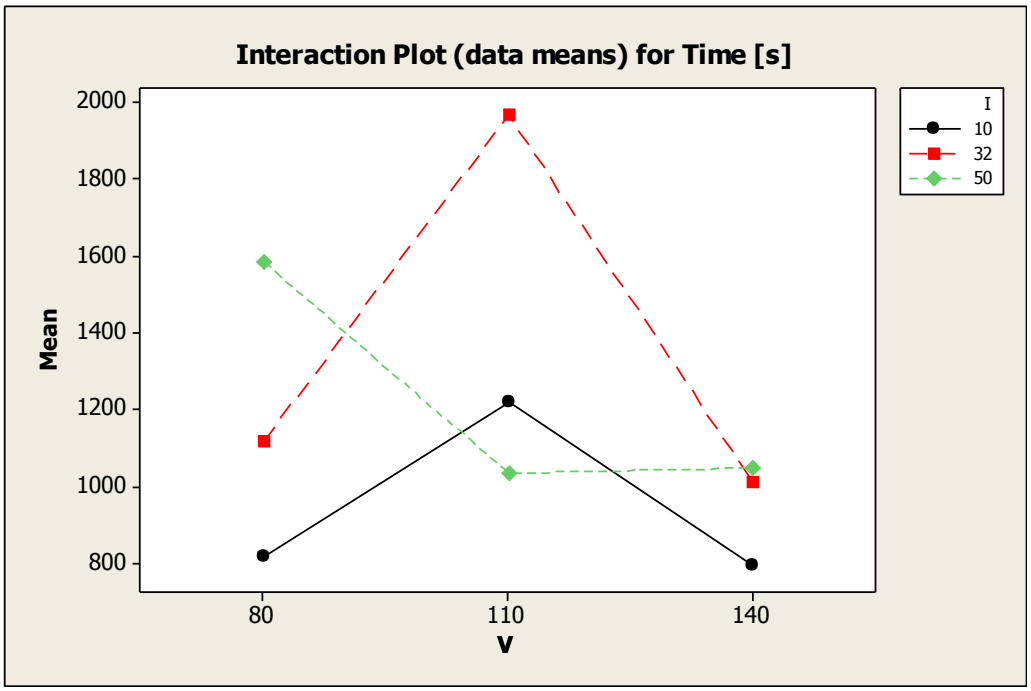

Figure 45: Interaction plot for machining time mean data as a function of I and V, d 300 μm, E 206

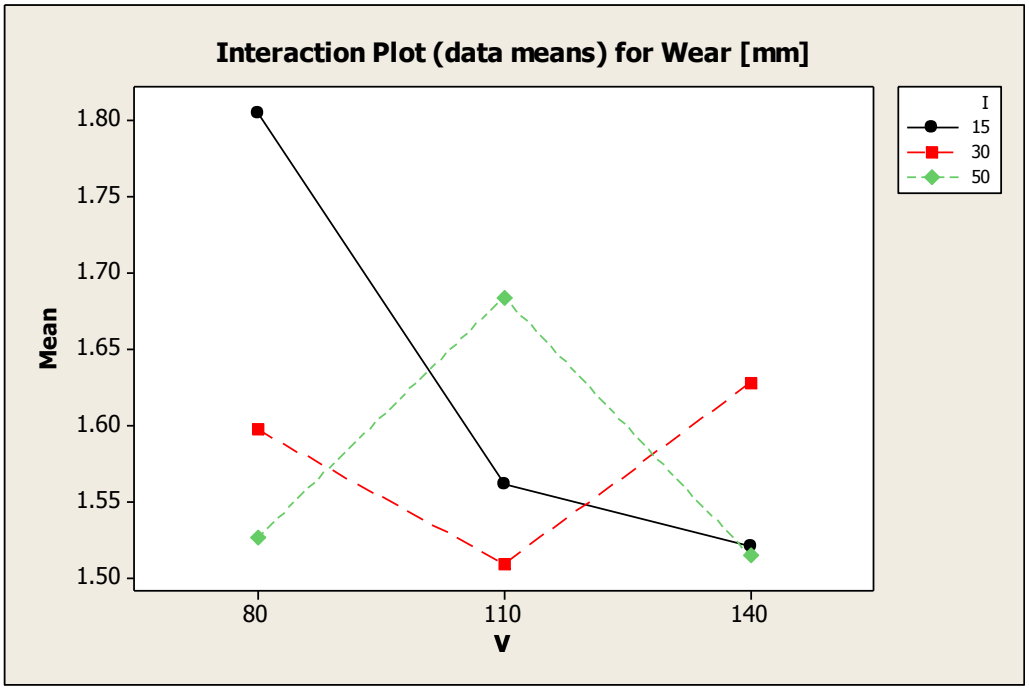

Figure 46: Interaction plot for electrode wear mean data as a function of I and V, d 300 μm, E 206

The main effects plots for both the indicators underline a considerable effect of the factors, but in both cases no direct proportionality can be found. The electrode wear main effects plot (Figure 47) can be considered representative of this situation: it is evident that the two factors affect the final value of the indicator, but with an opposite effect: for the peak current in fact, the "medium level" results in the maximum electrode wear, while for the voltage is the medium level that minimizes this physical phenomenon. The same pattern is recorded for the TWR indicator, as explained before. The same situation can be described for the geometrical indicator DOC. From both the main effects plots and the interaction plot it is evident how the interaction between the factors affects the final result (Figure 48 and Figure 49). In Figure 49 the maximum value of the DOC is ensured by the "medium" level of the indicators with a stronger effect of the voltage. In order to compare the results between the two energy levels, in Table 22 the p-values for both conditions are shown.

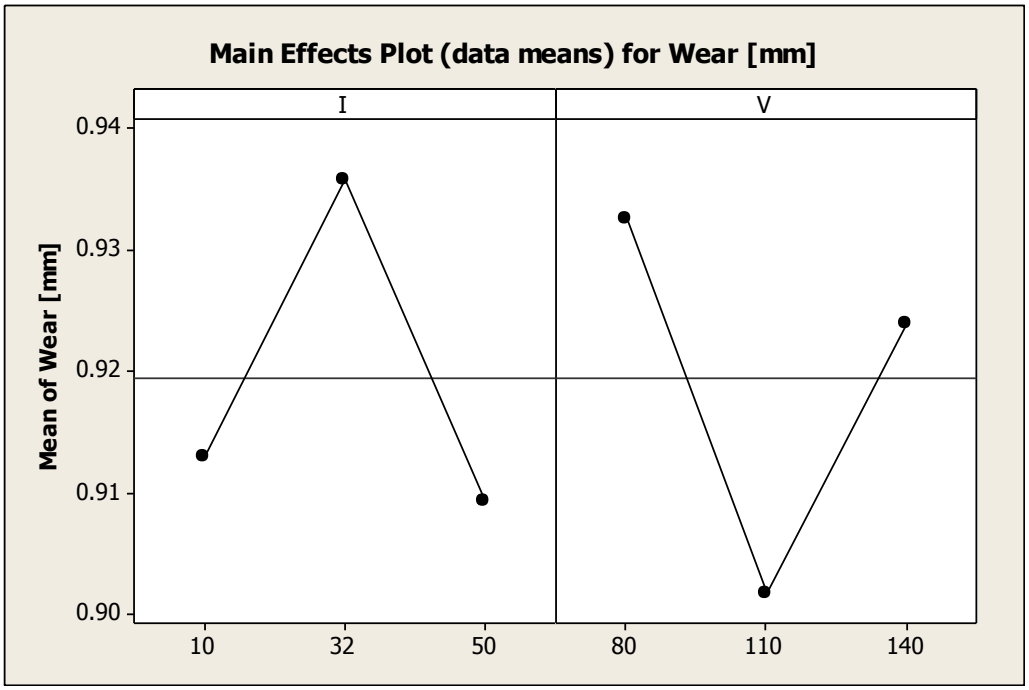

Figure 47: Main effects plot for electrode wear mean data as a function of I and V, d 300 μm, E 206

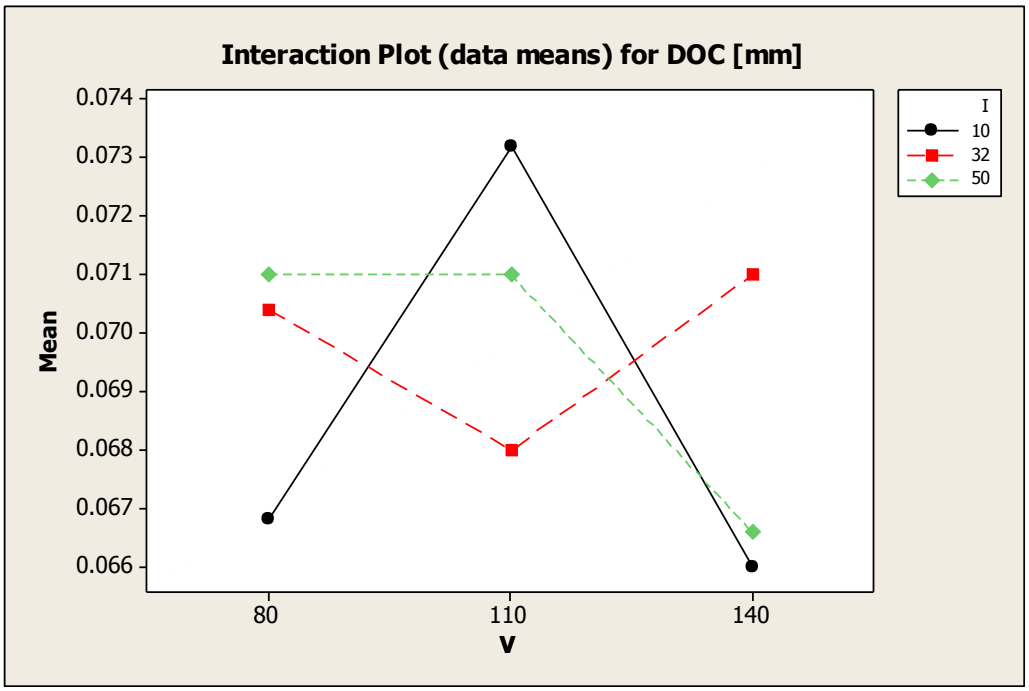

Figure 48: Interaction plot for DOC mean data as a function of I and V, d 300 µm, E 206

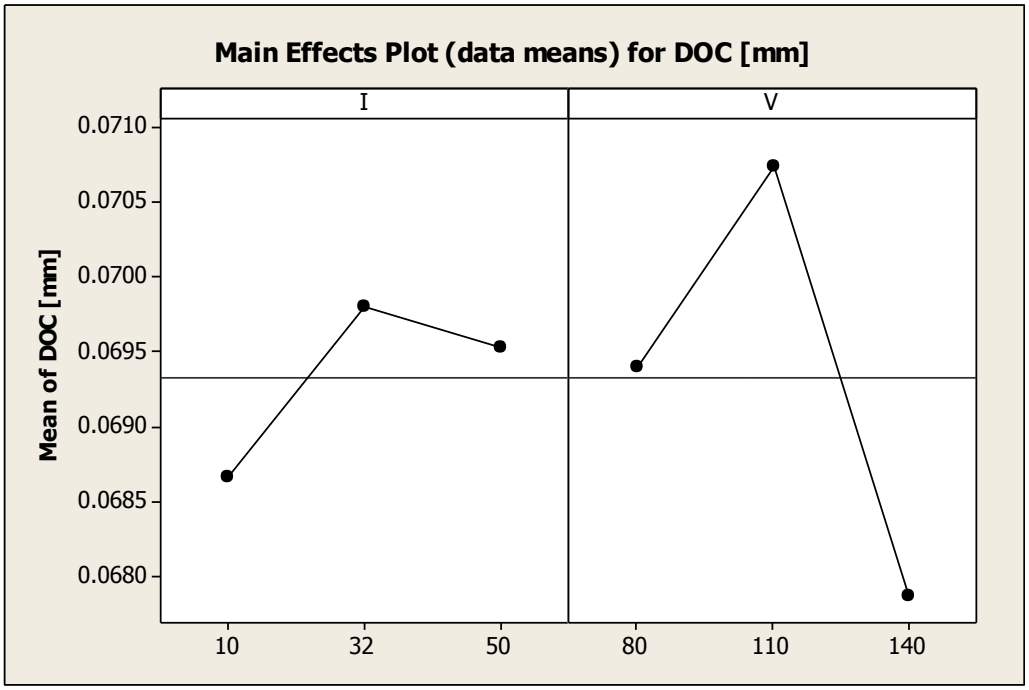

Figure 49: Main effects plot for DOC mean data as a function of I and V, d 300 µm, E 206

Table 22: Influence of the process parameters, d 300 µm, E206 and E365

Indicator	**Factors**	
	E365	**E 206**
Machining time	I, V	I, V, I*V
Electrode wear	I, V	V, I*V
DOC	I*V	I*V
TR	I*V	none
MRR	I, V	none
TWR	I, V	V, I*V

The energy level results in a completely different effect of the process parameters. Their influence, is more relevant for the high level of the energy if compared with the lower level. The same conclusion can be drawn for the interaction of the process parameters. These results underline the possibility to introduce the energy level as a factor of the model. This possibility is investigated in the second part of the present section.
For both energy levels, the interaction between the factors I and V is recorded, that is the only common pattern here identified. The same analysis have been executed for the 150 µm electrode diameter and the results will be discussed as follows.

TC, d 150 µm, E 365

Regarding the 150 micron diameter, Table 23 shows the indicators of the analysis of variance for the 365 energy level.

Table 23: Analysis of variance p-values for d 150 µm, E 365

	t	Wear	DOC	TR	MRR	TWR
I	**0**	**0**	**0**	**0**	**0**	**0**
V	**0**	**0**	**0**	**0**	**0**	**0**
I*V	**0**	**0**	**0.002**	**0**	**0**	**0**

In this case, all the indicators are strongly influenced by the process parameters and by their combination, too. Considering the machining time, a certain level of interaction has been recorded between the responses and the levels of the factors (Figure 50), even though it is not the most relevant so far.

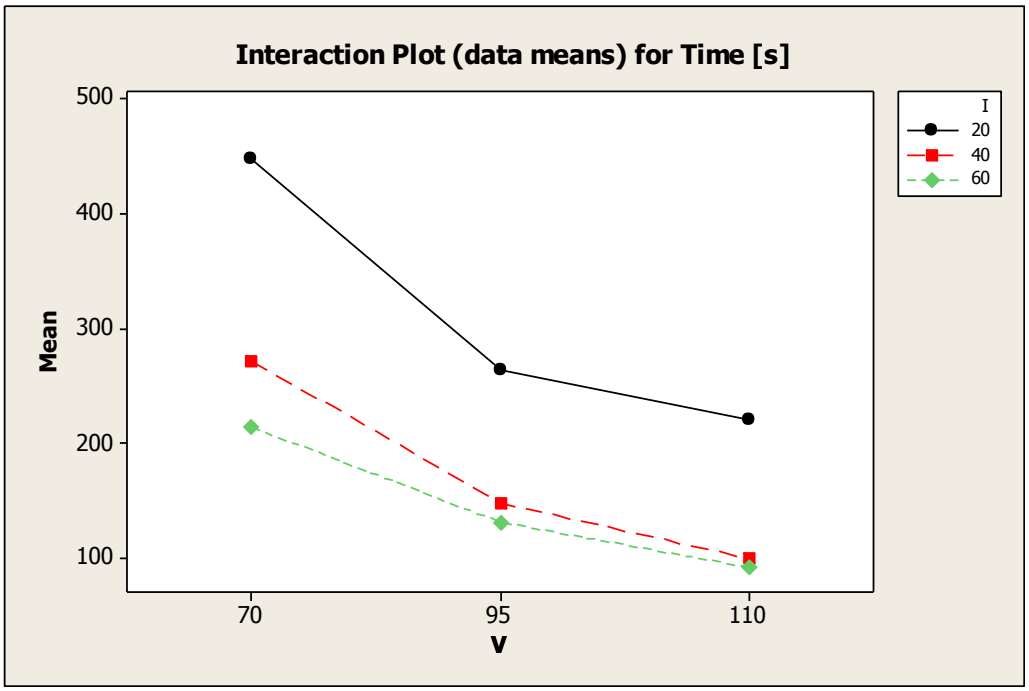

Figure 50: Interaction plot for machining time mean data as a function of I and V, d 150 µm, E 365

In this case, I and V have a similar effect on the machining time: the lower the mean value of the indicator the higher the machining time. This effect is explained by the aggressiveness of the process parameters that ensure the fastest removal process.

For all the process indicators, the effect of the factors' levels interaction is as relevant as the effect of the indicators considered singularly. The interaction plot and main effects plot for the electrode wear explain this kind of relationship.

In Figure 52 it is possible to find a certain interaction between the levels of the factors and the response (in this case the electrode wear). This plot is representative of all the interaction plots for DOC, TR, MRR and TWR indicators, that in order to simplify the analysis, are not here reported. The main effects plot for the electrode wear confirms this conclusion, since the trend for I and V are the opposite: the machining time mean data find the minimum and the maximum of the curves at the medium level of the factors, respectively. As mentioned before, the same conclusions can be drawn for the TWR.

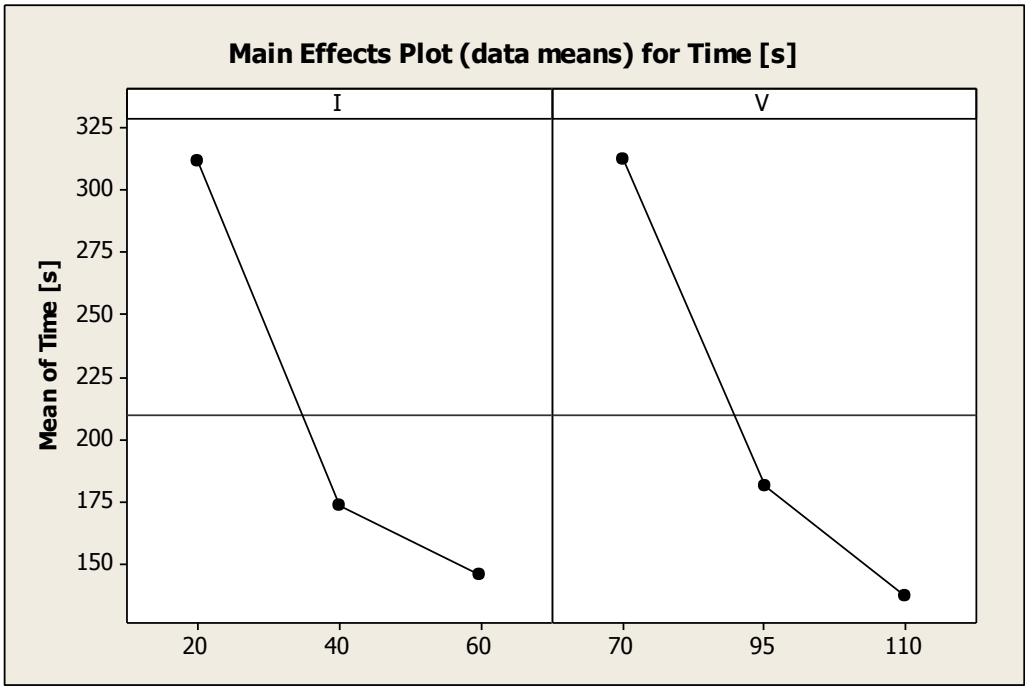

Figure 51: Main effects plot for machining time mean data as a function of I and V, d 150 μm, E 365

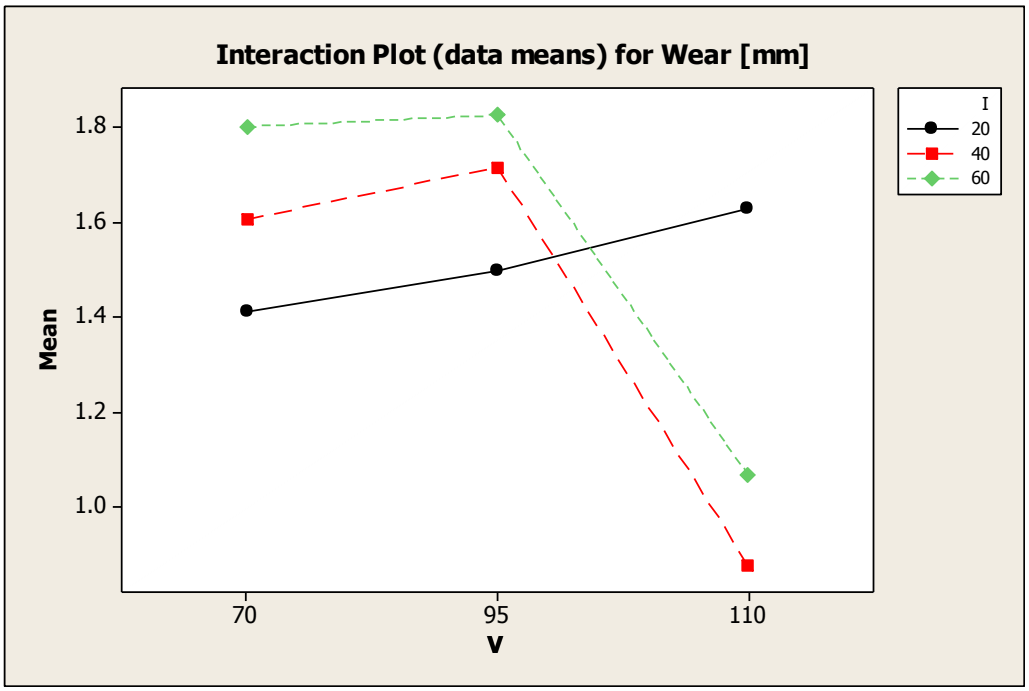

Figure 52: Interaction plot for electrode wear mean data as a function of I and V, d 150 µm, E 365

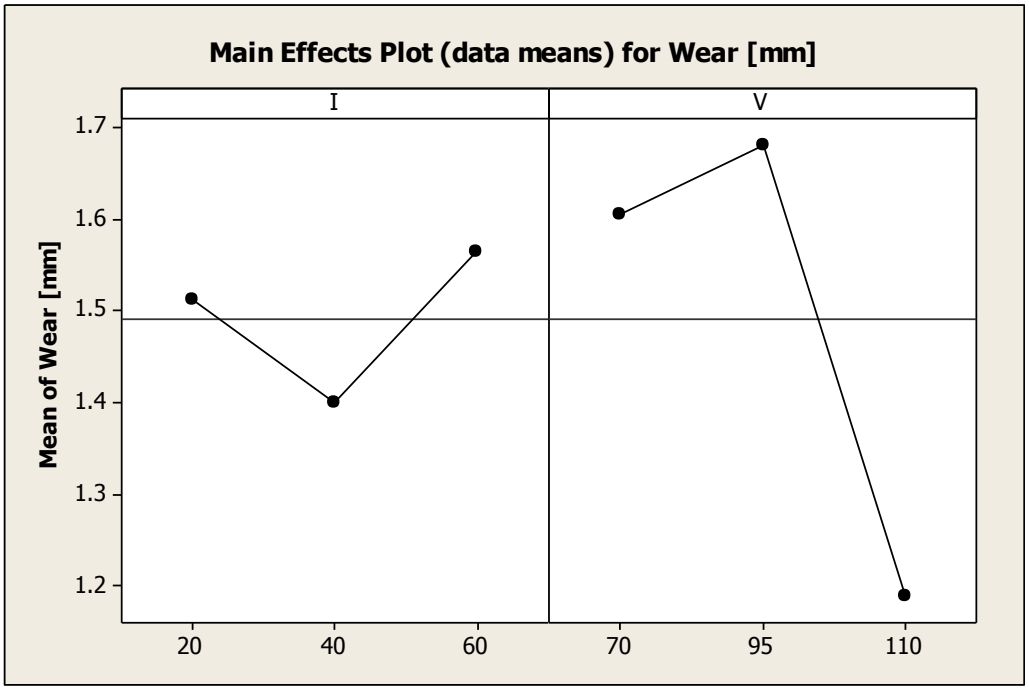

Figure 53: Main effects plot for electrode wear mean data as a function of I and V, d 150 µm, E 365

The influence of the peak current level is described by a monotonically increasing curve for both DOC and TR indicators (Figure 54 and Figure 55). This means that an increase in the peak current level results a worsening of the geometrical characteristics of the holes. The same cannot be concluded for the voltage.

Finally, for the MRR only a negligible interaction between the effects of the parameters on the response can be found (Figure 56). MRR trend is increasing monotone for both I and V levels (Figure 57). As for the 300 μm diameter, the following section describes the results obtained for the lower energy level.

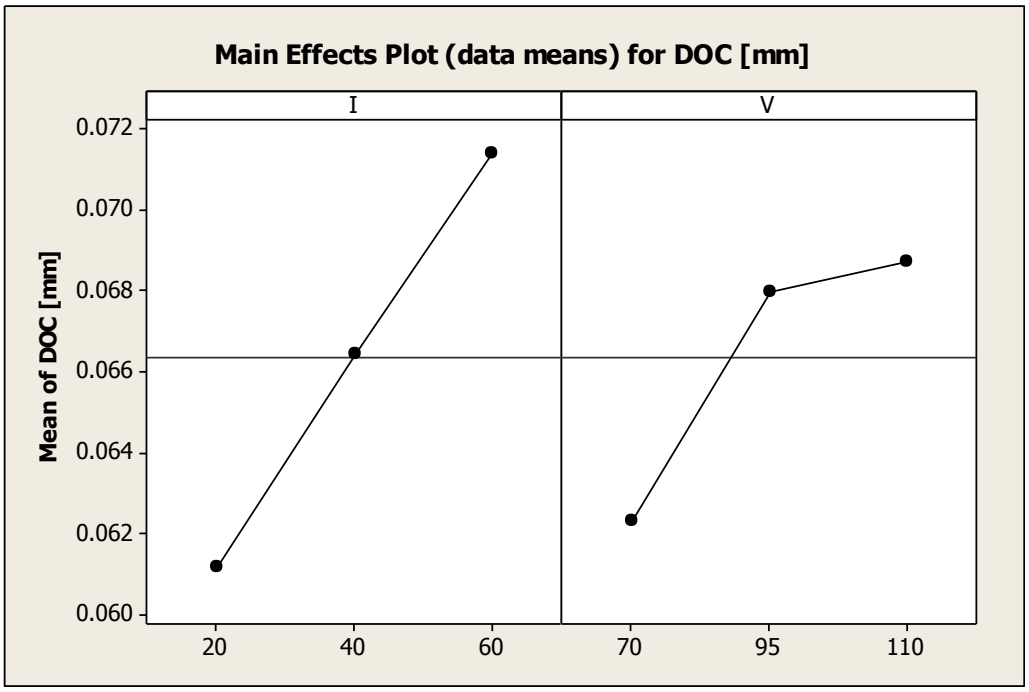

Figure 54: Main effects plot for DOC mean data as a function of I and V, d 150 μm, E 365

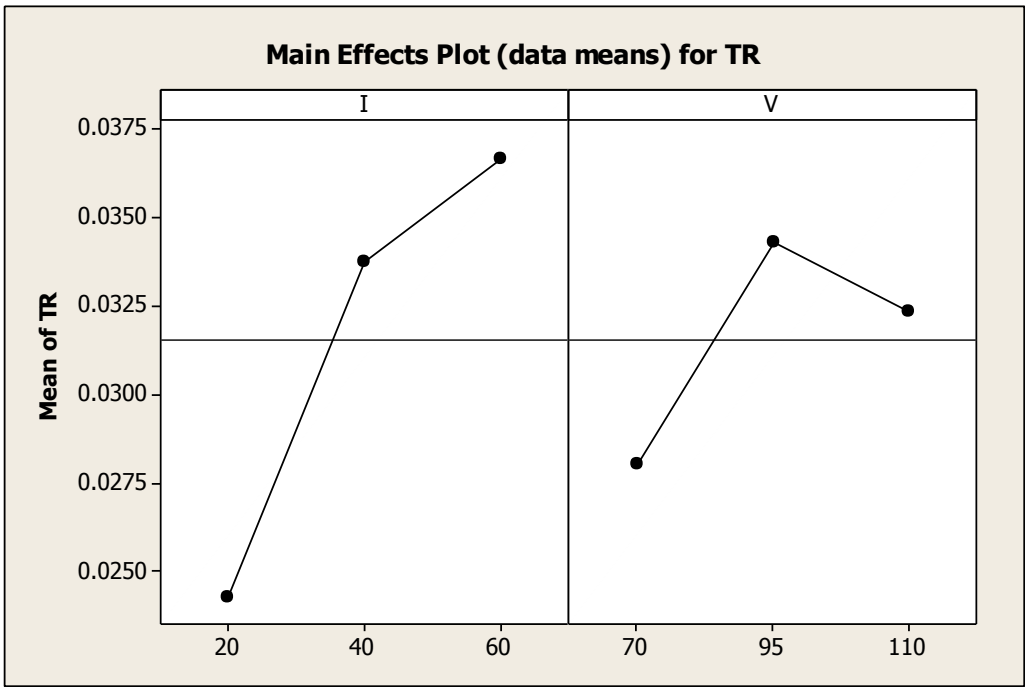

Figure 55: Main effects plot for TR mean data as a function of I and V, d 150 µm, E 365

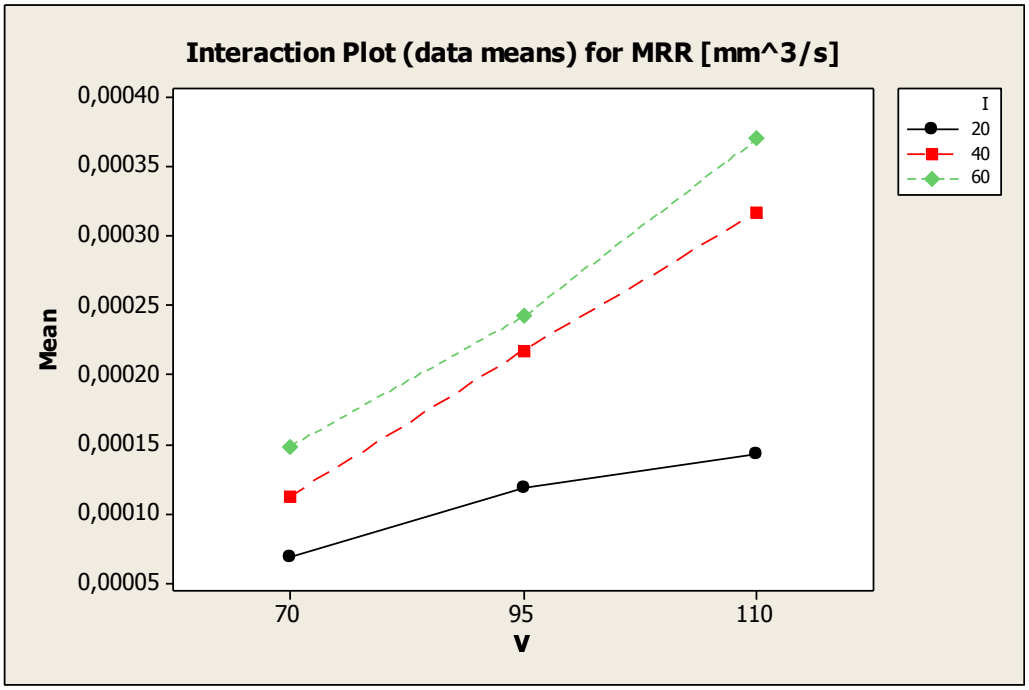

Figure 56: Interaction plot for MRR mean data as a function of I and V, d 150 µm, E 365

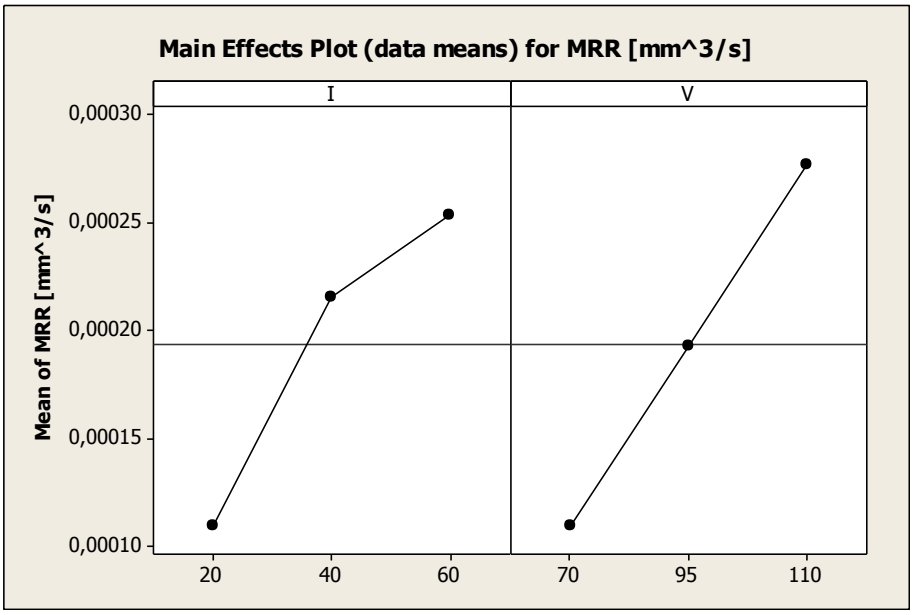

Figure 57: Main effects plot for MRR mean data as a function of I and V, d 150 μm, E 365

TC, d 150 μm, E 206

Table 24 summarizes the results for diameter 150 microns and energy level 206. It is possible to notice how the lower energy level affects the influence of the process parameters on the final response, similarly to the trend recorded for the 300 microns electrode diameter.

Table 24: Analysis of variance p-values for d 150 μm, E 206

	t	Wear	DOC	TR	MRR	TWR
I	**0.034**	0.481	0.620	0.599	0.106	0.559
V	**0.013**	0.209	0.798	0.564	0.200	0.130
I*V	**0.016**	**0.008**	0.171	0.271	0.173	0.189

In this case it is possible to notice that none of the indicators (DOC,TR, MRR and TWR) is consistently influenced by the factors of the model.

On the contrary, for the machining time and the electrode wear the combination of the parameters influence the final result. Moreover, the machining time is influenced by both peak current and voltage. For this reason the following analysis will take into account only the machining time and the electrode wear. Also in this case, an interaction between the factors is observed. Both machining time and electrode wear interaction plot's curves are characterized by intersections (Figure 58 and Figure 60). Figure 59 and Figure 61 show the main effects plot for the machining time and the electrode wear. These results confirm the conclusions drawn for the 300 μm diameter: the high energy level results in a more relevant influence of the process parameters.

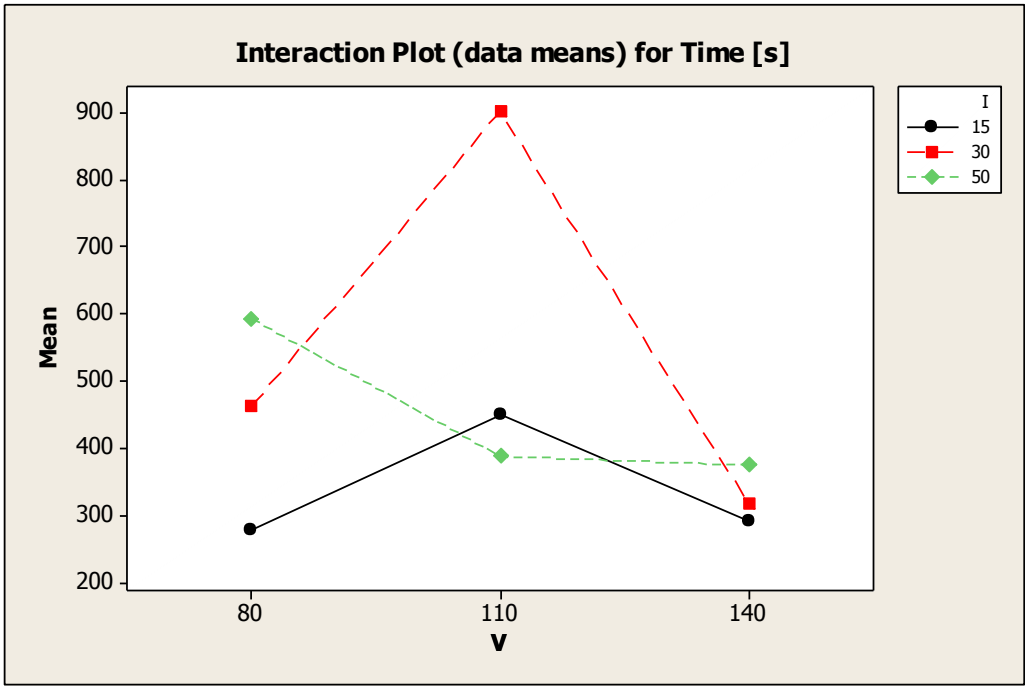

Figure 58: Interaction plot for machining time mean data as a function of I and V, d 150 μm, E 206

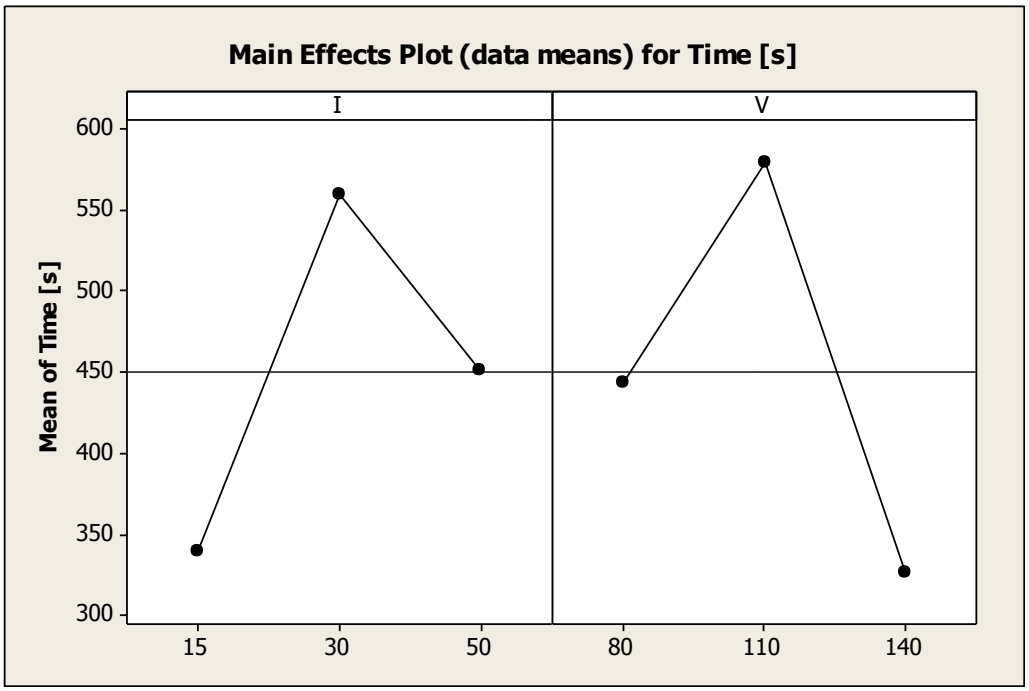

Figure 59: Main effects plot for machining time mean data as a function of I and V, d 150 µm, E 206

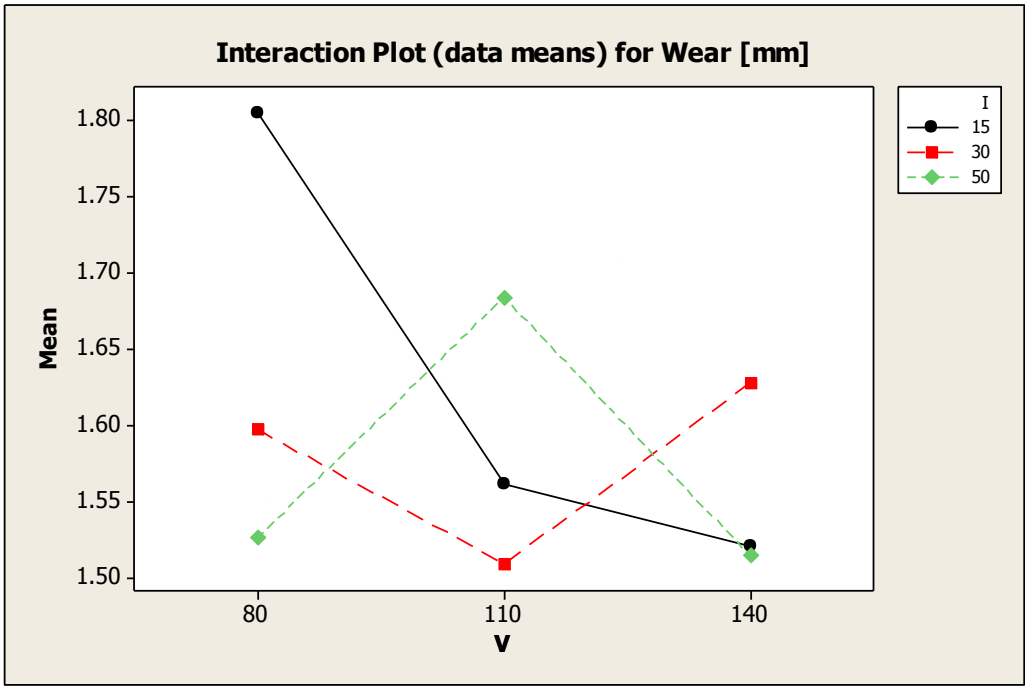

Figure 60: Interaction plot for electrode wear mean data as a function of I and V, d 150 µm, E 206

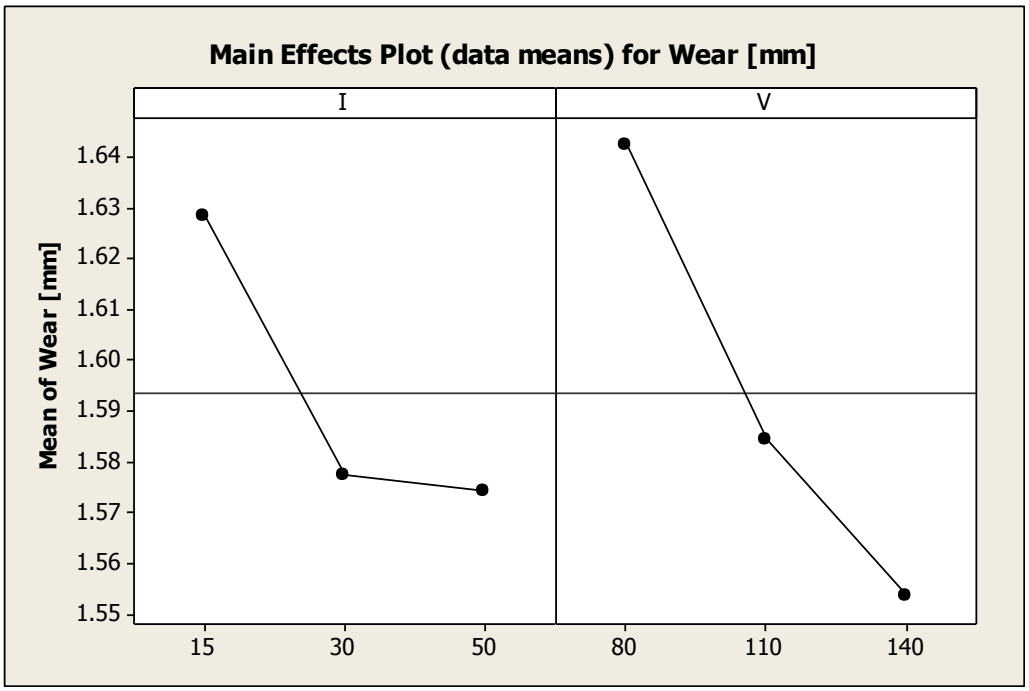

Figure 61: Main effects plot for electrode wear mean data as a function of I and V, d 150 μm, E 206

A summary of the final result for diameter 150 micron is reported below in Table 25.

Table 25: Influence of the process parameters, d 150 μm, E 206 and E 365

Indicator	**Factors**	
	E365	**E 206**
Machining time	I, V, I*V	I, V, I*V
Electrode wear	I, V, I*V	I*V
DOC	I, V, I*V	None
TR	I, V, I*V	None
MRR	I, V, I*V	None
TWR	I, V, I*V	None

It is possible to notice how, for the energy level 206, the influence of the process parameters becomes negligible if compared with the possible influence of other factors not considered yet, such as the energy level and the electrode material. This could be due to a possible influence of the energy level, as underlined for the 300 μm electrode. Moreover, also in this case a certain interaction between the factors is evident.

It is possible to conclude from the analysis carried out so far that the energy level has the most relevant influence on the final response. Moreover, the interaction between the factors is the only common aspect between all the process conditions (diameter and energy level) even though no common trend can be found. The persistent interaction between the two factors (I and V), shown in all the plots, can be representative of possible hidden phenomena or relationship between the parameters, that deserve to be investigated. In order to deepen the knowledge and better interpret the results, the energy level was introduced as a third factor in the plan. The next section will describe the details of the analysis.

4.2.1.2 Second level of Analysis: I , V and E

TC, d 300 μm

In the present section the analysis was carried out including the energy as a factor in the model. It is evident from the p-values comparison that the energy level is a factor having a considerable effect on the indicators. Table 26 shows the output of the analysis of variance.

The interaction plot underlines how the energy level influences the response (in this case, for the electrode wear).

It is evident that the electrode wear for the low energy level is less influenced by the process parameters if compared with the response for the high level of the energy, as shown in Figure 62 and Figure 63.

Table 26: Analysis of variance p-values for d 300 µm

	t	Wear	DOC	TR	MRR	TWR
I	**0.023**	**0.045**	0.111	**0.021**	**0.064**	**0.034**
V	**0.014**	**0.002**	0.082	0.094	**0.249**	**0.001**
E	**0.000**	**0.000**	**0.000**	**0.014**	**0.000**	**0.000**
I*V	**0.006**	0.566	**0.042**	**0.015**	0.668	0.640
I*E	**0.026**	**0.113**	**0.043**	0.377	**0.038**	**0.075**
V*E	**0.018**	**0.008**	0.282	0.233	**0.274**	**0.004**
I*V*E	**0.008**	0.819	**0.003**	**0.003**	0.643	0.598

A similar effect of the energy can be demonstrated for the machining time, but with an opposite trend as shown in Figure 64. In this case, for the high energy, the effect of the process parameters is less remarkable.

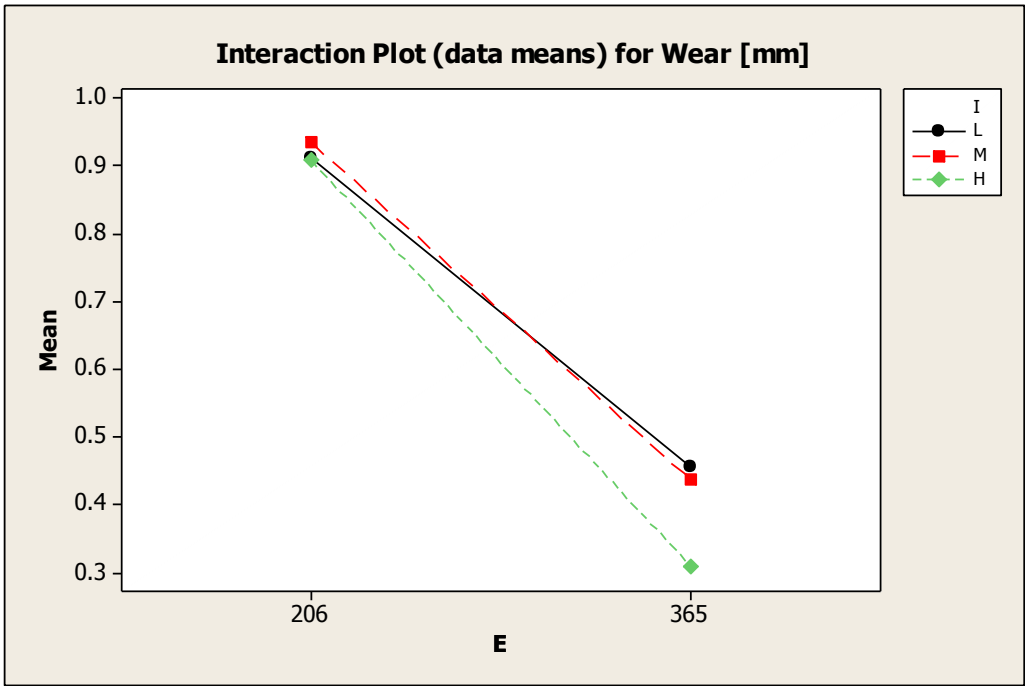

Figure 62: Interaction plot for electrode wear mean data as a function of I and E, d 300 µm

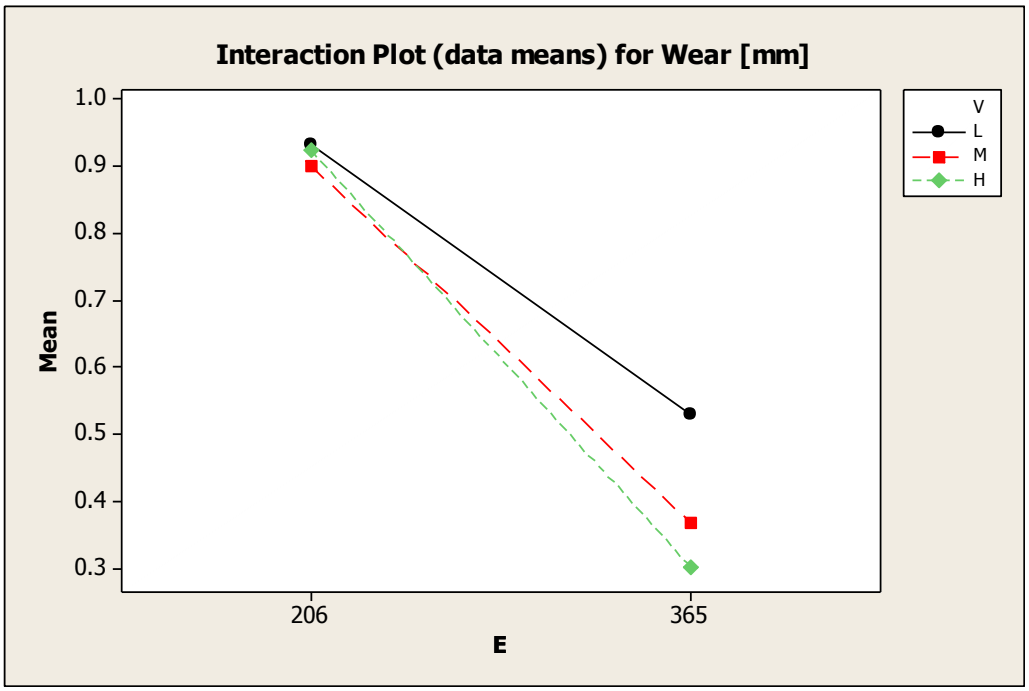

Figure 63: Interaction plot for electrode wear mean data as a function of V and E, d 300 μm

Figure 64: Interaction plot for machining time mean data as a function of I, V and E, d 300 μm

Such an effect of the energy factor is confirmed for the others indicators, as shown in Figure 65 and Figure 66.

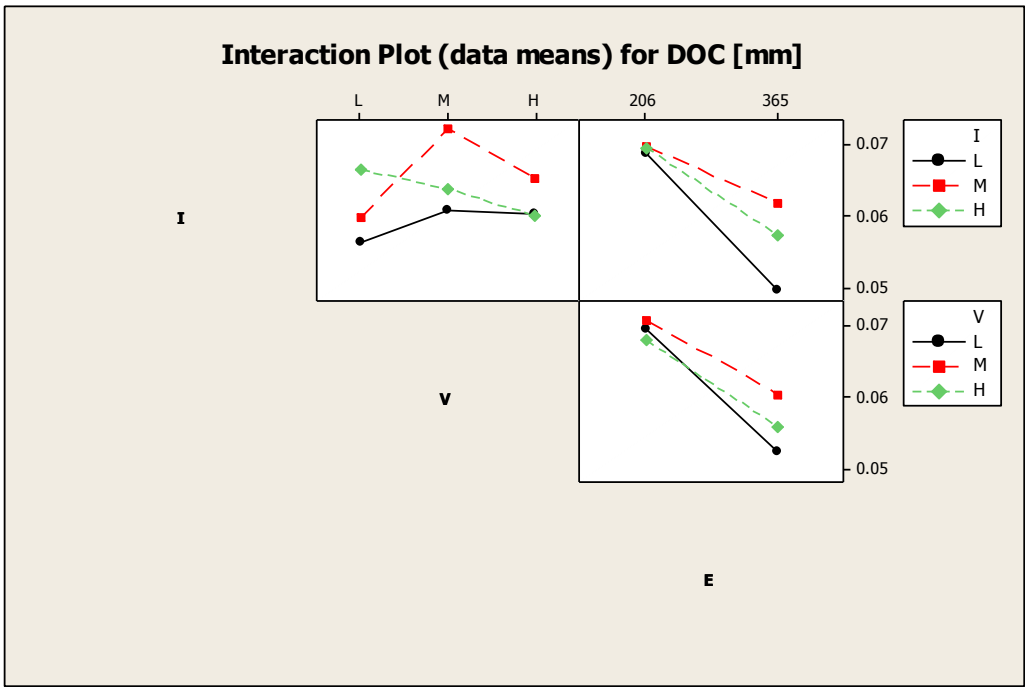

Figure 65: Interaction plot for DOC mean data as a function of I, V and E, d 300 µm

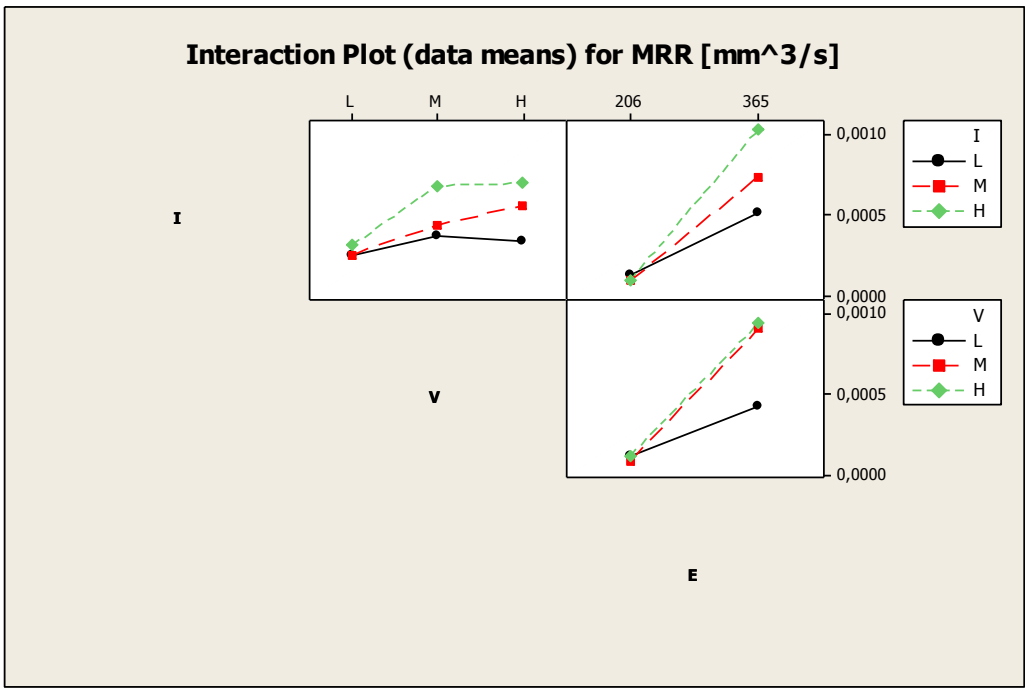

Figure 66: Interaction plot for MRR mean data as a function of I, V and E, d 300 µm

In order to have more detailed information about the influence of the energy level on the indicators, the interval plot graph has been used in order to produce the error bar graphs. The data has been divided into two panels, high energy level (365) and low energy level (206) and the standard error have been taken into account for the plot. The current and voltage level have been codified as “high” (H), “medium” (M) and “low” (L) in order to uniform the x axis for a better understanding of the plot (Figure 67). It is possible to notice that the higher energy level is characterized by higher standard error: for this reason, the 206 energy shape ensures a better process control. As mentioned before the effect of the process parameters, if compared with the effect of the energy level, is negligible. For the high level of the energy a common trend can be found: the electrode wear is always higher for low levels of the voltage. The same conclusions can be drawn considering the peak current as main variable of the analysis, as reported in Figure 68. From the analysis carried out so far, it is evident that the energy deserves to be introduced as a factor in the model. As a matter of fact, it results to be the most relevant factor (Figure 69) if compared with I and V.

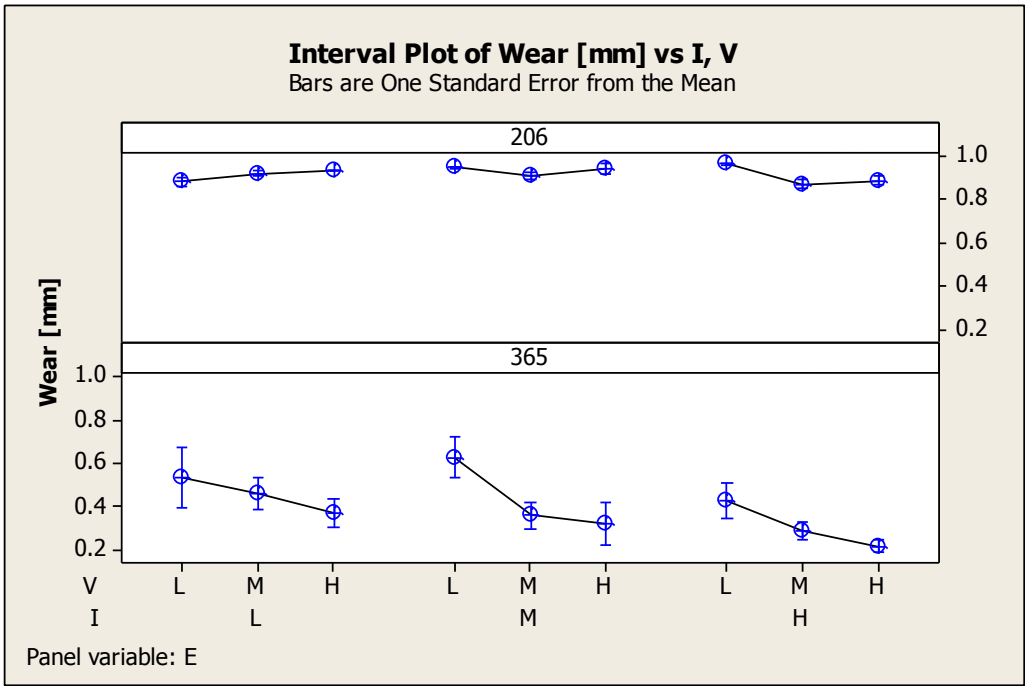

Figure 67: Interval plot for electrode wear as a function of I and V panelled considering E, d 300 μm

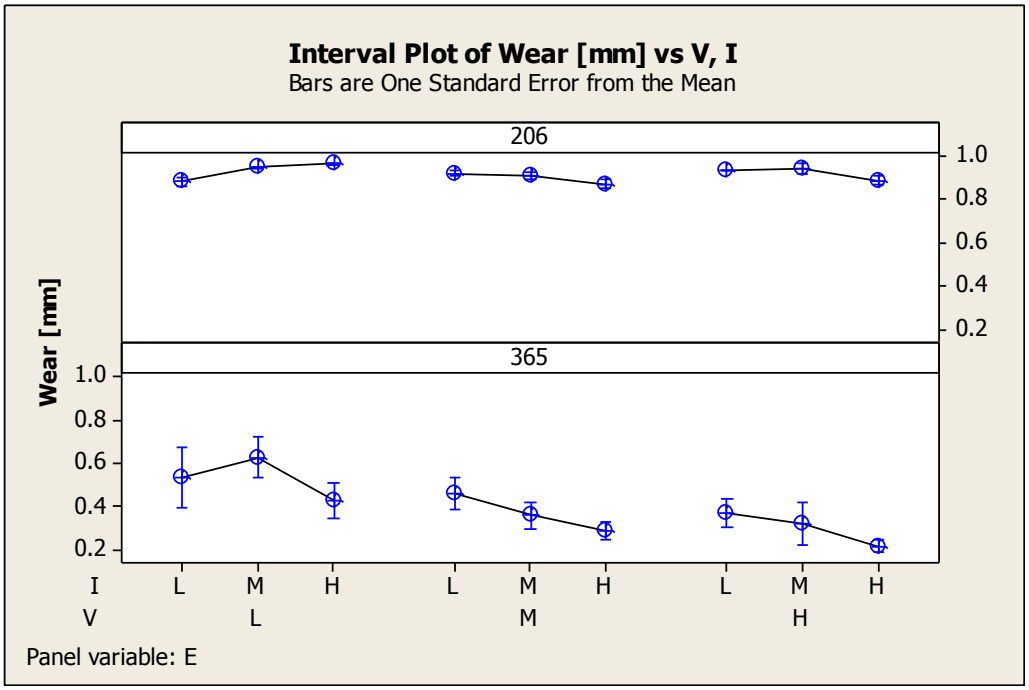

Figure 68: Interval plot for electrode wear as a function of V and I panelled considering E, d 300 µm

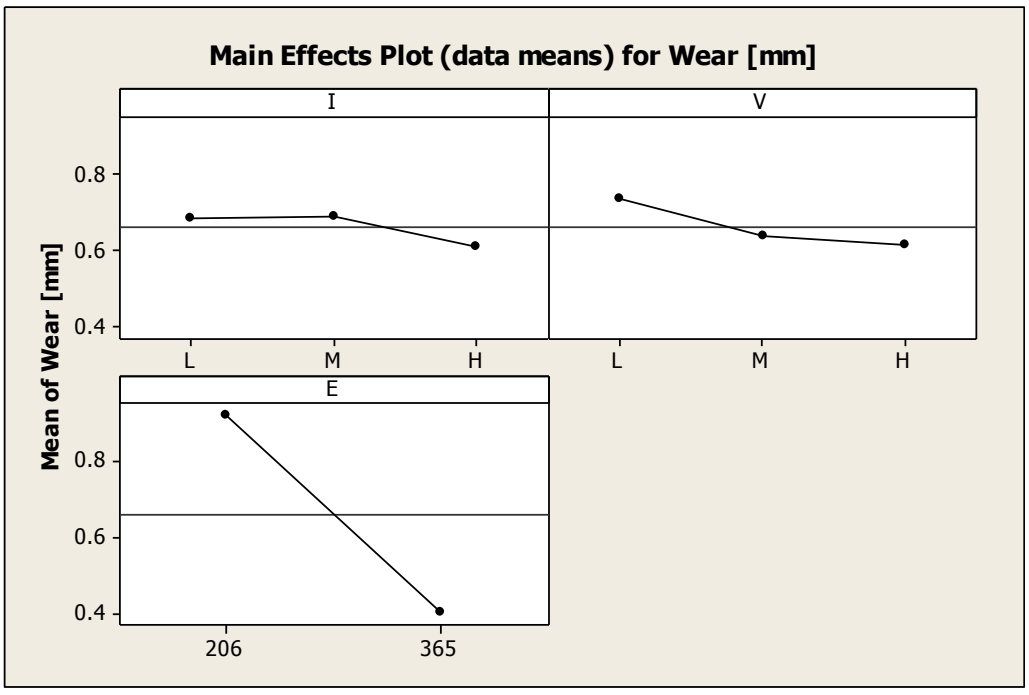

Figure 69: Main effects plot for electrode wear as a function of I, V and E, d 300 µm

Similar results have been identified for all the other indicators, testifying that the influence of the process parameters is determined by other aspects of the process, in this case the energy. The relevance of the energy level is confirmed by the main effects plot, too (Figure 69). The same analysis has been executed for the TC electrode 150 μm diameter. The results are summarized as follows.

TC, d 150 μm

In Table 27 the p-values obtained from the analysis of variance for all the factors is shown.

Table 27: Analysis of variance p-values for d 150 μm

	t	Wear	DOC	TR	MRR	TWR
I	0.071	0.548	0.782	0.868	0.280	0.497
V	**0.012**	0.397	0.425	0.943	0.309	0.406
E	**0.000**	0.062	**0.000**	**0.000**	**0.000**	**0.043**
I*V	**0.030**	0.936	0.471	0.715	0.735	0.997
I*E	**0.039**	0.415	0.612	0.659	0.486	0.586
V*E	**0.048**	0.897	0.874	0.573	0.712	0.882
I*V*E	**0.036**	0.241	0.511	0.787	0.823	0.596

It is evident that also in this case the energy is the factor influencing the majority of the indicators. The only exception is for the machining time, for which all the parameters except the peak current are relevant in the analysis.
Similarly to the 300 μm, for the 150 μm case the energy affects the response for different I and V levels, as shown in the following interaction plots (Figure 70 to Figure 74).

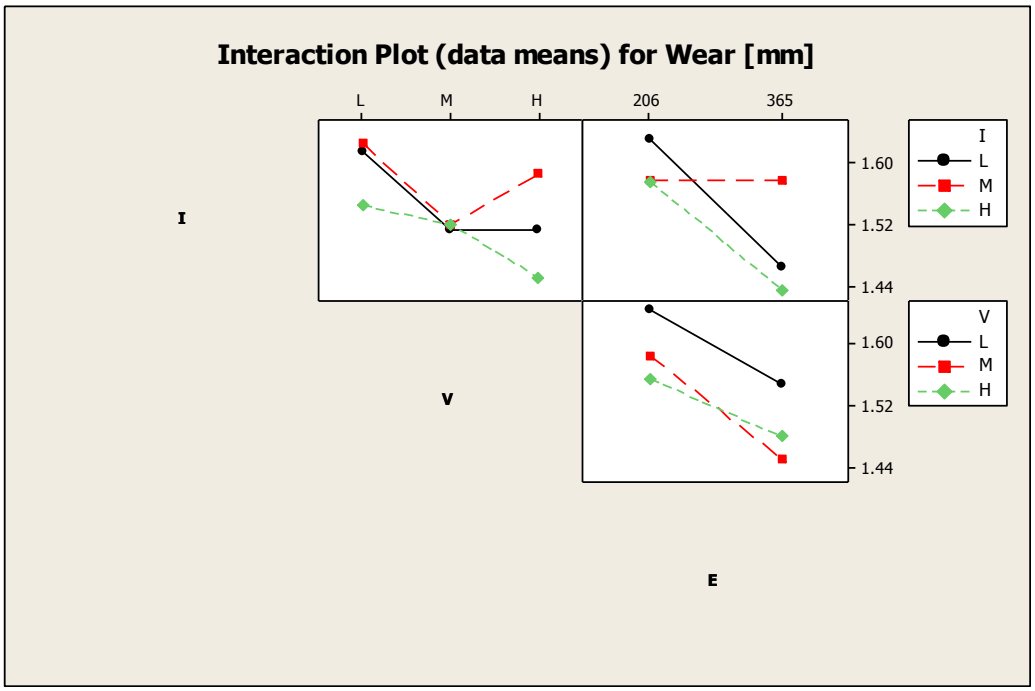

Figure 70: Interaction plot for electrode wear mean data as a function of I, V and E, d 150 µm

Figure 71: Interaction plot for machining time mean data as a function of I, V and E, d 150 µm

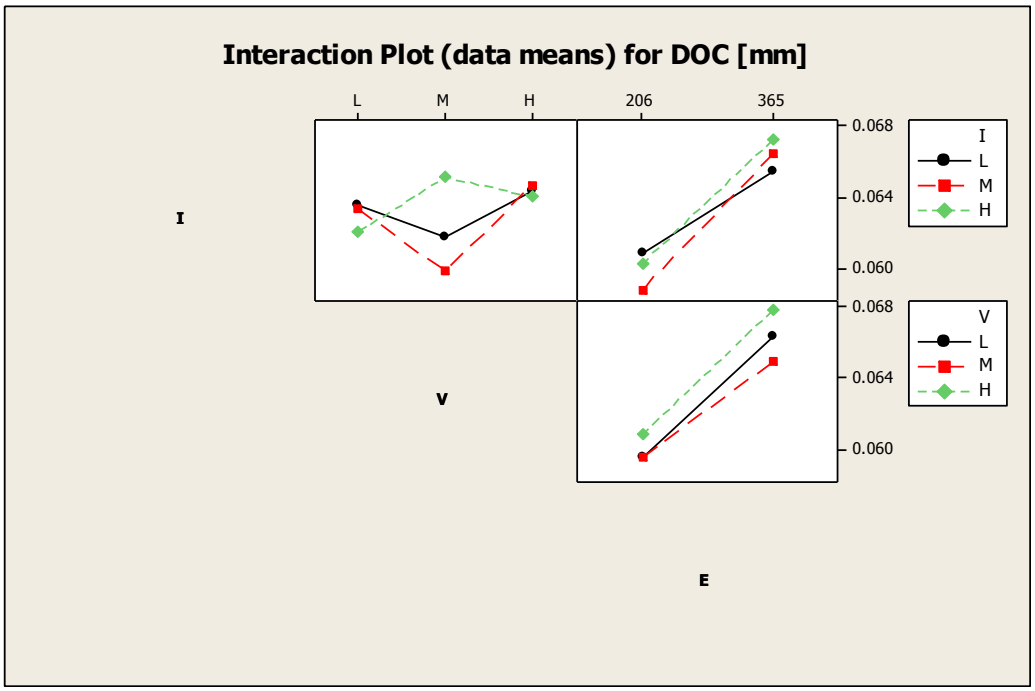

Figure 72: Interaction plot for DOC mean data as a function of I, V and E, d 150 µm

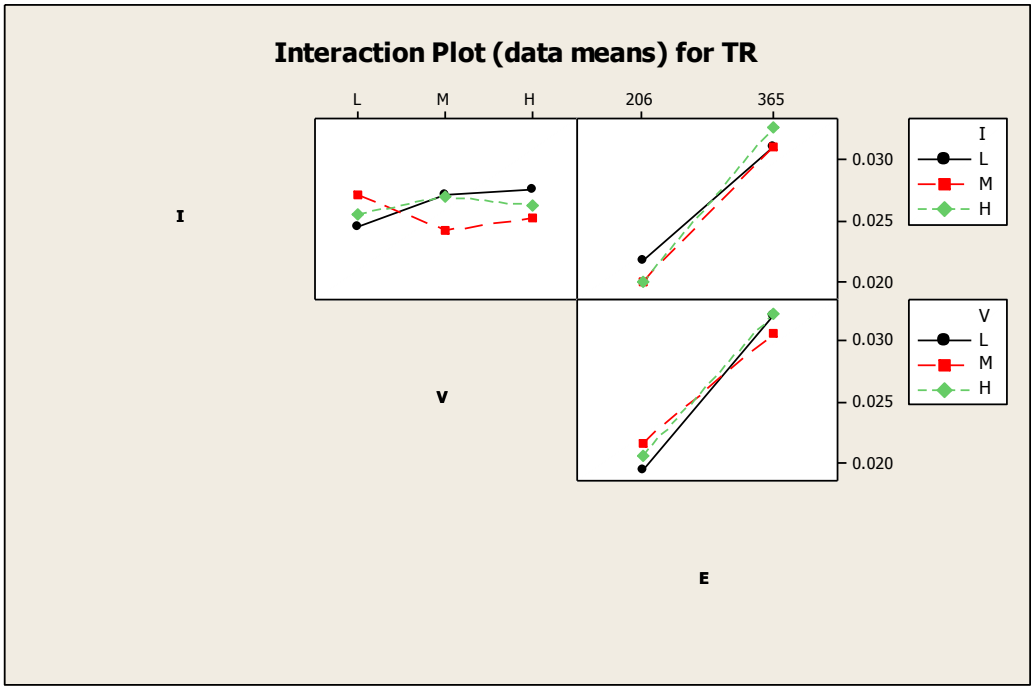

Figure 73: Interaction plot for TR mean data as a function of I, V and E, d 150 µm

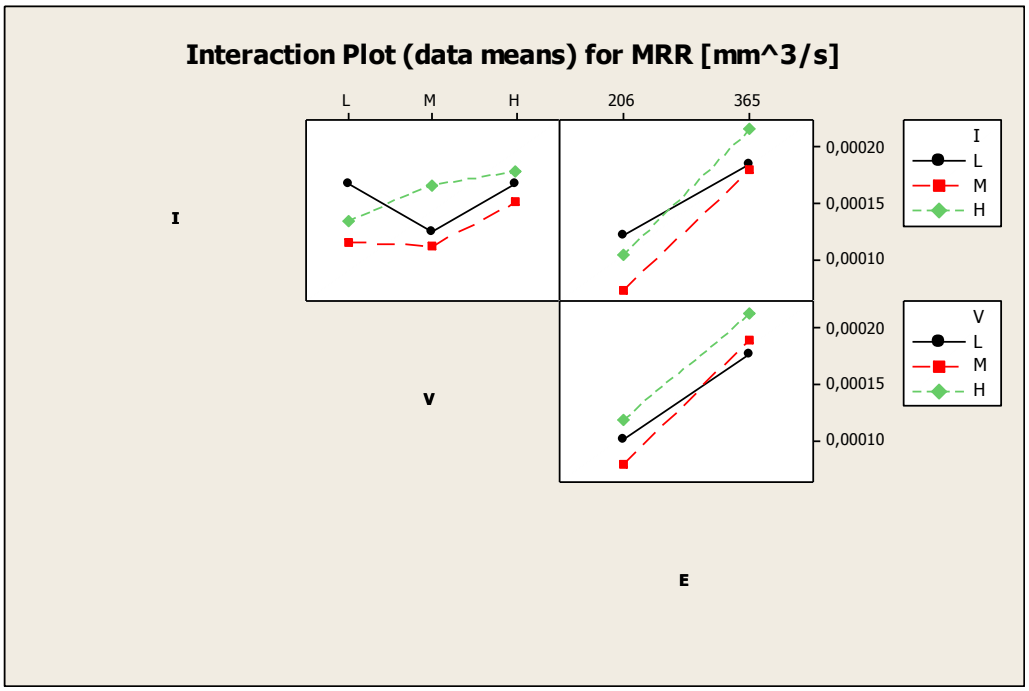

Figure 74: Interaction plot for MRR mean data as a function of I, V and E, d 150 µm

The interval plots (in Figure 75 and Figure 76) confirm the better process control ensured by the lower energy level, but no significant trend with the process parameters' combination can be found, neither for I (Figure 75) nor for V (Figure 76) factor. The main effects plot (Figure 77) confirms the result obtained for the 300 µm diameter, in other words confirms the relevance of the energy level if compared with the other factors.

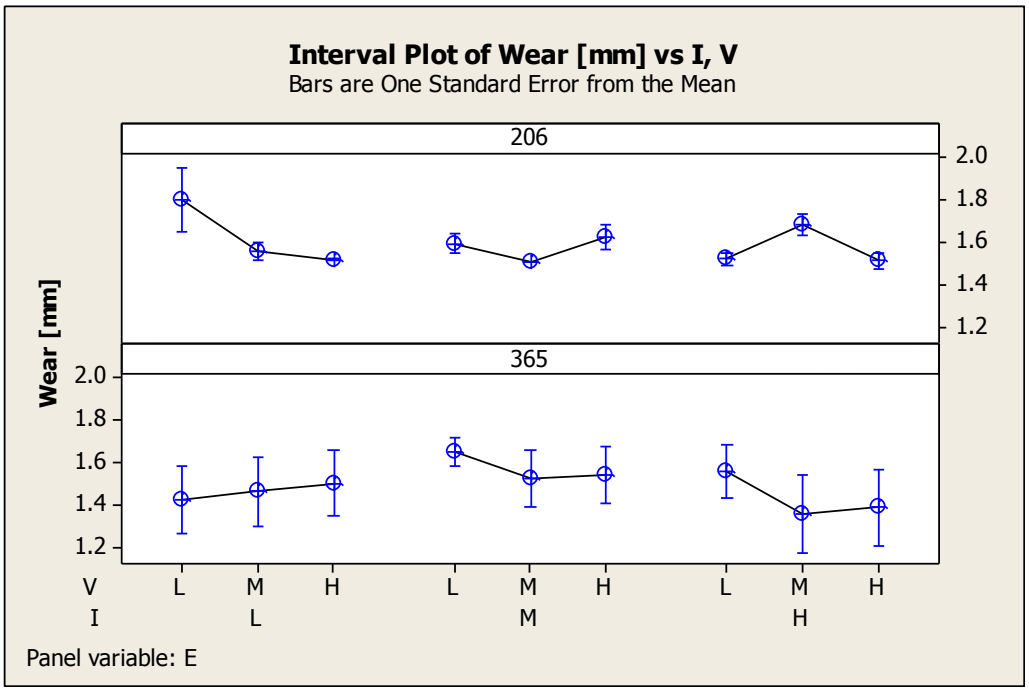

Figure 75: Interval plot for electrode wear as a function of I and V panelled considering E, d 150 μm

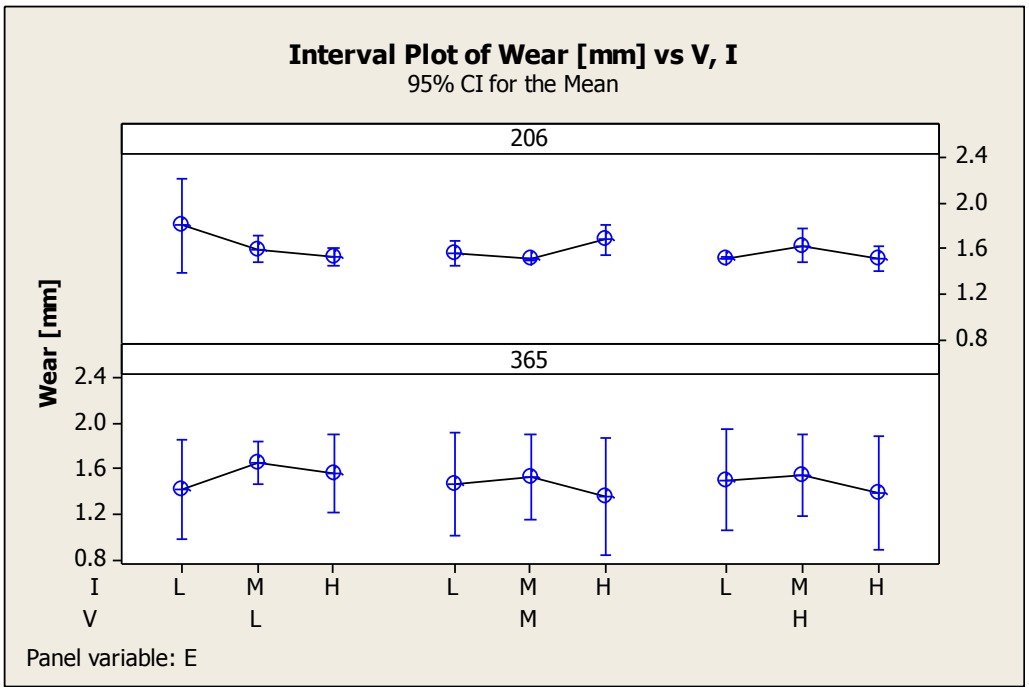

Figure 76: Interval plot for electrode wear as a function of V and I panelled considering E, d150 μm

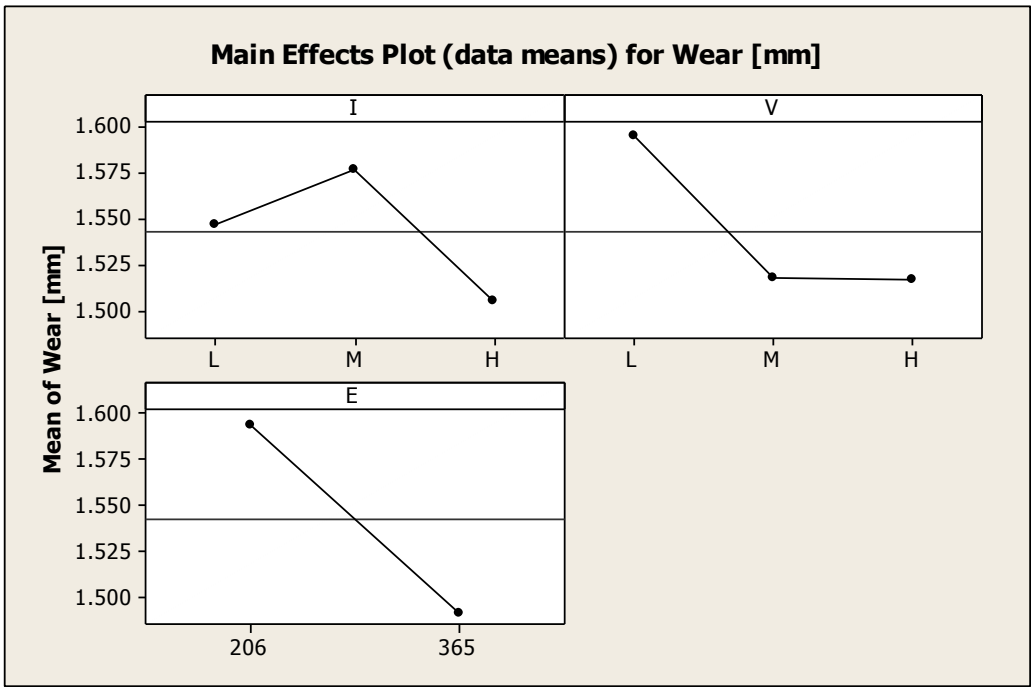

Figure 77: Main effects plot for electrode wear as a function of I, V and E, d 150 µm

From the analysis carried out so far, it is evident the influence of the energy level as well as the combined effect of the peak current and the voltage on the final output. This phenomenon was confirmed for both diameters. In order to investigate how these factors and their interaction influence the final result, the power exchanged during the process was taken into account as independent variable.

The definition of electrical power is shown in the following equation:

$$p(t) = i(t) \cdot V(t)$$

Where *p* is the power, *t* the time interval, *I* is the peak current and *V* is the peak voltage. As a matter of fact, the electrical power exchanged during the process was considered the most comprehensive indicator, able to identify not only the effective influence of the process parameters, but how these parameters influence the final value.

The information about the real power exchanged during the process was collected with the acquisition system dedicated to the Sarix machine that was previously described. In particular it was possible to collect information about:

- sparks per second (S/s);

- energy per spark (E/s);

From this starting point, it was possible to obtain the mean value of the exchanged power, expressed in watts, multiplying the energy per spark (E/s) by the sparks per second (S/s). The first part of the analysis was focused on the study of the real distribution of the electric power as a function of the process parameters combinations and on the verification of the correspondence between the indexes representing the process parameters' combinations (L-L, L-M, L-H, …, H-H) and the effective power exchanged during the process.

As mentioned before, the process parameters were varied on three levels each (codified as low, medium and high). For this reason the first combination corresponded to the low level for the peak current and the low level for the voltage, the second combination corresponded to the low level of the peak current and the medium value of the voltage and the third corresponded to the low level of the peak current and the high value of the voltage, et cetera. At the end of the analysis the power exchanged was plotted as a function of the nine different process parameters' combination. Figure 78 and Figure 79 show the trend obtained for both electrode diameters and energy levels.

It is demonstrated that the process parameters in this case are representative of the increasing power within the same peak current level: for all the peak current levels the voltage index is directly proportional to the electric power.

Secondly, it appears clear that the 365 energy level really corresponds to a more aggressive machining process: in other words, this wave shape corresponds to a higher electrical power exchanged between the tool and the electrode. On the contrary, the 206 energy wave shape is characterized by a lower level of the exchanged power.

Moreover, it is possible to notice the effect of the voltage within the three peak current data groups, low, mean and high. For example, considering the first three bars of the histogram (corresponding to the low level of the peak current and the low, medium and high levels of the voltage), it is possible to notice that the increasing values of the voltage correspond to an increasing value of the exchanged power. The same consideration can be drawn for the medium and high level of the peak current.

These plots confirm the assumptions made in the DOE design: it was assumed that the highest value of the peak current combined with the highest value of the voltage

corresponds to the highest power exchanged. Similar conclusions are drawn for the 150 µm electrode diameter. In other words, the trend of the indicators was evaluated as a function of the electrical power for the three different groups of the peak current level (low, medium and high), in order to investigate the influence of the voltage within each group.

Since the effective transitivity between the process parameters' indexes and the exchanged power is verified, the trends of the main indicators (DOC, TR, MRR and TWR) and of the two most relevant aspects of the process (machining time and electrode wear) were evaluated in this first stage of the analysis as a function of the electrical power at the same time taking into account the process parameters combination.

In this case the mean values of the five repetitions for each process parameters' combination were taken into account. Figure 78 and Figure 79 refer to the tungsten carbide electrode having diameter equal to 300 µm and 150 µm. For the sake of simplicity, only the more representative of the actual trends were here commented.

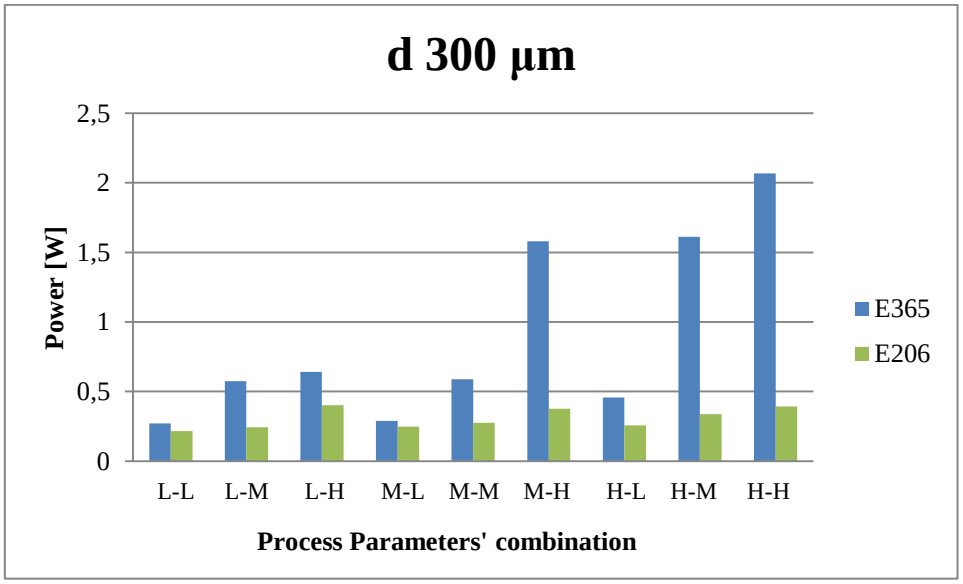

Figure 78: Electrical power as a function of the process parameters' combination, d 300 µm, E 365 and E 206

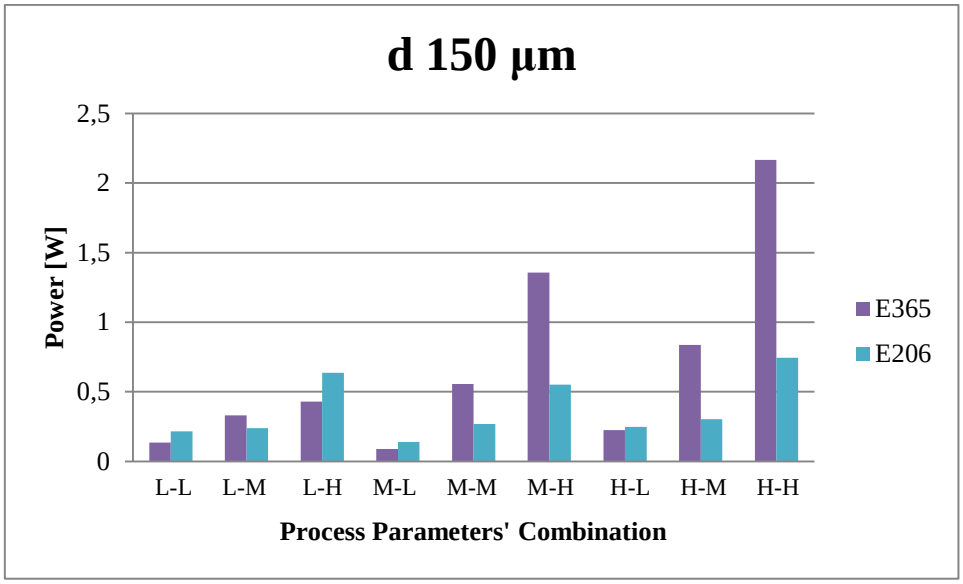

Figure 79: Electrical power as a function of the process parameters' combination, d 150 µm, E 365 and E 206

As regards the machining time, it is possible to notice a considerable effect of the energy level: for the 365 wave shape, a significant influence of the process parameters can be found, as shown in Figure 80 and Figure 81. In both cases, the power increment corresponds to decreasing machining durations. Moreover, the 365 energy level results in a faster erosion process.

In order to neglect the effect of the process parameters combination the machining time data was plotted as a function of the only electrical power, neglecting the process parameters' order, as shown in Figure 82. The 365 energy plot was considered representative of the trend identified for the 206 that, for the sake of simplicity is not here reported.

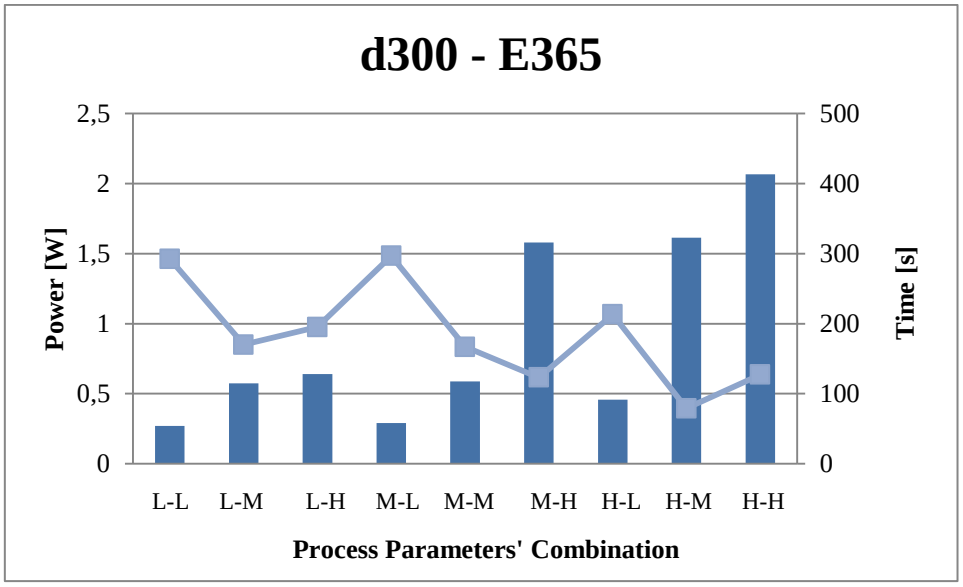

Figure 80: Machining time and electrical power as a function of the process parameters' combination, d 300 µm, E 365

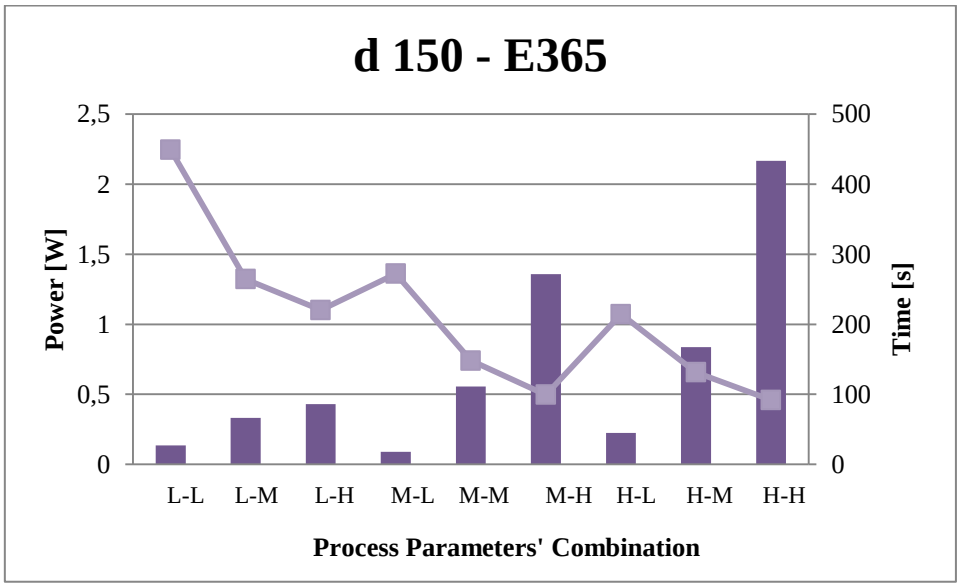

Figure 81: Machining time and electrical power as a function of the process parameters' combination, d 150 µm, E 365

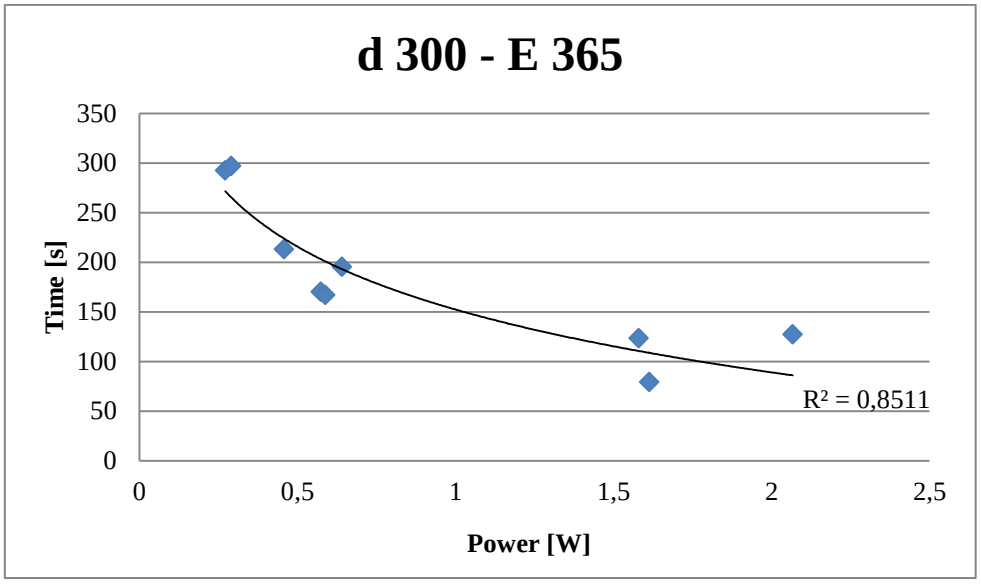

Figure 82: Machining time as a function of the electrical power, d 300 and E 365

It is evident how the electrical power affects the machining time: for increasing values of the exchanged power, the machining time is dramatically reduced. Regarding the electrode wear, it is possible to notice a similar but opposite effect: for high level of the electrical power, a lower electrode wear is recorded (Figure 83 and Figure 84).

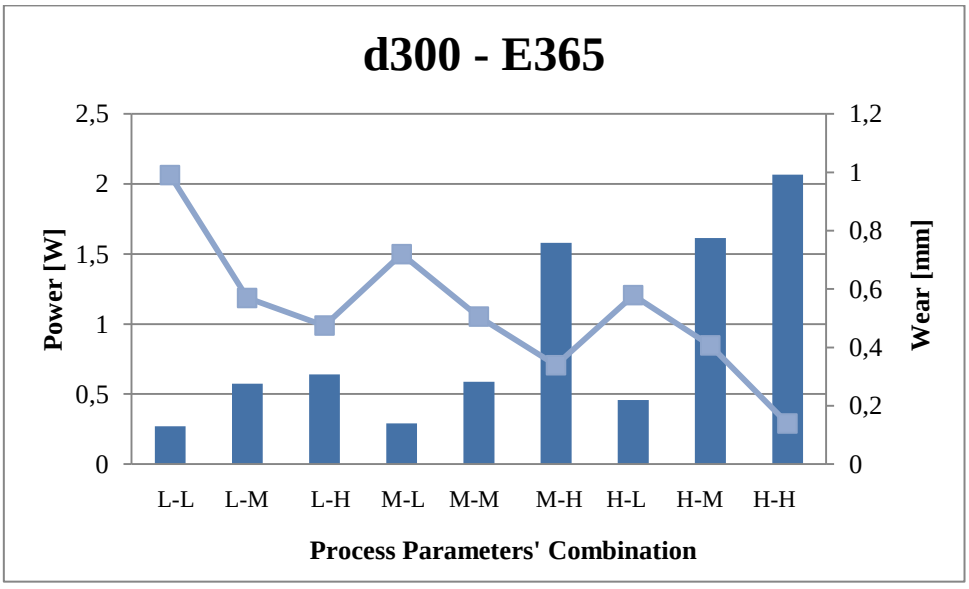

Figure 83: Electrode wear and electrical power as a function of the parameters' combination, d 300 μm, E 365

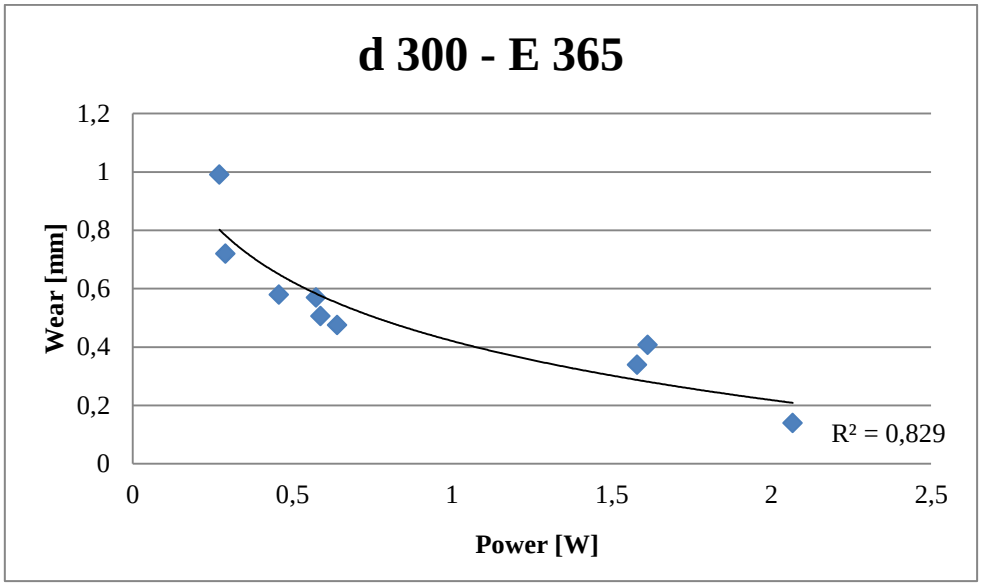

Figure 84: Electrode wear as a function of the electrical power, d 300 µm, E 365

This means that the higher the power the lower the electrode erosion. This result can be unexpected and misleading if not well explained. A possible explanation is the following: the higher the machining power the faster the process, and a faster process results in a lower electrode wear.

Regarding the process performance indicators, in particular the MRR, the same effect of the energy level is recorded: the 206 energy level ensures a damping as shown in Figure 85 and Figure 86. For the high energy level, a certain trend can be found: for increasing electrical power values an increment of the material removal rate is recorded: in other words, higher levels of the power result in a more aggressive and fast machining process. A similar trend is found for the 150 µm electrode, as shown in Figure 87. Figure 88 shows the MRR trend as a function of the electric power: this plot confirms the directly proportional effect of the electrical power and the machining time. As regards the TWR indicator, for increasing values of the electric power, a decrement in the indicator is found. This means that for increasing electrical power the amount of material removed from the workpiece is higher than the material removed from the tool. In other words, the machining process gets more effective. Figure 89 and Figure 90 show this effect of the exchanged power. Figure 91 confirms the dumping effect of the 206 energy level.

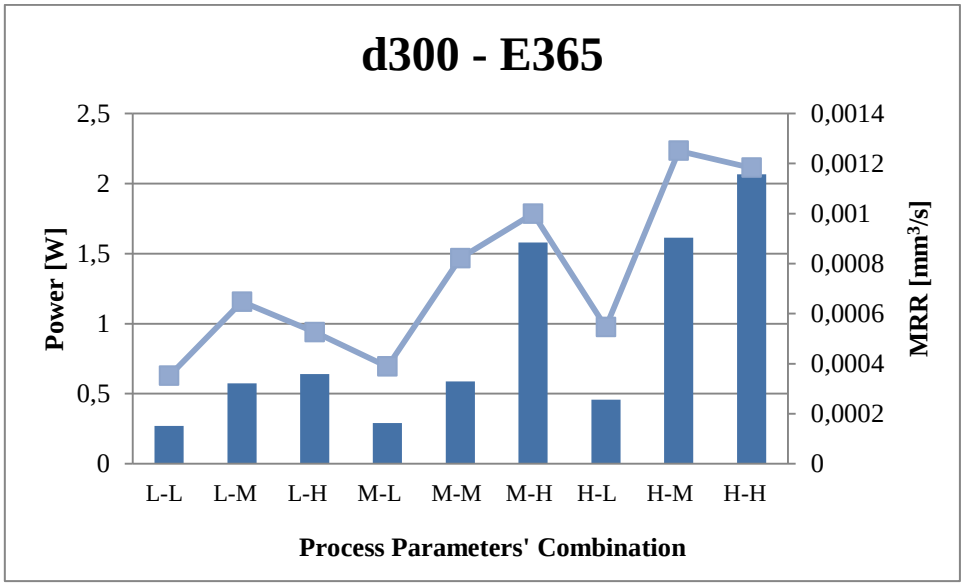

Figure 85: MRR and electrical power as a function of the process parameters' combination, d 300 µm, E 365

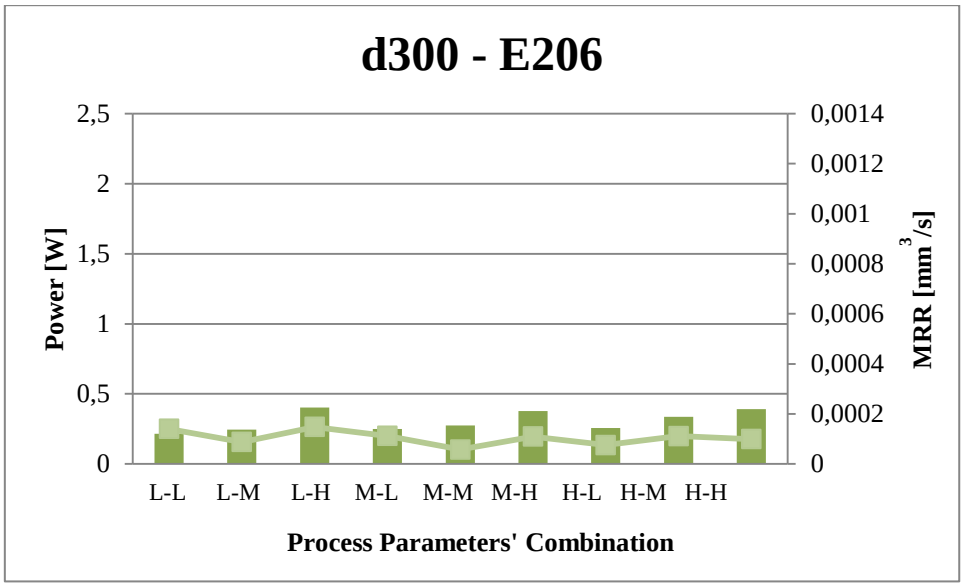

Figure 86: MRR and electrical power as a function of the process parameters' combination, d 300 µm, E 206

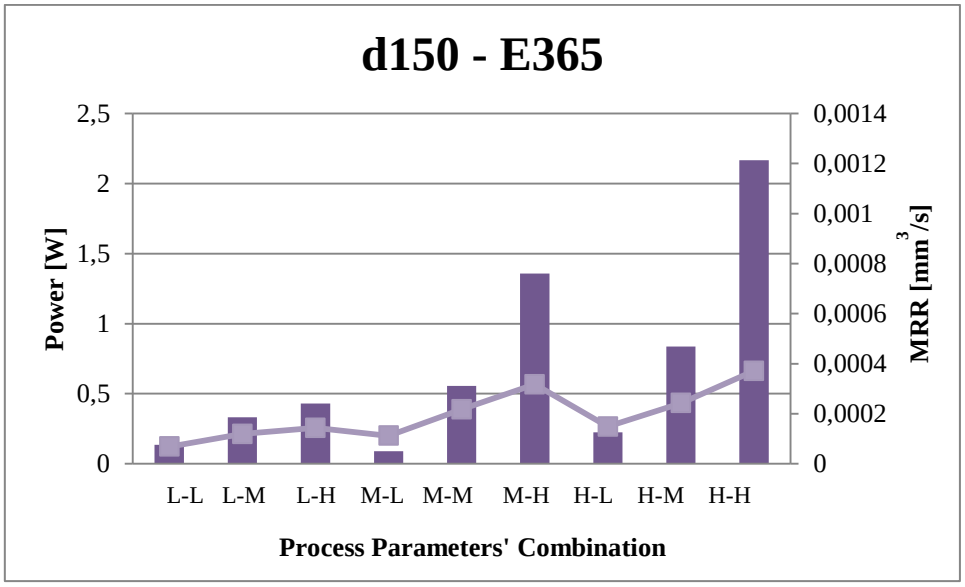

Figure 87: MRR and electrical power as a function of the process parameters' combination, d 150 µm, E 365

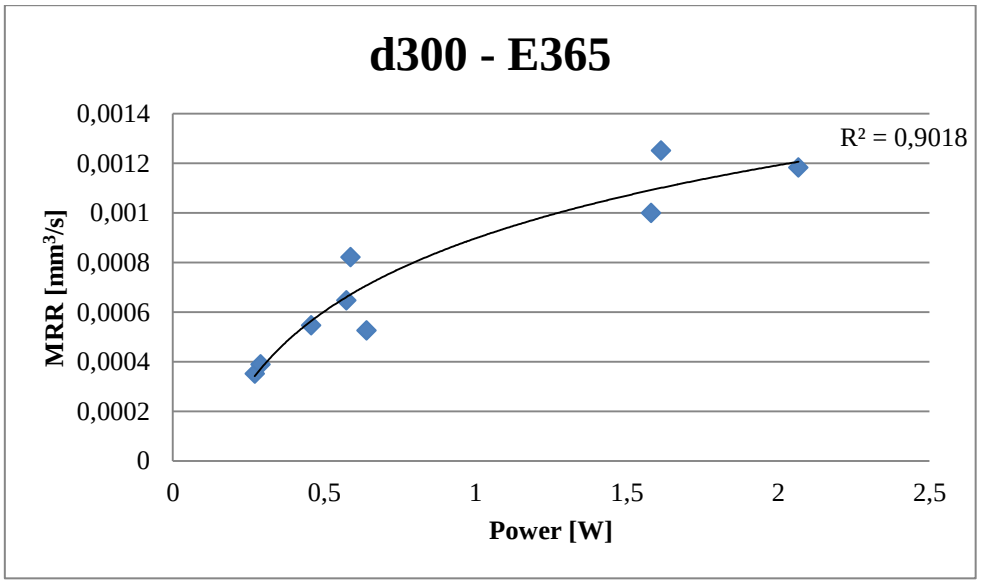

Figure 88: MRR as a function of the electrical power, d 300 µm, E 365

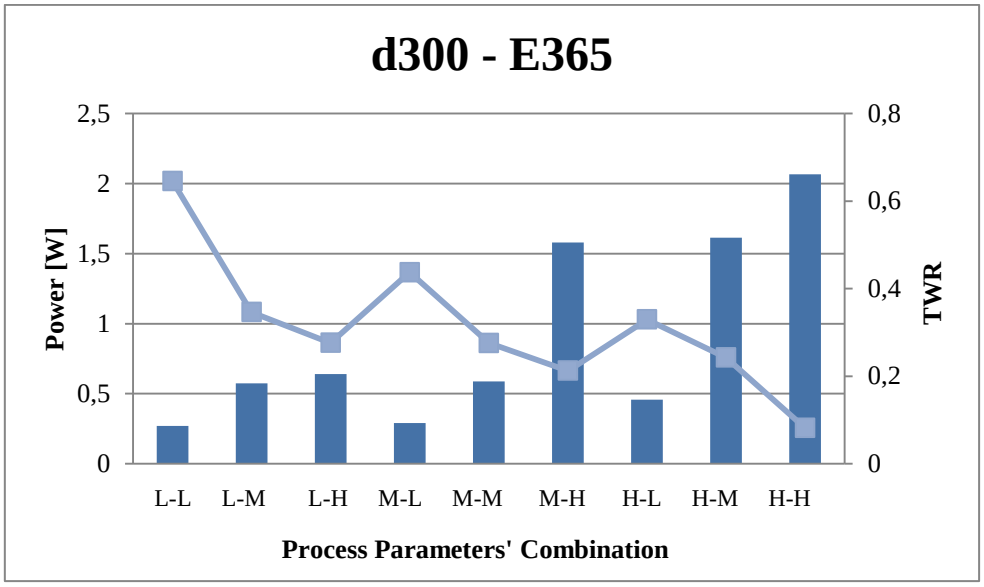

Figure 89: TWR and electrical power as a function of the process parameters' combination, d 300 µm, E 365

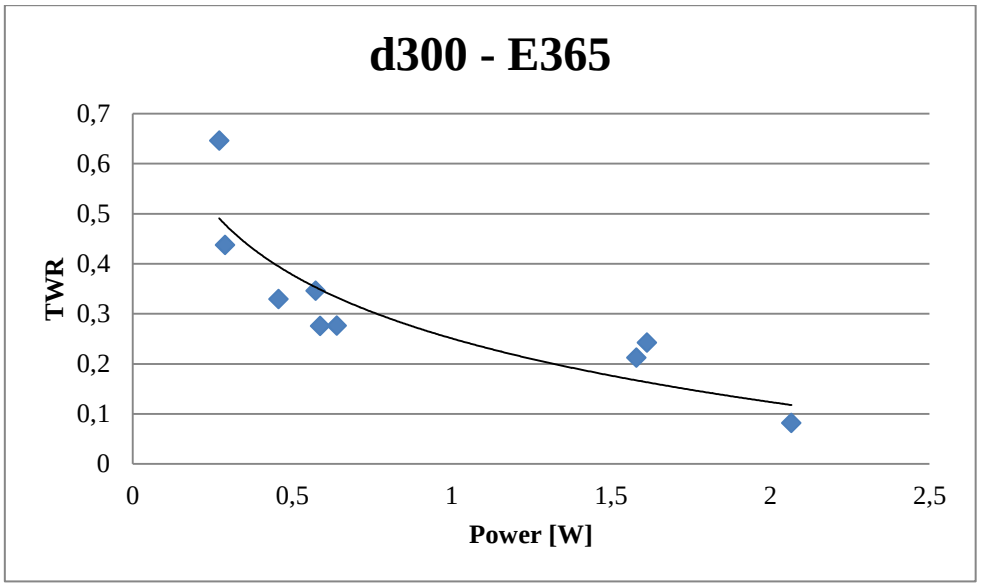

Figure 90: TWR as a function of the electrical power, d 300 µm, E 365

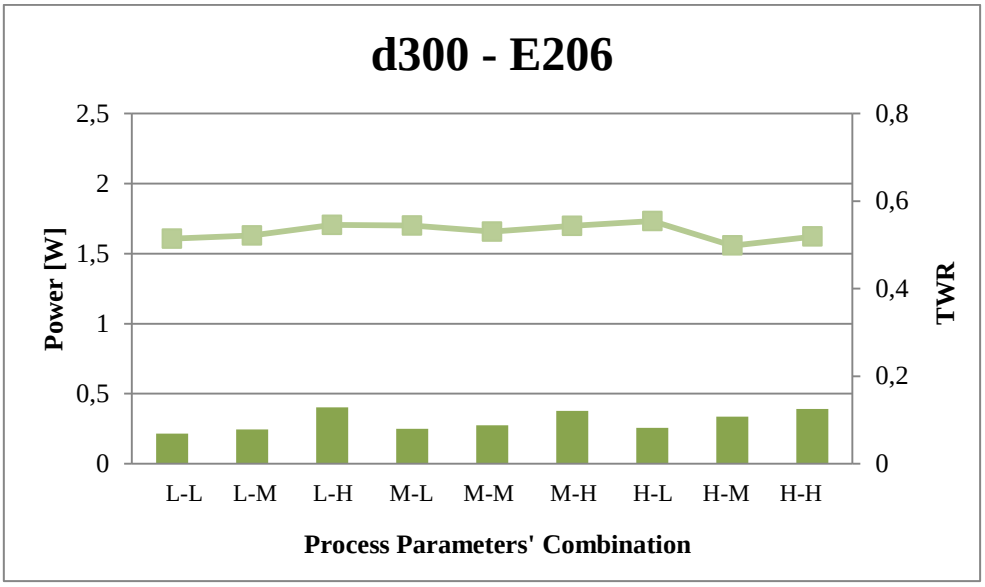

Figure 91: TWR and electrical power as a function of the process parameters' combination, d 300 µm, E 206

As regards the geometrical indicators, DOC and TR, no significant trend can be found for the 300 µm electrode diameter, as shown in Figure 92 and Figure 93. The only exception is for the DOC, with the low level of the peak current: in this case for increasing values of the exchanged energy bigger top diameters are recorded. In general, for both DOC and TR, a more considerable effect of the 365 energy is confirmed.

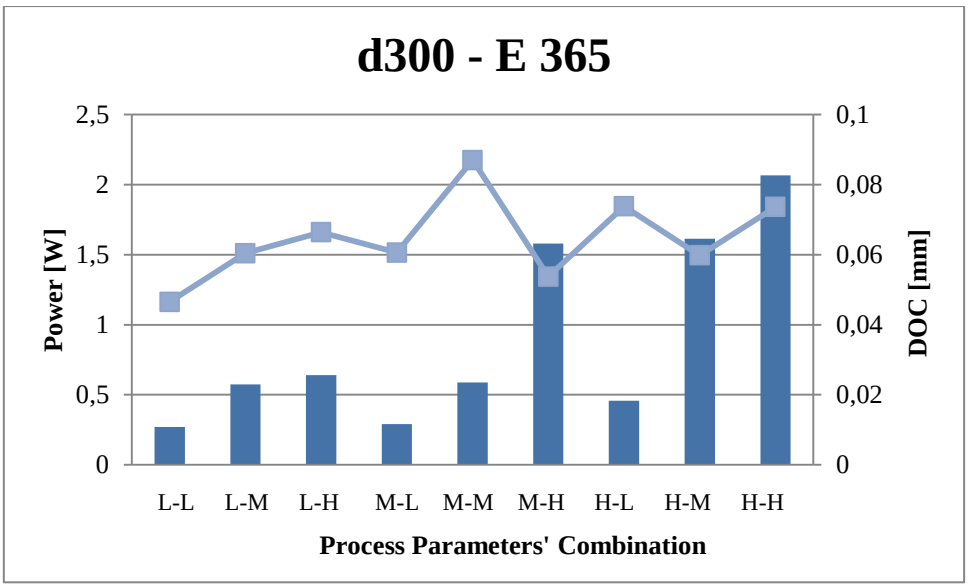

Figure 92: DOC and electrical power as a function of the process parameters' combination, d 300 µm, E 365

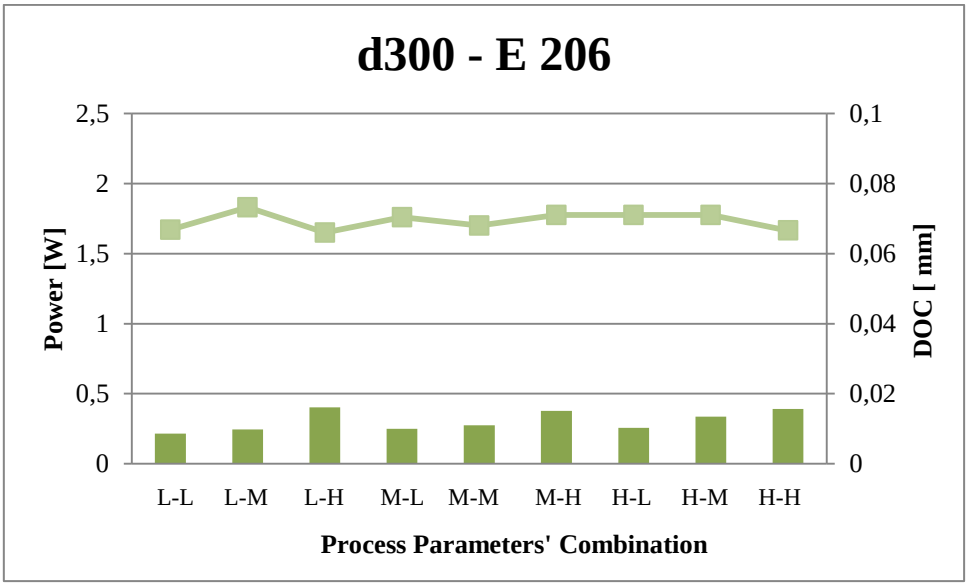

Figure 93: DOC and electrical power as a function of the process parameters' combination, d 300 µm, E 206

Different conclusions can be drawn for the 150 µm electrode diameter. In this case, a significant trend in the data is found: for increasing values of the exchanged power, the geometrical characteristics get worse, as shown in Figure 94.

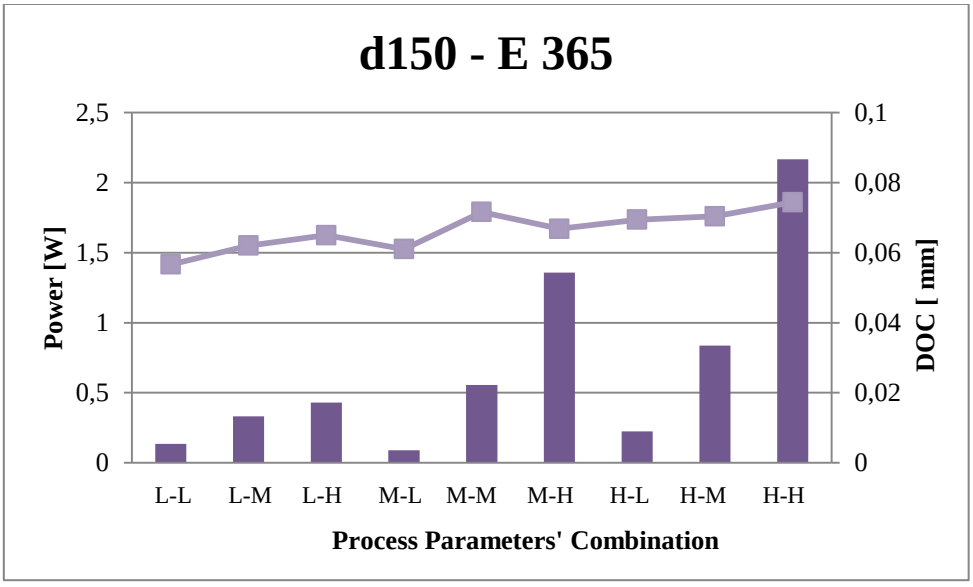

Figure 94: DOC and electrical power as a function of the process parameters' combination, d 150 µm, E 365

As a matter of fact, the tests concerning the 150 µm electrode diameter were executed with the use of the ceramic guide imposed by the dimensions of the electrode, as explained in the previous chapters. For this reason the geometrical data for the 150 µm electrode tests are less affected by the geometrical variability that may characterize the other tests, and an actual trend was found in this case.

In order to investigate the real influence of the exchanged power on the DOC indicator, the 150 µm diameter with 365 energy level was selected for the investigation. The same was done for the TR indicator. Figure 95 shows the trend of the DOC as a function of the exchanged electrical power. It is possible to notice how the exchanged power affects the indicator, for increasing exchange power values a worsening of the geometrical characteristics is recorded. Higher values of the exchange power result in a higher amount of the electrical power absorbed by the workpiece. This results in the melting and vaporizing of the material with a higher removal of the material from the workpiece. As a matter of fact, higher electrical power means a more aggressive process with consequent damaged entrance diameter.

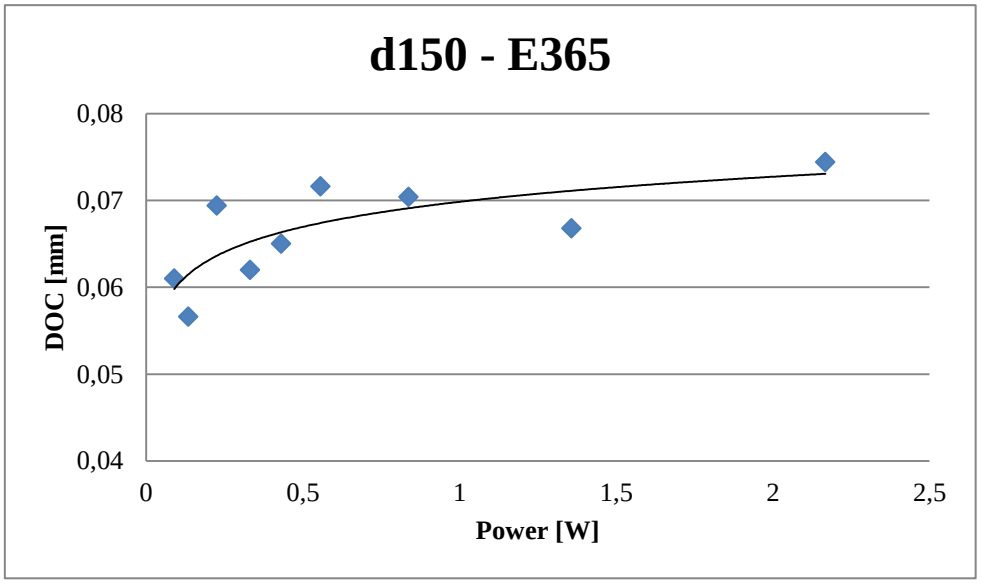

Figure 95: DOC as a function of the electrical power, d 150 µm, E 365

As regards the energy level 206 on the contrary, no significant trend can be found for, as shown in Figure 96. Similar conclusions can be drawn for the TR indicator. The effect of the energy is considerable and between the two diameters, the 150 µm electrode gives the best results in terms of influence of the process parameters in the form of the

exchanged power, as shown in Figure 97. In this case the increasing power has a negative effect on the geometrical characteristics of the holes, too. The same trend can be found for the TR as a function of the exchanged power, as shown in Figure 98.

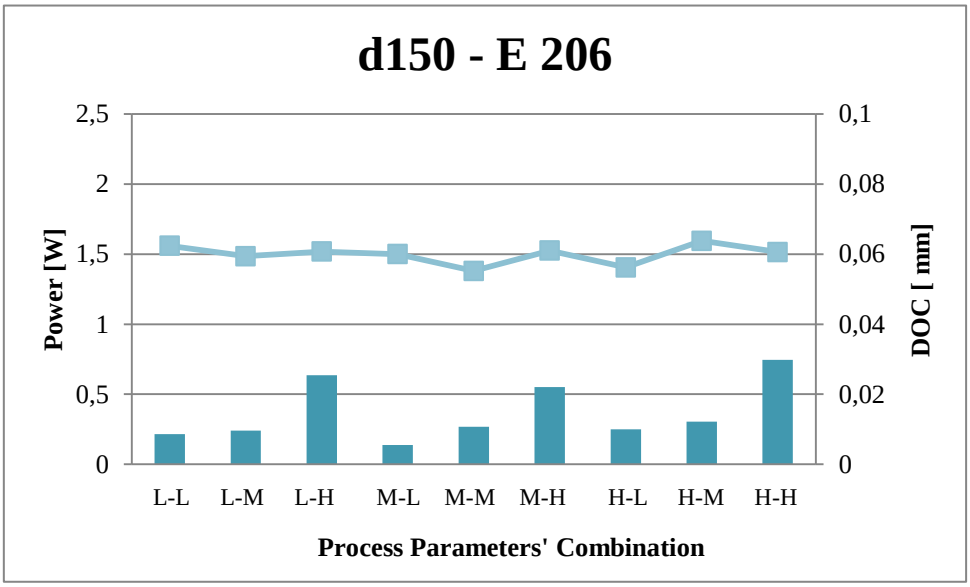

Figure 96: DOC and electrical power as a function of the process parameters' combination, d 150 µm, E 206

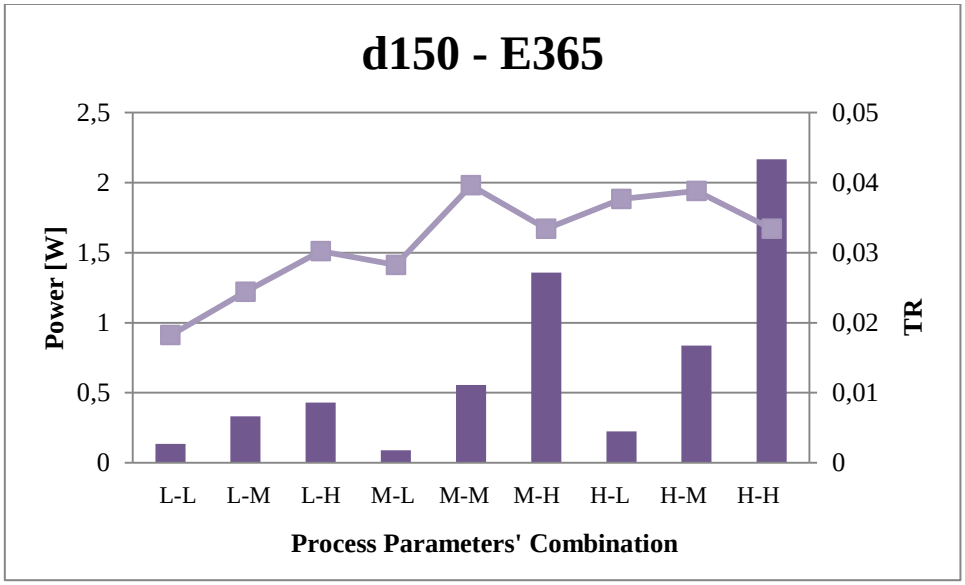

Figure 97: TR and electrical power as a function of the process parameters combination, d 150 µm, E 365

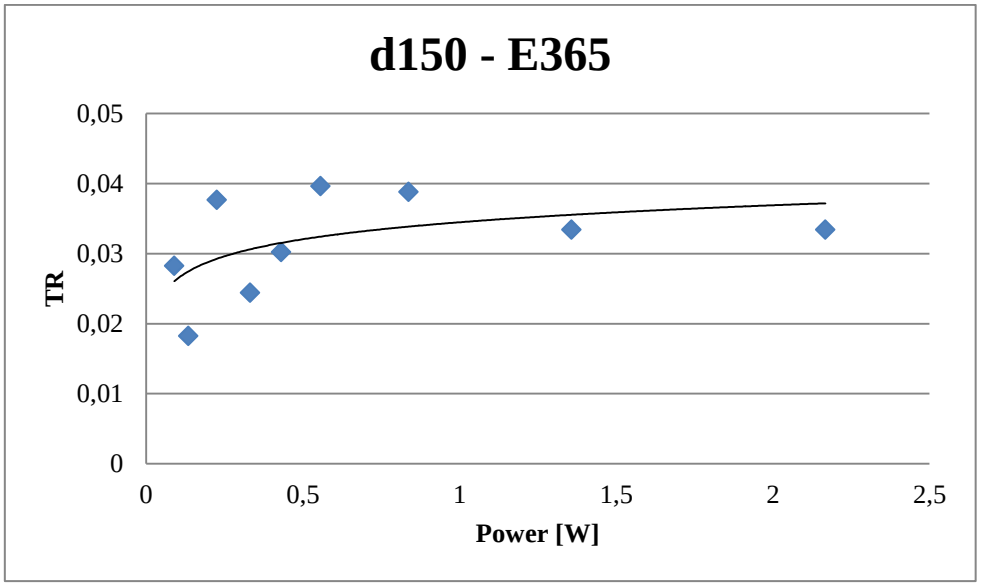

Figure 98: TR as a function of the exchanged power, d 150 µm, E 365

4.2.2 Copper electrode (Cu) Electrode

4.2.2.1 First level of Analysis: I and V

Cu, d 300 µm, E 365

In Table 28 the summarization of the analysis of variance output is shown. For all the indicators, the interaction between the factors has a consistent effect on the final response. Moreover, for all the indicators except TR and TWR, the peak current and the voltage have an influence on the final values.

Table 28: Analysis of variance output for d 300 µm and E 365

	t	Wear	DOC	TR	MRR	TWR
I	**0**	**0**	**0**	0.809	**0**	0
V	**0**	**0**	**0**	0.205	**0**	**0.035**
I*V	**0**	**0.007**	**0.122**	**0.006**	**0**	**0.014**

The interaction between the factors appears evident, as an example the interaction plot for the machining time is reported in Figure 99.

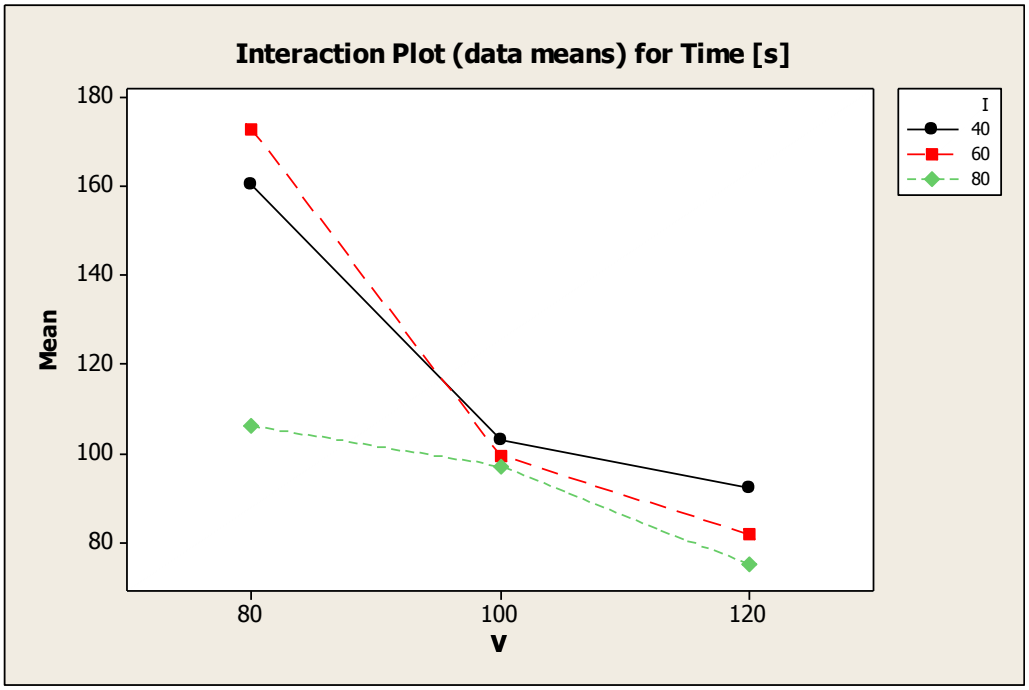

Figure 99: Interaction plot for machining time mean data as a function of I and V, d 300 μm, E 206

For all the indicators and for both energy levels an interaction between I and V is recorded, like for the TC electrode. For the sake of simplicity the energy level has been introduced in the model at this point of the analysis and the results are reported in the following section starting from this point of the analysis.

Cu, d 300 μm

Table 29: Analysis of variance p-values for d 300 μm

	t	Wear	DOC	TR	MRR	TWR
I	**0.000**	**0.005**	0.339	0.449	0.170	**0.000**
V	**0.000**	**0.005**	0.925	0.382	**0.000**	**0.000**
E	**0.000**	**0.000**	**0.000**	0.556	**0.000**	**0.000**
I*V	**0.000**	0.918	0.999	0.797	0.996	0.881
I*E	**0.000**	0.298	0.929	0.182	0.920	**0.040**
V*E	**0.000**	0.051	0.172	0.329	0.153	**0.000**
I*V*E	**0.000**	0.916	0.780	0.965	0.913	0.728

Similarly to the TC 300 μm electrode, the energy level influences the response, except for the taper rate (TR). For the sake of simplicity, only the interaction plots for the electrode wear are reported since they are representative of all the other parameters' effect. Since the TR is not influenced, it is not introduced in the analysis. Figure 100, Figure 101 and Figure 102 show the detail of the interaction plot for the electrode wear indicator. A certain effect of the energy level is recorded.

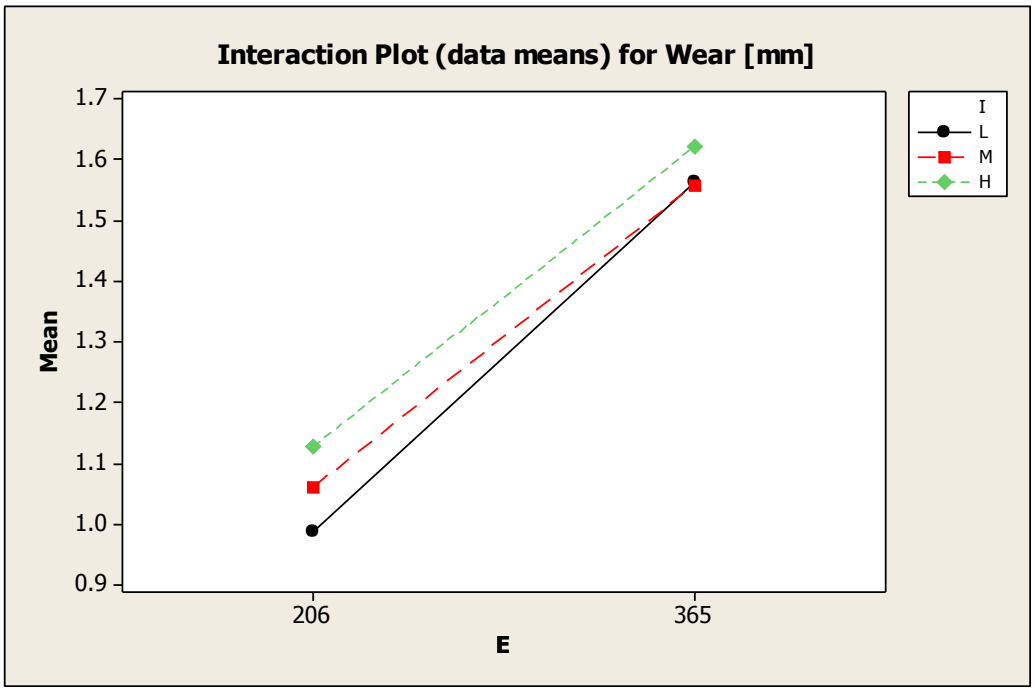

Figure 100: Interaction plot for electrode wear mean data as a function of I and E, d 300 µm

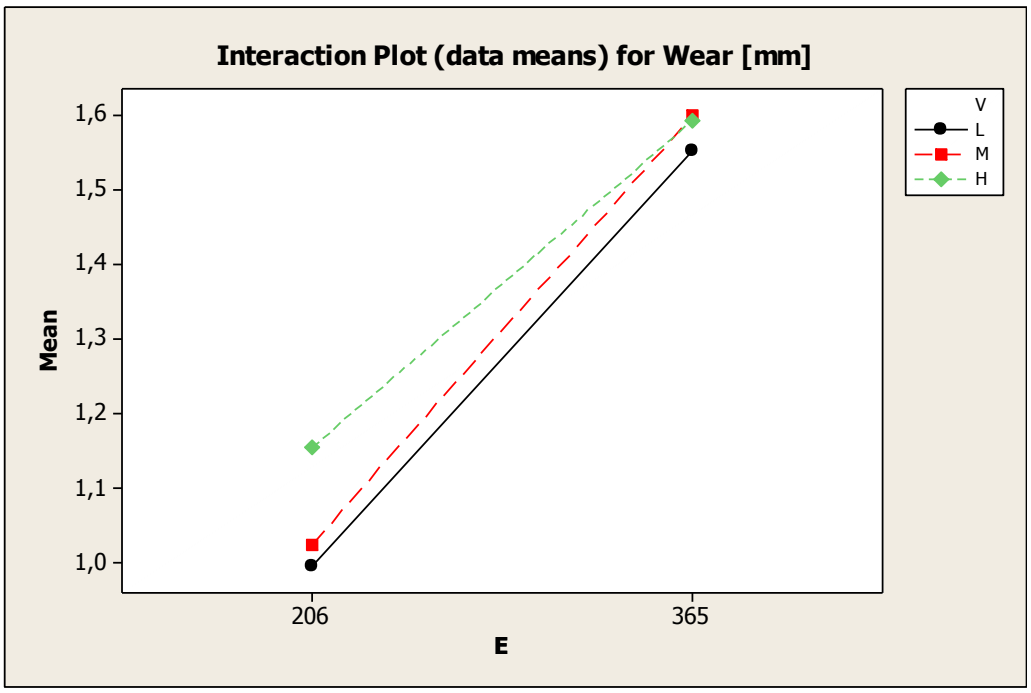

Figure 101: Interaction plot for electrode wear mean data as a function of V and E, d 300 µm

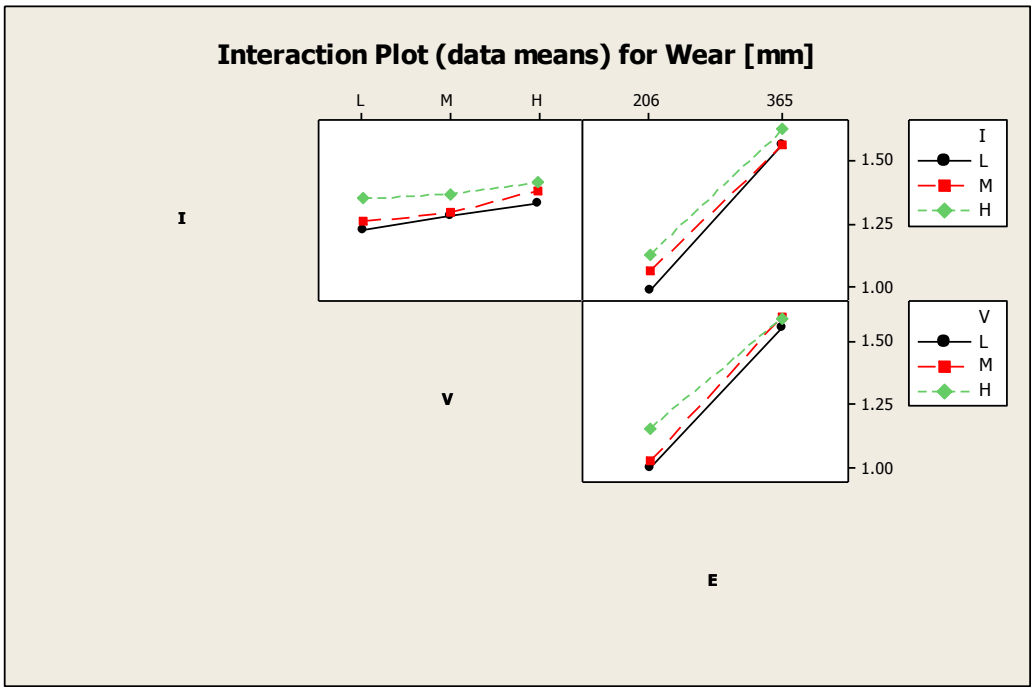

Figure 102: Interaction plot for electrode wear mean data as a function of I, V and E, d 300 μm

Figure 103 and Figure 104 report the details of the interval plot for the electrode wear panelled by the energy level. The dampening effect of the 206 energy level is here confirmed by the error bars, considerably lower, but no significant trend can be identified neither for the 365 nor for the 206 energy level. Finally in Figure 105 it is observed how the energy level is, also for the copper electrode, the most relevant factor on the final response.

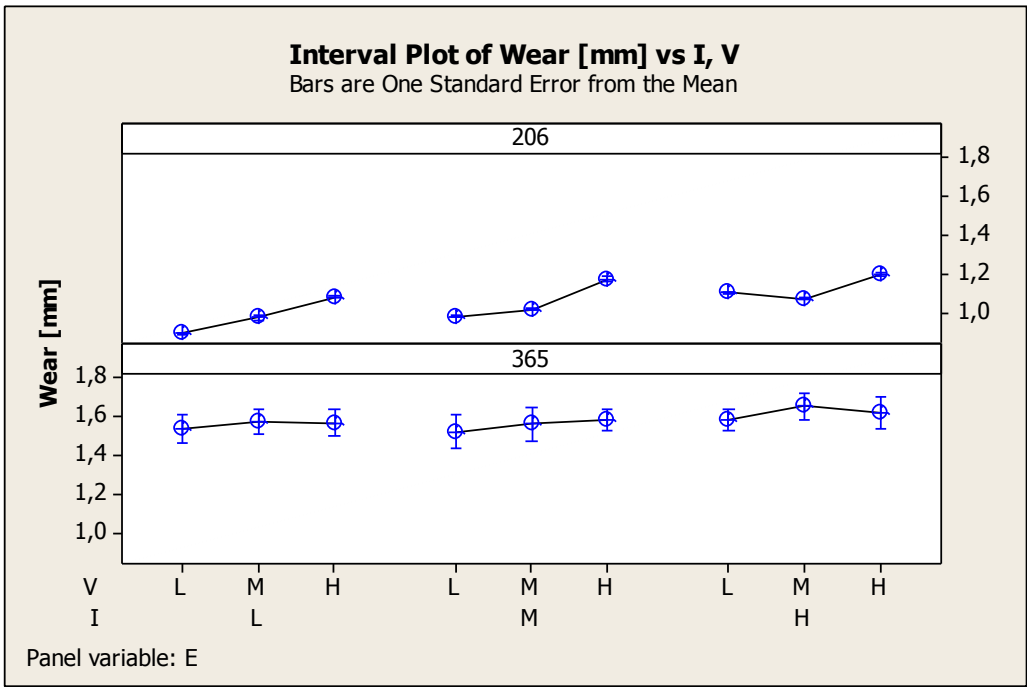

Figure 103: Interval plot for electrode wear as a function of I and V panelled considering E

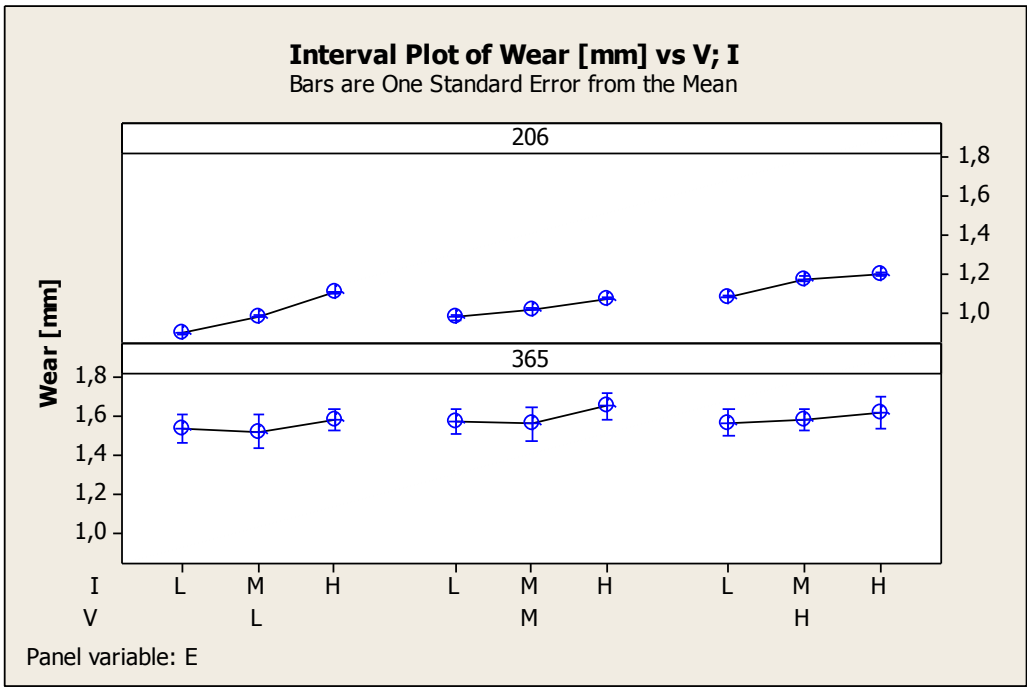

Figure 104: Interval plot for electrode wear as a function of V and I panelled considering E

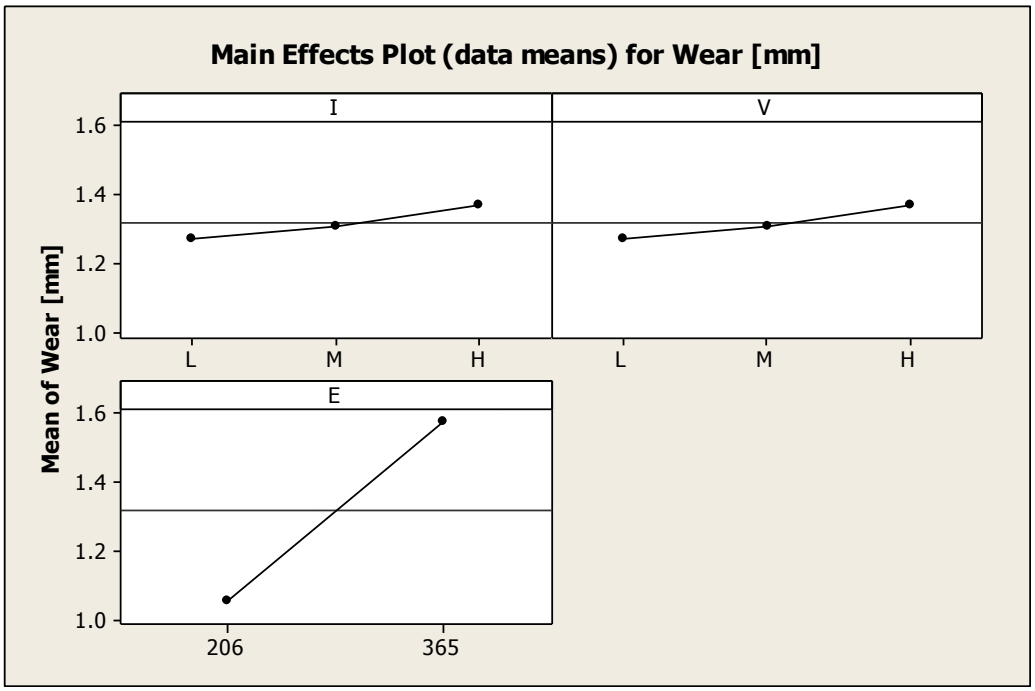

Figure 105: Main effects plot for electrode wear as a function of I, V and E

Cu, d 150 μm

Table 30 shows the results of the analysis of variance for all the indicators.

Table 30: Analysis of variance p-values for d 300 μm

	t	Wear	DOC	TR	MRR	TWR
I	**0.000**	**0.011**	0.815	0.265	0.244	**0.019**
V	**0.000**	0.209	0.642	0.311	**0.047**	**0.021**
E	**0.000**	**0.008**	0.176	0.933	**0.000**	**0.050**
I*V	**0.049**	0.580	0.544	0.778	0.937	0.626
I*E	**0.000**	0.498	0.987	0.247	0.510	0.162
V*E	**0.000**	0.747	0.952	0.171	0.313	0.588
I*V*E	**0.037**	**0.045**	0.212	0.858	0.576	0.341

The machining time indicator is the most influenced by the factors and their combination. As a matter of fact, in this case, the energy also has a considerable influence on the final result. For this diameter, the other factors are barely influenced by the process parameters and the energy level, if compared with the results obtained with the TC electrode. The effect of the energy level is shown in Figure 106 and in Figure 107, for the machining time indicator. It is possible to notice how the energy level affects the response and how in this case the high energy level results in a dumping effect of the response value. Figure 108 shows the main effects plot for the machining time, as a function of the three factors considered in the analysis. It is clear how the energy has the most relevant influence on the final response.

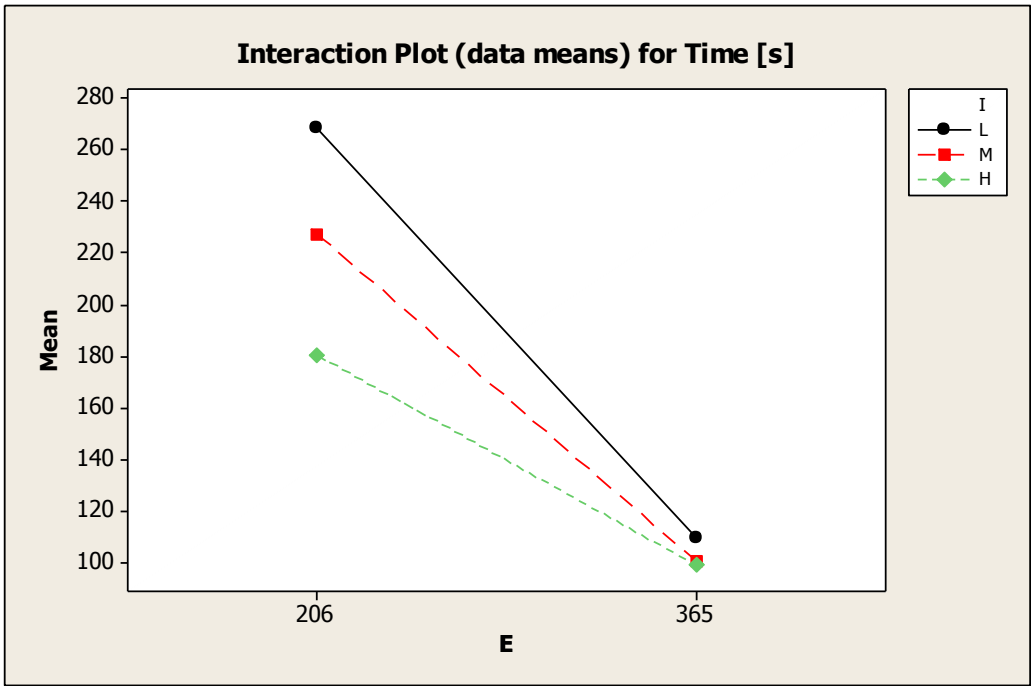

Figure 106: Interaction plot for machining time mean data as a function of I and E, d 300 µm

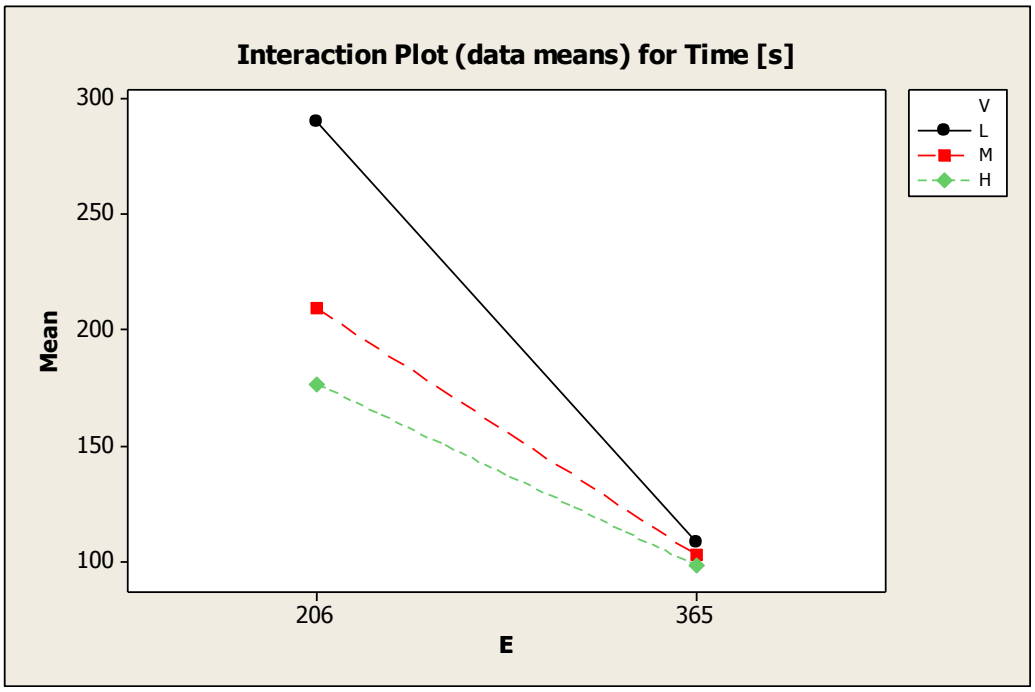

Figure 107: Interaction plot for machining time mean data as a function of V and E, d 300 µm

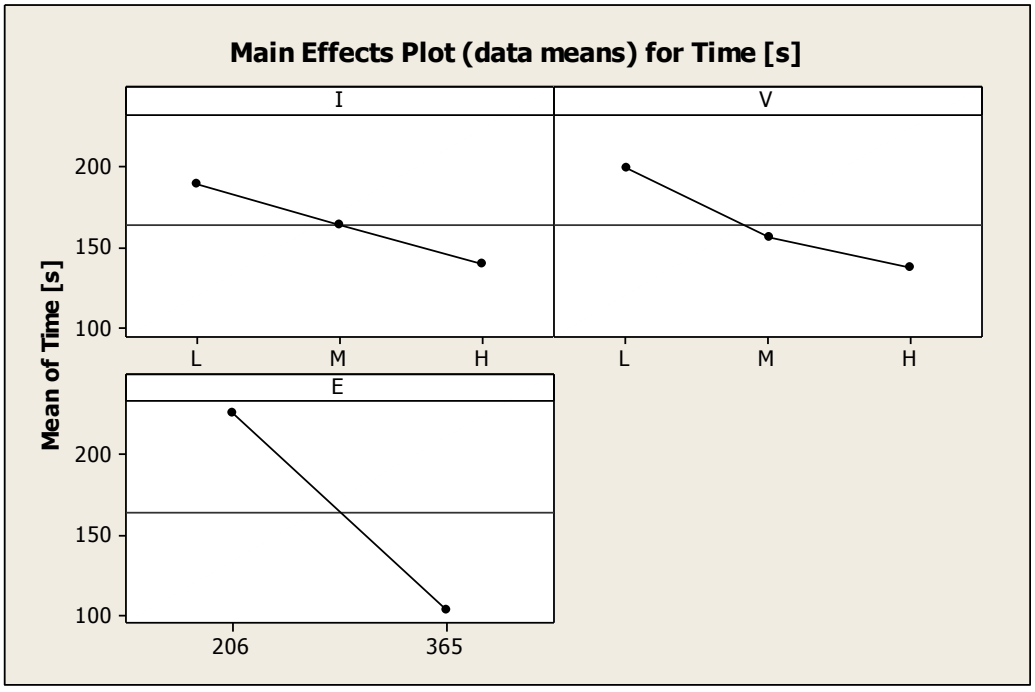

Figure 108: Main effects plot machining time as a function of I, V and E

The conclusion that can be drawn from this part of the analysis are several. From the diameter point of view, it is clear how the factors have a more consistent effect on the machining executed with the 300 μm electrode, for both electrode materials.

Moreover, the energy level is the most influencing factor, even though for the copper electrode this effect is less relevant than for the TC electrode, especially for the geometrical characteristics (TR and DOC). It is reasonable to suppose a certain relationship between the factors and the electrode material, or in other words, that the electrode material can be considered with full rights a factor of the model as well.

Similarly for the TC electrode, the power exchanged was evaluated for the Copper electrode, as well. The following plots show the power as a function of the process parameters' combination. As a matter of fact, it is possible to draw two main conclusions.

First of all, the amount of energy exchanged with the high level of the voltage parameter corresponds to the highest values of the electrical power recorded in the experimental campaign. In this case, in fact, the exchanged power is about ten times higher than the TC case with the same electrode diameter and energy level (Figure 109).

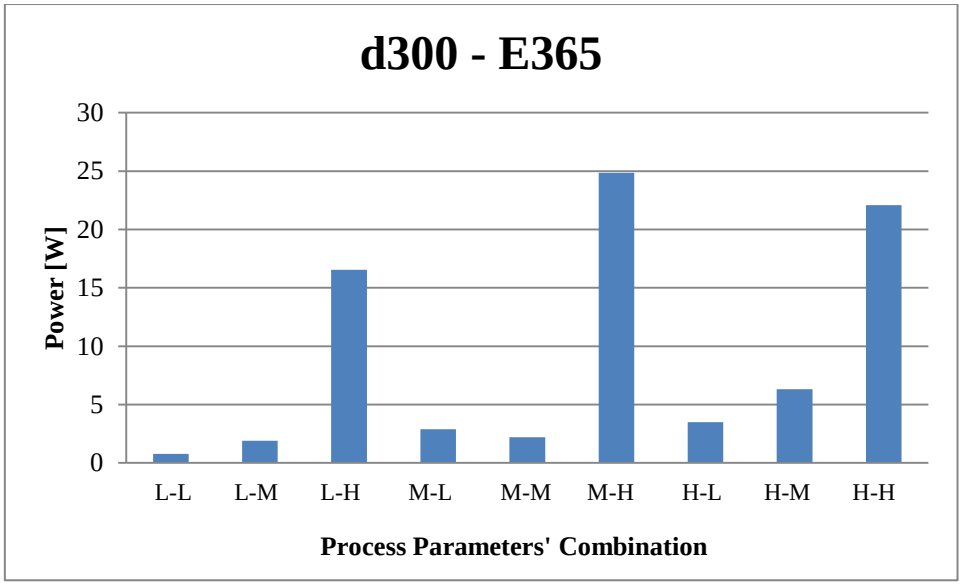

Figure 109: Copper electrode electrical power as a function of the process parameters' combination, d 300 μm, E 365

This phenomenon is recorded only for the high level of the energy, while the 206 energy level is characterised by lower exchanged powers, as shown in Figure 110. In this case, the exchanged power is in the same order of magnitude of the TC electrode tests, executed with the same electrode diameter and energy level.

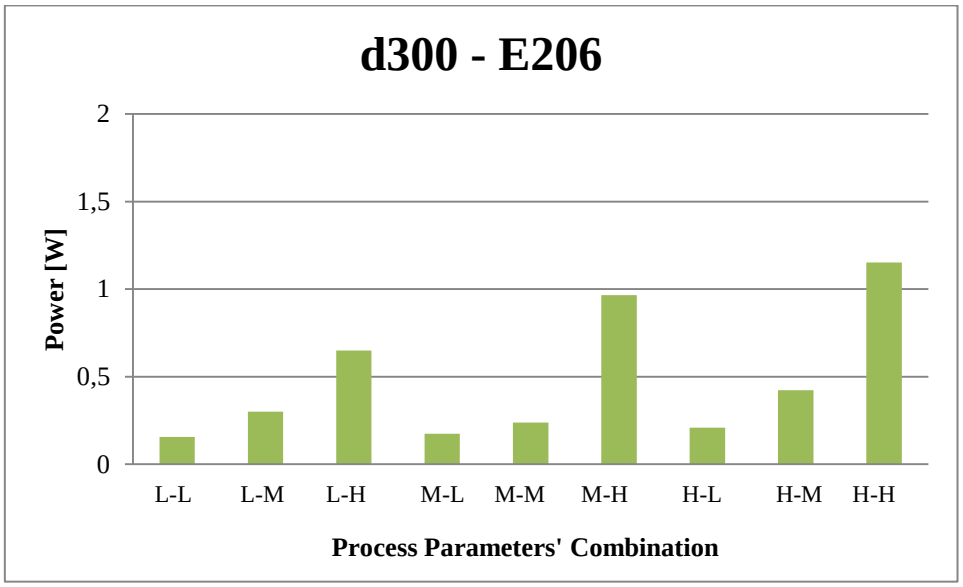

Figure 110: Copper electrode electrical power as a function of the process parameters' combination, d 300 μm, E 206

A possible explanation of this phenomenon is related to the process parameters: for the experiments carried out with the copper electrode having diameter equal to 300 μm and with the high level of the energy, the gap was increased at the value of 75 instead of 60, the gap value for all the other experiments.

This value of the parameter was chosen taking into account the results of the preliminary tests that allowed to investigate and chose the better process parameters aimed at the reduction of the electrode wear and machining time.

The increased gap in this particular case, was introduced in order to reduce the amount of short circuits that characterized the high energy level: a decreasing number of short circuits allowed an improvement of the process efficiency and with good level of confidence the exchanged power as well.

Another possible cause lies in the characteristics of the base material itself, since copper is characterized by a higher electrical conductivity than tungsten carbide. This aspect has been possibly enhanced by the high level of the energy, especially for the high level

of the voltage, as shown in Figure 109, since the medium and low levels resulted in comparable exchanged powers with the ones obtained in the previous tests.
The second conclusion regards the power exchanged during the tests measured with the 150 μm copper electrode. In this case, the order of magnitude of the exchanged power is comparable with the results obtained in the TC tests, but for the copper electrode the influence of the process parameters is completely negligible for both energy levels, as shown in Figure 111.

This result regarding the exchanged energy, forced the following part to be focused only on the 300 μm electrode diameter. The following graphs refer to the experiments carried out with the 206 energy level. As regards the machining time, it is possible to confirm the trend previously found for the TC electrode, increasing the power results in a decrement of the machining time (Figure 112).

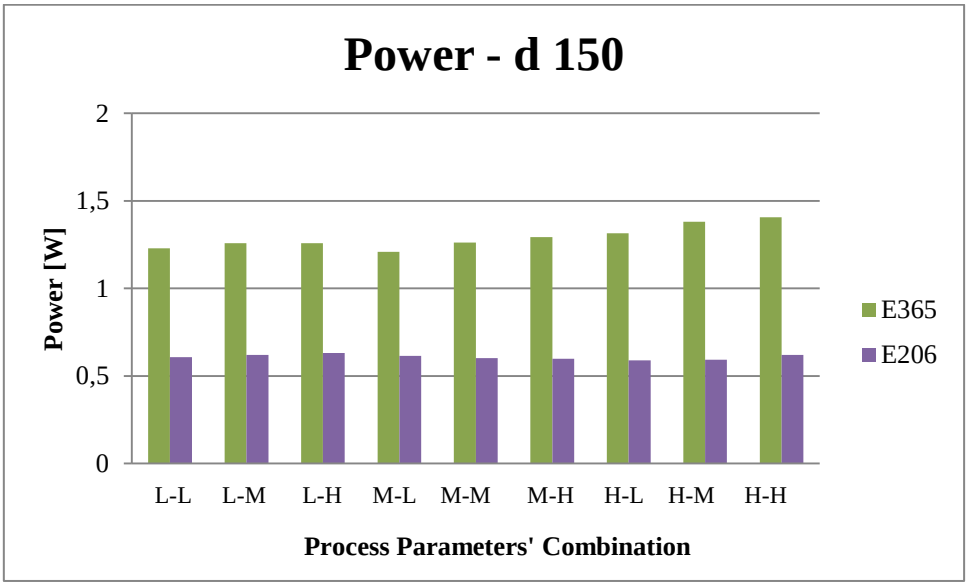

Figure 111: Copper electrode electrical power as a function of the process parameters' combination, d 150 μm

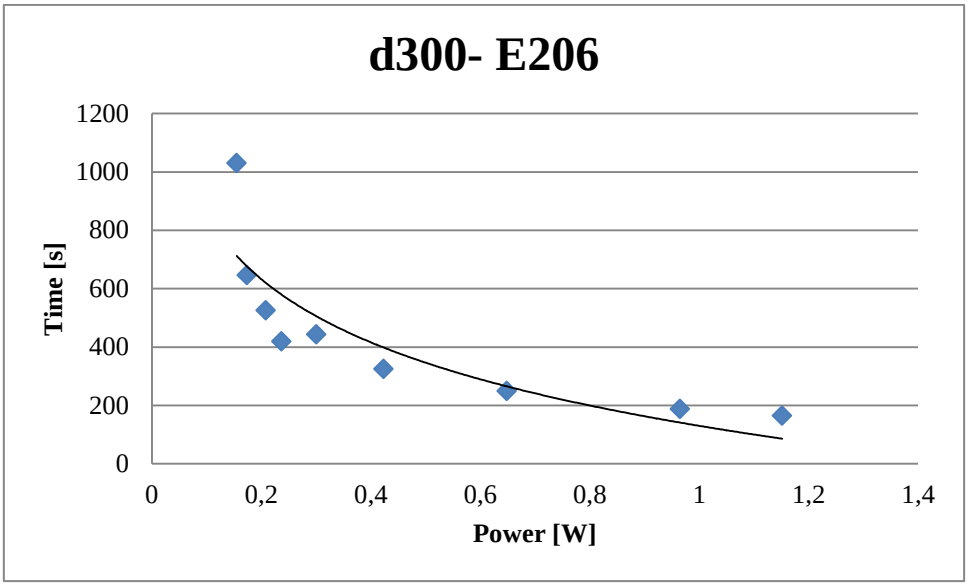

Figure 112: Copper electrode machining time as a function of the electrical power, d 300 μm, E 206

The same conclusions have been drawn for the electrode wear, as shown in Figure 113. In this case, differently from the TC electrode (which is characterized by a better wear resistance), for the copper electrode the increasing exchanged power results in a higher electrode wear. The lowest wear resistance of copper results in an inevitable erosion for higher values of the exchanged power, even if the machining time is lower. Similarly, the TWR indicator increases for increasing values of the power (Figure 114) and the same trend is recorded for the MRR (Figure 115).

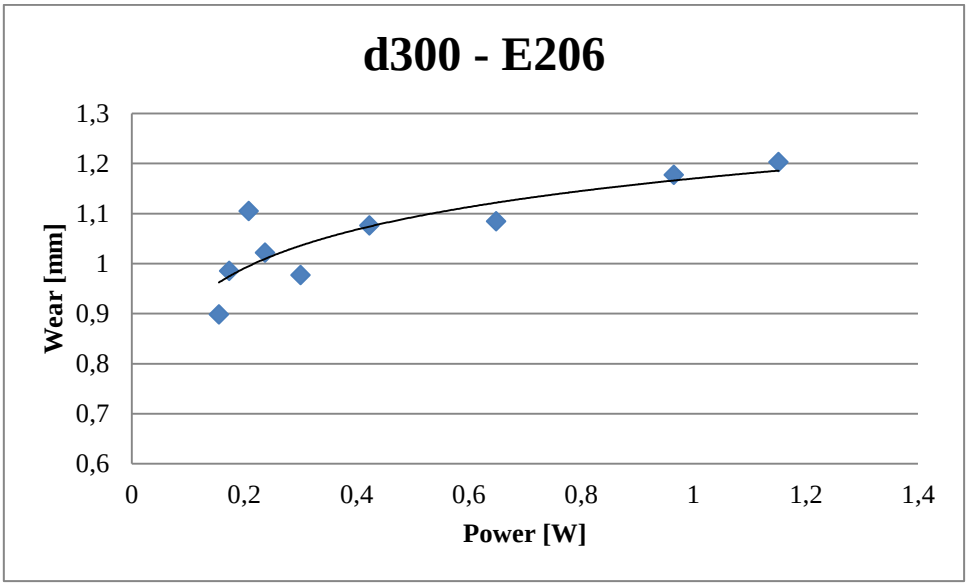

Figure 113: Copper electrode wear as a function of the electrical power, d 300 µm, E 206

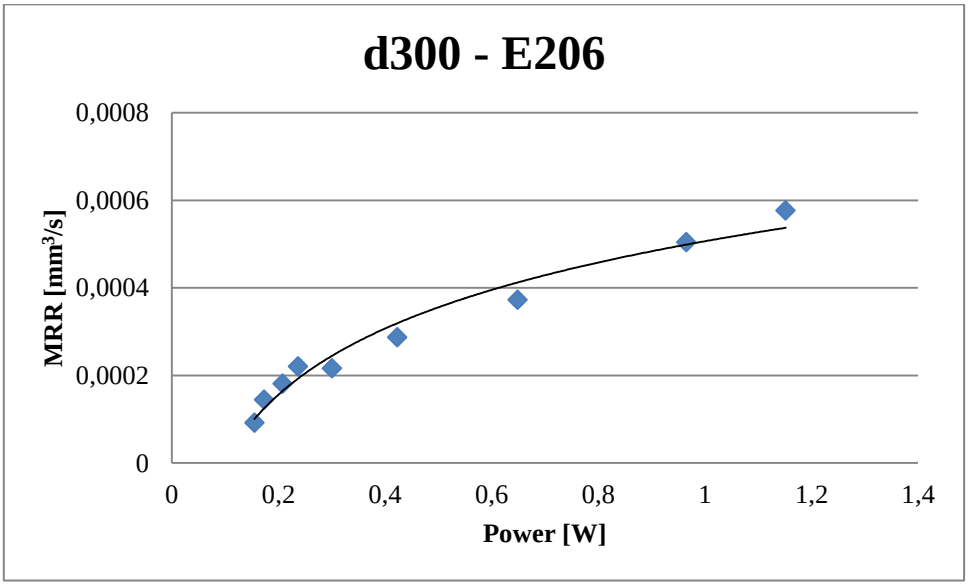

Figure 114: Copper electrode MRR as a function of the electrical power, d 300 µm, E 206

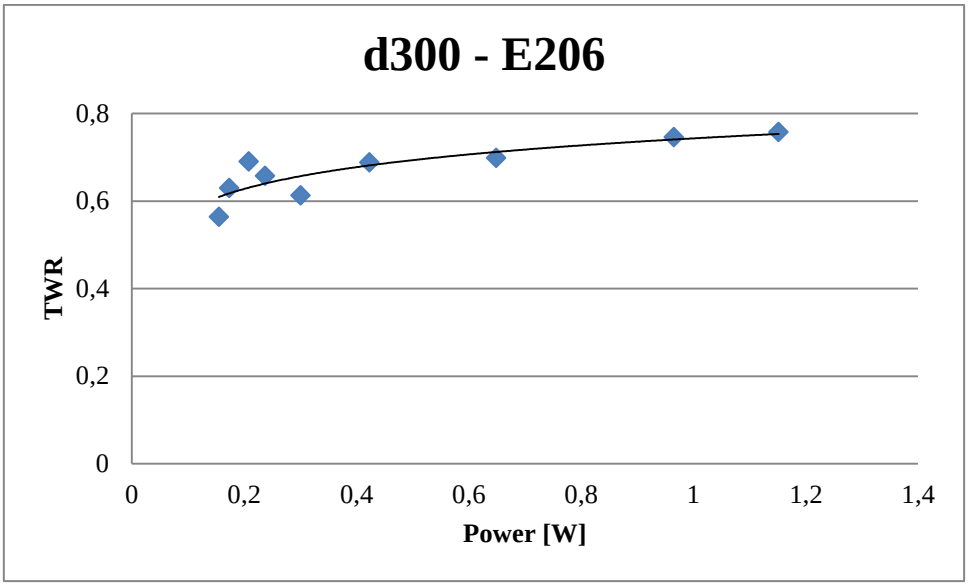

Figure 115: Copper electrode TWR as a function of the electrical power, d 300 µm, E 206

No significant trend has been found for the geometrical indicators.

Comparing the results obtained for the TC electrode and the copper electrode, it is possible to underline some differences and some common trends.

For both electrodes, the machining time is inversely proportional to the exchanged power: for the TC electrode the erosion duration is influenced by the electrode diameter and by the energy level, as well.

On the contrary, the electrode wear is characterized by different trends: for the TC electrode the lower machining time corresponds to the high value of the power; this results in decreasing values of the wear. On the contrary, for the Cu electrode, the increasing power results in a reduction of the machining time and an increment of the electrode wear. The copper electrode with high level of energy and with high electrode diameter ensures a machining time that is between 50 and 200 seconds, while with the same process conditions with the TC electrode the machining time is between 100 and 500 seconds. As a general remark, the copper electrode ensures a more aggressive machining process, lower machining time and higher exchanged power. Since the MRR and the TWR are directly dependent on the raw data “time” and “wear” the different trends are found for them as well.

Finally, no real trend can be found for the geometrical characteristics DOC and TR, for both the electrode diameters, as confirmed by the previous literature.

From the Minitab® analysis and considering the results described, it is evident how the electrode characteristics appear to be relevant and deserve to be inserted as a factor in the model. In order to investigate the relevance of these aspects of the process, the analysis was carried out including the electrode characteristics as a factor of the model. The results obtained are summarized in the following section.

4.2.3 Third level of Analysis: I, V, E and electrode material

Since in the previous section the relevance of the electrode characteristics were taken into account, in the present chapter the electrode material was added as a model factor. In the following sections the p-values from the analysis of variance are reported, for the 300 μm and for the 150 μm electrodes.

d 300 μm

Table 31 shows the p-values from the analysis of variance for all the indicators with I, V, E and the electrode material as factors of the model. The more considerable effect of the electrode material, if compared with the other factors, is observed. In this case all the indicators' responses are influenced by the electrode material.

Table 31: Analysis of variance p-values for 300 μm

	t	Wear	DOC	TR	MRR	TWR
I	0.166	0.536	0.209	0.835	**0.000**	0.182
V	**0.000**	**0.011**	0.433	0.474	**0.000**	**0.001**
E	**0.000**	**0.000**	**0.012**	0.072	**0.000**	**0.011**
Mat	**0.000**	**0.000**	**0.000**	**0.001**	**0.000**	**0.000**
I*V	**0.007**	0.851	0.092	0.257	0.500	0.746

I*E	0.160	**0.000**	0.486	0.684	**0.013**	**0.000**
I*Mat	**0.001**	**0.000**	0.130	0.146	0.217	**0.000**
V*E	**0.000**	**0.000**	0.136	0.257	**0.030**	**0.000**
V*Mat	**0.018**	**0.000**	0.231	0.341	0.161	**0.000**
E*Mat	**0.000**	**0.000**	**0.000**	0.318	0.482	**0.000**
I*V*E	**0.010**	0.220	**0.010**	0.165	0.850	**0.043**
I*V*Mat	**0.001**	0.905	**0.050**	0.123	0.684	0.562
I*E*Mat	**0.000**	0.070	0.270	0.247	**0.003**	**0.025**
V*E*Mat	**0.000**	**0.001**	0.847	0.909	**0.000**	**0.001**
I*V*E*Mat	**0.001**	0.805	**0.013**	0.109	0.460	0.414

As an example, Figure 116 shows the main effects plot for the electrode wear. For the plot the considerable effect of the electrode material is confirmed.

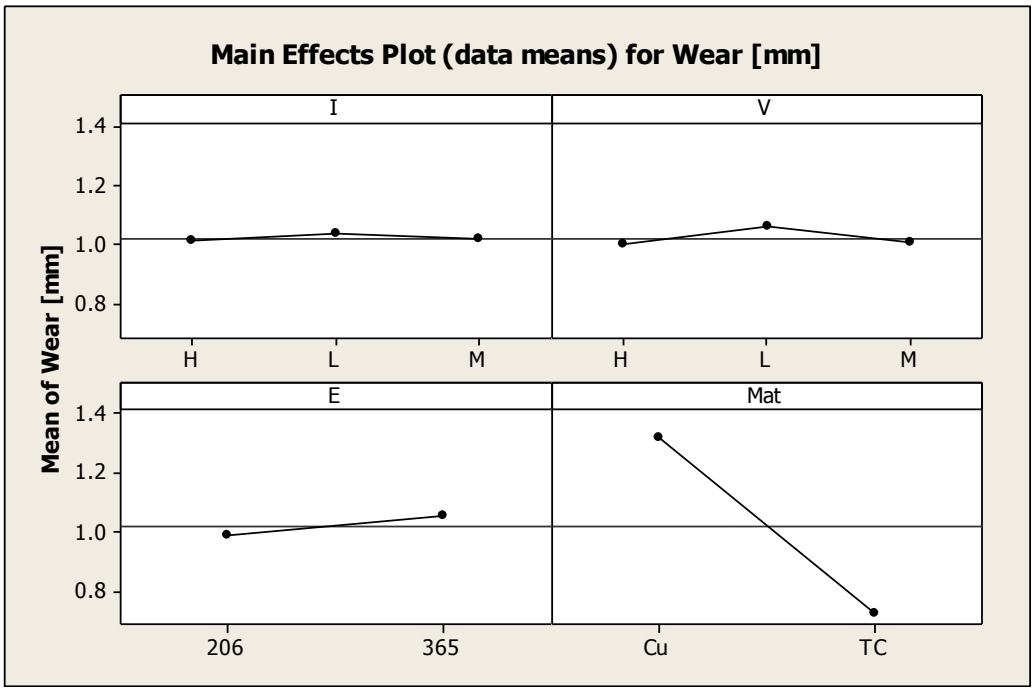

Figure 116: Main effects plot for electrode wear as a function of I, V, E and electrode material, d 300 µm

In order to compare the influence of the electrode material on both electrode diameter, in the following section the results of the same analysis are described.

d 150 µm

As shown in Table 32, the electrode material and the combined effect of the electrode material with the energy level are the most relevant factors, except for the geometrical characteristics DOC and TR, alternatively. This result confirms the assumptions according to which the electrode material and the energy level make the effect of the process parameters negligible.

Table 32: Analysis of variance p-values for 150 µm electrode

	t	Wear	DOC	TR	MRR	TWR
I	0.092	**0.034**	0.755	0.297	0.276	**0.035**
V	**0.001**	0.475	0.379	0.315	**0.026**	**0.037**
E	**0.000**	0.066	0.438	0.126	**0.000**	0.191
Mat	**0.000**	**0.000**	0.146	**0.000**	**0.000**	**0.000**
I*V	**0.044**	0.609	0.632	0.829	0.786	0.659
I*E	0.097	0.672	0.855	0.334	0.517	0.246
I*Mat	**0.020**	**0.008**	0.867	0.254	0.245	**0.015**
V*E	**0.019**	0.862	0.882	0.122	0.566	0.532
V*Mat	**0.019**	0.106	0.941	0.328	0.651	**0.017**
E*Mat	**0.002**	**0.002**	**0.001**	0.171	**0.001**	**0.014**
I*V*E	0.095	0.332	0.359	0.844	0.997	0.494
I*V*Mat	**0.016**	0.641	0.437	0.721	0.877	0.664
I*E*Mat	**0.009**	0.349	0.966	0.192	0.474	0.126

V*E*Mat	**0.036**	0.678	0.998	0.251	0.422	0.693
I*V*E*Mat	**0.011**	**0.007**	0.161	0.868	0.394	0.248

The main effects plot for the electrode wear confirms the relevance of the electrode material if compared with the other factors. This result is representative of the considerable effect of the electrode material if compared with the other factors.

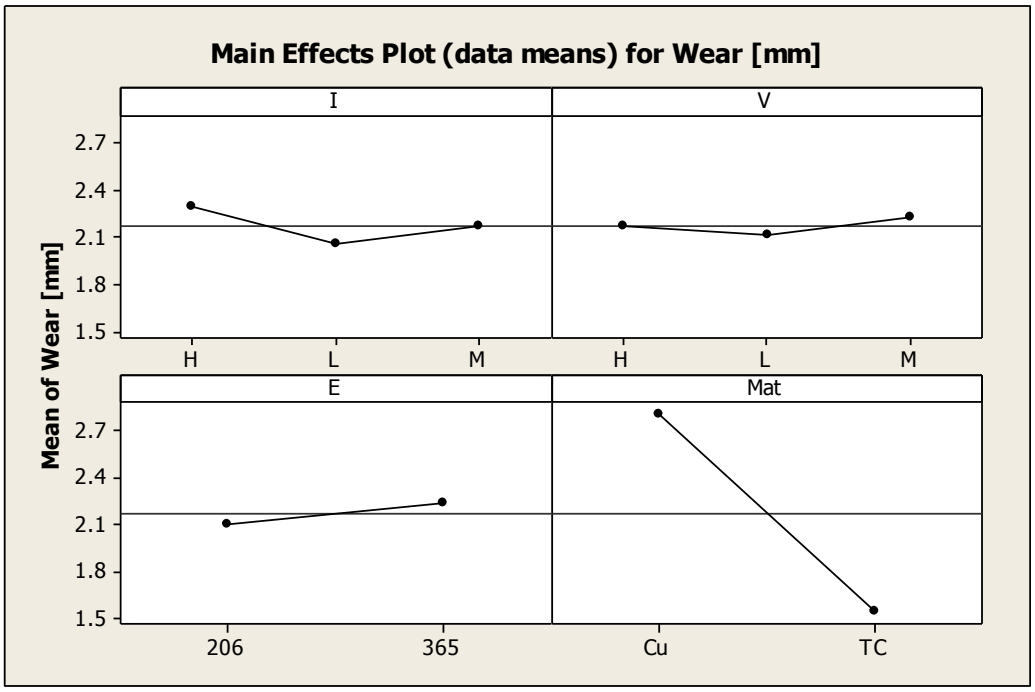

Figure 117: Main effects plot for electrode wear as a function of I, V, E and electrode material, d 150 µm

As a matter of fact, since the electrode materials (tungsten carbide and copper) are characterized by so different thermal and mechanical properties a certain influence was expected. But the most interesting result is the combined effect of the energy level and electrode material. This result emerged from the previous analysis, in particular regarding the 365 energy level tests. It was demonstrated that for the copper electrode tests executed with the 300 µm electrode diameter and with high energy level the exchanged power reached the value of about 25 watts. On the contrary, the experiments executed with the TC electrode resulted in a lower exchanged power, in particular, it was lower than 2.5 watts. Moreover, for the copper electrode with lower energy level,

the exchanged power is lower than 1.5 watts. This conclusion is confirmed by the TC results that in general are characterized by a lower exchanged of power when compared with the copper electrode. It is possible to conclude that the copper electrode with both energy levels ensures higher machining speeds, if compared with the TC electrode. A trade-off between the machining speed and electrode wear is still recorded, since the TC electrode ensures better results from this point of view. From the geometrical point of view, the DOC indicator is better for the copper electrode for the holes executed with low energy levels. Its value in fact is between 0.04 and 0.06 while for the TC electrode it is higher, since its value is between 0.06 and 0.08. For the high energy level, a different behaviour is recorded: the TC electrode results in more dispersed data, with values between 0.04 and 0.08. On the contrary, for the copper electrode, the values are 0.06 and 0.08. In general, even though a significant trend for the DOC cannot be found, the copper electrode provides better characteristics. This is possibly due to the lower machining time that decreases the probability of unwanted side discharges between the electrode and the workpiece, ensuring for this reason better geometrical qualities. This result is unexpected: the copper electrodes are characterized by a lower rigidity and possible effects on the geometrical characteristics, at least for the tests executed without the ceramic guide, were expected. The results instead confirm the better performance of the copper electrode, testifying that the machining time is a more relevant aspect for the geometrical quality of the holes.

In micro-EDM the electrode wear and the machining time are two of the most helpful indicators. Nowadays, even if information about time and wear could be of great help in the cost evaluation and in the production planning, a formal equation capable of predicting time and wear a priori is not available. In the following section, starting from the collected data about the real process parameters, some linear and non-linear predictive models have been developed. With these models it is possible to forecast not only the machining time and the electrode wear, but also the geometrical characteristics of the holes.

Chapter 5

Data mining and machine learning

In micro-EDM machining, the capability to predict the process performance and the geometrical quality of the holes can be very helpful. Especially from an industrial point of view, the possibility to forecast the time duration or the electrode wear, allows the evaluation of the machining process feasibility and leads to a more conscious estimation of time and costs. Nowadays a specific equation able to forecast the process performance or the geometrical characteristics of the holes is not available.

In order to identify a significant relationship between inputs (process parameters, electrode characteristics) and outputs (machining time, electrode wear and geometrical characteristics), a machine learning approach has been applied.

As mentioned before, no mathematical relationship has been found between the process parameters and the final output, expressed in terms of raw data like electrode wear and machining time. In order to identify this relationship and to forecast electrode wear and machining time, as well as the hole diameter, the Weka software has been used. Weka (Waikato Environment for Knowledge Analysis) is a free suite of data mining and machine learning software that is characterized by visualization tools and algorithms for data analysis and prediction modelling (Mark, et al. 2009).

The collected data about the process parameters has been used for the implementation of equations able to predict the final result with a good confidence level, especially for the holes' geometrical characteristics.

5.1 Data pre-processing, visualization and attribute selection

The first part of this elaboration consisted in the data preparation. The initial excel file containing all the collected data about diameters, process parameters and output, has been converted in ".csv" format. Starting from this point it is possible to convert in ".arff" weka file with a specific online application. Once the ".arff" file has been created

it is possible to visualize the raw data and eventually modify or update the data column. A typical pre-processing interface is shown in Figure 118.

In the picture it is possible to identify the so called “attributes” which correspond to all the data contained in the original starting excel file. In the left part of the figure it is possible to see the data visualization options: in particular, the “attributes” (the columns of the original excel file) and the “instances” (the rows of the original excel file). With the selection of each columns it is possible to open the “Explorer” window and to get information about the considered data set: the maximum value, the minimum, the average, the standard deviation and a graphical representation of the data.

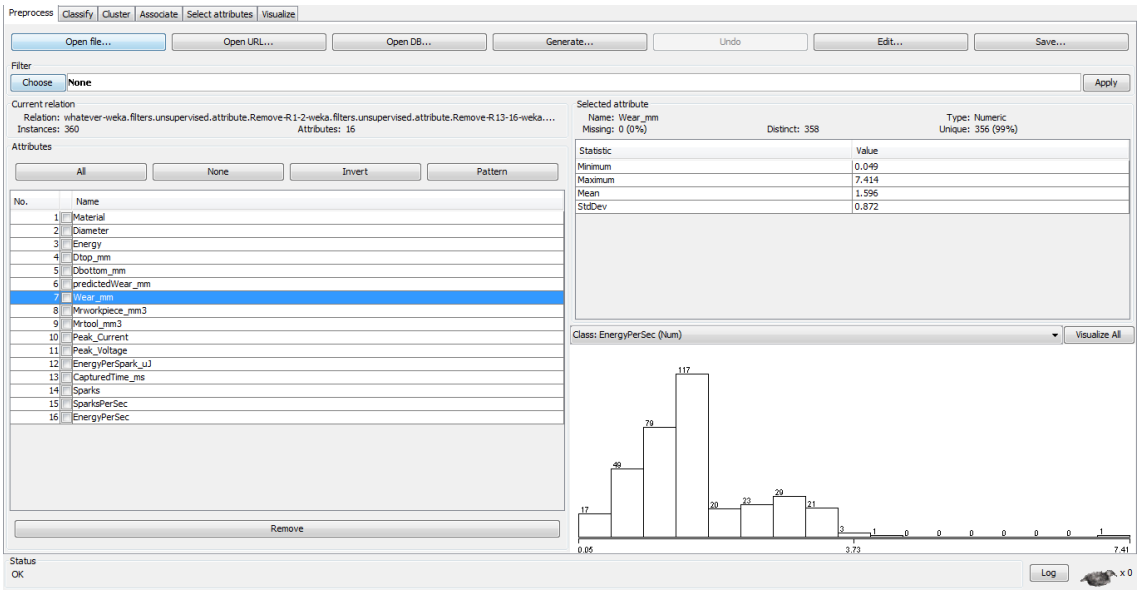

Figure 118: Weka pre-processing interface

The next step of the analysis consists in the creation of the model for the prediction of the selected attribute. The creation of the regression model can be carried out with the “Classify” option, as reported in Figure 119.

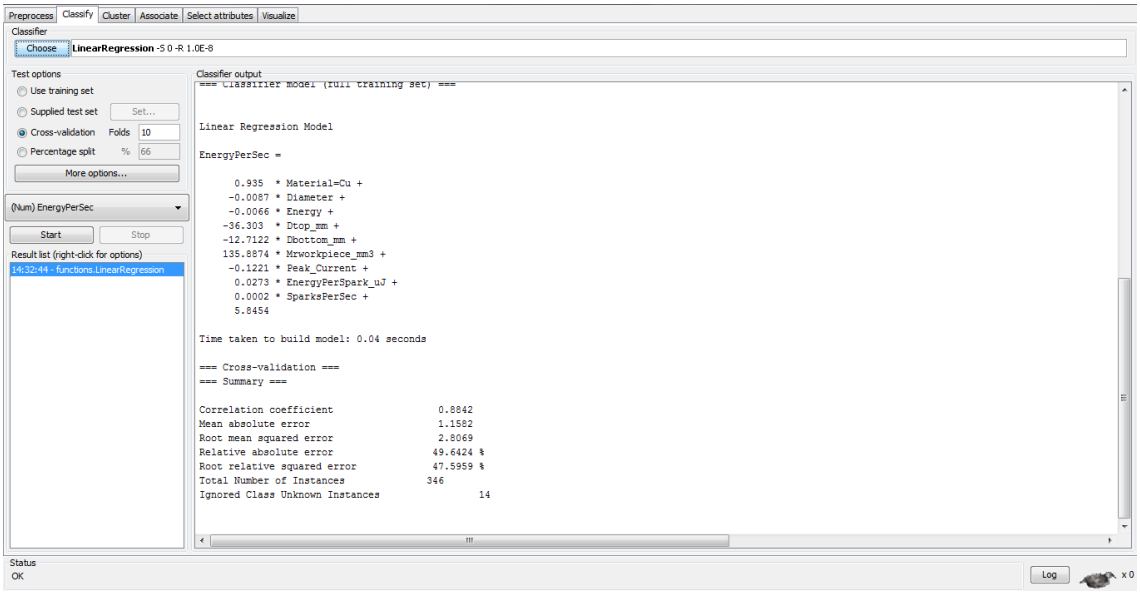

Figure 119: Weka regression model interface

Several models are available and can be chosen: the "LinearRegression" will be used for the first part of the present analysis. The linear regression approach is the simplest and the most used predicting technique in machine learning field, even though other more complex approaches allow more accurate results. For this reason the linear regression results were compared with the ones obtained with a non-linear regression approach. In particular, non-linear model trees were used, as well.

In general the linear regression model is used at the same time to predict the unknown dependent variable (Y), given the values of the independent variables (X_i), as reported in the following equation:

$$Y = \beta_0 + \beta_1 * X_1 + \beta_2 * X_2 + \ldots + \beta_n * X_n$$

The linear regression approach provides only the coefficients (β_i) while the "model tree" approach provides a more detailed relationship between the independent variables for numerous different experimental cases, describing the result with a higher level of confidence and with a lower error.

For this analysis a 10-fold cross validation approach has been applied: the regression model is built on 90% of the data (that represents the training dataset) and the remaining 10% (validation dataset) is used to validate the model able to predict the dependent variable. This result is compared with the already existing data for the selected 10%.

The proportion 10%-90% is considered optimal, because there is the need of a great amount of data for the model training (90%) but at the same time the statistical sample must be representative (10%). This procedure is repeated changing the 10%-90% proportion in order to avoid any over fitting problems and sample asymmetry.

Once the model has been chosen, it is possible to select between the attributes, in other words, it is possible to identify a minimal set of attributes for the model development. The initial dataset was made of the following attributes:

- Workpiece material (Mat),
- Electrode nominal diameter (Diam),
- Energy level (E),
- Peak current (I),
- Peak voltage (V),
- Energy per spark (E/spark),
- Energy per second (E/s),
- Total number of sparks (S),
- Number of sparks per second (S/s),
- Electrode wear,
- Machining time,
- Hole top diameter,
- Hole bottom diameter.

The pre-processing procedure, that is the selection of the attributes, has been differentiated for each case: for example, in order to identify the regression equation for the electrode wear some other attributes considered not relevant or correlated with the final output have been eliminated (for example, the machining time). The same has been done for the machining time and for the geometrical indicators. The details for each case and the obtained results will be described in the following sections.

Once the dependent attribute has been selected it is possible to carry out the regression between the inputs and the outputs in order to identify a mathematical relationship usable for the prediction of the results.

As a general remark, only columns that statistically give a contribution to the model accuracy are included, for this reason some of the attributes initially included in the model are ignored, since they do not contribute in creating a good model.

5.2 Regression models for electrode wear

Based on the previous assumptions, the first linear regression model has been carried out for the electrode wear. The data set here considered takes into account both materials (tungsten carbide and copper) and both diameters (300 and 150 microns). The linear regression model is reported below:

$$Wear = 0.9362 * Mat(Cu) - 0.0084 * Diam + 0.0023 \cdot E + 0.034 \cdot I + 2.3151$$

If the electrode material is copper, the coefficient 0.9362 must be included in the analysis, otherwise no coefficient must be considered. The summary of the regressions is reported in Table 33.

Table 33: Summary of the electrode wear linear regression

Coefficient	Value
Correlation coefficient	0.8601
Mean absolute error	0.2965
Root mean squared error	0.4443
Relative absolute error	46%
Root relative squared error	51%
Total number of Instances	360

As seen from the equation, some of the initial attributes have not been considered for the final equation. In particular, the peak voltage has not been included in the analysis as well as the energy per spark and the number of sparks. Some other parameters, the

number of sparks per second, are present in the model but with a null coefficient, for this reason they are not shown here. Figure 120 reports the plot of the classifier errors.

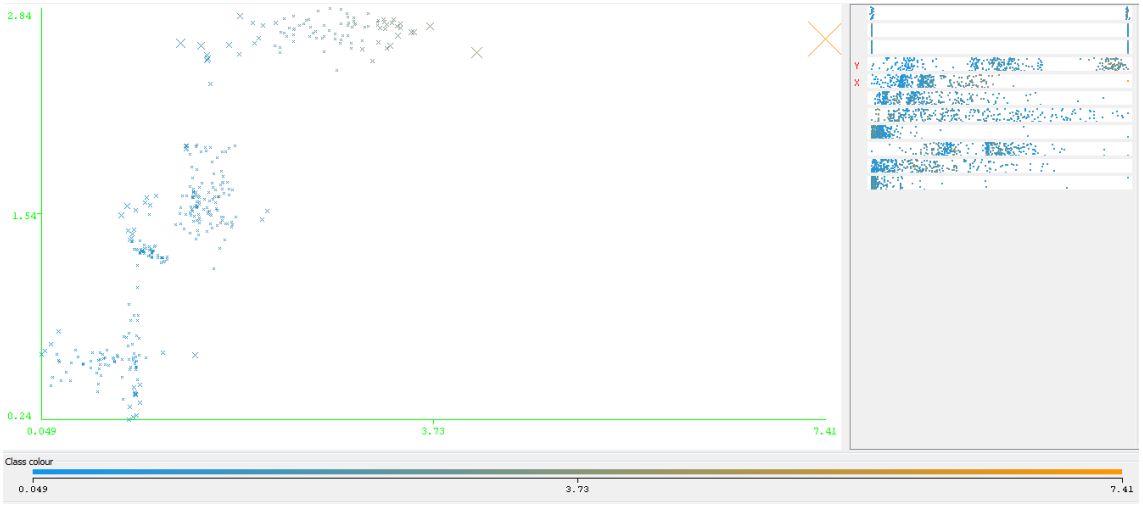

Figure 120: Classifier error plot for electrode wear linear regression

In this case it is possible to notice that a linear relationship exists between the predicted data and the real wear data. In particular, every cross represent the predicted data for the known initial data about the electrode wear. The predicted data appear to be distributed along an ideal line, which is not characterized by the 45° inclination because of the difference in scale of the x-y axises. The smaller the cross, the more accurate is the prediction of the final value.

With the non-linear approach it was possible to obtain a more accurate regression model, with lower errors, as reported in Table 34. A linear model tree is a decision tree with a linear functional model in each leaf, whereas in classical regression tree it is the sample mean of the response variable for statistical units in each leaf (hence, a constant) that is being considered. Linear model trees can be seen as a form of locally weighted regression, while regression tree are piecewise-constant regression (Torgo 1997). The structure of the tree obtained for the electrode wear is shown in Figure 121. It is possible to notice that the model considers only the electrode nominal diameter, the energy level and the electrode material, for the first level of the tree. Every branch of the tree is represented by a linear model (LM), in this case, LM1, LM2, LM3, LM4.

Table 34: Summary of the electrode wear non-linear regression

Coefficient	Value
Correlation coefficient	0.8708
Mean absolute error	0.2635
Root mean squared error	0.4283
Relative absolute error	40%
Root relative squared error	49%
Total number of Instances	360

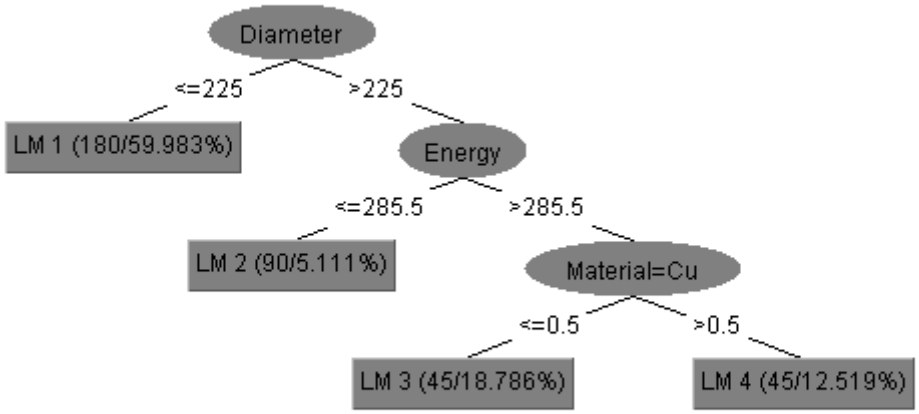

Figure 121: LM1 of the regression tree for the electrode wear

The other implemented linear models and the classifier errors (Figure 122) are shown below.

LM 1:

$$w = 1.1949 \cdot Mat(Cu) - 0.0006 \cdot D + 0.0022 \cdot E + 0.0026 \cdot I + 1.247$$

LM 2:

$$w = 0.072 \cdot Mat(Cu) - 0.0006 \cdot D + 0.0138 \cdot I - 0.0031 \cdot V - 0.0007 \cdot \frac{E}{S} +$$

$$-0.0001 \cdot S - 0.0122 \cdot \frac{E}{s} + 1.1491$$

LM 3:

$$w = 0.1689 \cdot Mat(Cu) - 0.0006 \cdot D + 0.0171 \cdot I - 0.0138 \cdot V - 0.004 \frac{E}{S} +$$

$$-0.0001 \cdot S + 0.0023 \cdot \frac{E}{s} + 1.5034$$

LM 4:

$$w = 0.1689 \cdot Mat(Cu) - 0.0006 \cdot D + 0.0364 \cdot I - 0.0054 \cdot V - 0.0001 \cdot \frac{E}{s}$$

$$- 0.0001 \cdot S + 0.0023 \cdot \frac{E}{s} + 1.3854$$

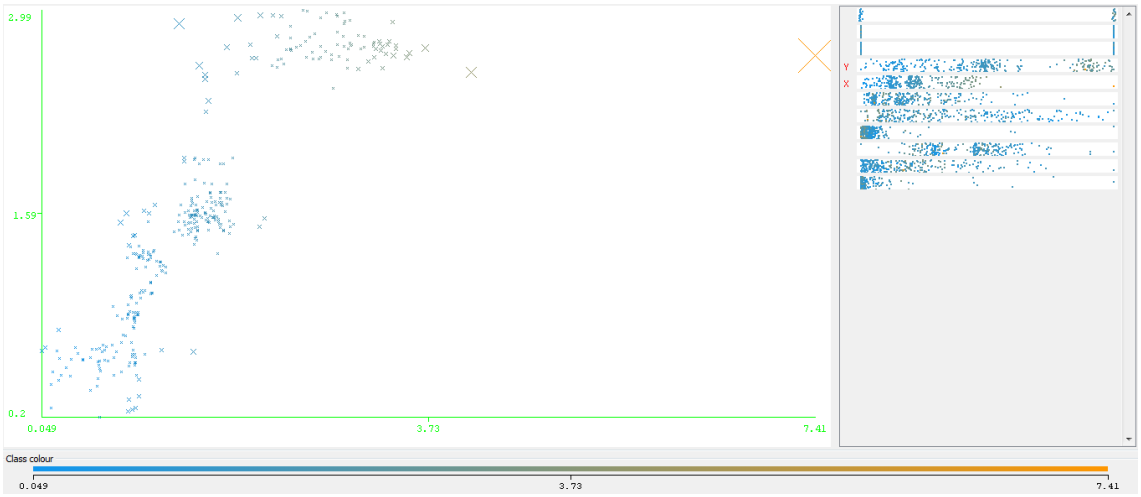

Figure 122: Classifier error plot for electrode wear non-linear regression

The non-linear approach ensures a lower error level and better regression capabilities than the simple linear regression. A trade-off between the usability of the model and the

prediction capabilities still exists: it is necessary to evaluate for each case if the real improvements in the regression capabilities are balanced by a considerable increment of complexity of the model.

5.3 Regression models for machining time

As explained for the electrode wear, the same linear regression has been made for the machining time, that with the electrode wear is one of the most important aspects describing the micro-EDM process. The obtained linear regression is reported below:

$$t = 506.6735 \cdot Mat(Tc) + 1.7624 \cdot D - 1.3055 \cdot E + 48.3054 \cdot I - 13.8123 \cdot V +$$

$$-0.2715 \cdot S + 251338$$

In this case, it is possible to notice that more factors have been included in the model, such as the number of sparks, the sparks per second and the voltage. The summary of the regression analysis is reported in Table 35.

Table 35: Summary of the machining time linear regression

Coefficient	Value
Correlation coefficient	0.794
Mean absolute error	168.4669
Root mean squared error	246.4101
Relative absolute error	61%
Root relative squared error	61%
Total number of Instances	360

In this case, the correlation coefficient is lower if compared with the electrode wear one. This is confirmed by the classifier errors plot, as reported in Figure 123.

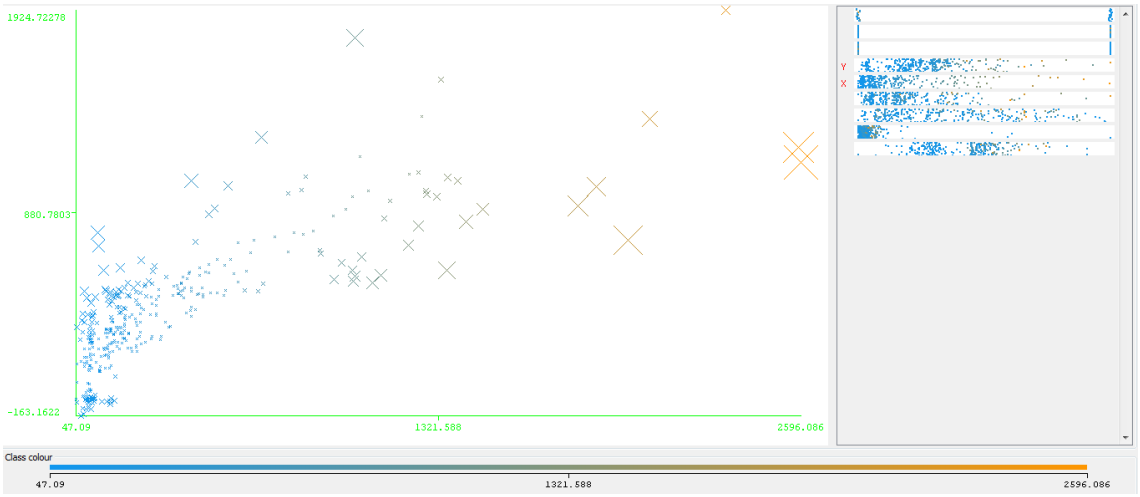

Figure 123: Classifier error plot for machining time linear regression

The regression tree provides a better correlation coefficient as shown in Table 36.

Table 36: Summary of the machining time non-linear regression

Coefficient	Value
Correlation coefficient	0.8316
Mean absolute error	130.4349
Root mean squared error	225.5382
Relative absolute error	47%
Root relative squared error	55%
Total number of Instances	360

The structure of the regression tree is shown in Figure 124. In this case only the energy level and the electrode material are included in the first model.

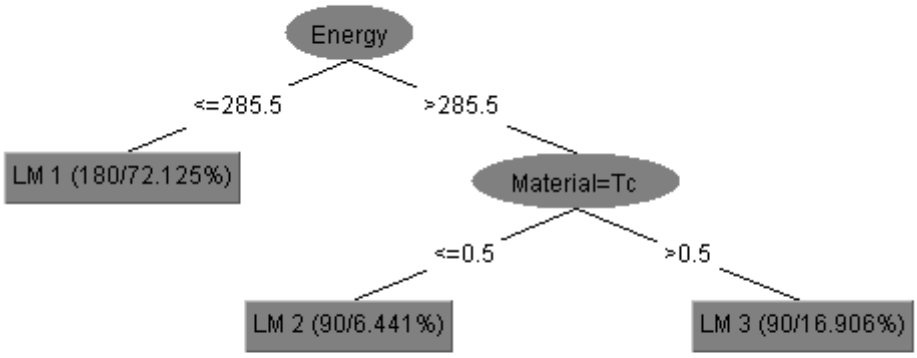

Figure 124: LM1 of the regression tree for the machining time

The details regarding the other models are reported below. Figure 125 shows the classifier errors.

LM 1:

$$t = 491.7175 \cdot Mat(TC) + 3.9493 \cdot D - 0.1004 \cdot E + 53.2883 \cdot I - 1.0625 \cdot V - 4.782 \cdot \frac{E}{S} + 1.272 \cdot S - 1173.5422$$

LM 2:

$$t = 68.4943 \cdot Mat(TC) + 0.3843 \cdot D - 0.1004 \cdot E - 0.1849 \cdot I - 1.8554 \cdot V - 0.0263 \cdot \frac{E}{S} + 0.0153 \cdot S + 75.4619$$

LM 3:

$$t = 68.4943 \cdot Mat(TC) + 0.6605 \cdot D - 0.1004 \cdot E + 26.9388 \cdot I - 8.4397 \cdot V - 0.0263 \cdot \frac{E}{S} + 0.0153 \cdot S + 191.1432$$

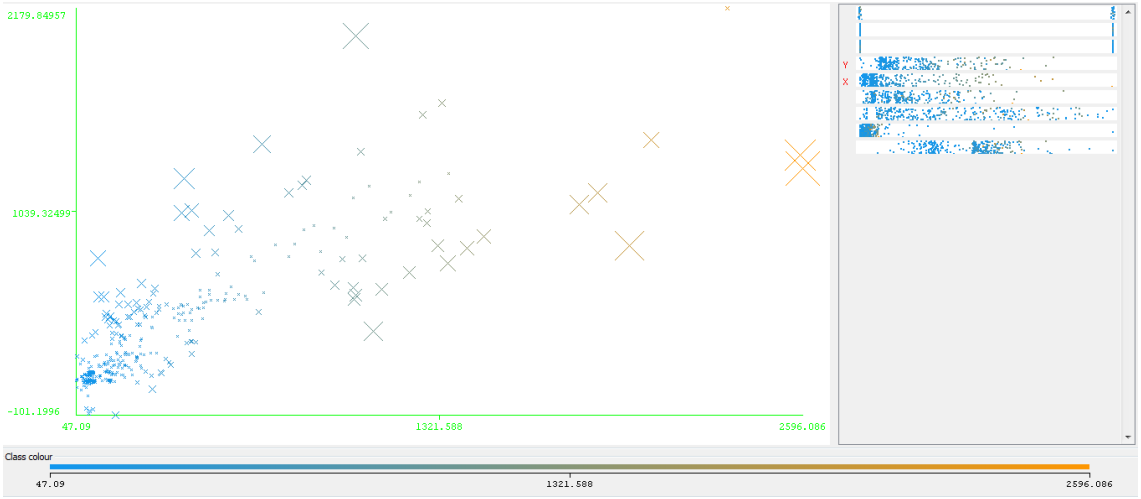

Figure 125: Classifier error plot for machining time non-linear regression

5.4 Regression models for hole top diameter

For the holes geometrical characteristics, both the top and the bottom diameter were taken into account for the analysis. It is well known that the top diameter in micro-EDM is always bigger than the bottom one, and that a certain relationship exists between the two. Anyway, they were analysed separately. The linear regression here obtained is the following:

$$D_{top} = 0.004 \cdot Mat(TC) + 0.001 \cdot D + 0.0005 \cdot I + 0.0002 \cdot V + 0.0576$$

Figure 122 shows the summary of the cross validation analysis. The correlation coefficient is highly satisfactory, for this reason no considerable incremental improvement provided by the non-linear model will be expected. In this case especially, the advantage given by a more complicated model is not balanced by the real improvements in the correlation coefficient.

Table 37: Summary of the top diameter linear regression

Coefficient	Value
Correlation coefficient	0.9901
Mean absolute error	0.0081
Root mean squared error	0.0107
Relative absolute error	11%
Root relative squared error	14%
Total number of Instances	360

Figure 126 shows the classifier errors. It is possible to notice the clusters referring to the 150 and 300 µm electrode diameter.

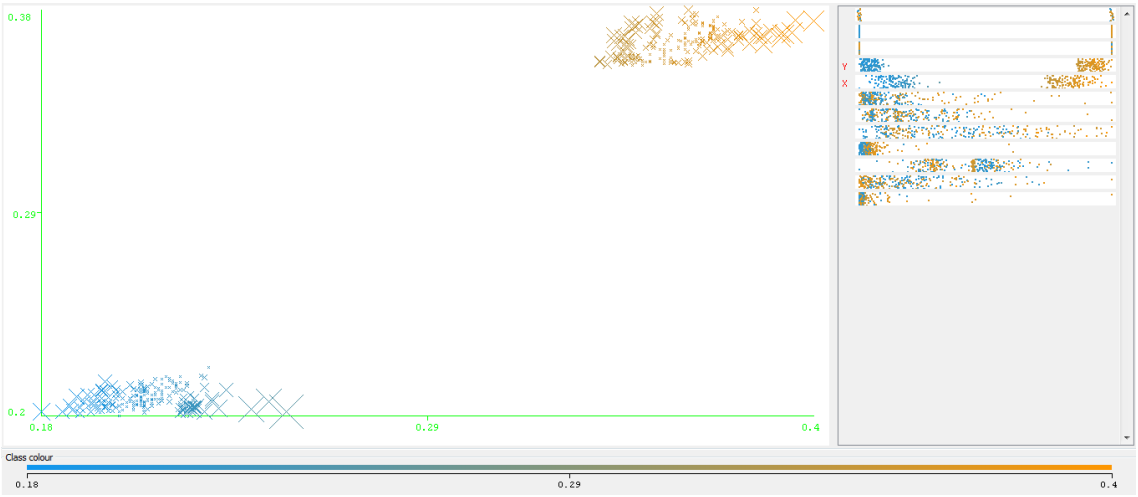

Figure 126: Classifier error plot for hole top diameter linear regression

Even if the non-linear regression with trees approach is based on building trees of linear models, in this case the tree corresponds to a singular linear model, which is reported below and corresponds to the first initial model:

LM 1:

$$D_{top} = 0.004 \cdot Mat(TC) + 0.001 \cdot D + 0.0005 \cdot I + 0.0002 \cdot V + 0.0576$$

The summary of the cross validation analysis is reported below:

Table 38: Summary of the top diameter non-linear regression

Coefficient	Value
Correlation coefficient	0.9903
Mean absolute error	0.0079
Root mean squared error	0.0106
Relative absolute error	11%
Root relative squared error	14%
Total number of Instances	360

As shown in Table 38, this is a particular case because the non-linear model corresponds to the linear model previously proposed. As a matter of fact, the correlation coefficient of the linear model did not allow many possible ways of improvement.

5.5 Regression models for hole bottom diameter

In the previous section the top diameter regression was implemented. In general, even if the conicity can vary with the process parameters combination, the bottom diameter is always the binding aspect. For this reason, the bottom diameter must fulfil certain dimensions and tolerances. The regression equation for the hole bottom diameter is the following:

$$D_{bottom} = 0.001 \cdot Diam + 0.0012 \cdot I + 0.0471$$

And the corresponding cross validation summary is reported in Table 39. If compared with the other regressions, the correlation coefficient is here notable. No considerable improvement is thus expected with the non-linear model approach that is reported below.

Table 39: Summary of the bottom diameter linear regression

Coefficient	Value
Correlation coefficient	0.9897
Mean absolute error	0.0079
Root mean squared error	0.011
Relative absolute error	10%
Root relative squared error	14%
Total number of Instances	360

In this case, the correlation coefficient is high and this result is confirmed by the plot reported in Figure 127. The data appears divided into two groups as expected: the blue one refers to the 150 µm diameter and the orange one refers to the 300 µm. Moreover, the classifier error for the 300 µm diameter are less relevant. The dispersion of the 150 µm electrode data is considerable, even though the regression can be considered very good. The non-linear regression results are shown in Figure 127.

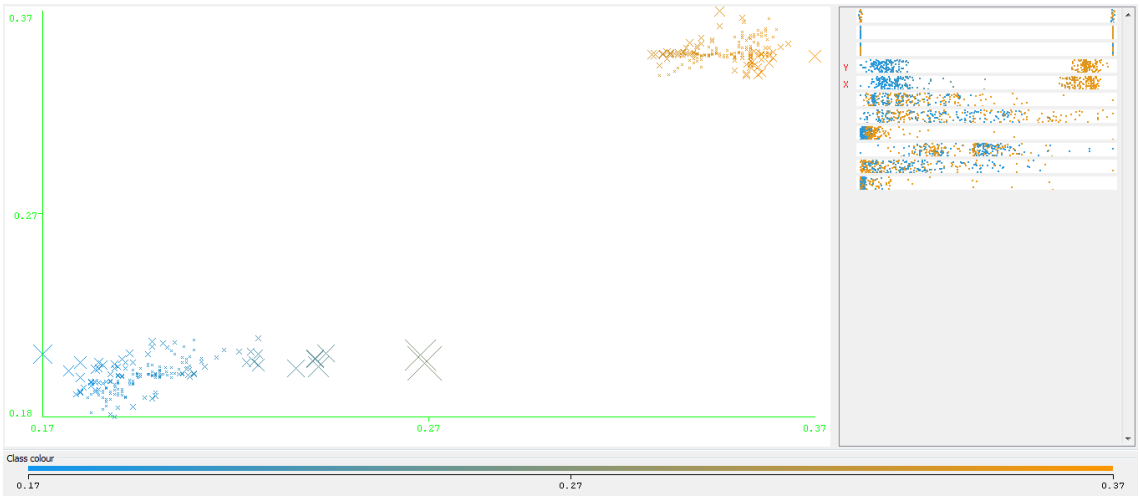

Figure 127: Classifier error plot for bottom diameter linear regression

Table 40: Summary of the bottom diameter non-linear regression

Coefficient	Value
Correlation coefficient	0.9838
Mean absolute error	0.0064
Root mean squared error	0.0138
Relative absolute error	8%
Root relative squared error	17%
Total number of Instances	360

From the analysis carried out so far, the regressions with the higher correlation coefficient are the geometrical ones, for the top and bottom diameter. For the top diameter in particular, the linear regression model, appears to be the best and corresponds to the non-linear model as well. The machining time on the contrary, is characterized by the worst predictive model.

It is possible to conclude that with the real data collected during the machining process (namely the exchanged energy and power, the number of sparks and the sparks per second and the peak current and voltage) it was possible to obtain simple linear or non-linear models with good correlation coefficients and acceptable errors.

The evaluation of the process performance is in general a very complicate aspect because of the non-deterministic nature of micro-EDM technology, and because of the unpredictable side effects like short circuits and unwanted side discharges.

Increasing the knowledge about the real process parameters (namely, I, V the energy and the power exchanged) allowed the introduction of regression equations useful to predict the process performances (machining time and electrode wear) and the geometrical characteristics of the holes (top and bottom diameter).

Conclusive Remarks and Future Work

The aim of the present work was to deepen the knowledge about the effect of process parameters and the electrode characteristics in micro-EDM and to investigate their influence on the process performance and on the geometrical characteristics of the micro-holes.

The relevance of the experimental conditions and their effect on the final output of micro-EDM was investigated by several authors and the present work gave a contribution, especially from the parameters measurement and analysis point of view.

First of all, a system for the acquisition of the electrical signal during micro-EDM machining was implemented: thanks to this system it was possible to collect information about the actual values of the peak current, the voltage and the energy exchanged during the process, data not available so far. Moreover, from the signal analysis, it was possible to obtain information about the number of sparks per second, the energy per spark, that resulted very useful information for the signal investigation and characterization.

In order to investigate the influence of the varied process parameters on the final output, the DOE approach was applied to the experimental campaign and the analysis of variance approach was used in order to investigate which factors of the model had an influence on the final response. The experimental campaign was executed with automatic programs and the machining time and the electrode wear were recorded at the end of each hole. The electrical signal regarding the peak current and voltage was recorded during the machining, too. The holes top and bottom diameters were measured by means of an optical microscope and the collected data were refined in order to eliminate all the outliers.

From the analysis of variance, a common trend for all the experiments carried out was identified: a certain interaction between the peak current and the voltage is always recorded even though no common trend was identified between the factors and the final response. Moreover, the considerable effect of the energy level was observed for all the experimental conditions, for this reason the model was extended a posteriori, including

in the analysis the energy level and the electrode material. The p-value comparison confirmed the assumptions previously made: the energy is with full rights a relevant factor of the model, and its influence can be considered the most relevant, in all the cases. The same was observed for the electrode material.

Once the factors having an influence on the final result were identified, the following step consisted in the investigation of their trend as a function of the electrical power. From this starting point, the measured values of the process parameters were used and the exchanged power was selected since it was considered a representative variable of I, V and E, or rather the relevant factors in the model.

The results can be summarized as follows. First of all, the measured exchanged power is directly proportional to the process parameters levels, as assumed before the effective measurement of the actual parameters. Moreover, it is demonstrated how the increasing exchanged power has a positive influence on the machining time, for both electrode diameters and materials. A different trend is found for the electrode wear: for the TC electrode, the increasing power decreases the electrode wear, exactly the opposite trend recorded for the copper electrode. This effect is due to the electrode material thermal and electrical characteristics. On the contrary, different trends were found for the geometrical characteristics indicators. In this case, the increasing power causes a worsening of the DOC and TR indicators, even though no significant trends can be found.

Finally, predictive models for the most relevant aspects of the micro-EDM process were implemented. The micro-EDM process aspects here considered relevant are the machining time and the electrode wear, as well as the hole top and bottom diameter.

Nowadays, no significant formalization is available to forecast the process performance, for this reason a simple linear regression with a cross validation approach was adopted. Although acceptable correlation coefficients were obtained, in order to improve the models, a non-linear regression approach was implemented as well. In this case, “model trees” were used, where every branch of the tree represents a linear model with different coefficients. Two different situations were obtained: for the hole geometrical characteristics the initial linear model was good to such an extent that no significant

improvement was ensured by the non-linear model. On the contrary, for the process performance (time and wear) the non-linear model ensures a certain improvement.

As a general remark, micro-EDM process is a non-deterministic process and many limitations to a real prediction of the final results is still present. The capability to collect and use real data from the electrical signal helps to overcome the previous limitations, even though some drawbacks due to the intrinsic characteristics of the technology still remain: for example, this process is characterized by short circuits and electric arcs, just to mention the most common. These electrical phenomena are almost impossible to forecast, nevertheless they affect the machining efficiency and they make every experimental campaign different from the others.

The study carried out so far took into account only one electrode geometry for the machining of stainless steel. In order to widen the knowledge about micro-EDM drilling and to implement more and more reliable forecasting models, other experimental campaign and characterization procedures can be carried out. The capability to investigate different workpiece materials, for example the so called “difficult to cut materials” (high hardness materials, like titanium), different electrode geometries and smaller electrode diameters could give a considerable contribution to the electrode wear and machining time forecasting.

In conclusion, the capability to monitor, record and use the experimental data allows a better understanding of the technology. Moreover, it allows to overcome the previous lack of knowledge related to the expected hole diameter, and to implement predictive models for the most relevant aspects of the process.

References

Alting L, Kimura F, Hansen H N, Bissacco G. "Micro Engineering." *CIRP Annals - Manufacturing Technology*, 2003: 52(2):635-657.

Arbizu I D, Pérez C J L. *History and foundations of EDM: the least conventional of the machining.*, http://www.interempresas.net/MetalWorking/Articles/12068-The-least-conventional-of-the-machining.html, (last accessed April 24, 2013).

Chow H M, Yan B H, Huang F Y, Hung J C. "Study of added powder in kerosene for the micro-slit machining of titanium alloy using electro-discharge machining." *J Mater Process Technol*, 2000: 101:95-103.

Chow H M, Yang L D, Lin C T, Chen Y F. "The use of SiC powder in water as dielectric for micro-slit EDM machining." *J Mater Process Technol*, 2008: 195:160-170.

Denkena, B, Hoffmeister H W, M Reichstein, S Illenseer, and M Hlavac. "Micromachining process for micro system technology." *Microsystems Technology*, 2006: 659-664.

Deshmukh, A. *Modelling of Anode Crater Formation in Micro-Electrical Discharge Machining,2*013,http://digitalcommons.unl.edu/cgi/viewcontent.cgi?article=1044&context=imsediss.

D'Urso, G, G Maccarini, C Merla, C Ravasio, and A Surleraux. "Comparison EDM / Dry-EDM in microdrilling process." *Proceedings of 4M Conference*, 2015.

D'Urso G., Merla C. "Workpiece and electrode influence on micro-EDM drilling performance." *Precision Engineering*, 2014, 38 (4), 903-914.

D'Urso, G, C Merla, and G Maccarini. "EDM drilling of high aspect ratio micro holes." *Proceedings of AITeM Conference*, 2013.

D'Urso, G, G Maccarini, and C Merla. "The dowsizing effects in EDM drilling of micro holes." *Proceedeings of SheMet Conference*, 2013.

D'Urso, G, G Maccarini, C Merla, and C Ravasio. "Micro-EDM machining of small features on magnesium plates." *ProMed - 1st International Conference on Design and PROcesses for MEdical Devices*, 2012.

D'Urso, G, G Maccarini, C Merla, and C Ravasio. “The influence of electrode shape and material on micro-EDM drilling process.” *Proceedings of 4M Conference*, 2012.

D'Urso, G, M Longo, G Maccarini, and C ravasio. "Electrical discharge machining of micro holes on titanium sheets." *Proceedings of the 5th International Conference on Micro and Nanosystems, ICOM 14*, 2011.

Garn, R, A Schubert, and H Zeidler. “Analysis of the effect of vibration on the micro-EDM process at the workpiece surface.” *Precision Engineering*, 2011: 35, 364-368.

Geiger, M et al. "Microforming." *Annals of the CIRP*, 2001: 50(2):445-462.

Ho K H, Newman S T. "State of the Art Electrical Discharge Machining (EDM)." *INternational Journal of Machine Tools and Manufacture* 43 (2003): 1287-1300.

Ho K H, Newman S T, Rahimifard S, Allen R D. “State of the Art Wire Electrical Discharge Machining.” *International Journal of Machine Tools and Manufacture* 44 (2004): 1247-1259.

Innovaciòn, Ministero de Ciencia e. *Micro manufacturing, differences between macro and micro-EDM,* http://www.micromanufacturing.net/didactico/Desarollo/edm-eng/6-differences-between-macro-and-micro-edm. (last accessed Dec 2013).

Jaham, M. P. “Micro-Electrical Discharge Machining.” *Nontraditional machining processes*, by J. P. Davim. 2013.

Jahan, M P, M Rahman, and Y S Wong. "A review on the conventional and micro-electro discharge machining of tungsten carbide." *International Journal of Machine Tools & Manufacture*, 2011: (51) 837–858.

Jahan, M P, Y S Wong, and M Rahman. “A comparative experimental investigation of deep-hole micro-EDM drilling capability for cemented carbide (WC-Co) against austenitic stainless steel (SUS 304).” *International Journal of Advanced Manufacturing Technology*, 2010: 46, 1145-1160.

Jeswani, M L. "Effect of the addition of graphite powder to kerosene used as the dielectric fluid in electrical discharge machining." *Wear*, 1981: 70:133-139.

Kansal H K, Singh S, Kumar P. "Technology and research developments in powder mixed electric discharge machining (PMEDM)." *Journal of Material Processing Technologies*, 2007: 184:32-41.

Karafuji H, Masuzawa T. "Micro-EDM of Cemented Carbide Alloys." *Japanese Society of Electrical Machining Engineers* 2, no. 3 (1968): 1-16.

Katz Z, Tibbles C J. "Analysis of micro-scale EDM process." *International Journal of Advanced Manufacturing Technologies*, 2005: 25:923-928.

Kibria G, Sarkar B R, Pradhan B B, Bhattacharyya B. "Comparative Study of different dielectics for micro-EDM performance during micro-hole machining of Ti-6Al-4V alloy." *International Journal of Advanced Manufacturing Technologies*, 2010: 48: 557-570.

Klocke, F, M Schwade, A Klink, and A Kopp. "EDM machining capabilities of magnesium (Mg) alloy WE43 for medical applications." *Procedia Engineering*, 2011: 19, 190-195.

Kumar S, Singh R, Singh T P, Sethi B L. "Surface modification by electrical discharge machining: A review"." *Journal of Materials Processing Technology*, 2009: 209:3675-3687.

Kunieda M, Lauwers B, Rajurkar K P, Schumacher B M. "Advancing EDM though fundamental insight into the process." *Annals of the CIRP*, 2005: 54(2):64:87.

Kuppan, P, A Rajadurai, and S Narayanan. “Influence of EDM process parameters in deep hole drilling of Inconel 718.” *International Journal of Advanced manufacturing Technology*, 2008: 38, 74-78.

L, Jeswani M. "Electrical discharge machining in distilled water." *Wear*, 1981: 72:81-88.

Lazarenko B R, Lazarenko N J. "Electrical Erosion of Metals (in Russian)." 1944: 27, 7 figures.

Lim H S, Wong Y S, Rahman M, Lee E M K. "A study on the machining of high-aspect ratio micro-structures using micro EDM." *Journal of Material Processing Technologies*, 2003: 140:318-325.

Lim, H S, S M Son, Y S WOng, and Rahman M. "Develpoment and evaluation of an on-machine optical measurement device." *International Journal of machine Tools and Manufacture*, 2007: 1556-1562.

Livshiz, A L. "Electroerosive machining Metals (in Russian)." *German edition 1959 by VEB Verlag Technik*, 1957: 145 pages, 62 figures, 7 charts.

Luo, Y F. "The dependence of interspace discharge transitivity upon the gap debris in precision electro-discharge machining." *Journal of Material Processing Technologies,* 1997: 68:127-131.

MacGeogh J A, et al. "Electroforming process and application to micro/macro manufacturing." *Annals of the CIRP*, 2001: 50(2):499-514.

Mahendran S, Devarajan R, Nagarajan T, Majdi A. "A review of Micro-EDM." *Proceedings of the International MultiConference of Engineers and Computer Scientists Vol. II, IMECS*, 2010.

Mark, Hall, Frank Eibe, Holmes Geoffrey, Pfahringer Bernhard, Reutemann Peter, and Witten Ian H. "The WEKA Data Mining Software: An Update." *SIGKDD Explorations*, 2009, 11(1).

Masuzawa, T. "State of the Art of Micromachining." *Annals of the CIRP*, 2000: 49(2):473-488.

Menz, W et al. "Non-conventional technologies for fabrication of micro-systems." *Proceedings of the 3rd Euspen International Conference*, 2002: 3-6.

Mounier, E. "MEMS, the alternative semiconductor business." *Proceedings of the 3rd Euspen International Conference*, 2002: 391-394.

Pham D T, Dimov S S, Bigot S, Ivanov A, Popov K. "Micro-EDM recent developments and research issues." *J Mater Process Technol*, 2004: 149:50-57.

Pham, D T, A Ivanov, S Bigot, K Popov, and S Dimov. "A study of micro-electro discharge machining electrode wear." *Journal of Mechanical Engineering Science*, 2007: 605-612.

Ponappa, P, S Aravindan, P V Rao, J Ramkumar, and M Gupta. "The effect of process parameters on machining of magnesium nano alumina composites through EDM." *International Journal of Advanced Manufacturing Technologies*, 2010: 46, 1035-1042.

Pradhan, B B, M Masanta, B R Sarkar, and B Bhattacharyya. "Investigation of electro-discharge micro-machining of titanium super alloy." *International Journal of Advanced Manifacturing technology*, 2009: 41, 1094-1106.

Rajurkar K P, Levy G, Malshe A, Sundaram M M, McGeough J, Hu X, Resnick R, De Silva A. "Mico and nano machining by electro-physical and chemical processes." *Ann CIRP, 55(2):643-666*, 2006.

Rajurkar K P, Wang W M. "On-line monitor and control for wire breakage in WEDM." *Ann CIRP, 40(1):219-222*, 1991.

Reynaerts D, Heeren P H, Van Brussel H, Beuret C, Larsson O, Bertholds A. "Micro structuring of silicon by electro-discharge machining (EDM) part II: applications." *Sens Actuators*, 1997: 61:379-386.

SA, Sairx. "Sarix User Manual." Losone (Swisse) , 2012.

Sanchez, J A, et al. "Electrode set-up for EDM-drilling of large aspect-ratio microholes." *Procedia CIRP 6 - The Seventeenth CIRP Conference on Electro Physical and Chemical Machining (ISEM)*, 2013, pp 275 – 280.

Schumacher B M, Krampitz R, Kruth J P. “Historical phases of EDM development driven by the dual influence of "Market Pull" and "Science Push"” *Procedia CIRP*, 2013: 5-12.

Solotych, N B. "Physical Fundamentals of Electrical Spark Machining of Metals (in Russian)." *German Edition 1955 by VEB Verlag Technnik*, 1952: 90 pages, 50 figures.

Takahata, K. "Micro-electro-discharge machining technology for MEMS." *Micro Electron Mech Syst INTECH*, 2009: 144-164.

Torgo, L. "Functional Models for Regression Tree Leaves." 1997.

Uhlmann E, Piltz S, Doll U. "Machining of Micro/Miniature dies and moulds by electrical discharge machining-recent developments." *Journal of Material Processing Technology*, 2005: 167:488-493.

Van Brussel, H et al. "Assembly of micro-systems." *Annals of the CIRP*, 2000: 49(2):451-472.

Yilmaz, O N, and A Okka. "Effect of single and multi-channel electrodes applicationon EDM fast hole drilling performance." *International Journal of Advanced Manufacturing Technology*, 2010.

Yu, Z Y, K P Rajurkar, and H Shen. “High aspect ratio and complex shaped blind micro holes by micro EDM.” *Department of Industrial and Management Systems Engineering, University of Nebraska, Lincoln (USA)*, 2002.

Yu, Z Y, T Masuzawa, and M Fyjino. "Micro-EDM for three dimensional cavities - Development of uniform wear method." *Annals of the CIRP*, 1998: 47 (1), 169-172.

Zahiruddin M, Masanori K. "Comparison of energy and removal efficiencies between micro and macro EDM." *CIRP Annals - Manufacturing Technology*, 2012: 61:187-190.

Zhang L, Jia Z, Liu W, Li A. "A two-stage servo feed controller of micro-EDM based on interval type-2 fuzzy logic." *International Journal of Advanced Manuacturingf Technologies*, 2012: 59(5-8):633-645.

Zhang Q H, Du R, Zhang J H, Zhang Q. "An investigation of ultrasonic-assisted electrical discharge machining in gas." *International Journal of Machine Tool and Manufacturing*, 2006: 46(12-13):1582-1588.

List of Tables

List of Figures

Appendix

Tungsten Carbide (TC) Electrode

First level of Analysis: I and V

TC, d 300 µm, E 365

General Linear Model: Time [s], Wear [mm], ... versus I, V

```
Factor  Type   Levels  Values
I       fixed       3  40, 60, 80
V       fixed       3  80, 100, 120


Analysis of Variance for Time [s], using Adjusted SS for Tests

Source  DF  Seq SS  Adj SS  Adj MS     F      P
I        2   50198   50198   25099  8.55  0.001
V        2   57801   57801   28901  9.85  0.000
I*V      4   17121   17121    4280  1.46  0.235
Error   36  105674  105674    2935
Total   44  230794


S = 54.1792   R-Sq = 54.21%   R-Sq(adj) = 44.04%


Unusual Observations for Time [s]

Obs  Time [s]      Fit  SE Fit  Residual  St Resid
 22   128.390  263.947  24.230  -135.557     -2.80 R
 23   278.292  154.145  24.230   124.147      2.56 R

R denotes an observation with a large standardized residual.


Analysis of Variance for Wear [mm], using Adjusted SS for Tests

Source  DF   Seq SS   Adj SS   Adj MS      F      P
I        2  0.54518  0.54518  0.27259  28.94  0.000
V        2  1.01400  1.01400  0.50700  53.82  0.000
```

I*V	4	0.02116	0.02116	0.00529	0.56	0.692
Error	36	0.33913	0.33913	0.00942		
Total	44	1.91947				

S = 0.0970581 R-Sq = 82.33% R-Sq(adj) = 78.41%

Unusual Observations for Wear [mm]

Obs	Wear [mm]	Fit	SE Fit	Residual	St Resid
3	0.215662	0.405565	0.043406	-0.189903	-2.19 R
6	0.599213	0.322810	0.043406	0.276404	3.18 R
21	0.600302	0.405565	0.043406	0.194737	2.24 R
24	0.081982	0.322810	0.043406	-0.240827	-2.77 R

R denotes an observation with a large standardized residual.

Analysis of Variance for DOC [mm], using Adjusted SS for Tests

Source	DF	Seq SS	Adj SS	Adj MS	F	P
I	2	0.0011173	0.0011173	0.0005586	10.77	0.000
V	2	0.0005689	0.0005689	0.0002845	5.48	0.008
I*V	4	0.0056669	0.0056669	0.0014167	27.30	0.000
Error	36	0.0018682	0.0018682	0.0000519		
Total	44	0.0092213				

S = 0.00720378 R-Sq = 79.74% R-Sq(adj) = 75.24%

Unusual Observations for DOC [mm]

Obs	DOC [mm]	Fit	SE Fit	Residual	St Resid
12	0.046000	0.060000	0.003222	-0.014000	-2.17 R
21	0.078000	0.060000	0.003222	0.018000	2.79 R
25	0.090000	0.065500	0.003222	0.024500	3.80 R

R denotes an observation with a large standardized residual.

Analysis of Variance for TR, using Adjusted SS for Tests

Source	DF	Seq SS	Adj SS	Adj MS	F	P
I	2	0.0001562	0.0001562	0.0000781	5.03	0.012
V	2	0.0000745	0.0000745	0.0000373	2.40	0.105
I*V	4	0.0019408	0.0019408	0.0004852	31.21	0.000
Error	36	0.0005596	0.0005596	0.0000155		
Total	44	0.0027312				

S = 0.00394264 R-Sq = 79.51% R-Sq(adj) = 74.96%

Unusual Observations for TR

Obs	TR	Fit	SE Fit	Residual	St Resid
3	0.009000	0.016200	0.001763	-0.007200	-2.04 R
9	0.020000	0.012800	0.001763	0.007200	2.04 R
21	0.025000	0.016200	0.001763	0.008800	2.50 R
24	0.002000	0.009700	0.001763	-0.007700	-2.18 R
27	0.003000	0.012800	0.001763	-0.009800	-2.78 R

R denotes an observation with a large standardized residual.

Analysis of Variance for MRR [mm/s], using Adjusted SS for Tests

Source	DF	Seq SS	Adj SS	Adj MS	F	P
I	2	0.0000022	0.0000022	0.0000011	11.21	0.000
V	2	0.0000020	0.0000020	0.0000010	10.12	0.000
I*V	4	0.0000006	0.0000006	0.0000002	1.59	0.198
Error	36	0.0000035	0.0000035	0.0000001		
Total	44	0.0000082				

S = 0.000311432 R-Sq = 57.66% R-Sq(adj) = 48.25%

Unusual Observations for MRR [mm/s]

Obs	MRR [mm/s]	Fit	SE Fit	Residual	St Resid
5	0.001709	0.001020	0.000139	0.000689	2.47 R
9	0.000518	0.001352	0.000139	-0.000834	-2.99 R
23	0.000382	0.001020	0.000139	-0.000638	-2.29 R
24	0.001338	0.000760	0.000139	0.000578	2.07 R
27	0.001910	0.001352	0.000139	0.000559	2.01 R

R denotes an observation with a large standardized residual.

Analysis of Variance for TWR, using Adjusted SS for Tests

Source	DF	Seq SS	Adj SS	Adj MS	F	P
I	2	0.245006	0.245006	0.122503	34.56	0.000
V	2	0.443255	0.443255	0.221628	62.52	0.000
I*V	4	0.027001	0.027001	0.006750	1.90	0.131
Error	36	0.127621	0.127621	0.003545		
Total	44	0.842884				

S = 0.0595402 R-Sq = 84.86% R-Sq(adj) = 81.49%

Unusual Observations for TWR

Obs	TWR	Fit	SE Fit	Residual	St Resid
6	0.376155	0.202971	0.026627	0.173185	3.25 R
7	0.405309	0.284048	0.026627	0.121261	2.28 R
24	0.051473	0.202971	0.026627	-0.151498	-2.84 R

R denotes an observation with a large standardized residual.

TC, d 300 µm, E 206

Factor	Type	Levels	Values
I	fixed	3	10, 32, 50
V	fixed	3	80, 110, 140

Analysis of Variance for Wear [mm], using Adjusted SS for Tests

Source	DF	Seq SS	Adj SS	Adj MS	F	P
I	2	0.006169	0.006169	0.003084	2.40	0.105
V	2	0.007597	0.007597	0.003798	2.96	0.065
I*V	4	0.027967	0.027967	0.006992	5.44	0.002
Error	36	0.046229	0.046229	0.001284		
Total	44	0.087961				

S = 0.0358350 R-Sq = 47.44% R-Sq(adj) = 35.76%

Unusual Observations for Wear [mm]

Obs	Wear [mm]	Fit	SE Fit	Residual	St Resid
33	1.03414	0.94729	0.01603	0.08685	2.71 R
36	0.82526	0.88948	0.01603	-0.06421	-2.00 R
37	0.81798	0.88405	0.01603	-0.06606	-2.06 R
42	0.88270	0.94729	0.01603	-0.06459	-2.02 R

R denotes an observation with a large standardized residual.

Analysis of Variance for Time [s], using Adjusted SS for Tests

Source	DF	Seq SS	Adj SS	Adj MS	F	P
I	2	1374513	1374513	687256	3.94	0.028
V	2	1560606	1560606	780303	4.47	0.018
I*V	4	2749542	2749542	687386	3.94	0.009
Error	36	6282831	6282831	174523		
Total	44	11967491				

S = 417.760 R-Sq = 47.50% R-Sq(adj) = 35.83%

Unusual Observations for Time [s]

Obs	Time [s]	Fit	SE Fit	Residual	St Resid
23	1029.92	1966.17	186.83	-936.25	-2.51 R
25	2596.09	1583.44	186.83	1012.64	2.71 R
31	1988.69	1115.53	186.83	873.16	2.34 R

R denotes an observation with a large standardized residual.

Analysis of Variance for DOC [mm], using Adjusted SS for Tests

Source	DF	Seq SS	Adj SS	Adj MS	F	P
I	2	0.0000105	0.0000105	0.0000053	0.38	0.688
V	2	0.0000617	0.0000617	0.0000309	2.21	0.124
I*V	4	0.0001837	0.0001837	0.0000459	3.29	0.021
Error	36	0.0005020	0.0005020	0.0000139		
Total	44	0.0007580				

S = 0.00373423   R-Sq = 33.77%   R-Sq(adj) = 19.06%

Unusual Observations for DOC [mm]

Obs	DOC [mm]	Fit	SE Fit	Residual	St Resid	
1	0.059000	0.066800	0.001670	-0.007800	-2.34	R
26	0.064000	0.071000	0.001670	-0.007000	-2.10	R
37	0.075000	0.066800	0.001670	0.008200	2.46	R

R denotes an observation with a large standardized residual.

Analysis of Variance for TR, using Adjusted SS for Tests

Source	DF	Seq SS	Adj SS	Adj MS	F	P
I	2	0.0000267	0.0000267	0.0000133	0.98	0.386
V	2	0.0000132	0.0000132	0.0000066	0.48	0.622
I*V	4	0.0000755	0.0000755	0.0000189	1.38	0.259
Error	36	0.0004915	0.0004915	0.0000137		
Total	44	0.0006068				

S = 0.00369497   R-Sq = 19.00%   R-Sq(adj) = 1.01%

Unusual Observations for TR

Obs	TR	Fit	SE Fit	Residual	St Resid	
1	0.005000	0.012000	0.001652	-0.007000	-2.12	R
18	0.004000	0.012800	0.001652	-0.008800	-2.66	R
26	0.007000	0.014000	0.001652	-0.007000	-2.12	R

R denotes an observation with a large standardized residual.

Analysis of Variance for MRR [mm/s], using Adjusted SS for Tests

Source	DF	Seq SS	Adj SS	Adj MS	F	P
I	2	0.0000000	0.0000000	0.0000000	3.01	0.062
V	2	0.0000000	0.0000000	0.0000000	2.79	0.075
I*V	4	0.0000000	0.0000000	0.0000000	2.35	0.072

Error	36	0.0000001	0.0000001	0.0000000
Total	44	0.0000001		

S = 0.0000395986 R-Sq = 36.86% R-Sq(adj) = 22.83%

Unusual Observations for MRR [mm/s]

Obs	MRR [mm/s]	Fit	SE Fit	Residual	St Resid
37	0.000226	0.000140	0.000018	0.000086	2.42 R
39	0.000226	0.000147	0.000018	0.000079	2.22 R

R denotes an observation with a large standardized residual.

Analysis of Variance for TWR, using Adjusted SS for Tests

Source	DF	Seq SS	Adj SS	Adj MS	F	P
I	2	0.0020029	0.0020029	0.0010014	1.67	0.203
V	2	0.0040188	0.0040188	0.0020094	3.35	0.046
I*V	4	0.0073639	0.0073639	0.0018410	3.07	0.028
Error	36	0.0216009	0.0216009	0.0006000		
Total	44	0.0349865				

S = 0.0244954 R-Sq = 38.26% R-Sq(adj) = 24.54%

Unusual Observations for TWR

Obs	TWR	Fit	SE Fit	Residual	St Resid
9	0.568485	0.518681	0.010955	0.049805	2.27 R
33	0.596505	0.543441	0.010955	0.053064	2.42 R
36	0.468262	0.518681	0.010955	-0.050419	-2.30 R
37	0.460299	0.513924	0.010955	-0.053625	-2.45 R

R denotes an observation with a large standardized residual.

TC, d 150 µm, E 365

Factor	Type	Levels	Values
I	fixed	3	20, 40, 60

V fixed 3 70, 95, 110

Analysis of Variance for Wear [mm], using Adjusted SS for Tests

Source	DF	Seq SS	Adj SS	Adj MS	F	P
I	2	0.21284	0.21284	0.10642	68.55	0.000
V	2	2.09193	2.09193	1.04597	673.72	0.000
I*V	4	1.97168	1.97168	0.49292	317.50	0.000
Error	36	0.05589	0.05589	0.00155		
Total	44	4.33235				

S = 0.0394021 R-Sq = 98.71% R-Sq(adj) = 98.42%

Unusual Observations for Wear [mm]

Obs	Wear [mm]	Fit	SE Fit	Residual	St Resid
2	1.58201	1.49783	0.01762	0.08418	2.39 R
6	0.80118	0.87664	0.01762	-0.07546	-2.14 R

R denotes an observation with a large standardized residual.

Analysis of Variance for Time [s], using Adjusted SS for Tests

Source	DF	Seq SS	Adj SS	Adj MS	F	P
I	2	235546	235546	117773	1558.09	0.000
V	2	247564	247564	123782	1637.59	0.000
I*V	4	18161	18161	4540	60.07	0.000
Error	36	2721	2721	76		
Total	44	503992				

S = 8.69413 R-Sq = 99.46% R-Sq(adj) = 99.34%

Unusual Observations for Time [s]

Obs	Time [s]	Fit	SE Fit	Residual	St Resid
3	203.682	220.278	3.888	-16.596	-2.13 R
19	468.998	448.962	3.888	20.036	2.58 R
43	230.672	214.409	3.888	16.263	2.09 R

R denotes an observation with a large standardized residual.

Analysis of Variance for DOC [mm], using Adjusted SS for Tests

Source	DF	Seq SS	Adj SS	Adj MS	F	P
I	2	0.0007806	0.0007806	0.0003903	47.99	0.000
V	2	0.0003680	0.0003680	0.0001840	22.63	0.000
I*V	4	0.0001649	0.0001649	0.0000412	5.07	0.002
Error	36	0.0002928	0.0002928	0.0000081		
Total	44	0.0016063				

S = 0.00285190 R-Sq = 81.77% R-Sq(adj) = 77.72%

Unusual Observations for DOC [mm]

Obs	DOC [mm]	Fit	SE Fit	Residual	St Resid
5	0.078000	0.071600	0.001275	0.006400	2.51 R
9	0.067000	0.074400	0.001275	-0.007400	-2.90 R

R denotes an observation with a large standardized residual.

Analysis of Variance for TR, using Adjusted SS for Tests

Source	DF	Seq SS	Adj SS	Adj MS	F	P
I	2	0.0012534	0.0012534	0.0006267	47.66	0.000
V	2	0.0003054	0.0003054	0.0001527	11.61	0.000
I*V	4	0.0004586	0.0004586	0.0001147	8.72	0.000
Error	36	0.0004734	0.0004734	0.0000132		
Total	44	0.0024908				

S = 0.00362629 R-Sq = 80.99% R-Sq(adj) = 76.77%

Unusual Observations for TR

Obs	TR	Fit	SE Fit	Residual	St Resid
35	0.032000	0.038800	0.001622	-0.006800	-2.10 R

R denotes an observation with a large standardized residual.

Analysis of Variance for MRR [mm/s], using Adjusted SS for Tests

Source	DF	Seq SS	Adj SS	Adj MS	F	P
I	2	0.0000002	0.0000002	0.0000001	486.27	0.000
V	2	0.0000002	0.0000002	0.0000001	615.28	0.000
I*V	4	0.0000000	0.0000000	0.0000000	50.05	0.000
Error	36	0.0000000	0.0000000	0.0000000		
Total	44	0.0000004				

S = 0.0000130833 R-Sq = 98.52% R-Sq(adj) = 98.20%

Unusual Observations for MRR [mm/s]

Obs	MRR [mm/s]	Fit	SE Fit	Residual	St Resid	
5	0.000248	0.000218	0.000006	0.000031	2.63	R
9	0.000334	0.000371	0.000006	-0.000037	-3.13	R
32	0.000193	0.000218	0.000006	-0.000024	-2.07	R
36	0.000409	0.000371	0.000006	0.000038	3.22	R

R denotes an observation with a large standardized residual.

Analysis of Variance for TWR, using Adjusted SS for Tests

Source	DF	Seq SS	Adj SS	Adj MS	F	P
I	2	0.03286	0.03286	0.01643	31.88	0.000
V	2	0.52158	0.52158	0.26079	506.02	0.000
I*V	4	0.45193	0.45193	0.11298	219.22	0.000
Error	36	0.01855	0.01855	0.00052		
Total	44	1.02493				

S = 0.0227020 R-Sq = 98.19% R-Sq(adj) = 97.79%

Unusual Observations for TWR

Obs	TWR	Fit	SE Fit	Residual	St Resid	
8	0.893961	0.851828	0.010153	0.042133	2.07	R

R denotes an observation with a large standardized residual.

TC, d 150 µm, E 206

Multilevel Factorial Design

Factors:	2	Replicates:	5
Base runs:	9	Total runs:	45
Base blocks:	1	Total blocks:	1

Number of levels: 3, 3

General Linear Model: Wear [mm], Time [s], ... versus I, V

Factor	Type	Levels	Values
I	fixed	3	15, 30, 50
V	fixed	3	80, 110, 140

Analysis of Variance for Wear [mm], using Adjusted SS for Tests

Source	DF	Seq SS	Adj SS	Adj MS	F	P
I	2	0.02774	0.02774	0.01387	0.75	0.481
V	2	0.06082	0.06082	0.03041	1.64	0.209
I*V	4	0.30370	0.30370	0.07592	4.09	0.008
Error	36	0.66843	0.66843	0.01857		
Total	44	1.06068				

S = 0.136262 R-Sq = 36.98% R-Sq(adj) = 22.98%

Unusual Observations for Wear [mm]

Obs	Wear [mm]	Fit	SE Fit	Residual	St Resid	
1	1.50966	1.80454	0.06094	-0.29488	-2.42	R
19	2.12542	1.80454	0.06094	0.32088	2.63	R
28	2.17182	1.80454	0.06094	0.36728	3.01	R
37	1.46798	1.80454	0.06094	-0.33656	-2.76	R

R denotes an observation with a large standardized residual.

Analysis of Variance for Time [s], using Adjusted SS for Tests

Source	DF	Seq SS	Adj SS	Adj MS	F	P
I	2	364064	364064	182032	3.73	0.034
V	2	476552	476552	238276	4.89	0.013
I*V	4	689567	689567	172392	3.54	0.016
Error	36	1755050	1755050	48751		
Total	44	3285232				

S = 220.797 R-Sq = 46.58% R-Sq(adj) = 34.71%

Unusual Observations for Time [s]

Obs	Time [s]	Fit	SE Fit	Residual	St Resid
7	1091.99	592.09	98.74	499.90	2.53 R
14	503.51	901.11	98.74	-397.61	-2.01 R
23	406.07	901.11	98.74	-495.05	-2.51 R
32	1318.39	901.11	98.74	417.28	2.11 R

R denotes an observation with a large standardized residual.

Analysis of Variance for DOC [mm], using Adjusted SS for Tests

Source	DF	Seq SS	Adj SS	Adj MS	F	P
I	2	0.0000353	0.0000353	0.0000176	0.48	0.620
V	2	0.0000165	0.0000165	0.0000083	0.23	0.798
I*V	4	0.0002478	0.0002478	0.0000620	1.70	0.171
Error	36	0.0013108	0.0013108	0.0000364		
Total	44	0.0016103				

S = 0.00603405 R-Sq = 18.60% R-Sq(adj) = 0.52%

Unusual Observations for DOC [mm]

Obs	DOC [mm]	Fit	SE Fit	Residual	St Resid
28	0.075000	0.062400	0.002699	0.012600	2.33 R

R denotes an observation with a large standardized residual.

Analysis of Variance for TR, using Adjusted SS for Tests

Source	DF	Seq SS	Adj SS	Adj MS	F	P
I	2	0.0000324	0.0000324	0.0000162	0.52	0.599
V	2	0.0000363	0.0000363	0.0000181	0.58	0.564
I*V	4	0.0001679	0.0001679	0.0000420	1.35	0.271
Error	36	0.0011214	0.0011214	0.0000312		
Total	44	0.0013580				

S = 0.00558122 R-Sq = 17.42% R-Sq(adj) = 0.00%

Unusual Observations for TR

Obs	TR	Fit	SE Fit	Residual	St Resid
34	0.031000	0.017200	0.002496	0.013800	2.76 R
35	0.013000	0.023000	0.002496	-0.010000	-2.00 R

R denotes an observation with a large standardized residual.

Analysis of Variance for MRR [mm/s], using Adjusted SS for Tests

Source	DF	Seq SS	Adj SS	Adj MS	F	P
I	2	0.0000000	0.0000000	0.0000000	2.39	0.106
V	2	0.0000000	0.0000000	0.0000000	1.68	0.200
I*V	4	0.0000000	0.0000000	0.0000000	1.69	0.173
Error	36	0.0000001	0.0000001	0.0000000		
Total	44	0.0000002				

S = 0.0000614598 R-Sq = 29.31% R-Sq(adj) = 13.61%

Unusual Observations for MRR [mm/s]

Obs	MRR [mm/s]	Fit	SE Fit	Residual	St Resid
8	0.000248	0.000117	0.000027	0.000130	2.37 R
12	0.000266	0.000129	0.000027	0.000137	2.49 R

```
 28    0.000275  0.000162  0.000027  0.000114      2.07 R

R denotes an observation with a large standardized residual.
```

Analysis of Variance for TWR, using Adjusted SS for Tests

```
Source  DF    Seq SS    Adj SS    Adj MS     F      P
I        2  0.004217  0.004217  0.002109  0.59  0.559
V        2  0.015406  0.015406  0.007703  2.16  0.130
I*V      4  0.023193  0.023193  0.005798  1.63  0.189
Error   36  0.128280  0.128280  0.003563
Total   44  0.171096


S = 0.0596937   R-Sq = 25.02%   R-Sq(adj) = 8.36%


Unusual Observations for TWR

Obs       TWR       Fit    SE Fit   Residual  St Resid
 19  0.941062  0.821023  0.026696   0.120039      2.25 R
 37  0.703607  0.821023  0.026696  -0.117416     -2.20 R
 44  0.939080  0.781093  0.026696   0.157987      2.96 R

R denotes an observation with a large standardized residual.
```

Second level of Analysis: I, V and E

TC, d 300 µm

General Linear Model: Time [s], Wear [mm], ... versus I, V, ...

```
Factor  Type   Levels  Values
I       fixed       3  L, M, H
V       fixed       3  L, M, H
E       fixed       2  206, 365


Analysis of Variance for Time [s], using Adjusted SS for Tests

Source  DF    Seq SS    Adj SS    Adj MS       F      P
I        2    717856    717856    358928    4.00  0.023
```

V	2	809980	809980	404990	4.51	0.014
E	1	23962446	23962446	23962446	266.86	0.000
I*V	4	1411888	1411888	352972	3.93	0.006
I*E	2	686034	686034	343017	3.82	0.026
V*E	2	767399	767399	383699	4.27	0.018
I*V*E	4	1349308	1349308	337327	3.76	0.008
Error	72	6465186	6465186	89794		
Total	89	36170097				

S = 299.657 R-Sq = 82.13% R-Sq(adj) = 77.91%

Unusual Observations for Time [s]

Obs	Time [s]	Fit	SE Fit	Residual	St Resid	
14	847.38	1583.44	134.01	-736.07	-2.75	R
46	1029.92	1966.17	134.01	-936.25	-3.49	R
50	2596.09	1583.44	134.01	1012.64	3.78	R
62	1988.69	1115.53	134.01	873.16	3.26	R
64	2588.33	1966.17	134.01	622.17	2.32	R

R denotes an observation with a large standardized residual.

Analysis of Variance for Wear [mm], using Adjusted SS for Tests

Source	DF	Seq SS	Adj SS	Adj MS	F	P
I	2	0.11510	0.11510	0.05755	3.23	0.045
V	2	0.23893	0.23893	0.11946	6.71	0.002
E	1	6.06823	6.06823	6.06823	340.61	0.000
I*V	4	0.05292	0.05292	0.01323	0.74	0.566
I*E	2	0.08003	0.08003	0.04001	2.25	0.113
V*E	2	0.18339	0.18339	0.09169	5.15	0.008
I*V*E	4	0.02742	0.02742	0.00685	0.38	0.819
Error	72	1.28275	1.28275	0.01782		
Total	89	8.04875				

S = 0.133477 R-Sq = 84.06% R-Sq(adj) = 80.30%

Unusual Observations for Wear [mm]

Obs	Wear [mm]	Fit	SE Fit	Residual	St Resid	
11	0.59921	0.32019	0.05969	0.27903	2.34	R
55	0.08198	0.53475	0.05969	-0.45277	-3.79	R
79	0.27410	0.62977	0.05969	-0.35567	-2.98	R
85	0.15502	0.42704	0.05969	-0.27202	-2.28	R

R denotes an observation with a large standardized residual.

Analysis of Variance for DOC [mm], using Adjusted SS for Tests

Source	DF	Seq SS	Adj SS	Adj MS	F	P
I	2	0.0006751	0.0006751	0.0003375	4.81	0.011
V	2	0.0003640	0.0003640	0.0001820	2.60	0.082
E	1	0.0039072	0.0039072	0.0039072	55.71	0.000
I*V	4	0.0007351	0.0007351	0.0001838	2.62	0.042
I*E	2	0.0004597	0.0004597	0.0002298	3.28	0.043
V*E	2	0.0001806	0.0001806	0.0000903	1.29	0.282
I*V*E	4	0.0012236	0.0012236	0.0003059	4.36	0.003
Error	72	0.0050499	0.0050499	0.0000701		
Total	89	0.0125951				

S = 0.00837481 R-Sq = 59.91% R-Sq(adj) = 50.44%

Unusual Observations for DOC [mm]

Obs	DOC [mm]	Fit	SE Fit	Residual	St Resid	
27	0.093000	0.076200	0.003745	0.016800	2.24	R
41	0.078000	0.054600	0.003745	0.023400	3.12	R
49	0.090000	0.062000	0.003745	0.028000	3.74	R
63	0.055000	0.076200	0.003745	-0.021200	-2.83	R
65	0.090000	0.059600	0.003745	0.030400	4.06	R
69	0.072500	0.056500	0.003745	0.016000	2.14	R

R denotes an observation with a large standardized residual.

Analysis of Variance for TR, using Adjusted SS for Tests

Source	DF	Seq SS	Adj SS	Adj MS	F	P
I	2	0.0001946	0.0001946	0.0000973	4.09	0.021
V	2	0.0001162	0.0001162	0.0000581	2.44	0.094

E	1	0.0001495	0.0001495	0.0001495	6.28	0.014
I*V	4	0.0003139	0.0003139	0.0000785	3.30	0.015
I*E	2	0.0000471	0.0000471	0.0000235	0.99	0.377
V*E	2	0.0000708	0.0000708	0.0000354	1.49	0.233
I*V*E	4	0.0004314	0.0004314	0.0001078	4.53	0.003
Error	72	0.0017136	0.0017136	0.0000238		
Total	89	0.0030371				

S = 0.00487852 R-Sq = 43.58% R-Sq(adj) = 30.26%

Unusual Observations for TR

Obs	TR	Fit	SE Fit	Residual	St Resid	
36	0.004000	0.012800	0.002182	-0.008800	-2.02	R
41	0.025000	0.012600	0.002182	0.012400	2.84	R
47	0.002000	0.011600	0.002182	-0.009600	-2.20	R
63	0.013000	0.024400	0.002182	-0.011400	-2.61	R
85	0.003000	0.012600	0.002182	-0.009600	-2.20	R

R denotes an observation with a large standardized residual.

Analysis of Variance for MRR [mm/s], using Adjusted SS for Tests

Source	DF	Seq SS	Adj SS	Adj MS	F	P
I	2	0.0000006	0.0000006	0.0000003	2.86	0.064
V	2	0.0000003	0.0000003	0.0000002	1.42	0.249
E	1	0.0000145	0.0000145	0.0000145	132.44	0.000
I*V	4	0.0000003	0.0000003	0.0000001	0.59	0.668
I*E	2	0.0000007	0.0000007	0.0000004	3.42	0.038
V*E	2	0.0000003	0.0000003	0.0000001	1.32	0.274
I*V*E	4	0.0000003	0.0000003	0.0000001	0.63	0.643
Error	72	0.0000079	0.0000079	0.0000001		
Total	89	0.0000249				

S = 0.000331078 R-Sq = 68.33% R-Sq(adj) = 60.85%

Unusual Observations for MRR [mm/s]

Obs	MRR [mm/s]	Fit	SE Fit	Residual	St Resid

9	0.001709	0.000844	0.000148	0.000866	2.92 R
75	0.001432	0.000811	0.000148	0.000620	2.10 R
79	0.001323	0.000610	0.000148	0.000712	2.41 R
83	0.001905	0.000968	0.000148	0.000937	3.16 R
85	0.001910	0.000889	0.000148	0.001021	3.45 R

R denotes an observation with a large standardized residual.

Analysis of Variance for TWR, using Adjusted SS for Tests

Source	DF	Seq SS	Adj SS	Adj MS	F	P
I	2	0.04973	0.04973	0.02487	3.54	0.034
V	2	0.10347	0.10347	0.05173	7.36	0.001
E	1	1.79136	1.79136	1.79136	254.83	0.000
I*V	4	0.01784	0.01784	0.00446	0.63	0.640
I*E	2	0.03783	0.03783	0.01891	2.69	0.075
V*E	2	0.08507	0.08507	0.04253	6.05	0.004
I*V*E	4	0.01952	0.01952	0.00488	0.69	0.598
Error	72	0.50614	0.50614	0.00703		
Total	89	2.61095				

S = 0.0838432 R-Sq = 80.61% R-Sq(adj) = 76.04%

Unusual Observations for TWR

Obs	TWR	Fit	SE Fit	Residual	St Resid
1	0.507711	0.350524	0.037496	0.157187	2.10 R
11	0.376155	0.190017	0.037496	0.186138	2.48 R
19	0.507316	0.350524	0.037496	0.156792	2.09 R
55	0.051473	0.350524	0.037496	-0.299051	-3.99 R
75	0.136739	0.293388	0.037496	-0.156649	-2.09 R
79	0.170517	0.400818	0.037496	-0.230301	-3.07 R
85	0.093785	0.255521	0.037496	-0.161736	-2.16 R

R denotes an observation with a large standardized residual.

TC d 150 µm

General Linear Model: Time [s], Wear [mm], ... versus I, V, ...

Factor	Type	Levels	Values
I	fixed	3	L, M, H
V	fixed	3	L, M, H
E	fixed	2	206, 365

Analysis of Variance for Time [s], using Adjusted SS for Tests

Source	DF	Seq SS	Adj SS	Adj MS	F	P
I	2	169818	169818	84909	2.74	0.071
V	2	289909	289909	144955	4.67	0.012
E	1	1296044	1296044	1296044	41.80	0.000
I*V	4	353571	353571	88393	2.85	0.030
I*E	2	210314	210314	105157	3.39	0.039
V*E	2	195849	195849	97924	3.16	0.048
I*V*E	4	337124	337124	84281	2.72	0.036
Error	72	2232639	2232639	31009		
Total	89	5085269				

S = 176.093 R-Sq = 56.10% R-Sq(adj) = 45.73%

Unusual Observations for Time [s]

Obs	Time [s]	Fit	SE Fit	Residual	St Resid
9	1279.97	901.11	78.75	378.86	2.41 R
13	1091.99	592.09	78.75	499.90	3.17 R
27	503.51	901.11	78.75	-397.61	-2.52 R
45	406.07	901.11	78.75	-495.05	-3.14 R
49	206.73	592.09	78.75	-385.36	-2.45 R
63	1318.39	901.11	78.75	417.28	2.65 R

R denotes an observation with a large standardized residual.

Analysis of Variance for Wear [mm], using Adjusted SS for Tests

Source	DF	Seq SS	Adj SS	Adj MS	F	P
I	2	0.07828	0.07828	0.03914	0.61	0.548
V	2	0.12103	0.12103	0.06052	0.94	0.397
E	1	0.23243	0.23243	0.23243	3.60	0.062
I*V	4	0.05218	0.05218	0.01304	0.20	0.936

I*E	2	0.11492	0.11492	0.05746	0.89	0.415
V*E	2	0.01405	0.01405	0.00703	0.11	0.897
I*V*E	4	0.36262	0.36262	0.09066	1.40	0.241
Error	72	4.64994	4.64994	0.06458		
Total	89	5.62546				

S = 0.254131 R-Sq = 17.34% R-Sq(adj) = 0.00%

Unusual Observations for Wear [mm]

Obs	Wear [mm]	Fit	SE Fit	Residual	St Resid	
52	0.80118	1.35557	0.11365	-0.55438	-2.44	R
54	0.92094	1.38837	0.11365	-0.46742	-2.06	R
56	0.86854	1.42438	0.11365	-0.55584	-2.45	R
58	0.85814	1.46392	0.11365	-0.60578	-2.67	R
60	0.93438	1.50507	0.11365	-0.57069	-2.51	R
72	1.88006	1.38837	0.11365	0.49170	2.16	R
82	1.06594	1.52965	0.11365	-0.46371	-2.04	R
84	1.04078	1.54402	0.11365	-0.50324	-2.21	R

R denotes an observation with a large standardized residual.

Analysis of Variance for DOC [mm], using Adjusted SS for Tests

Source	DF	Seq SS	Adj SS	Adj MS	F	P
I	2	0.0000193	0.0000193	0.0000096	0.25	0.782
V	2	0.0000676	0.0000676	0.0000338	0.87	0.425
E	1	0.0009296	0.0009296	0.0009296	23.81	0.000
I*V	4	0.0001400	0.0001400	0.0000350	0.90	0.471
I*E	2	0.0000386	0.0000386	0.0000193	0.49	0.612
V*E	2	0.0000106	0.0000106	0.0000053	0.14	0.874
I*V*E	4	0.0001295	0.0001295	0.0000324	0.83	0.511
Error	72	0.0028111	0.0028111	0.0000390		
Total	89	0.0041463				

S = 0.00624850 R-Sq = 32.20% R-Sq(adj) = 16.19%

Unusual Observations for DOC [mm]

Obs	DOC [mm]	Fit	SE Fit	Residual	St Resid
10	0.053000	0.064400	0.002794	-0.011400	-2.04 R
55	0.075000	0.062400	0.002794	0.012600	2.25 R
88	0.079000	0.066400	0.002794	0.012600	2.25 R

R denotes an observation with a large standardized residual.

Analysis of Variance for TR, using Adjusted SS for Tests

Source	DF	Seq SS	Adj SS	Adj MS	F	P
I	2	0.0000139	0.0000139	0.0000070	0.14	0.868
V	2	0.0000057	0.0000057	0.0000029	0.06	0.943
E	1	0.0027445	0.0027445	0.0027445	55.76	0.000
I*V	4	0.0001040	0.0001040	0.0000260	0.53	0.715
I*E	2	0.0000413	0.0000413	0.0000206	0.42	0.659
V*E	2	0.0000552	0.0000552	0.0000276	0.56	0.573
I*V*E	4	0.0000846	0.0000846	0.0000211	0.43	0.787
Error	72	0.0035440	0.0035440	0.0000492		
Total	89	0.0065933				

S = 0.00701586 R-Sq = 46.25% R-Sq(adj) = 33.56%

Unusual Observations for TR

Obs	TR	Fit	SE Fit	Residual	St Resid
4	0.017000	0.031200	0.003138	-0.014200	-2.26 R
6	0.017000	0.031600	0.003138	-0.014600	-2.33 R
8	0.018000	0.031800	0.003138	-0.013800	-2.20 R
10	0.015000	0.029450	0.003138	-0.014450	-2.30 R
67	0.031000	0.017200	0.003138	0.013800	2.20 R

R denotes an observation with a large standardized residual.

Analysis of Variance for MRR [mm/s], using Adjusted SS for Tests

Source	DF	Seq SS	Adj SS	Adj MS	F	P
I	2	0.0000000	0.0000000	0.0000000	1.29	0.280
V	2	0.0000000	0.0000000	0.0000000	1.19	0.309
E	1	0.0000002	0.0000002	0.0000002	27.34	0.000
I*V	4	0.0000000	0.0000000	0.0000000	0.50	0.735

I*E	2	0.0000000	0.0000000	0.0000000	0.73	0.486
V*E	2	0.0000000	0.0000000	0.0000000	0.34	0.712
I*V*E	4	0.0000000	0.0000000	0.0000000	0.38	0.823
Error	72	0.0000005	0.0000005	0.0000000		
Total	89	0.0000008				

S = 0.0000859101 R-Sq = 34.54% R-Sq(adj) = 19.08%

Unusual Observations for MRR [mm/s]

Obs	MRR [mm/s]	Fit	SE Fit	Residual	St Resid
82	0.000334	0.000179	0.000038	0.000155	2.02 R
84	0.000364	0.000196	0.000038	0.000168	2.19 R
86	0.000369	0.000196	0.000038	0.000173	2.25 R
88	0.000409	0.000215	0.000038	0.000193	2.52 R

R denotes an observation with a large standardized residual.

Analysis of Variance for TWR, using Adjusted SS for Tests

Source	DF	Seq SS	Adj SS	Adj MS	F	P
I	2	0.02126	0.02126	0.01063	0.71	0.497
V	2	0.02744	0.02744	0.01372	0.91	0.406
E	1	0.06367	0.06367	0.06367	4.23	0.043
I*V	4	0.00248	0.00248	0.00062	0.04	0.997
I*E	2	0.01621	0.01621	0.00811	0.54	0.586
V*E	2	0.00377	0.00377	0.00189	0.13	0.882
I*V*E	4	0.04201	0.04201	0.01050	0.70	0.596
Error	72	1.08284	1.08284	0.01504		
Total	89	1.25969				

S = 0.122635 R-Sq = 14.04% R-Sq(adj) = 0.00%

Unusual Observations for TWR

Obs	TWR	Fit	SE Fit	Residual	St Resid
52	0.379790	0.637419	0.054844	-0.257629	-2.35 R
54	0.430028	0.654331	0.054844	-0.224303	-2.04 R
56	0.403397	0.676333	0.054844	-0.272936	-2.49 R

58	0.404380	0.701974	0.054844	-0.297594	-2.71 R
60	0.446756	0.692549	0.054844	-0.245792	-2.24 R
72	0.893961	0.654331	0.054844	0.239630	2.18 R
82	0.485769	0.725040	0.054844	-0.239271	-2.18 R
84	0.447141	0.716049	0.054844	-0.268907	-2.45 R
86	0.500495	0.732166	0.054844	-0.231672	-2.11 R

R denotes an observation with a large standardized residual.

Copper electrode (Cu) Electrode

First level of Analysis: I and V

Cu, d 300 µm, E 365

General Linear Model: Time [s], Wear [mm], ... versus I, V

Factor	Type	Levels	Values
I	fixed	3	40, 60, 80
V	fixed	3	80, 100, 120

Analysis of Variance for Time [s], using Adjusted SS for Tests

Source	DF	Seq SS	Adj SS	Adj MS	F	P
I	2	6559.1	6559.1	3279.6	87.66	0.000
V	2	32604.6	32604.6	16302.3	435.73	0.000
I*V	4	6929.5	6929.5	1732.4	46.30	0.000
Error	36	1346.9	1346.9	37.4		
Total	44	47440.1				

S = 6.11671 R-Sq = 97.16% R-Sq(adj) = 96.53%

Unusual Observations for Time [s]

Obs	Time [s]	Fit	SE Fit	Residual	St Resid
12	103.430	91.974	2.735	11.456	2.09 R
39	78.344	91.974	2.735	-13.630	-2.49 R

R denotes an observation with a large standardized residual.

Analysis of Variance for Wear [mm], using Adjusted SS for Tests

Source	DF	Seq SS	Adj SS	Adj MS	F	P
I	2	0.75445	0.75445	0.37723	113.94	0.000
V	2	0.08127	0.08127	0.04064	12.27	0.000
I*V	4	0.05542	0.05542	0.01386	4.18	0.007
Error	36	0.11919	0.11919	0.00331		
Total	44	1.01033				

S = 0.0575391 R-Sq = 88.20% R-Sq(adj) = 85.58%

Unusual Observations for Wear [mm]

Obs	Wear [mm]	Fit	SE Fit	Residual	St Resid
3	1.60846	1.48097	0.02573	0.12749	2.48 R
5	1.64318	1.53928	0.02573	0.10390	2.02 R
18	1.64238	1.75544	0.02573	-0.11306	-2.20 R
21	1.37222	1.48097	0.02573	-0.10875	-2.11 R

R denotes an observation with a large standardized residual.

Analysis of Variance for DOC [mm], using Adjusted SS for Tests

Source	DF	Seq SS	Adj SS	Adj MS	F	P
I	2	0.0005503	0.0005503	0.0002752	9.49	0.000
V	2	0.0006375	0.0006375	0.0003187	10.99	0.000
I*V	4	0.0002271	0.0002271	0.0000568	1.96	0.122
Error	36	0.0010437	0.0010437	0.0000290		
Total	44	0.0024586				

S = 0.00538439 R-Sq = 57.55% R-Sq(adj) = 48.12%

Unusual Observations for DOC [mm]

Obs	DOC [mm]	Fit	SE Fit	Residual	St Resid
5	0.072000	0.059000	0.002408	0.013000	2.70 R
23	0.047000	0.059000	0.002408	-0.012000	-2.49 R

```
 29  0.054000  0.063750  0.002408  -0.009750     -2.02 R

R denotes an observation with a large standardized residual.


Analysis of Variance for TR, using Adjusted SS for Tests

Source  DF     Seq SS     Adj SS     Adj MS     F      P
I        2  0.0000128  0.0000128  0.0000064  0.21  0.809
V        2  0.0000994  0.0000994  0.0000497  1.65  0.205
I*V      4  0.0005096  0.0005096  0.0001274  4.24  0.006
Error   36  0.0010812  0.0010812  0.0000300
Total   44  0.0017029


S = 0.00548014   R-Sq = 36.51%   R-Sq(adj) = 22.40%


Unusual Observations for TR

Obs        TR       Fit    SE Fit   Residual  St Resid
 29  0.003000  0.013750  0.002451  -0.010750     -2.19 R

R denotes an observation with a large standardized residual.


Analysis of Variance for MRR [mm/s], using Adjusted SS for Tests

Source  DF     Seq SS     Adj SS     Adj MS       F      P
I        2  0.0000006  0.0000006  0.0000003   36.19  0.000
V        2  0.0000023  0.0000023  0.0000011  147.99  0.000
I*V      4  0.0000002  0.0000002  0.0000001    7.88  0.000
Error   36  0.0000003  0.0000003  0.0000000
Total   44  0.0000034


S = 0.0000878137   R-Sq = 91.74%   R-Sq(adj) = 89.91%


Unusual Observations for MRR [mm/s]

Obs  MRR [mm/s]       Fit    SE Fit   Residual  St Resid
 18    0.001243  0.001421  0.000039  -0.000177     -2.26 R
 39    0.001281  0.001094  0.000039   0.000187      2.39 R
```

```
 42    0.001481  0.001267  0.000039   0.000214      2.72 R
 45    0.001660  0.001421  0.000039   0.000240      3.05 R

R denotes an observation with a large standardized residual.


Analysis of Variance for TWR, using Adjusted SS for Tests

Source  DF    Seq SS    Adj SS    Adj MS       F      P
I        2  0.150903  0.150903  0.075452  119.35  0.000
V        2  0.004672  0.004672  0.002336    3.69  0.035
I*V      4  0.009135  0.009135  0.002284    3.61  0.014
Error   36  0.022759  0.022759  0.000632
Total   44  0.187470


S = 0.0251435   R-Sq = 87.86%   R-Sq(adj) = 85.16%


Unusual Observations for TWR

Obs      TWR      Fit   SE Fit  Residual  St Resid
  3  0.95738  0.88131  0.01124   0.07607      3.38 R
 36  1.04124  0.98895  0.01124   0.05228      2.32 R

R denotes an observation with a large standardized residual.
```

Second level of Analysis: I, V and E

Cu, d 300 µm

General Linear Model: Time [s], Wear [mm], ... versus I, V, ...

```
Factor  Type   Levels  Values
I       fixed       3  L, M, H
V       fixed       3  L, M, H
E       fixed       2  206, 365


Analysis of Variance for Time [s], using Adjusted SS for Tests

Source  DF   Seq SS   Adj SS   Adj MS        F      P
I        2   234086   234086   117043   100.35  0.000
```

V	2	1149059	1149059	574530	492.60	0.000
E	1	2496735	2496735	2496735	2140.71	0.000
I*V	4	166041	166041	41510	35.59	0.000
I*E	2	198873	198873	99437	85.26	0.000
V*E	2	1040554	1040554	520277	446.09	0.000
I*V*E	4	155954	155954	38989	33.43	0.000
Error	72	83975	83975	1166		
Total	89	5525278				

S = 34.1513 R-Sq = 98.48% R-Sq(adj) = 98.12%

Unusual Observations for Time [s]

Obs	Time [s]	Fit	SE Fit	Residual	St Resid	
7	572.94	645.83	15.27	-72.89	-2.39	R
19	955.14	1029.84	15.27	-74.70	-2.45	R
32	172.96	110.42	15.27	62.54	2.05	R
36	177.86	106.75	15.27	71.11	2.33	R
73	1120.07	1029.84	15.27	90.23	2.95	R
79	707.65	645.83	15.27	61.82	2.02	R

R denotes an observation with a large standardized residual.

Analysis of Variance for Wear [mm], using Adjusted SS for Tests

Source	DF	Seq SS	Adj SS	Adj MS	F	P
I	2	0.15358	0.15358	0.07679	5.75	0.005
V	2	0.15137	0.15137	0.07568	5.67	0.005
E	1	6.14313	6.14313	6.14313	460.08	0.000
I*V	4	0.01251	0.01251	0.00313	0.23	0.918
I*E	2	0.03291	0.03291	0.01645	1.23	0.298
V*E	2	0.08271	0.08271	0.04136	3.10	0.051
I*V*E	4	0.01275	0.01275	0.00319	0.24	0.916
Error	72	0.96138	0.96138	0.01335		
Total	89	7.55034				

S = 0.115553 R-Sq = 87.27% R-Sq(adj) = 84.26%

Unusual Observations for Wear [mm]

Obs	Wear [mm]	Fit	SE Fit	Residual	St Resid	
6	1.35694	1.57009	0.05168	-0.21314	-2.06	R
8	1.31158	1.52493	0.05168	-0.21334	-2.06	R
10	1.35510	1.56491	0.05168	-0.20981	-2.03	R
16	1.44526	1.65425	0.05168	-0.20899	-2.02	R
18	1.39374	1.62093	0.05168	-0.22718	-2.20	R
62	1.75174	1.52493	0.05168	0.22682	2.19	R
82	1.77654	1.56491	0.05168	0.21163	2.05	R
90	1.84310	1.62093	0.05168	0.22218	2.15	R

R denotes an observation with a large standardized residual.

Analysis of Variance for DOC [mm], using Adjusted SS for Tests

Source	DF	Seq SS	Adj SS	Adj MS	F	P
I	2	0.0001293	0.0001293	0.0000647	1.10	0.339
V	2	0.0000092	0.0000092	0.0000046	0.08	0.925
E	1	0.0035188	0.0035188	0.0035188	59.73	0.000
I*V	4	0.0000054	0.0000054	0.0000013	0.02	0.999
I*E	2	0.0000087	0.0000087	0.0000043	0.07	0.929
V*E	2	0.0002125	0.0002125	0.0001063	1.80	0.172
I*V*E	4	0.0001036	0.0001036	0.0000259	0.44	0.780
Error	72	0.0042418	0.0042418	0.0000589		
Total	89	0.0082292				

S = 0.00767549 R-Sq = 48.45% R-Sq(adj) = 36.28%

Unusual Observations for DOC [mm]

Obs	DOC [mm]	Fit	SE Fit	Residual	St Resid	
46	0.047000	0.061600	0.003433	-0.014600	-2.13	R
82	0.079000	0.061600	0.003433	0.017400	2.53	R
89	0.068000	0.052400	0.003433	0.015600	2.27	R
90	0.083000	0.065200	0.003433	0.017800	2.59	R

R denotes an observation with a large standardized residual.

Analysis of Variance for TR, using Adjusted SS for Tests

Source	DF	Seq SS	Adj SS	Adj MS	F	P
I	2	0.0000675	0.0000675	0.0000338	0.81	0.449
V	2	0.0000812	0.0000812	0.0000406	0.97	0.382
E	1	0.0000146	0.0000146	0.0000146	0.35	0.556
I*V	4	0.0000692	0.0000692	0.0000173	0.41	0.797
I*E	2	0.0001454	0.0001454	0.0000727	1.74	0.182
V*E	2	0.0000941	0.0000941	0.0000471	1.13	0.329
I*V*E	4	0.0000241	0.0000241	0.0000060	0.14	0.965
Error	72	0.0030009	0.0030009	0.0000417		
Total	89	0.0034970				

S = 0.00645599 R-Sq = 14.19% R-Sq(adj) = 0.00%

Unusual Observations for TR

Obs	TR	Fit	SE Fit	Residual	St Resid
1	0.028000	0.013400	0.002887	0.014600	2.53 R
37	-0.002000	0.013400	0.002887	-0.015400	-2.67 R

R denotes an observation with a large standardized residual.

Analysis of Variance for MRR [mm/s], using Adjusted SS for Tests

Source	DF	Seq SS	Adj SS	Adj MS	F	P
I	2	0.0000002	0.0000002	0.0000001	1.82	0.170
V	2	0.0000009	0.0000009	0.0000005	10.57	0.000
E	1	0.0000111	0.0000111	0.0000111	253.65	0.000
I*V	4	0.0000000	0.0000000	0.0000000	0.05	0.996
I*E	2	0.0000000	0.0000000	0.0000000	0.08	0.920
V*E	2	0.0000002	0.0000002	0.0000001	1.93	0.153
I*V*E	4	0.0000000	0.0000000	0.0000000	0.24	0.913
Error	72	0.0000032	0.0000032	0.0000000		
Total	89	0.0000156				

S = 0.000209454 R-Sq = 79.75% R-Sq(adj) = 74.97%

Unusual Observations for MRR [mm/s]

Obs	MRR [mm/s]	Fit	SE Fit	Residual	St Resid

6	0.000623	0.001040	0.000094	-0.000417	-2.23 R
10	0.000599	0.000997	0.000094	-0.000398	-2.12 R
32	0.000558	0.000980	0.000094	-0.000422	-2.25 R
34	0.000589	0.001033	0.000094	-0.000444	-2.37 R
36	0.000538	0.001066	0.000094	-0.000528	-2.82 R
60	0.001481	0.001040	0.000094	0.000441	2.35 R
88	0.001503	0.001033	0.000094	0.000470	2.51 R
90	0.001660	0.001066	0.000094	0.000595	3.17 R

R denotes an observation with a large standardized residual.

Analysis of Variance for TWR, using Adjusted SS for Tests

Source	DF	Seq SS	Adj SS	Adj MS	F	P
I	2	0.04715	0.04715	0.02357	9.14	0.000
V	2	0.04625	0.04625	0.02312	8.96	0.000
E	1	1.55118	1.55118	1.55118	601.26	0.000
I*V	4	0.00303	0.00303	0.00076	0.29	0.881
I*E	2	0.01736	0.01736	0.00868	3.37	0.040
V*E	2	0.04842	0.04842	0.02421	9.38	0.000
I*V*E	4	0.00527	0.00527	0.00132	0.51	0.728
Error	72	0.18575	0.18575	0.00258		
Total	89	1.90442				

S = 0.0507928   R-Sq = 90.25%   R-Sq(adj) = 87.94%

Unusual Observations for TWR

Obs	TWR	Fit	SE Fit	Residual	St Resid
8	0.81625	0.91274	0.02272	-0.09649	-2.12 R
16	0.85722	0.96209	0.02272	-0.10487	-2.31 R
18	0.84798	0.95070	0.02272	-0.10272	-2.26 R
66	1.03166	0.93014	0.02272	0.10152	2.23 R
74	1.02261	0.92501	0.02272	0.09760	2.15 R
76	1.05240	0.94285	0.02272	0.10955	2.41 R
78	1.00633	0.91133	0.02272	0.09500	2.09 R

R denotes an observation with a large standardized residual.

Cu, d 150 µm

General Linear Model: Time [s], Wear [mm], ... versus I, V, ...

Factor	Type	Levels	Values
I	fixed	3	L, M, H
V	fixed	3	L, M, H
E	fixed	2	206, 365

Analysis of Variance for Time [s], using Adjusted SS for Tests

Source	DF	Seq SS	Adj SS	Adj MS	F	P
I	2	36210	36210	18105	18.74	0.000
V	2	59865	59865	29933	30.98	0.000
E	1	336452	336452	336452	348.25	0.000
I*V	4	9692	9692	2423	2.51	0.049
I*E	2	22856	22856	11428	11.83	0.000
V*E	2	42833	42833	21416	22.17	0.000
I*V*E	4	10442	10442	2610	2.70	0.037
Error	72	69562	69562	966		
Total	89	587912				

S = 31.0827 R-Sq = 88.17% R-Sq(adj) = 85.37%

Unusual Observations for Time [s]

Obs	Time [s]	Fit	SE Fit	Residual	St Resid
2	185.078	110.575	13.901	74.503	2.68 R
4	168.596	107.621	13.901	60.975	2.19 R
6	168.106	109.259	13.901	58.847	2.12 R
10	170.910	107.030	13.901	63.880	2.30 R
17	212.982	156.271	13.901	56.711	2.04 R
61	373.102	314.864	13.901	58.238	2.09 R
80	47.090	108.091	13.901	-61.001	-2.19 R

R denotes an observation with a large standardized residual.

Analysis of Variance for Wear [mm], using Adjusted SS for Tests

Source	DF	Seq SS	Adj SS	Adj MS	F	P

I	2	4.1402	4.1402	2.0701	4.81	0.011
V	2	1.3762	1.3762	0.6881	1.60	0.209
E	1	3.1871	3.1871	3.1871	7.40	0.008
I*V	4	1.2425	1.2425	0.3106	0.72	0.580
I*E	2	0.6066	0.6066	0.3033	0.70	0.498
V*E	2	0.2527	0.2527	0.1263	0.29	0.747
I*V*E	4	4.4296	4.4296	1.1074	2.57	0.045
Error	72	31.0024	31.0024	0.4306		
Total	89	46.2371				

S = 0.656193 R-Sq = 32.95% R-Sq(adj) = 17.12%

Unusual Observations for Wear [mm]

Obs	Wear [mm]	Fit	SE Fit	Residual	St Resid	
7	4.14281	2.63209	0.29346	1.51072	2.57	R
70	7.41361	3.79297	0.29346	3.62064	6.17	R
88	2.41841	3.79297	0.29346	-1.37456	-2.34	R

R denotes an observation with a large standardized residual.

Analysis of Variance for DOC [mm], using Adjusted SS for Tests

Source	DF	Seq SS	Adj SS	Adj MS	F	P
I	2	0.0000775	0.0000775	0.0000388	0.21	0.815
V	2	0.0001684	0.0001684	0.0000842	0.45	0.642
E	1	0.0003520	0.0003520	0.0003520	1.87	0.176
I*V	4	0.0005861	0.0005861	0.0001465	0.78	0.544
I*E	2	0.0000051	0.0000051	0.0000025	0.01	0.987
V*E	2	0.0000186	0.0000186	0.0000093	0.05	0.952
I*V*E	4	0.0011306	0.0011306	0.0002827	1.50	0.212
Error	72	0.0135813	0.0135813	0.0001886		
Total	89	0.0159196				

S = 0.0137342 R-Sq = 14.69% R-Sq(adj) = 0.00%

Unusual Observations for DOC [mm]

Obs	DOC [mm]	Fit	SE Fit	Residual	St Resid

6	0.032000	0.059800	0.006142	-0.027800	-2.26	R
7	0.101000	0.070800	0.006142	0.030200	2.46	R
43	0.038000	0.070800	0.006142	-0.032800	-2.67	R
77	0.096000	0.070200	0.006142	0.025800	2.10	R

R denotes an observation with a large standardized residual.

Analysis of Variance for TR, using Adjusted SS for Tests

Source	DF	Seq SS	Adj SS	Adj MS	F	P
I	2	0.003363	0.003363	0.001681	1.35	0.265
V	2	0.002953	0.002953	0.001476	1.19	0.311
E	1	0.000009	0.000009	0.000009	0.01	0.933
I*V	4	0.002200	0.002200	0.000550	0.44	0.778
I*E	2	0.003546	0.003546	0.001773	1.42	0.247
V*E	2	0.004510	0.004510	0.002255	1.81	0.171
I*V*E	4	0.001635	0.001635	0.000409	0.33	0.858
Error	72	0.089601	0.089601	0.001244		
Total	89	0.107817				

S = 0.0352769 R-Sq = 16.89% R-Sq(adj) = 0.00%

Unusual Observations for TR

Obs	TR	Fit	SE Fit	Residual	St Resid	
81	0.210750	0.043550	0.015776	0.167200	5.30	R
87	0.230000	0.046000	0.015776	0.184000	5.83	R

R denotes an observation with a large standardized residual.

Analysis of Variance for MRR [mm/s], using Adjusted SS for Tests

Source	DF	Seq SS	Adj SS	Adj MS	F	P
I	2	0.0000000	0.0000000	0.0000000	1.44	0.244
V	2	0.0000000	0.0000000	0.0000000	3.19	0.047
E	1	0.0000007	0.0000007	0.0000007	116.79	0.000
I*V	4	0.0000000	0.0000000	0.0000000	0.20	0.937
I*E	2	0.0000000	0.0000000	0.0000000	0.68	0.510
V*E	2	0.0000000	0.0000000	0.0000000	1.18	0.313
I*V*E	4	0.0000000	0.0000000	0.0000000	0.73	0.576

Error	72	0.0000004	0.0000004	0.0000000
Total	89	0.0000012		

S = 0.0000778095 R-Sq = 64.96% R-Sq(adj) = 56.69%

Unusual Observations for MRR [mm/s]

Obs	MRR [mm/s]	Fit	SE Fit	Residual	St Resid	
2	0.000156	0.000327	0.000035	-0.000171	-2.46	R
4	0.000174	0.000319	0.000035	-0.000146	-2.09	R
6	0.000160	0.000325	0.000035	-0.000165	-2.37	R
8	0.000192	0.000353	0.000035	-0.000161	-2.31	R
10	0.000175	0.000333	0.000035	-0.000158	-2.28	R
70	0.000614	0.000381	0.000035	0.000233	3.34	R
80	0.000676	0.000353	0.000035	0.000323	4.64	R

R denotes an observation with a large standardized residual.

Analysis of Variance for TWR, using Adjusted SS for Tests

Source	DF	Seq SS	Adj SS	Adj MS	F	P
I	2	1.3844	1.3844	0.6922	4.16	0.019
V	2	1.3498	1.3498	0.6749	4.06	0.021
E	1	0.6596	0.6596	0.6596	3.97	0.050
I*V	4	0.4344	0.4344	0.1086	0.65	0.626
I*E	2	0.6208	0.6208	0.3104	1.87	0.162
V*E	2	0.1776	0.1776	0.0888	0.53	0.588
I*V*E	4	0.7633	0.7633	0.1908	1.15	0.341
Error	72	11.9660	11.9660	0.1662		
Total	89	17.3558				

S = 0.407670 R-Sq = 31.05% R-Sq(adj) = 14.78%

Unusual Observations for TWR

Obs	TWR	Fit	SE Fit	Residual	St Resid	
70	3.43004	1.71731	0.18232	1.71272	4.70	R
81	3.60699	1.68990	0.18232	1.91710	5.26	R
87	3.01465	1.59444	0.18232	1.42022	3.89	R

R denotes an observation with a large standardized residual.

Third level of Analysis: I, V, E and electrode material

D 300 µm

General Linear Model: Time [s], Wear [mm], ... versus I, V, ...

Factor	Type	Levels	Values
I	fixed	3	H, L, M
V	fixed	3	H, L, M
E	fixed	2	206, 365
Mat	fixed	2	Cu, TC

Analysis of Variance for Time [s], using Adjusted SS for Tests

Source	DF	Seq SS	Adj SS	Adj MS	F	P
I	2	166643	166643	83321	1.82	0.166
V	2	1611606	1611606	805803	17.61	0.000
E	1	19799551	19799551	19799551	432.61	0.000
Mat	1	7310694	7310694	7310694	159.73	0.000
I*V	4	674832	674832	168708	3.69	0.007
I*E	2	169656	169656	84828	1.85	0.160
I*Mat	2	659316	659316	329658	7.20	0.001
V*E	2	992379	992379	496189	10.84	0.000
V*Mat	2	379670	379670	189835	4.15	0.018
E*Mat	1	4906497	4906497	4906497	107.20	0.000
I*V*E	4	629075	629075	157269	3.44	0.010
I*V*Mat	4	928191	928191	232048	5.07	0.001
I*E*Mat	2	871786	871786	435893	9.52	0.000
V*E*Mat	2	929003	929003	464502	10.15	0.000
I*V*E*Mat	4	850694	850694	212674	4.65	0.001
Error	144	6590551	6590551	45768		
Total	179	47470145				

S = 213.934 R-Sq = 86.12% R-Sq(adj) = 82.74%

Unusual Observations for Time [s]

Obs	Time [s]	Fit	SE Fit	Residual	St Resid
2	1218.77	814.32	95.67	404.45	2.11 R
14	847.38	1583.44	95.67	-736.07	-3.85 R
44	582.93	1115.53	95.67	-532.60	-2.78 R
46	1029.92	1966.17	95.67	-936.25	-4.89 R
50	2596.09	1583.44	95.67	1012.64	5.29 R
52	1418.70	1033.44	95.67	385.26	2.01 R
62	1988.69	1115.53	95.67	873.16	4.56 R
64	2588.33	1966.17	95.67	622.17	3.25 R
66	1477.58	1009.59	95.67	467.98	2.45 R
88	619.17	1033.44	95.67	-414.27	-2.17 R

R denotes an observation with a large standardized residual.

Analysis of Variance for Wear [mm], using Adjusted SS for Tests

Source	DF	Seq SS	Adj SS	Adj MS	F	P
I	2	0.01868	0.01868	0.00934	0.63	0.536
V	2	0.13866	0.13866	0.06933	4.65	0.011
E	1	0.19242	0.19242	0.19242	12.90	0.000
Mat	1	15.98513	15.98513	15.98513	1071.92	0.000
I*V	4	0.02025	0.02025	0.00506	0.34	0.851
I*E	2	0.27420	0.27420	0.13710	9.19	0.000
I*Mat	2	0.46836	0.46836	0.23418	15.70	0.000
V*E	2	0.56489	0.56489	0.28244	18.94	0.000
V*Mat	2	0.78380	0.78380	0.39190	26.28	0.000
E*Mat	1	9.40355	9.40355	9.40355	630.58	0.000
I*V*E	4	0.08660	0.08660	0.02165	1.45	0.220
I*V*Mat	4	0.01531	0.01531	0.00383	0.26	0.905
I*E*Mat	2	0.08069	0.08069	0.04035	2.71	0.070
V*E*Mat	2	0.20498	0.20498	0.10249	6.87	0.001
I*V*E*Mat	4	0.02418	0.02418	0.00604	0.41	0.805
Error	144	2.14742	2.14742	0.01491		
Total	179	30.40911				

S = 0.122117 R-Sq = 92.94% R-Sq(adj) = 91.22%

Unusual Observations for Wear [mm]

Obs	Wear [mm]	Fit	SE Fit	Residual	St Resid

1	0.76278	0.99012	0.05461	-0.22734	-2.08	R
5	0.21566	0.47456	0.05461	-0.25889	-2.37	R
11	0.59921	0.33901	0.05461	0.26020	2.38	R
31	0.33102	0.57861	0.05461	-0.24759	-2.27	R
37	0.72822	0.99012	0.05461	-0.26190	-2.40	R
47	0.08198	0.33901	0.05461	-0.25703	-2.35	R
73	1.49422	0.99012	0.05461	0.50410	4.62	R
83	0.57878	0.33901	0.05461	0.23977	2.20	R
108	1.39374	1.62093	0.05461	-0.22718	-2.08	R
152	1.75174	1.52493	0.05461	0.22682	2.08	R
180	1.84310	1.62093	0.05461	0.22218	2.03	R

R denotes an observation with a large standardized residual.

Analysis of Variance for DOC [mm], using Adjusted SS for Tests

Source	DF	Seq SS	Adj SS	Adj MS	F	P
I	2	0.0003072	0.0003072	0.0001536	1.58	0.209
V	2	0.0001634	0.0001634	0.0000817	0.84	0.433
E	1	0.0006235	0.0006235	0.0006235	6.43	0.012
Mat	1	0.0039293	0.0039293	0.0039293	40.52	0.000
I*V	4	0.0007910	0.0007910	0.0001977	2.04	0.092
I*E	2	0.0001405	0.0001405	0.0000703	0.72	0.486
I*Mat	2	0.0004019	0.0004019	0.0002010	2.07	0.130
V*E	2	0.0003920	0.0003920	0.0001960	2.02	0.136
V*Mat	2	0.0002872	0.0002872	0.0001436	1.48	0.231
E*Mat	1	0.0034716	0.0034716	0.0034716	35.80	0.000
I*V*E	4	0.0013459	0.0013459	0.0003365	3.47	0.010
I*V*Mat	4	0.0009433	0.0009433	0.0002358	2.43	0.050
I*E*Mat	2	0.0002561	0.0002561	0.0001281	1.32	0.270
V*E*Mat	2	0.0000323	0.0000323	0.0000162	0.17	0.847
I*V*E*Mat	4	0.0012739	0.0012739	0.0003185	3.28	0.013
Error	144	0.0139655	0.0139655	0.0000970		
Total	179	0.0283248				

S = 0.00984798 R-Sq = 50.70% R-Sq(adj) = 38.71%

Unusual Observations for DOC [mm]

Obs	DOC [mm]	Fit	SE Fit	Residual	St Resid
13	0.055000	0.073800	0.004404	-0.018800	-2.13 R

17	0.048000	0.070200	0.004404	-0.022200	-2.52	R
23	0.046000	0.066400	0.004404	-0.020400	-2.32	R
31	0.055000	0.073800	0.004404	-0.018800	-2.13	R
57	0.085000	0.060400	0.004404	0.024600	2.79	R
71	0.094000	0.070200	0.004404	0.023800	2.70	R
75	0.081000	0.060400	0.004404	0.020600	2.34	R
79	0.085000	0.060600	0.004404	0.024400	2.77	R
87	0.083000	0.059800	0.004404	0.023200	2.63	R
89	0.099000	0.070200	0.004404	0.028800	3.27	R
180	0.083000	0.065200	0.004404	0.017800	2.02	R

R denotes an observation with a large standardized residual.

Analysis of Variance for TR, using Adjusted SS for Tests

Source	DF	Seq SS	Adj SS	Adj MS	F	P
I	2	0.0000161	0.0000161	0.0000081	0.18	0.835
V	2	0.0000671	0.0000671	0.0000336	0.75	0.474
E	1	0.0001467	0.0001467	0.0001467	3.28	0.072
Mat	1	0.0005305	0.0005305	0.0005305	11.86	0.001
I*V	4	0.0002401	0.0002401	0.0000600	1.34	0.257
I*E	2	0.0000341	0.0000341	0.0000171	0.38	0.684
I*Mat	2	0.0001744	0.0001744	0.0000872	1.95	0.146
V*E	2	0.0001227	0.0001227	0.0000614	1.37	0.257
V*Mat	2	0.0000970	0.0000970	0.0000485	1.08	0.341
E*Mat	1	0.0000450	0.0000450	0.0000450	1.01	0.318
I*V*E	4	0.0002955	0.0002955	0.0000739	1.65	0.165
I*V*Mat	4	0.0003310	0.0003310	0.0000827	1.85	0.123
I*E*Mat	2	0.0001264	0.0001264	0.0000632	1.41	0.247
V*E*Mat	2	0.0000086	0.0000086	0.0000043	0.10	0.909
I*V*E*Mat	4	0.0003448	0.0003448	0.0000862	1.93	0.109
Error	144	0.0064420	0.0064420	0.0000447		
Total	179	0.0090220				

S = 0.00668851 R-Sq = 28.60% R-Sq(adj) = 11.24%

Unusual Observations for TR

Obs	TR	Fit	SE Fit	Residual	St Resid	
53	0.003000	0.019600	0.002991	-0.016600	-2.77	R
57	0.030000	0.014600	0.002991	0.015400	2.57	R

71	0.036000	0.019600	0.002991	0.016400	2.74	R
79	0.030000	0.013600	0.002991	0.016400	2.74	R
85	0.033000	0.020000	0.002991	0.013000	2.17	R
89	0.034000	0.019600	0.002991	0.014400	2.41	R
91	0.028000	0.013400	0.002991	0.014600	2.44	R
127	-0.002000	0.013400	0.002991	-0.015400	-2.57	R

R denotes an observation with a large standardized residual.

Analysis of Variance for MRR [mm/s], using Adjusted SS for Tests

Source	DF	Seq SS	Adj SS	Adj MS	F	P
I	2	0.0000009	0.0000009	0.0000005	8.32	0.000
V	2	0.0000019	0.0000019	0.0000010	17.59	0.000
E	1	0.0000207	0.0000207	0.0000207	377.61	0.000
Mat	1	0.0000020	0.0000020	0.0000020	35.70	0.000
I*V	4	0.0000002	0.0000002	0.0000000	0.84	0.500
I*E	2	0.0000005	0.0000005	0.0000002	4.51	0.013
I*Mat	2	0.0000002	0.0000002	0.0000001	1.54	0.217
V*E	2	0.0000004	0.0000004	0.0000002	3.60	0.030
V*Mat	2	0.0000002	0.0000002	0.0000001	1.85	0.161
E*Mat	1	0.0000000	0.0000000	0.0000000	0.50	0.482
I*V*E	4	0.0000001	0.0000001	0.0000000	0.34	0.850
I*V*Mat	4	0.0000001	0.0000001	0.0000000	0.57	0.684
I*E*Mat	2	0.0000007	0.0000007	0.0000003	5.97	0.003
V*E*Mat	2	0.0000010	0.0000010	0.0000005	9.41	0.000
I*V*E*Mat	4	0.0000002	0.0000002	0.0000000	0.91	0.460
Error	144	0.0000079	0.0000079	0.0000001		
Total	179	0.0000370				

S = 0.000234269 R-Sq = 78.64% R-Sq(adj) = 73.44%

Unusual Observations for MRR [mm/s]

Obs	MRR [mm/s]	Fit	SE Fit	Residual	St Resid	
9	0.001709	0.000822	0.000105	0.000888	4.24	R
11	0.000547	0.001000	0.000105	-0.000453	-2.16	R
29	0.000467	0.001000	0.000105	-0.000533	-2.54	R
35	0.001905	0.001295	0.000105	0.000610	2.91	R
45	0.000382	0.000822	0.000105	-0.000439	-2.10	R
53	0.001910	0.001295	0.000105	0.000615	2.94	R

65	0.001855	0.001000	0.000105	0.000855	4.08 R
89	0.000470	0.001295	0.000105	-0.000825	-3.94 R
122	0.000558	0.000980	0.000105	-0.000422	-2.01 R
124	0.000589	0.001033	0.000105	-0.000444	-2.12 R
126	0.000538	0.001066	0.000105	-0.000528	-2.52 R
150	0.001481	0.001040	0.000105	0.000441	2.11 R
178	0.001503	0.001033	0.000105	0.000470	2.24 R
180	0.001660	0.001066	0.000105	0.000595	2.84 R

R denotes an observation with a large standardized residual.

Analysis of Variance for TWR, using Adjusted SS for Tests

Source	DF	Seq SS	Adj SS	Adj MS	F	P
I	2	0.01513	0.01513	0.00757	1.72	0.182
V	2	0.06646	0.06646	0.03323	7.57	0.001
E	1	0.02933	0.02933	0.02933	6.69	0.011
Mat	1	6.44407	6.44407	6.44407	1468.93	0.000
I*V	4	0.00852	0.00852	0.00213	0.49	0.746
I*E	2	0.13111	0.13111	0.06555	14.94	0.000
I*Mat	2	0.18422	0.18422	0.09211	21.00	0.000
V*E	2	0.26295	0.26295	0.13148	29.97	0.000
V*Mat	2	0.28664	0.28664	0.14332	32.67	0.000
E*Mat	1	2.52837	2.52837	2.52837	576.34	0.000
I*V*E	4	0.04430	0.04430	0.01108	2.52	0.043
I*V*Mat	4	0.01310	0.01310	0.00328	0.75	0.562
I*E*Mat	2	0.03312	0.03312	0.01656	3.77	0.025
V*E*Mat	2	0.06751	0.06751	0.03375	7.69	0.001
I*V*E*Mat	4	0.01742	0.01742	0.00435	0.99	0.414
Error	144	0.63172	0.63172	0.00439		
Total	179	10.76396				

S = 0.0662338 R-Sq = 94.13% R-Sq(adj) = 92.70%

Unusual Observations for TWR

Obs	TWR	Fit	SE Fit	Residual	St Resid
1	0.50771	0.64573	0.02962	-0.13802	-2.33 R
5	0.13737	0.27601	0.02962	-0.13864	-2.34 R
11	0.37616	0.21236	0.02962	0.16380	2.76 R
19	0.50732	0.64573	0.02962	-0.13841	-2.34 R

31	0.20603	0.32948	0.02962	-0.12345	-2.08	R
37	0.48183	0.64573	0.02962	-0.16390	-2.77	R
47	0.05147	0.21236	0.02962	-0.16089	-2.72	R
69	0.36612	0.24231	0.02962	0.12381	2.09	R
73	0.97707	0.64573	0.02962	0.33134	5.59	R
83	0.36257	0.21236	0.02962	0.15021	2.54	R

R denotes an observation with a large standardized residual.

D 150 µm

General Linear Model: Time [s], Wear [mm], ... versus I, V, ...

Factor	Type	Levels	Values
I	fixed	3	H, L, M
V	fixed	3	H, L, M
E	fixed	2	206, 365
Mat	fixed	2	Cu, TC

Analysis of Variance for Time [s], using Adjusted SS for Tests

Source	DF	Seq SS	Adj SS	Adj MS	F	P
I	2	77627	77627	38813	2.43	0.092
V	2	219526	219526	109763	6.87	0.001
E	1	1476594	1476594	1476594	92.36	0.000
Mat	1	1242129	1242129	1242129	77.69	0.000
I*V	4	161033	161033	40258	2.52	0.044
I*E	2	75905	75905	37952	2.37	0.097
I*Mat	2	128402	128402	64201	4.02	0.020
V*E	2	129888	129888	64944	4.06	0.019
V*Mat	2	130249	130249	65124	4.07	0.019
E*Mat	1	155902	155902	155902	9.75	0.002
I*V*E	4	129027	129027	32257	2.02	0.095
I*V*Mat	4	202230	202230	50558	3.16	0.016
I*E*Mat	2	157266	157266	78633	4.92	0.009
V*E*Mat	2	108794	108794	54397	3.40	0.036
I*V*E*Mat	4	218539	218539	54635	3.42	0.011
Error	144	2302200	2302200	15988		
Total	179	6915310				

S = 126.442   R-Sq = 66.71%   R-Sq(adj) = 58.62%

Unusual Observations for Time [s]

Obs	Time [s]	Fit	SE Fit	Residual	St Resid	
6	469.00	212.85	56.55	256.15	2.26	R
9	1279.97	901.11	56.55	378.86	3.35	R
13	1091.99	592.09	56.55	499.90	4.42	R
15	144.00	387.47	56.55	-243.46	-2.15	R
27	503.51	901.11	56.55	-397.61	-3.52	R
45	406.07	901.11	56.55	-495.05	-4.38	R
49	206.73	592.09	56.55	-385.36	-3.41	R
53	673.17	374.30	56.55	298.87	2.64	R
63	1318.39	901.11	56.55	417.28	3.69	R
73	535.26	278.40	56.55	256.87	2.27	R

R denotes an observation with a large standardized residual.

Analysis of Variance for Wear [mm], using Adjusted SS for Tests

Source	DF	Seq SS	Adj SS	Adj MS	F	P
I	2	1.7193	1.7193	0.8596	3.47	0.034
V	2	0.3700	0.3700	0.1850	0.75	0.475
E	1	0.8491	0.8491	0.8491	3.43	0.066
Mat	1	71.2715	71.2715	71.2715	287.87	0.000
I*V	4	0.6701	0.6701	0.1675	0.68	0.609
I*E	2	0.1971	0.1971	0.0985	0.40	0.672
I*Mat	2	2.4992	2.4992	1.2496	5.05	0.008
V*E	2	0.0738	0.0738	0.0369	0.15	0.862
V*Mat	2	1.1272	1.1272	0.5636	2.28	0.106
E*Mat	1	2.5705	2.5705	2.5705	10.38	0.002
I*V*E	4	1.1462	1.1462	0.2866	1.16	0.332
I*V*Mat	4	0.6245	0.6245	0.1561	0.63	0.641
I*E*Mat	2	0.5244	0.5244	0.2622	1.06	0.349
V*E*Mat	2	0.1929	0.1929	0.0965	0.39	0.678
I*V*E*Mat	4	3.6459	3.6459	0.9115	3.68	0.007
Error	144	35.6524	35.6524	0.2476		
Total	179	123.1341				

S = 0.497580   R-Sq = 71.05%   R-Sq(adj) = 64.01%

Unusual Observations for Wear [mm]

Obs	Wear [mm]	Fit	SE Fit	Residual	St Resid	
92	1.92201	2.88429	0.22252	-0.96228	-2.16	R
97	4.14281	2.63209	0.22252	1.51072	3.39	R
133	1.61081	2.63209	0.22252	-1.02128	-2.29	R
142	2.65041	3.79297	0.22252	-1.14256	-2.57	R
160	7.41361	3.79297	0.22252	3.62064	8.14	R
178	2.41841	3.79297	0.22252	-1.37456	-3.09	R

R denotes an observation with a large standardized residual.

Analysis of Variance for DOC [mm], using Adjusted SS for Tests

Source	DF	Seq SS	Adj SS	Adj MS	F	P
I	2	0.0000642	0.0000642	0.0000321	0.28	0.755
V	2	0.0002221	0.0002221	0.0001111	0.98	0.379
E	1	0.0000688	0.0000688	0.0000688	0.60	0.438
Mat	1	0.0002433	0.0002433	0.0002433	2.14	0.146
I*V	4	0.0002934	0.0002934	0.0000734	0.64	0.632
I*E	2	0.0000358	0.0000358	0.0000179	0.16	0.855
I*Mat	2	0.0000326	0.0000326	0.0000163	0.14	0.867
V*E	2	0.0000286	0.0000286	0.0000143	0.13	0.882
V*Mat	2	0.0000138	0.0000138	0.0000069	0.06	0.941
E*Mat	1	0.0012129	0.0012129	0.0012129	10.65	0.001
I*V*E	4	0.0005010	0.0005010	0.0001252	1.10	0.359
I*V*Mat	4	0.0004327	0.0004327	0.0001082	0.95	0.437
I*E*Mat	2	0.0000079	0.0000079	0.0000039	0.03	0.966
V*E*Mat	2	0.0000006	0.0000006	0.0000003	0.00	0.998
I*V*E*Mat	4	0.0007592	0.0007592	0.0001898	1.67	0.161
Error	144	0.0163924	0.0163924	0.0001138		
Total	179	0.0203091				

S = 0.0106694 R-Sq = 19.29% R-Sq(adj) = 0.00%

Unusual Observations for DOC [mm]

Obs	DOC [mm]	Fit	SE Fit	Residual	St Resid	
96	0.032000	0.059800	0.004772	-0.027800	-2.91	R
97	0.101000	0.070800	0.004772	0.030200	3.16	R

104	0.082000	0.059600	0.004772	0.022400	2.35	R
115	0.051000	0.070800	0.004772	-0.019800	-2.07	R
131	0.049000	0.070200	0.004772	-0.021200	-2.22	R
133	0.038000	0.070800	0.004772	-0.032800	-3.44	R
150	0.080000	0.059800	0.004772	0.020200	2.12	R
167	0.096000	0.070200	0.004772	0.025800	2.70	R
169	0.091000	0.070800	0.004772	0.020200	2.12	R
172	0.080000	0.059150	0.004772	0.020850	2.18	R
177	0.080000	0.060800	0.004772	0.019200	2.01	R

R denotes an observation with a large standardized residual.

Analysis of Variance for TR, using Adjusted SS for Tests

Source	DF	Seq SS	Adj SS	Adj MS	F	P
I	2	0.0015859	0.0015859	0.0007930	1.23	0.297
V	2	0.0015066	0.0015066	0.0007533	1.16	0.315
E	1	0.0015315	0.0015315	0.0015315	2.37	0.126
Mat	1	0.0124245	0.0124245	0.0124245	19.21	0.000
I*V	4	0.0009591	0.0009591	0.0002398	0.37	0.829
I*E	2	0.0014296	0.0014296	0.0007148	1.11	0.334
I*Mat	2	0.0017906	0.0017906	0.0008953	1.38	0.254
V*E	2	0.0027575	0.0027575	0.0013787	2.13	0.122
V*Mat	2	0.0014520	0.0014520	0.0007260	1.12	0.328
E*Mat	1	0.0012218	0.0012218	0.0012218	1.89	0.171
I*V*E	4	0.0009053	0.0009053	0.0002263	0.35	0.844
I*V*Mat	4	0.0013446	0.0013446	0.0003362	0.52	0.721
I*E*Mat	2	0.0021580	0.0021580	0.0010790	1.67	0.192
V*E*Mat	2	0.0018081	0.0018081	0.0009040	1.40	0.251
I*V*E*Mat	4	0.0008143	0.0008143	0.0002036	0.31	0.868
Error	144	0.0931450	0.0931450	0.0006468		
Total	179	0.1268344				

S = 0.0254331   R-Sq = 26.56%   R-Sq(adj) = 8.71%

Unusual Observations for TR

Obs	TR	Fit	SE Fit	Residual	St Resid	
105	-0.004000	0.046000	0.011374	-0.050000	-2.20	R
123	-0.001000	0.046000	0.011374	-0.047000	-2.07	R
153	-0.002000	0.043550	0.011374	-0.045550	-2.00	R

159	-0.001000	0.046000	0.011374	-0.047000	-2.07	R
171	0.210750	0.043550	0.011374	0.167200	7.35	R
177	0.230000	0.046000	0.011374	0.184000	8.09	R

R denotes an observation with a large standardized residual.

Analysis of Variance for MRR [mm/s], using Adjusted SS for Tests

Source	DF	Seq SS	Adj SS	Adj MS	F	P
I	2	0.0000000	0.0000000	0.0000000	1.30	0.276
V	2	0.0000001	0.0000001	0.0000000	3.76	0.026
E	1	0.0000008	0.0000008	0.0000008	123.89	0.000
Mat	1	0.0000005	0.0000005	0.0000005	79.01	0.000
I*V	4	0.0000000	0.0000000	0.0000000	0.43	0.786
I*E	2	0.0000000	0.0000000	0.0000000	0.66	0.517
I*Mat	2	0.0000000	0.0000000	0.0000000	1.42	0.245
V*E	2	0.0000000	0.0000000	0.0000000	0.57	0.566
V*Mat	2	0.0000000	0.0000000	0.0000000	0.43	0.651
E*Mat	1	0.0000001	0.0000001	0.0000001	11.42	0.001
I*V*E	4	0.0000000	0.0000000	0.0000000	0.04	0.997
I*V*Mat	4	0.0000000	0.0000000	0.0000000	0.30	0.877
I*E*Mat	2	0.0000000	0.0000000	0.0000000	0.75	0.474
V*E*Mat	2	0.0000000	0.0000000	0.0000000	0.87	0.422
I*V*E*Mat	4	0.0000000	0.0000000	0.0000000	1.03	0.394
Error	144	0.0000010	0.0000010	0.0000000		
Total	179	0.0000026				

S = 0.0000819599 R-Sq = 62.60% R-Sq(adj) = 53.51%

Unusual Observations for MRR [mm/s]

Obs	MRR [mm/s]	Fit	SE Fit	Residual	St Resid	
56	0.000322	0.000171	0.000037	0.000151	2.06	R
82	0.000334	0.000179	0.000037	0.000155	2.12	R
84	0.000364	0.000196	0.000037	0.000168	2.29	R
86	0.000369	0.000196	0.000037	0.000173	2.36	R
88	0.000409	0.000215	0.000037	0.000193	2.64	R
92	0.000156	0.000327	0.000037	-0.000171	-2.33	R
96	0.000160	0.000325	0.000037	-0.000165	-2.25	R
98	0.000192	0.000353	0.000037	-0.000161	-2.19	R
100	0.000175	0.000333	0.000037	-0.000158	-2.16	R

160	0.000614	0.000381	0.000037	0.000233	3.17 R
170	0.000676	0.000353	0.000037	0.000323	4.41 R

R denotes an observation with a large standardized residual.

Analysis of Variance for TWR, using Adjusted SS for Tests

Source	DF	Seq SS	Adj SS	Adj MS	F	P
I	2	0.62111	0.62111	0.31055	3.43	0.035
V	2	0.61179	0.61179	0.30590	3.38	0.037
E	1	0.15670	0.15670	0.15670	1.73	0.191
Mat	1	13.09033	13.09033	13.09033	144.46	0.000
I*V	4	0.21986	0.21986	0.05497	0.61	0.659
I*E	2	0.25686	0.25686	0.12843	1.42	0.246
I*Mat	2	0.78453	0.78453	0.39226	4.33	0.015
V*E	2	0.11479	0.11479	0.05739	0.63	0.532
V*Mat	2	0.76542	0.76542	0.38271	4.22	0.017
E*Mat	1	0.56654	0.56654	0.56654	6.25	0.014
I*V*E	4	0.30912	0.30912	0.07728	0.85	0.494
I*V*Mat	4	0.21700	0.21700	0.05425	0.60	0.664
I*E*Mat	2	0.38018	0.38018	0.19009	2.10	0.126
V*E*Mat	2	0.06657	0.06657	0.03329	0.37	0.693
I*V*E*Mat	4	0.49617	0.49617	0.12404	1.37	0.248
Error	144	13.04887	13.04887	0.09062		
Total	179	31.70585				

S = 0.301027 R-Sq = 58.84% R-Sq(adj) = 48.84%

Unusual Observations for TWR

Obs	TWR	Fit	SE Fit	Residual	St Resid
105	1.03165	1.59444	0.13462	-0.56279	-2.09 R
117	1.05168	1.68990	0.13462	-0.63822	-2.37 R
135	1.13071	1.68990	0.13462	-0.55919	-2.08 R
160	3.43004	1.71731	0.13462	1.71272	6.36 R
171	3.60699	1.68990	0.13462	1.91710	7.12 R
177	3.01465	1.59444	0.13462	1.42022	5.27 R
178	1.15992	1.71731	0.13462	-0.55740	-2.07 R

R denotes an observation with a large standardized residual.